Methodology for Assessing Transport Properties of Wells Used in the Geological Storage of Carbon Dioxide

by

Francisco Moreno Tellez

A thesis submitted in partial fulfillment of the requirements for the degree of

Doctor of Philosophy

in
Geotechnical Engineering

Department of Civil and Environmental Engineering
University of Alberta

ABSTRACT

One of the aspects of climate change is global warming, which can be defined as the increase in the average temperature of the Earth's near-surface air and the oceans and its projected continuation. Scientific understanding of the cause of global warming has been increasing. In its fourth assessment of the relevant scientific literature, the Intergovernmental Panel on Climate Change (IPCC) reported that scientists were more than 90% certain that most of global warming was being caused by increasing concentrations of greenhouse gases (GHG) produced by human activities. Common GHGs in the Earth's atmosphere include water vapor, carbon dioxide, methane, nitrous oxide, ozone, and chlorofluorocarbons.

Carbon dioxide (CO_2) is the most important anthropogenic GHG that has significant contribution to the climate change. Carbon dioxide (CO_2) emissions come mostly from fossil fuel combustion, cement production, and land use changes such as deforestation. Ways to lessen the environmental impact of fossil fuel combustion technologies, which currently comprise a substantial portion of the planet energy supply, are being evaluated internationally. One promising option is carbon capture and storage (CCS).

CCS involves capturing CO_2 emissions from large point sources and storing them underground in suitable geological formations. The process of storing CO_2 is defined as geological CO_2 sequestration or CO_2 geo-sequestration. Suitable geological formations include declining oil reservoirs, un-minable coal seams, depleted oil and gas reservoirs, and saline formations. Storage options such as enhanced oil recovery (EOR) for declining oil reservoirs and enhanced coal-bed methane (ECBM) recovery for un-mineable coal seams provide short-term storage opportunities. On the other hand, storage in depleted oil and gas reservoirs and deep saline formations can be considered longer-term options.

The storage of CO_2 is not risk-free, but if it is properly planned, operated and monitored, risk can be reduced substantially. Leakage of stored CO_2 from a storage formation may take place due a loss in the structural integrity of the cap rock. This integrity is controlled by two mechanisms, which are geological leakage mechanism and wellbore leakage mechanism. Wellbores provide access to a reservoir and may serve as preferential flow paths by allowing upward migration of injected CO_2. This migration, unlike the lateral movement of the CO_2 plume in the reservoir, might occur in a very short time frame, on the order of years to tens of years and, in some critical cases, less. This can have potential adverse

effects in relation to safety and/or environmental damage, thus posing a risk to the success of CO_2 underground disposal.

For CO2 storage, the ultimate goal for well-leakage models is to serve as inputs for a certification framework and risk analysis. In order to achieve this goal, there is a need to further investigate a more realistic representation of wellbore element bulk permeability that can differ from element to element within a wellbore system. Researchers have adopted the concept of wellbore lifecycle and recognized its importance in understanding wellbore behavior under different states. However, all of these efforts are scattered and dispersed due to either the various approaches of the study and the multi-disciplinary nature of the problem. In addition, direct measurements of wellbore bulk permeability along well segments are limited and very expensive to obtain. As a result, there is a need to develop a unified method and a conceptual model, which can be used as a practical engineering platform to assess wellbore integrity.

A methodology to assess the transport properties of wells is introduced. The methodology presented systematically identifies and estimates the effect of each of the physical and chemical processes responsible for the alteration of the transport properties of wells. Based on the physics involved in these permeability alteration processes, a four-group classification is proposed: geomechanical damage, hydrochemical

damage, mud removal, and deterioration damage (cement). These processes can occur during the various phases of a well's life, namely drilling, completion, production, and abandonment.

Example of wellbore bulk permeability calculation for a typical 54 –year old vertical well, drilled in the Weyburn oil field in southeastern Saskatchewan, Canada, using the proposed methodology is presented. Estimate of permeability is in good agreement with direct measurements conducted as a component of the IEAGHG Weyburn-Midale CO_2 Monitoring and Storage Project.

DEDICATION

I dedicate this thesis to my parents Wilfrido and Amparo, my wife Claudia, and my daughters Silvia and Gabriela.

ACNOWLEDGMENTS

I express my gratitude to Dr. Rick Chalaturnyk for his valuable support, patience, and assistance offered throughout this project. His helpful advice and encouragement are appreciated.

My thanks go to my friends, Santiago Paz and Dr. Kin Wan Soe Moe, for their friendship and help.

Appreciation is also extended to Sally Petaske and Stephen Gamble of the Department of Civil and Environmental Engineering, for their assistance at the university. The support and encouragement of other faculty and staff in the department are always in my heart.

TABLE OF CONTENTS

LIST OF TABLES

LIST OF FIGURES

LIST OF SYMBOLS

A	aging weight function [dimensionless]
a_{df}	activity of drill fluid [dimensionless]
a_{sh}	shale activity [dimensionless]
c	cohesion [MPa]
cc	cake compressibility factor [dimensionless]
cm	mud specific heat [J/kg .°C]
cp	mass concentration of particles in mud [g/cm^3]
d	cement pore diameter [μm]
Do	outer casing diameter [m]
Ds	stability margin
D_2	open-hole size [m]
E	rock Young's modulus [GPa]
Ec	cement Young's modulus [GPa]
Ed	dynamic Young's modulus [GPa]
Eh	average rock Young's modulus [GPa]
Es	static Young's modulus [GPa]
Et	steel Young's modulus [GPa]
Eu	undrained Young's modulus [GPa]
Gm	mud temperature gradient [°C/m]
Gt	geothermal gradient [°C/m]
h	cake efficiency [ ]
hi	thickness of corresponding section [m]

H	Hamacker coefficient [J]
H_T	total thickness [m]
hc	casing-wall thickness [m]
I	separation distance between particle surfaces [μm]
Jd	discontinuity dip rating [ ]
Jp	support pressure rating [ ]
Js	discontinuity spacing rating [ ]
Jt	temperature rating [ ]
kc	cake permeability [D]
kd	cement permeability [D]
ki	permeability of individual section [D]
kf	formation permeability [D]
k_I	effective permeability for flow in horizontal direction [D]
k_{II}	effective permeability for flow in vertical direction, [D]
lc	critical pore diameter [μm]
L	well depth [m]
Ld	annular cement thickness [mm]
nc	critical value of capillary porosity [%]
Ne	lateral load on centralizer [N]
Nw	well stability rating [ ]
P	pressure differential function [ ]
P_{max}	maximum operational pressure [MPa]

Po	mean stress $(\sigma_1 + \sigma_3)/2$ [MPa]
P_{temp}	equivalent pressure, [MPa]
PV	mud plastic viscosity [cp]
pw	drill fluid pressure [MPa]
Q	mud flow rate [m^3/min]
Q_D	actual mud flow rate [m^3/min]
Qe	equivalent mud flow rate [m^3/min]
q	gas flow rate [Mscf/D]
r_c	average particle radius [μm]
R	gas constant [8.314 m^3 Pa/K.mol]
$RF_{67\%}$	restoring force [N]
Ro	outer casing radius [m]
R_2	open-hole radius [m]
s	centralizer spacing [m]
Sa	swelling activity [dimensionless]
So	deviatoric stress $(\sigma_1 - \sigma_3)$ [MPa]
SRF	stress reduction factor [dimensionless]
STO	standoff [%]
Sw	shear stress on filter cake function [dimensionless]
t	time [day]
T	axial tension [N]
Ta	annular mud temperature [°C]
Ti	inlet mud temperature [°C]

T_{max}	maximum operational temperature, [°C]
To	far-field temperature [°C]
Tr	reservoir temperature [°R]
Ts	surface-formation temperature [°C]
TY	mud yield strength [lb./100 ft.^{2}]
u	pore pressure [MPa]
UCS	unconfined compressive strength [MPa]
V	mean partial molar volume of water [m^3]
Vb	base fluid-viscosity change due to temperature function [ ]
V_{clay}	volume fraction of clay minerals [dimensionless]
Ve	equivalent mud velocity [m/min]
vi	discharge velocity of corresponding section [m/sec]
V_{narrow}/V_{avg}	ratio of interface velocity on narrow side and average velocity in the annulus [dimensionless]
Vp	compressive wave velocity [km/sec]
Vs	shear wave velocity [km/sec]
V_T	volume of turbulent fluid flow [m^3]
ws	casing weight [kg/m]
Z	depth [m]
z	gas deviation factor [dimensionless]
α	Biot's constant [dimensionless]
β	dogleg [°]

ΔL	well length [m]
ΔP	reservoir pressure [psi]
δ	cake thickness [mm]
δ_c	centralizer deflection [m]
δ_{cg}	casing deflection [m]
δ_T	total casing deflection [m]
ΔPm	osmotic pressure [MPa]
ϕ	friction angle [°]
γ	unit weight [N/m^3]
I	casing moment of inertia [in.^{4}]
θ	well inclination [°]
ρ_d	bulk rock density [kg/m^3]
ρ_m	mud density [kg/m^3]
ρ_s	steel density [kg/m^3]
μ	gas viscosity [cp]
σ	osmosis efficiency [ ]
σ_e	restrained expansion pressure [MPa]
σ_h	minimum horizontal stress [MPa]
σ_H	maximum horizontal stress [MPa]
σ_s	hydrostatic pressure [MPa]
σ_T	total stress [MPa]
σ_v	vertical stress [MPa]

σ'	effective stress [MPa]
σ_1, σ_3	major and minor stress [MPa]
υ	Poisson's ratio [dimensionless]
υ_d	dynamic Poisson's ratio [dimensionless]
υ_s	static Poisson's ratio [dimensionless]
υ_u	undrained Poisson's ratio [dimensionless]
τ_c	cake yield strength [dyne/cm^2]
τ_w	shear stress at wall [dyne/cm^2]
Ω	volumetric thermal expansion of steel [in./in.] °F^{-1}

1 Introduction

1.1 General

It is now generally accepted that man-made greenhouse gas emissions are contributing to the global rise in atmospheric greenhouse gas levels. Most man-made greenhouse gas emissions are caused by our use of fossil fuels. At present, however, the use of fossil fuels is central to the well-being of any industrial society and cannot simply be stopped. One way of reducing anthropogenic greenhouse gas emissions, without radically altering our use of fossil fuels for power generation, is to dispose of them underground rather than emitting them to the atmosphere. This technology is better known as carbon dioxide (CO_2) capture and storage, and it has been identified as an important means of reducing greenhouse gas emissions. Geological storage of CO_2 is particularly attractive for Western Canada because a large percentage of CO_2 emissions come from large stationary sources, such as fossil-fuel power plants, oil sands plants, refineries, cement plants and petrochemical plants.

There are several means of geologically storing CO_2: in depleted oil and gas reservoirs, in deep saline aquifers, in CO_2-flood enhanced oil recovery (EOR) operations, and in enhanced coalbed methane recovery. The last two also provide an economic benefit in that they enable the production of additional oil or methane, respectively.

In the past, however, CO_2 injection into the subsurface by the oil industry has not attracted the attention of environmentalists or government control. As a result, little relevant data or published research are available in the EOR industry that relate to CO_2 storage. Recognizing this need, several multiyear research projects at both large- and small-scale carbon sequestration projects are being conducted by international teams of researchers. Results from these studies have recognized two possible leakage paths: wellbores (both new and existing) and caprock (Moreno et al., 2004). Wellbores that provide access to a reservoir may serve as preferential flow paths by allowing upward migration of injected CO_2. This migration, unlike the lateral movement of the CO_2 plume in the reservoir, might occur in a very short time frame, on the order of years to tens of years and, in some critical cases, less. This can have potential adverse effects in relation to safety and/or environmental damage, thus posing a risk to the success of CO_2 underground disposal.

Possible leakage through existing wells appears to be especially important in mature sedimentary basins that have been intensively explored and exploited for hydrocarbon production. One good example would be the mature Alberta basin. There are close to 400,000 wells, of which some 120,000 have been abandoned. As drilling and completion techniques have evolved with time, we can expect a wide variety of transport conditions in these wells (Moreno et al., 2004). In addition, the cement

used in their completion, historically of variable quality and quantity, has probably degraded. Unfortunately, our knowledge of how those properties evolve under the different life stages of a well is limited. Thus, if geological storage of CO_2 is to be a reality, a methodology that can reliably assess the performance of wells as sealing barriers to the upward migration of CO_2 is needed.

1.2 Objective and Scope of work

In this context, the purpose of this research is, first, to understand the response of wells as a sealing system and, second, to develop the framework for a performance assessment of wells. Given that one of the objectives is to develop a credible assessment of wells as sealing barriers, the methodology will have to withstand public scrutiny and, as such, it must be auditable. Therefore, the theoretical, empirical and subjective background for each index will be fully described. The understanding proceeds through a process that identifies each one of the main components responsible for the transport properties of wells, recognizing how each of the stages during the life of a wellbore (drilling, completion, history and abandonment) contributes to the final sealing conditions.

Investigation work was organized in this thesis in the following chapters:

Part 1 (Theoretical background) presents first a general overview of typical oil wellbore completion. Given that a wellbore goes through a series of

stages during its life, an explanation of the major activities associated with these periods is given. Second, from a transport-properties perspective, a wellbore system is defined and its components are described. Finally, the main permeability-alteration mechanisms, identified as being responsible for the response of active and abandoned wells, are pointed out. Their effect on the transport properties on each of the components of the wellbore system is also explained.

The ability to capture the 'exact' state of all wellbores is extremely difficult. In order to quantify the main processes associated with the hydraulic integrity of the wells, the methodology will implement 'integrity indices' as a tool to assess the most likely future performance of wellbores. These integrity indices will permit the identification of possible high-risk areas associated with the CO_2 injection and will allow focused effort in that area to refine the elements associated with the risk of leakage. All indices will be a function of time, to capture factors such age of well, change in temperature and pressure, etc. An outline of the general procedure to implement the methodology, and the charts needed for the calculation of each index, are presented in *Part 2 (Procedure outline and calculation charts)*.

Part 3 describes and summarizes the work carried out for collecting 'real' wellbore data from an actual CO_2-EOR project. This information is used

as an example of the application of the methodology throughout this research. A brief description of the project is also presented.

Part 4 presents the main processes associated with the transport of CO_2 through the wellbore system. A typical Weyburn wellbore configuration, as determined in the previous part, is used to illustrate these processes. The effect of different possible configurations for the wellbore on gas leakage is also discussed. *Part 5* presents the main flaws and research needs of the methodology and enumerates the main conclusions extracted from this research. Suggestions are also given for further research in the use of the methodology presented here for geological storage of CO_2.

2 Theoretical Background

2.1 General

Any assessment methodology for wellbore integrity, from the perspective of hydraulic or transport properties, must be based on identifying relevant leakage paths within a wellbore system and the processes or mechanisms that influence the characteristics of these leakage paths. To accomplish this, the key elements of the wellbore system must first be defined. For the purpose of this thesis, the wellbore system has been chosen to include the casing, the annular cement (between casing and formation), the formation near the wellbore, and all the interfaces that exist between these components.

2.2 Conductivity-Alteration Mechanisms

A wide variety of processes and mechanisms can modify the transport properties of the wellbore system. For instance, casing permeability can be modified with time due to corrosion, and cement permeability can be increased, usually due of cracking or chemical alteration. Interface permeability is augmented by debonding or the presence of a mud cake.

Based on the physics involved in these permeability-alteration mechanisms, a four-group classification is proposed: geomechanical damage, hydrochemical damage, mud removal and deterioration damage (cement). Geomechanical damage encompasses any stress-induced

changes to the hydraulic conductivity properties of materials within the wellbore system. Hydrochemical damage refers to any alteration of hydraulic conductivity in the near-well region due to particulate processes; this is typically called 'formation damage'. The third group covers the development of mud channels during cementing operations and its impact on hydraulic integrity of the wellbore system. Cement deterioration refers to porosity alterations due to geochemical processes pre– and post–CO_2 injection.

2.3 Hydrochemical Damage

Permeability reduction of the near-wellbore or deep into the rock of a permeable formation usually occurs by exposure to drilling fluids. This alteration of the far-field characteristics of a formation is generally referred to as formation damage. Although formation damage is caused by several mechanisms, it has been generally recognized that plugging of pore spaces by fine particles is one of the major causes (Liu and Civan, 1995, Rahmani et al., 2009, Patnana et al., 2013). There are three primary sources of fine particles in permeable formations (Civan, 2000, Christanti et al., 2011)):

- Externally introduced with fluids used during drilling; depth of invasion will be a function of the relationship between pores and particles, large pores and small particles being the most

unfavourable case; this source causes extremely severe damage, even though particles usually do not invade the formation deeply

- Generated by chemical reactions
- In situ mobilization of clay and other fine mineral species attached to the pore surface of permeable formations due to injected and rock-fluid incompatibility or high hydrodynamic shear of the fluid flowing through porous media

Formation fines are composed of silica, feldspar, mica, calcite, dolomite, siderite and chloride. Commonly found clay minerals include smectite, kaolinite, chlorite and illite (Liu and Civan, 1995). According to its origin, clay in sedimentary rocks can be classified as detrital or authigenic. Detrital clays form an integral part of the rock formation, whereas authigenic clays occur as deposits lining or filling in the pore system.

A detailed description and examples of the different sources of fine particles can be found in Liu and Civan (1995) and Civan (2000).

Migration and deposition of fine particles by the fluids flowing through porous media are controlled by four primary mechanisms: diffusion, adsorption, sedimentation and hydrodynamics (Wojtanowicz et al., 1987). The main difference between these is the forces acting upon particles. Ives (1985) grouped these into

- forces related to the transport mechanisms,

- forces related to the attachment mechanisms, and
- forces related to the detachment mechanisms.

Figure 1 shows the different forces acting upon a particle and their relationship to the different stages, along with the associated mechanisms.

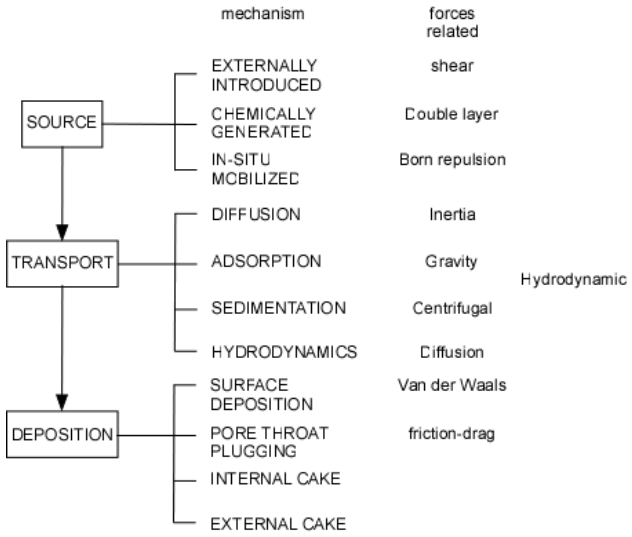

Figure 1 Stages of formation damage and the associated forces acting upon a particle.

According to Civan (2000), the various particulate processes can be classified in two groups: internal and external. External processes occur over the formation face, whereas internal processes occur in the porous media.

2.3.1 Internal processes

Internal processes can be classified as (Wojtanowicz, 1988):

- pore-surface processes (gradual pore reduction),
- pore-throat processes (throat plugging), and

- pore-volume processes (internal cake).

The dominant process is dictated by the ratios of particle size to pore-throat size (β; Hassen, 1980, Ershaghi, 1980, Peden et al., 1982, Peden et al., 1984, Fraser et al., 1995, Francis, 1997, Martins et al., 2004, Whitfill, 2008)

$$\beta = \frac{Dt}{Dp}, \quad \textbf{[1]}$$

where the pore-throat diameter is given by

$$Dt = \frac{Dg}{(1-\phi)^{1/3}}\left(1-(1-\phi)^{1/3}\right). \quad \textbf{[2]}$$

Where

Dt = pore throat diameter,

Dg = mean hydraulic equivalent diameter,

ϕ = porosity.

When the mean size of the particles is much smaller than those of pore bodies and pore throats ($\beta > 7$), they will deposit on the pore walls (Figure 2). This gradual reduction in pore size (pore filling) will continue until it eventually becomes small enough to be plugged by particles, after which an internal cake begins (El-Sayed et al., 2007, Savari et al, 2011). Particles with sizes smaller than that of a pore throat can plug the pore throat as they flow through the porous media. This mechanism of pore plugging is analogous to shutting off a valve, since pore throats act like gates or valves that allow connection between pore bodies. Thus,

permeability diminishes without the pore space being completely filled (Chang and Civan, 1991). Pore filling follows pore-throat plugging, leading to an internal cake formation. Finally, particles slightly larger than a given pore-throat size stick ($1 < \beta < 3$) form bridges just inside the surface pores. Once a primary bridge is established, successively smaller particles are trapped, creating an external cake (King and Adegbesan, 1997). Particles larger than the pore opening ($\beta < 1$) cannot enter the pore and are swept away by the mud stream (Darley and Gray, 1988).

The extent to which these processes occur is a function of several factors that can be grouped into three categories: rock attributes, fluid properties, and environmental properties in the well. Rock attributes include tortuosity, relative permeability, mean pore size, and porosity, type of fluid, viscosity, particle concentration, and particle-size distribution are considered main fluid properties. Environmental properties in the wellbore comprise fluid temperature, differential pressure between borehole and formation, flow rate, wellbore inclination, and drilling rate (Vasquez and Curtice, 2013).

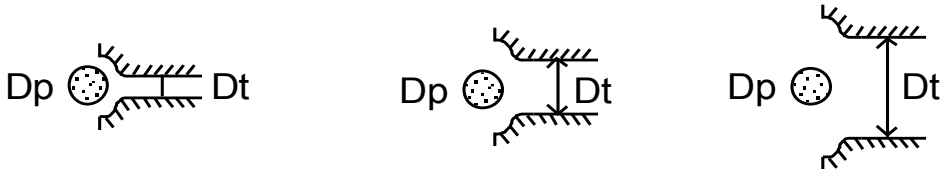

Figure 2 Internal processes (from King and Adegbesan, 1997).

Several models can predict permeability impairment caused by any of these particulate processes, but most have been developed for single-phase fluid systems. As a result, they have little applicability to the assessment of formation damage at the reservoir level, where multiphase effects must be considered. However, they could still offer valuable information on permeability impairment in the near-wellbore region for the specific case of fluid invasion into brine-saturated aquifers dealt with here. A discussion of the four most relevant models available for prediction of damage in literature is presented in this chapter. The following is a summary of the modelling approaches and assumptions identified, interpreted and compared by Civan (2000):

- The thin-slice algebraic model assumes the porous media can be represented by Nh tubes of the same mean hydraulic equivalent diameter Dg, the core has cross-sectional area A and length L. Given that a unique pore size is assumed to exist, only one distinct internal process can dominate. A set of diagnostic equations was developed for the cases of 1) deposition of externally introduced particles, and 2) mobilization and subsequent deposition of in situ particles. Given that high concentrations of solids are normally found during drilling, only the case where particles originate from external sources is considered.

- The compartments-in-series ordinary differential model assumes the porous medium has one unique pore-throat size and that particles of sizes comparable to or larger than the pore throat are trapped within (throat plugging). It also considers that the particle concentration of the fluid leaving a compartment will be a fraction of the fluid in the compartment, as some of the particles might be retained at the pore throats. Both externally introduced and in situ–mobilized particles are simultaneously considered.
- The simplified partial-differential model assumes the porous medium has one unique pore-throat size and that particles with sizes comparable to or larger than the pore throat are trapped within (throat plugging). It also neglects the contribution of the small amount of particles in the flowing suspension (only considers in situ–mobilized particles). As with the previous model, deposited particles will be entrained by hydrodynamic mobilization when a critical shear stress necessary to detach the particles is exceeded.
- The plugging-nonplugging parallel-pathways partial-differential model assumes there are two type of pathways: a smooth and large-diameter nonplugging pathway, where only gradual pore reduction is involved; and a highly tortuous and small-diameter plugging pathway, where retention of particles occurs by jamming and blocking of pore throats. Only the external particle invasion is considered. Unfortunately, this model relies heavily on

mathematical expressions derived empirically, which causes uncertainty regarding the validity of its results.

In all four models, the porous medium is assumed to be uncompressible, homogeneous, and isotropic, and the fluid and particles are uncompressible with constant physical properties. An in-depth review of these models can be found in Civan (2000). Figure 3 is a comparison of these models.

	pore size	particle source	internal process
THIN-SLICE MODEL	single	external or in-situ mobilized	gradual pore reduction or pore plugging or internal cake
COMPARTMENTS-IN SERIES ORDINARY DIFFERENTIAL MODEL	single	external and/or in-situ mobilized	pore plugging
SIMPLIFIED PARTIAL DIFFERENTIAL MODEL	single	in-situ mobilized	pore plugging
PLUGGIN-NONPLUGGING PARALLEL PATHWAYS DIFFERENTIAL MODEL	dual	external	gradual pore reduction and/or pore plugging

Figure 3 Stages in formation damage and the associated forces acting upon particles.

2.3.2 External processes

During drilling, the drilling mud is usually maintained at a pressure higher than that of the formation to prevent formation fluid from invading the

wellbore (Gdanski and Bryant, 2011). Because of this overbalance pressure, the mud tends to invade the permeable formation. Massive loss of mud into the formation usually does not occur because the invading particles are filtered out onto the walls of the hole. This creates a cake of relatively low permeability through which only filtrate can pass (Darley and Gray, 1988, and Suri and Sharma, 2004).

As a result of the bridging process, three zones of mud particles have been identified (Darley and Gray, 1988):

- an external filter cake on the walls of the borehole
- an internal filter cake, extending a couple of grain diameters into the formation
- a zone invaded by the fine particles during the mud-spurt period, which normally extends about an inch into the formation.

In general, dynamic filtration increases as a $t^{1/2}$ function when the surface rock is first exposed, filtration rate is very high, and the cake grows rapidly (Peden et al., 1982). As time passes, the growth rate decreases until it eventually equals the erosion rate (Figure 4).

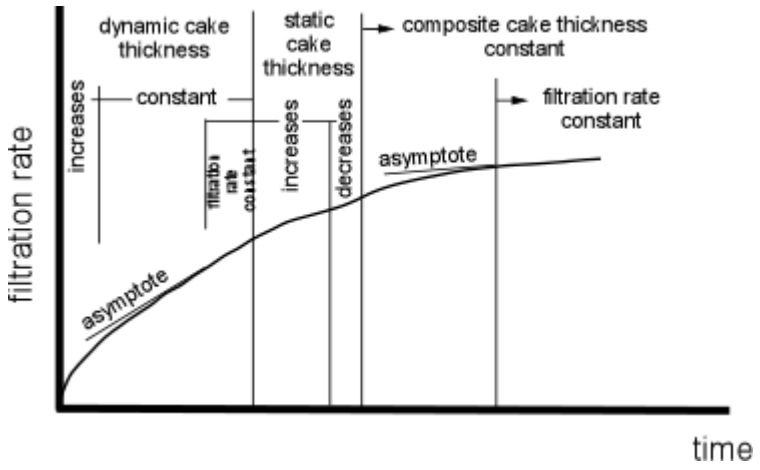

Figure 4 Dynamic filtration stages (from Outmans, 1963).

Down-hole filtration properties of a fluid, along with cake thickness, are measured routinely in the field using the static fluid-loss test (Hassen, 1980). The properties of diverse muds are evaluated by filtering the fluid through paper under standard temperature and pressure, and measuring the filtrate volume accumulating in a standard time (Darley and Gray, 1988). This is better known as the API standard fluid-loss test. Typical test conditions are as follows:

time: 30 minutes

pressure: 100 psi

filtration area: approximately 7 sq. in. (45 cm^2)

filter paper: Whatman 50, S & S No. 576 or equivalent (the thinnest of all Whatman filter papers, with an average pore size of 2.7 μm (20–40 mD)

The thickness of the filter cake is measured to the nearest 1/32 in. (1 mm) after washing off the excess mud with a gentle stream of water. The 30-minute filtrate volume is sometimes predicted by measuring the filtrate volume at 7.5 minutes and doubling the value obtained (since $\sqrt{30}/\sqrt{7.5} = 2$). In some cases, the error introduced by neglecting the mud spurt is small. In others, however, the initial mud spurt can be substantial; this practice can result in serious errors and should therefore be avoided (Arthur and Peden, 1988). They estimated that filtrate volume calculated in this manner was less than the actual value for about 90% of the muds they tested, with an average error of 9.7%. Still, the API static fluid-loss test is qualitatively and comparatively useful to an experienced driller as a mean of periodically checking the mud. However, due to the absence of fluid motion during the test, this is clearly not a good tool for measuring the dynamic fluid-loss characteristics of the mud (Hassen, 1980, Fisk et al., 1981, Chesser et al., 1994, Bailey et al., 1998, and Santos et al., 1999). In addition, this procedure uses a filter paper to simulate the formation, which is not realistic because the structure of a real, permeable formation is quite different (Santos et al., 1999). To overcome this problem, several studies have been undertaken to define a substitute for the API filtration test (Santos, 2000); however, none of these proposed procedures has been adopted as a standard by the oil industry.

Filtration properties can also be measured at high temperatures and pressures. Usually, the standard working pressure is 1000 psi (6.89 MPa) and the maximum temperature is 450˚F (232˚C). Filtration time is 30 minutes at the temperature of interest, but the volume of filtrate collected is doubled to allow for the difference in filtration area between the high- and low-pressure filtration cells (Darley and Gray, 1998). These conditions can generally be found when drilling deep high-permeability formations at high overbalanced pressures, with differential pressures >6.89 MPa (1000 psi) when gas pockets are encountered (Fisk et al., 1991).

When assessing the impact of filter cake on wellbore transport properties, two parameters are of interest: cake thickness and permeability. The variables that can affect cake permeability can be classified into rock properties (formation permeability), drilling-fluid properties (chemical activity), and environmental conditions of the wellbore (temperature, and differential pressure between borehole and formation). The effect of these variables on cake permeability is presented below. A discussion of the parameters known to affect cake thickness is left for a subsequent section.

2.3.2.1. Effect of formation permeability

It is obvious that the pore-size distribution of the formation plays an important role in the filtration process, as it determines the bridging size of

the cake. Large-pore-size formations will capture larger particles than smaller size pore formations; as a result, cake will have higher permeability. Dynamic filtration experiments conducted on cores with permeability and mean pore sizes in specific ranges indicate that greater fluid loss results from increased core permeability and mean pore size (Peden et al., 1982). Similar results were obtained by Browne and Smith (1994), Zain and Sharma (1999) and Suri and Sharma (2001). They observed that high pressures were needed to initiate clean-up of filter cakes in open-hole completion for low-permeability core, with the flow-initiation pressure gradually decreasing as the core permeability increases. Fraser et al. (1995) focused on the performance aspects of three commercially available drill-in fluids. Three rock types were used, covering a wide range of permeabilities (2.6–0.04 D) and average pore diameters (17.9–0.2 μm). Results from these tests indicated lower fluid loss using the tighter formation. They concluded that, when a formation has small pore size, drilling fluids will more rapidly bridge the pores, thereby arresting the invasion of damaging solids.

Effect of mud additive

The electrochemical conditions in a mud are a major factor determining the permeability of its filter cake. For instance, flocculation of mud causes the particles to associate in a loose open network. As the degree of flocculation increases, so does the degree of flocculation of the filter-cake

solids, causing considerable increase in permeability (Chesser et al., 1994). On the other hand, when the mud is deflocculated, clay platelets become detached from each other and can lie flat to form a thin, low-permeability filter cake (Schlumberger Oilfield Glossary).

The electrochemical conditions in a mud can be determined if the type of mud used is known. As a generalization, three distinct mud types can be defined: thinned mud, lightly treated mud, and inhibited mud (Figure 5). Each will form with very distinct cake and associated permeability properties. As a general rule, additives and mud systems share their names. For example, a mud using thinners is called thinned mud and, if the thinner used is a lignosulfonate, then the mud system can be named a lignosulfonate mud.

The remainder of this section describes the complicated chemistry of each mud type, and how its particular electrochemical conditions determine the permeability of its cake.

Thinned (dispersed) mud: Clay (cuttings from the well) is deflocculated throughout the fluid. Deflocculation of a mud by the addition of a thinning agent causes a decrease in cake permeability. Moreover, if deflocculation is accompanied by dispersion of clay aggregates, cake permeability is further reduced.

These muds are used at greater depths, where higher densities are required, or where borehole conditions may be problematic. Deflocculation is achieved by adding polyphosphates, tannins, lignite, and lignosulfonate:

- **Polyphosphate mud:** Polyphosphates are added to the mud as a very effective clay deflocculant and treatment for cement contamination. They were among the first thinners for mud, but they hydrolyze back to orthophosphates as the temperature approaches the boiling point of water, thus limiting their use to relatively shallow

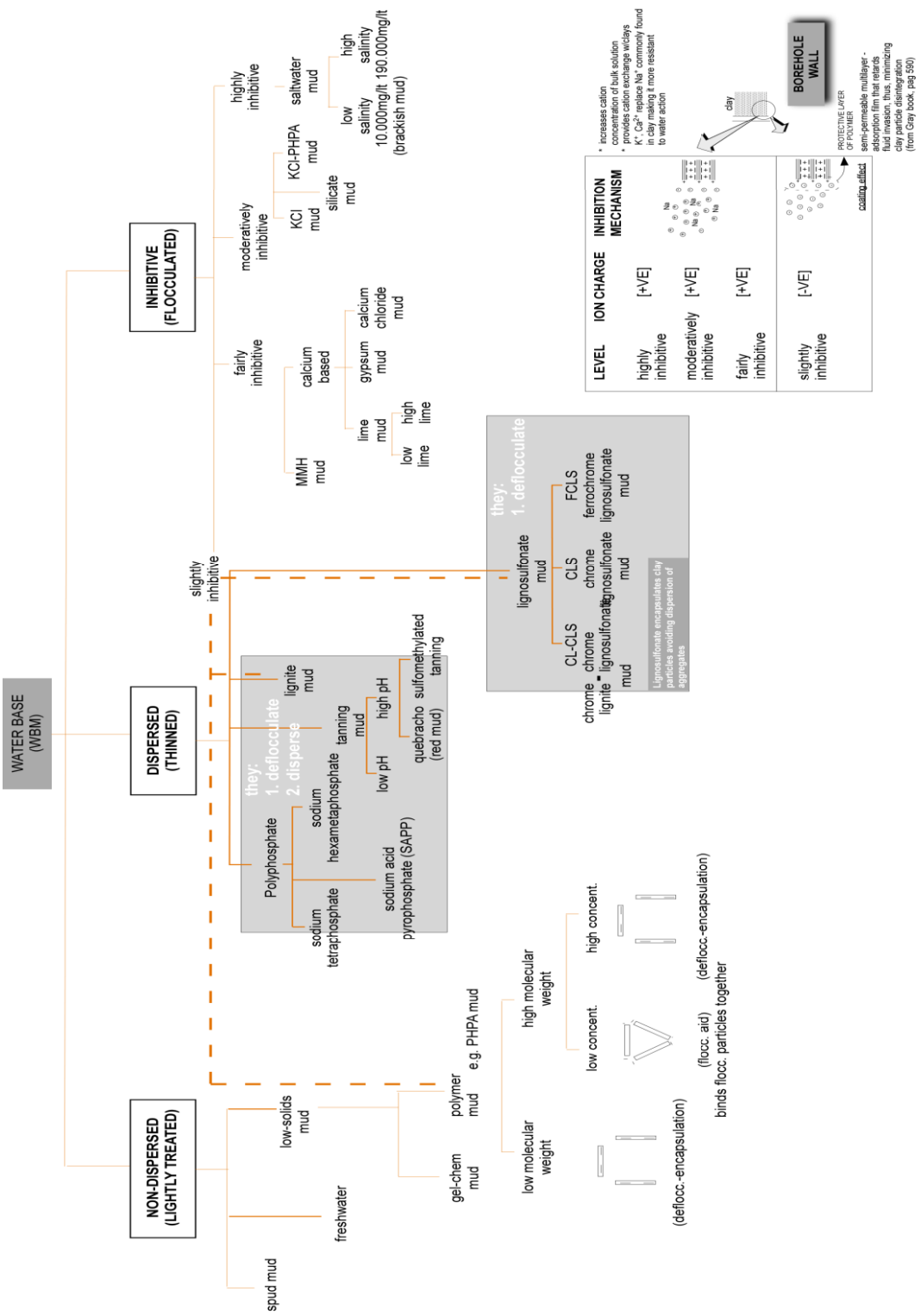

Figure 5 Summary of mud types.

drilling. They also tend to increase disintegration and dispersion of shale cuttings, thus, increasing solids content, an unwanted property in drilling muds.

- **Tanning mud:** The most popular is the red mud, a clay-based water mud that used quebracho as the clay deflocculant and lignite for fluid-loss control (Schlumberger, 2005). It was one of the first thinners used in the United States, but its use declined in the late 1950s.
- **Lignite mud:** Introduced as a partial substitute for quebracho (red) mud in 1947, it is a thinner for muds and now it can be regarded as a filtrate reducer, oil emulsifier and property stabilizer.
- **Lignosulfonate mud:** Deflocculation of clays by lignosulfonate is believed to result mainly from the adsorption of the negative lignosulfonate on the edge surfaces of the clay particle. In addition to clay deflocculation, the adsorption layer of lignosulfonate that surrounds clay particles reduces clay swelling and dispersion by acting as an impermeable membrane that retards water invasion. At the borehole wall, the adsorption layer acts as a buffer in the form of a plastering and blocking agent, thus promoting borehole stabilization. Several mud systems can be included in this classification: 1) calcium lignosulfonate (CL) was used initially as a thinner in lime mud and came into use as a mud in 1949; 2 chrome lignosulfonate (CLS) replaced lime mud for drilling deep holes (Darley and Gray, 1988) chrome lignite–chrome lignosulfonate (CL-CLS) afforded a

relatively simple chemical system that was applicable over a wide range of pH, salinity, and solids content, lignite being added to provide thermal stability to the system (Darley and Gray, 1988).

Lightly to non-treated (non-dispersed) mud: Thinners are not added to some muds, so as to avoid the undesirable dispersion of shale cuttings and clay particles (Darley and Gray, 1988). Consequently, cake permeabilities and porosities of non-dispersed muds are considerably greater than those of thinned (dispersed) muds. These systems include spud muds, low-solids muds, and any other lightly treated systems that are generally used for shallow wells. The term 'low-solids muds' does not apply to any specific composition, but to a number of systems that use chemical and mechanical methods (e.g., shale shaker, desander, hydrocyclone, and centrifuge) to maintain the minimum practical solids content relative to conventional clay muds of the same density (Darley and Gray, 1988, and Schlumberger, 2005). Two of the main chemical methods to control the solids are substitution of polymers for bentonite in the control of viscosity and filtration properties (Darley and Gray, 1988), and the introduction of a bentonite extender polymer to link bentonite particles together and improve rheology without increased solids loading (Schlumberger, 2005). No attempt will be made here to describe the complicated chemistry of polymers, although a few features are highlighted to emphasize the variety and versatility of these substances,

which have assumed such importance in drilling fluids (Figure 6). Monographs can be consulted for details on the extensive research into polymer chemistry (Darley and Gray, 1988).

Inhibited mud: This is a mud used to stop or slow hydration and disintegration of shales when drilling thick sections of dispersible mud-making shale (Darley and Gray, 1988, and Schlumberger, 2005). Flocculation of a mud by the addition of an inhibiting agent causes an increase in cake permeability, because the cake is then built of thicker packets of clay platelets associated in the form of a loose open network (Darley and Gray, 1988). According to the Schlumberger Oilfield Glossary, the degree of inhibition ranges from highly inhibitive (oil mud, saltwater mud), through moderately inhibitive (potassium mud, silicate mud), fairly inhibitive (calcium-based mud, mixed-metal hydroxide [MMH] mud), and slightly inhibitive (lignosulfonate mud, lignite mud, polymer mud), to non-inhibitive (slightly to non-treated mud).

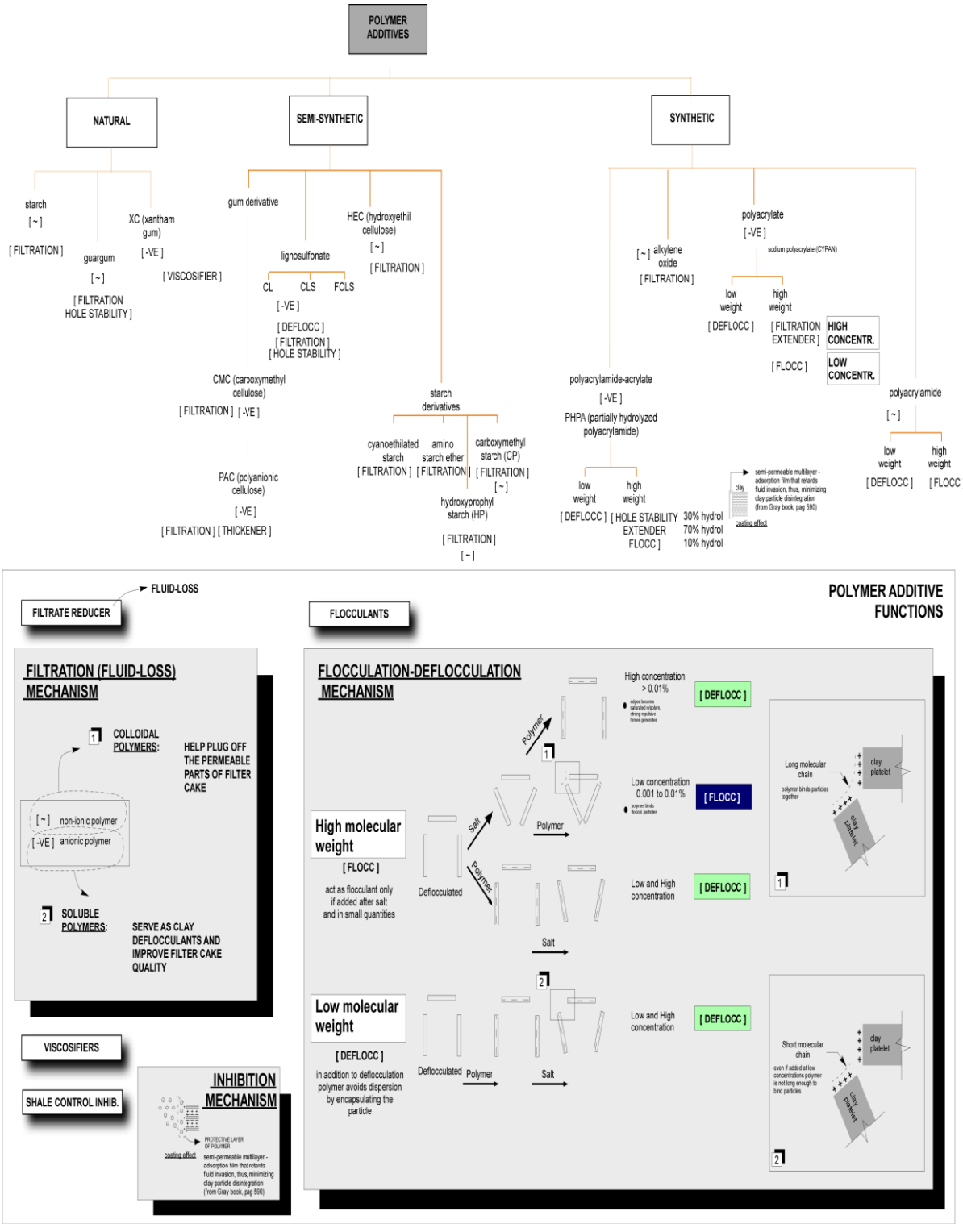

Figure 6 Summary of polymer additives.

Effect of temperature

In general, higher temperature increases the filtration rate due to viscosity reduction of the base fluid (Hassen, 1980, Peden et al., 1984, and Darley and Gray, 1988). Hassen (1980) proposed the following equation to consider this effect when calculating filtration rate under static fluid conditions

$$q_2 = q_1 e^{\frac{B}{2}\left(\frac{T_2 - T_1}{T_2 T_1}\right)}, \quad \textbf{[3]}$$

where

q_1 = filtration rate under condition 1,

q_2 = filtration rate under condition 2,

T_1 = temperature under condition 1,

T_2 = temperature under condition 2,

B = is a viscosity constant for Newtonian fluids (3000 for water or brine).

According to the same author and several other researchers (Peden et al., 1984, Arthur and Peden, 1988, Darley and Gray, 1988, Hartmann et al., 1988, Chesser et al., 1994, and Liu and Civan, 1995), higher filtration rates might actually be recorded than indicated by this equation. A rise in temperature may also increase the filtrate volume by affecting the properties of the filter media, usually in the form of changes in the degree of flocculation or degradation of the mud constituents.

Analysis of mudcake structures in several drilling muds, under simulated borehole conditions, revealed that thermal stress causes an increase in the filtrate volume of bentonite-freshwater mud (gel mud). This process can be associated with a flocculation of the bentonite particles, resulting in enlargement of the effective flow cross-section within the filter cake (Hartmann et al., 1988). As the degree of flocculation increases, so does the flocculation of the filter-cake solids, resulting in an increase of cake permeability (Chesser et al., 1994). Larssen (1938) also concluded that changes in the cake structure due to bentonite flocculation would be the dominant process at intermediate temperatures. An increase in fluid loss of up to 16.7% was measured at 93˚C. Byck (1939) found that permeability of the cakes he tested increased as a result of a temperature increase from 21˚ to 70˚C, with the maximum increase being greater than 100%.

At a critical temperature, many organic filtration-control additives and viscosifiers start to break down rapidly, inhibiting the sealing action in the filter cake and thereby altering the permeability of the cake. This breakdown process is accelerated with further increases in temperature. This critical temperature is approximately 107˚C for starch, 135˚C for cellulosic polymers (sodium carboxymethylcellulose [CMC] and hydroxyethylcellulose [HEC]), 177˚C for CL-CLS muds, and 120˚C for XC polymer (Darley and Gray, 1988). Hartmann et al. (1988) found that three

of the four muds they tested had 4–15 times greater filter loss at 180˚C than at 21˚C. This is equivalent to an increase in permeability of 1–2 orders of magnitude.

Effect of differential pressure

A direct mean of assessing permeability changes with pressure drop across the cake was developed by Courteille and Zurdo (1985)

$$kc = kc_0 \left(\frac{\Delta P_o}{\Delta P} \right)^{CC}, \quad \textbf{[4]}$$

where

ΔP_0 = pressure drop across the cake at reference condition,

ΔP = actual pressure drop across the cake,

kc_0 = cake permeability at reference condition,

kc = cake permeability at actual pressure drop,

cc = compressibility index (equals to zero when cake is uncompressible).

Generally speaking, bentonite, starches, modified cellulosic polymers and certain other soluble organic polymers are among a number of materials that give the cake increased compressibility (Chesser et al., 1994). In the case of bentonite, the cakes are so compressible that the exponent (cc) is zero. However, consideration of maximum borehole temperature and fluid

salinity is important when evaluating cake compressibility, as this property is also a function of the degree of flocculation in the mud. In general, highly deflocculated systems tend to show less compressibility (Chesser et al., 1994), addition of ferrochrome-lignosulfonate in increasing amounts producing less compressible cakes due to the deflocculation of bentonite (Arthur and Peden, 1988). In addition, rigid particles such as barite are less easily deformed under pressure. A cake containing a high proportion of rigid particles should itself be more rigid (less compressible; Peden et al., 1984). Arthur and Peden (1988) defined a critical value of 0.7 for the mass fraction of barite below which the concentration of barite has no effect on compressibility.

According to Outmans (1963), for an uncompressible filter cake cc = 0 and, for materials with a size distribution comparable to that of drilling clay, the exponent (cc) ranges between 0.7 and 0.8. According to Darley and Gray (1988), experiments have shown that the same exponent varies from from 0.6 to 1.0. Hassen (1980) estimated that this parameter for a typical good mud ranges from 0.6 to 0.8 and, in the worst case, is cc = 0 (uncompressible filter cake). Thus, for the normal range of pressures found during drilling operations, filtrate-cake permeability is relatively sensitive to pressure changes (Outmans, 1963, and Darley and Gray, 1988).

Cake thickness can be affected by several significant parameters, which can be categorized as rock properties (formation permeability), wellbore hydraulic conditions (shear stress on the filter cake surface), and environmental conditions of the wellbore (temperature). A review of the effect of these parameters on cake thickness is presented in the next section.

Effect of temperature on cake thickness

As pointed out by Chesser et al. (1994), down-hole temperature has a profound effect on filtration rates of drilling muds. In general, filtration rate increases during a rise in temperature due to reduction in viscosity of the base fluid (Hassen, 1980, Peden et al., 1984, Darley and Gray, 1988, and Chesser et al., 1994). Larsen (1938) proposed the following expression to consider this effect when calculating filtration rate under static fluid conditions

$$q_2 = q_1 \left[\frac{\mu_{T1}}{\mu_{T2}} \right]^{1/2} . \quad \textbf{[5]}$$

where

q_1 = filtration rate under condition 1,

q_2 = filtration rate under condition 2,

μ_{T1} = fluid viscosity at temperature 1,

μ_{T2} = fluid viscosity at temperature 2.

This expression assumes that only the change in viscosity with temperature affects fluid loss. Arthur and Peden (1988) stated that this relationship provides reasonably good estimates of fluid loss when borehole temperature is similar to standard test temperature. They attributed this to the minimal changes that will occur in cake structure due to flocculation or aging of mud components over small temperature ranges.

Effect of shear stress (annular velocity)

In practice, the evaluation of the filtration properties of a drilling fluid is based on static tests (Outmans, 1963); under dynamic conditions, however, one should expect a lower cake thickness. This can be attributed to the shear stress exerted on the filter cake by the circulating fluid (Outmans, 1963, Davidson et al., 2012). During circulation of the mud, the upper part of the cake is removed because the effective stress is extremely small in this top layer. Erosion continues to the point where the effective stress at a certain distance below the eroding surface is sufficiently large to resist the shearing action of the drilling mud (Outmans, 1963). In the case of compressible cakes, the solid pressure in the filter cake increases rapidly only in the more compacted portion, making this highly compressed layer difficult to remove from the surface (Outmans, 1963, Ershaghi and Azari, 1980, Arthur and Peden, 1988, and Cerassi et al., 2001). On the other hand, relatively uncompressible cakes will have a

more uniform, solid pressure distribution inside the cake (Figure 7). Thus, removal of this type of cake can be difficult (Arthur and Peden, 1988).

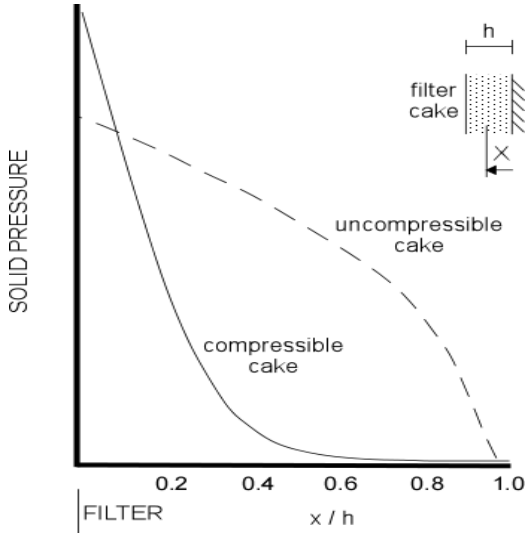

Figure 7 Solid stress distribution with cake thickness.

As mentioned previously, cake erosion will take place as long as the shear stress at the point of contact between the circulating fluid and the cake (τ_w) exceeds the yield stress of the cake (τ_{yc}). Thus, if the cake thickness is to be determined, these two parameters must be first determined. Filter-cake resistance to erosion can be calculated using the model proposed by Ravi et al. (1992), in which particles stick at the cake surface by an adhesion mechanism. Cake resistance can then be estimated using the equation developed by Potanin et al. (1991)

$$\tau_{yc} = \frac{1}{4r_c^{\,2}} \frac{H \times d_c}{12 \times l^2} \times 1.99x10^{24}, \quad \textbf{[6]}$$

where τ_{yc} is the calculated shear strength of the filter cake in lb./100 sq. ft., r_c is the average particle radius in μm, H is the Hamaker coefficient (3 x 10^{-20} joules), and l is the separation distance between particle surfaces in nm.

Shear stress (τ_w) on the filter cake will be a function of the rheological properties of the circulating fluid, the most popular models being the power-law model and the Bingham plastic model.

If the power-law model is used to calculate wall shear stress, the equation can be written as

$$\tau_w = k \times \dot{\gamma}_w^{\,n}, \quad \textbf{[7]}$$

where n, the power-law index, is a dimensionless parameter that quantifies the degree of non-Newtonian behaviour of the fluid, and k, the consistency index, is proportional to the apparent viscosity of a power-law fluid. $\dot{\gamma}_w$ is the shear rate at the wall and, for narrow concentric annuli, can be calculated using

$$\dot{\gamma}_w = \frac{6V}{(R_2 - R_1)}. \quad \textbf{[8]}$$

If the Bingham plastic model is used to calculate wall shear stress, the equation can be written as

$$\tau_w = \tau_y + PV \times \dot{\gamma}_w ,$$

[9]

where τ_y is the fluid yield stress, usually expressed in Pa, and PV is the plastic viscosity of the fluid, expressed in centipoises (cp).

2.4 Mud Removal

Effectively cementing production casing to isolate productive zones is essential to the successful completion of oil or gas wells. To meet this objective, the drilling mud and the pre-flush (if any) must be fully removed from the annulus, and the annular space must be completely filled with cement slurry (Denney et al., 2009). Once in place, the cement must harden and develop the necessary mechanical properties to maintain a hydraulic seal throughout the life of the well. Therefore, good mud removal and proper cement-slurry placement are essential to obtain well isolation. However, ensuring adequate primary cementing jobs still poses some difficult problems in many areas. The consequences of poor primary cementing jobs can be severe (Bellabarba et al., 2008). First, a continuous mud channel can form on the narrow side of the eccentric annulus. Second, residual mud or spacer can contaminate the cement as it sets. Third, mud may remain as a layer on the wellbore walls. In the first or last case, the residual mud dehydrates as the cement sets and allows a porous conduit to develop in the annulus, thereby favouring communication between subsurface zones or to surface (Fraser et al.,

1996, and Frigaard et al., 2001). In the second case, contaminated cement will possess lower strength and durability (transport) properties.

2.4.1 Mud conditioning

Drilling-fluid properties are generally tailored to clean the cutting and caving particles from the wellbore, and to provide some inhibiting properties in certain formations (Smith, 1990, Vargo et al., 2007). However, they are not necessarily conducive to efficient mud displacement. Prior to cementing, therefore, the mud must be circulated to break the mud's gel strength and to lower its yield point and plastic viscosity (Haut and Crook, 1979, and Brady et al., 1992). Reducing the mud's gel and yield strength, and its plastic viscosity is recognized as being very beneficial because its mobility is increased. It is also desirable to reduce the mud density to the minimum density limit (Zuiderwijk, 1974). The aim is usually to achieve 90% (or greater) annular volume circulation while running casing and prior to pumping cement (Smith, 1984, and Brady et al., 1992). For cementing in the case of water-based drilling fluids, the plastic viscosity is usually reduced to less than 30 cp and the yield point to 5 Pa (Smith, 1990). Table 1 lists some recommended drilling-mud properties to optimize the primary cementing job. In general, the conditioned mud should have the lowest plastic viscosity/yield point acceptable for that mud system, a flat and a low 10 s/10 min gel and a low fluid-loss value (Silva et al., 1996). Static periods after mud conditioning

and prior to the cementing job are avoided. Although oil-based muds are used on a regular basis in some areas of the world, the greatest amount of work has been with water-based muds. Thus, only their rheological properties were considered in this thesis.

Table 1 Recommended drilling-fluid properties for vertical wells (from Soter, 2003, and Silva et al., 1996).

Property	Recommended	Preferred
Yield point (lb./100 sq. ft.)	< 10	2
Plastic viscosity (cp)	< 20	15
Fluid loss (cc/30 min)	15	5
Gel strength (10 s/10 min)	Flat profile	

2.4.2 Casing centralization

Past work in controlled laboratory tests, field experience and analytical approaches have recognized the importance of centralization in improving the displacement process (McLean et al., 1967, Childer, 1968, Zuiderwijk, 1974, Martin et al., 1978, Haut and Crook, 1979, Lockyear and Hibbert, 1989, Guillot et al., 1990, 2008, and Tehrani et al., 1992). Centralizing the casing helps to create a uniform annular flow area and equalizes flow resistance, thereby improving cement placement around the casing string (Haut and Crook, 1979, and Lee et al., 1986). Conversely, in a highly eccentric situation, the cement slurry will tend to flow and displace the drilling fluid on the wide side of the annulus, where the resistance is less, and bypass the mud on the narrow side (Soter, 2003).

There are two basic types of centralizer: rigid and spring-bow (Nelson, 1990). Rigid centralizers are built with a fixed bow height and are sized to fit a specific casing or hole size. They are ideally suited to cementing in a near-gauge hole. Bow centralizers are made of two collars and a number of oversized spring-like bows attached to them that are flexible yet stiff enough to provide adequate standoff in various holes and shapes (Nelson, 1990). Bow centralizers can be used in washed-out sections. Because casings are normally reciprocated, the centralizers are allowed to float between casing collars or between stop collars (Smith, 1990).

Casing centralization is defined using the common parameter in the oil industry, casing standoff (STO). This parameter is defined by the formula

$$\mathrm{STO} = 100 \times \left[1 - \frac{\delta_T}{R_2 - R_o} \right],$$

[10]

where R_2 and R_o are the hole and casing radius respectively, and δ_T is the total casing deflection. The result of this formula is given as a percentage where 0% represents a casing in contact with the wellbore wall and 100% represents perfectly centered casing.

The recognized industry standard for casing standoff usually varies from a minimum of 67% to a maximum of 85% (Lee et al., 1986, Sauer, 1987,

Silva et al., 1996, and Kinzel and Koithan, 1997). In the field, standoffs rarely exceed 85% (Guillot et al., 1990). In a vertical hole, centralizers are routinely run one per casing joint, as well as across the intervals where zonal isolation is required (Smith, 1990).

2.4.3 Primary cementing techniques

The displacement of mud during cementing has received a considerable amount of attention during the past 75 years. As a result, cementing techniques have evolved with time. Most of the practices considered as sound today were identified in the 1940s. Recommended practices for improving displacement of mud included pipe movement during displacement, gauge holes, centralizing the casing in the borehole, mud thinning before cementing, and the use of a bottom plug to isolate the cement while it is circulated down the casing (McLean et al., 1967, and Sauer, 1987). The benefits of turbulent flow in accomplishing effective mud removal have also been known since the early 1940s (Sauer, 1987). However, practical limitations in equipment and cement slurries precluded its application at that time (Brice and Holmes, 1964). The common practice, up to the 1950s, was to have a single slurry cement to perform the function of removing the mud and to provide adequate strength characteristics opposite the pay zones.

It was not until the early 1960s that developments in primary cementing techniques made turbulent flow possible within practical limits (Sauer, 1987). As a result, the widely accepted practice of using two slurries, the lead and the tail slurries, evolved. The lead slurry is a low-density, highly dispersed cement slurry that is designed for placement in turbulent flow at a reasonable pump rate. On the other hand, the tail slurry is a high-density slurry designed to give adequate strength opposite the zones of interest (Brice and Holmes, 1964). It was also recognized during this time that pumping a fluid in turbulent flow across the zone of interest for a contact time in excess of 10 minutes would result in optimal mud removal (Brice and Holmes, 1964).

In the early 1970s, investigators started analyzing how to obtain good cement jobs in deviated holes. Best practices, such as increased centralizer placement on the casing, small solids settling on the low side of the hole, and pipe movement in the hole, were identified.

Finally, in the late 1970s and early 1980s, the industry adopted the philosophy of dealing with fluid incompatibilities of lead slurries and most muds using a cement-mud spacer fluid. This type of fluid is capable of going into turbulent flow at reasonable pump rates and still suspending the solids required to achieve a density greater than the mud (Sauer, 1987).

In order to achieve laminar displacements, the design is more sophisticated and modified fluids are often needed; however, criteria have been established to ensure optimal displacement efficiency (Fraser et al., 1996, Martin-Hayden et al., 2014). Criteria to ensure efficient turbulent flow displacement have also been developed. The remainder of this section provides an overview of the criteria established in both displacement techniques.

2.3.2.1. Effective laminar-flow criteria

Field results, together with laboratory studies, show that the effective laminar-displacement rate can be used in those cases when turbulent-flow techniques are impractical (mechanical limitations, presence of large washouts, high eccentricity, and/or concerns of breaking exposed formations -low fracture gradient- Parker et al., 1965, Brady et al., 1992, Soter, 2003, and Fraser et al., 1996). Four criteria must be met during the design of effective laminar flow (Brady et al., 1992):

- **Density hierarchy:** For better mud removal, the density of the displacing fluid must be 10% higher than the fluid displaced. This helps to maintain a flat fluid interface and breaks down the gelled mud due to gravity forces (buoyancy). When mud is displaced by a spacer, the density of the spacer must be higher than that of the drilling mud but lower than that of the cement slurry (Parker et al., 1965, Flumerfelt, 1975, Beirute and Flumerfelt, 1977, Guillot, 1990,

Lockyear et al., 1990, Nelson, 1990, Soter, 2003, and Javora et al., 2008).

- **Friction pressure hierarchy:** The design of the spacer and rheology of the cement must be such that the friction pressure generated by the displacing fluid is 20% higher than the fluid displaced. This helps to minimize fingering and maintain a flat interface (Parker et al., 1965, Flumerfelt, 1975, Beirute and Flumerfelt, 1977, and Tehrani et al., 1992). This criterion leads to minimum and maximum annular-flow rates. Laboratory testing has shown that the more viscous the cement and the less viscous the mud, the greater the percentage of mud displaced (Parker et al., 1965, McLean et al., 1967, Childers, 1968, Zuiderwijk, 1974, Tehrani et al., 1992, and Silva et al., 1996). Theoretical studies have reached the same conclusions (Flumerfelt, 1975, Beirute and Flumerfelt, 1977, Martin et al., 1978, and Guillot et al., 1990).
- **Minimum pressure gradient:** The fluid displaced must be flowing all around the annulus. In an eccentric casing, the wall-shear stress is higher on the wide side than on the narrow side. This implies that, when a fluid exhibits a yield stress the wall-shear stress on the narrow side should exceed the fluid yield stress in order to have motion all around the casing (Beirute and Flumerfelt, 1977, and Guillot et al., 1990). This criterion leads to a minimum acceptable flow rate. McLean et al. (1967) noted that optimum mud

displacement is reached when the yield strength of cement is higher than a critical value, which in turns exceeds the gel strength. Conversely, theoretical studies carried out by Beirut and Flumerfelt (1977) showed that, when the yield strength of cement is lower than that of mud, the penetrating front becomes very thin, promoting channelling.

- **Differential velocity criterion:** It is important to achieve a value of V_{narrow}/V_{avg} as close as possible to 1. In other words, the displacing fluid does not flow faster on the wide side than the displaced fluid on the narrow side of the annulus. This ensures that no mud channels are left behind (Lockyear et al., 1990).

Some well conditions and problems can limit the application of the laminar-flow technique, including free fall during cementing due to density differential and casing length; use of high-viscosity muds due to particle removal constraints; and a deep well, where the extra time needed for the laminar-pumping method of placement is not viable (Parker et al., 1965).

Turbulent-flow criteria

It is generally accepted that turbulent flow for the displacing fluid is an effective way to remove the mud from the annulus (Brice and Holmes, 1964, Clark and Carter, 1973, Haut and Crook, 1979, Guillot et al., 1990, Smith, 1990, and Soter, 2003). This can be attributed to more uniform

velocity distribution in the annulus and the erosive action of turbulent eddies (Buckingham et al., 1994).

Design centres on achieving turbulent flow all around the annulus and on the amount of contact time the fluid has with the formation (Brady et al., 1992). The contact time is defined as the period of contact between the formation and the flowing slurry. Density hierarchy is not necessary in turbulent flow, as evidenced by water efficiently displacing fluids several pounds per gallon heavier (Guillot et al., 1990). However, large density differences can reduce the efficiency of the displacement (i.e., a very thin cement slurry may be completely turbulent but unable to move a thick mud; McLean et al., 1967). Thus, rheological properties of the displacing fluid should be as close as possible to those of the displaced fluid.

Calculations of critical flow rate for turbulence are usually performed assuming a concentric casing in the annulus. However, this practice may lead to a continuous strip of mud left on the annulus. Since standoffs in the field rarely exceed 85%, displacing fluids will only be in partial turbulent flow at the calculated flow rates (Guillot et al., 1990).

2.4.4 Pre-flushes

The drilling mud and cement are incompatible under certain circumstances, resulting in the formation of a highly viscous mass at the

cement–drilling mud interface. When incompatibility exists, the cement tends to bypass through the interface, leaving channels of contaminated mud. Incompatibility is a problem especially with oil-based drilling muds, which are almost always incompatible with cements (Smith, 1984). Properties of mud and cement can be changed to a limited extent, but too large a change may adversely affect their primary function. Pre-flushes, on the other hand, can be varied greatly to help prevent potential contamination problems associated with incompatibility between drilling fluid and cement (Nelson, 1990). Pre-flushes must also remove all drilling mud from the wellbore ahead of the cement, provide fluid-loss control where applicable, and leave the annular surfaces receptive (water-wet) to enhance bonding with cement (Nelson, 1990).

There are two basic types of pre-flush:

- **Washes:** These are thin fluids with a density and viscosity very close to that of water. A wash must be compatible with the drilling fluid and the cement slurry. It removes the drilling mud by a combination of dispersion and turbulent action (Waremburg et al., 1980). The simplest form of wash is freshwater. In addition to the turbulent action and due to the low density of water, mud sloughs from the wall into the displacing fluid. This additional eroding action of water improves the removal of even high-yield-stress mud-filter cake (Haut and Crook, 1981). Another commonly used type is a chemical wash. It contains a

mixture of dispersants and surfactants that provides a more efficient thinning and dispersion of the mud (Nelson, 1990).

- **Spacers:** These are generally viscous fluids that are capable of being weighted to a high density (higher solid particle content than washes). Spacers are chemically more complicated than washes. As rule of thumb, the preferred flow regime for a spacer is turbulent flow; however, in many cases the pumping rates necessary for turbulent flow are not achievable in the field because of hydraulics limitations (pumping equipment availability, low fracture pressure gradient or oversized holes - washouts). In such cases, spacers are designed to be pumped in using laminar displacement techniques (Nelson, 1990). When pumped in turbulent flow, the viscosity should be as low as possible, to allow reasonable pumping rates but sufficiently high to effectively suspend the weighting agent (Nelson, 1990). In all cases, density and viscosity of the spacer should be selected between those of the fluid it is displacing and the fluid displacing it (Martin et al., 1978).

2.4.5 Casing movement

Extensive studies on the effect of casing movement on the displacement process have shown better mud-removal efficiencies when the casing is placed in motion (McLean et al., 1967, Childers, 1968, Clark and Carter,

1973, Landrum et al., 1985, and Arceneaux and Smith, 1986). In some cases, poor standoff and unfavourable rheological properties between the mud and the cement can even be compensated by casing movement (Childers, 1968).

There are two types of casing movement: rotation and reciprocation (Haut and Crook, 1979, Nelson, 1990, and Soter, 2003). Efficiency increase during reciprocation is related with a relative velocity increase (fluid relative to pipe) equal to the speed of the downstroke during casing movement (McLean et al., 1967, and Childers, 1968). On the other hand, rotation may provide a dragging force on the cement and pull it around to displace the mud (McLean et al., 1967).

Since rotation is much more difficult to implement in terms of obtaining swivels, rotating heads, proper centralizers, and equipment with adequate torque, drillers generally opt for casing reciprocation (Sauer, 1987, Smith, 1990, and Brady et al., 1992). Rotation is chosen over reciprocation only in those cases where seizing of the casing in the borehole is a concern (highly deviated or horizontal well) or when swab/surge pressures must be avoided (i.e., formation with a low fracture-pressure gradient; Landrum et al., 1985, and Arceneaux and Smith, 1986).

Relative velocity increase during reciprocation depends on wellbore geometry, speed of pipe movement, and casing-end conditions (Figure 8). The remainder of this section presents a detailed description of the various types of casing end.

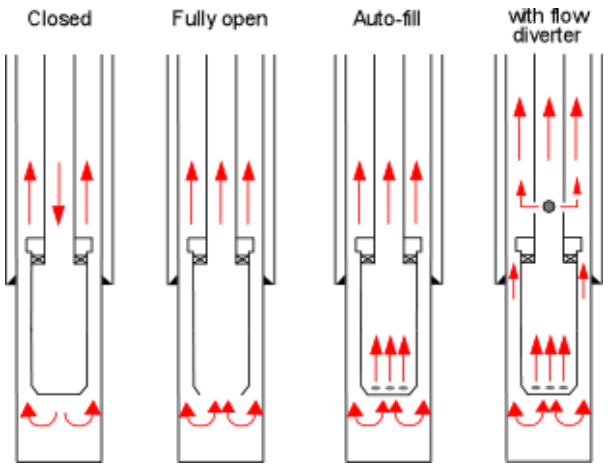

Figure 8 Casing-end conditions (from Liu, 2001).

Closed casing

As the casing is moved downward into the well, the mud is displaced by the new volume of the extended casing and the mud must move upward (Liu, 2001). Assuming the flow rate of the mud in the annulus is equal to casing displacement rate and considering velocity-profile distortion due to movement of the casing wall (Figure 9), the equivalent velocity can be calculated as

$$Ve = Vp\left[\frac{D_1^2}{D_2^2 - D_1^2} + \kappa\right],$$

[11]

where Ve and Vp are the equivalent mud and casing velocities, respectively; D_1 and D_2 are the outer casing and borehole diameters, respectively; and κ is the mud-clinging constant. This constant represents the proportion of pipe velocity that must be added to mud velocity to determine the equivalent mud velocity and is a function of flow regime and the casing diameter to borehole diameter ratio (D_2/D_1). In the field, it is a common practice to assume a clinging constant of 0.45. Although this can introduce a considerable error (Liu, 2001), it will not be significant for the common range of annular clearance found on intermediate and production sections (75–40 mm).

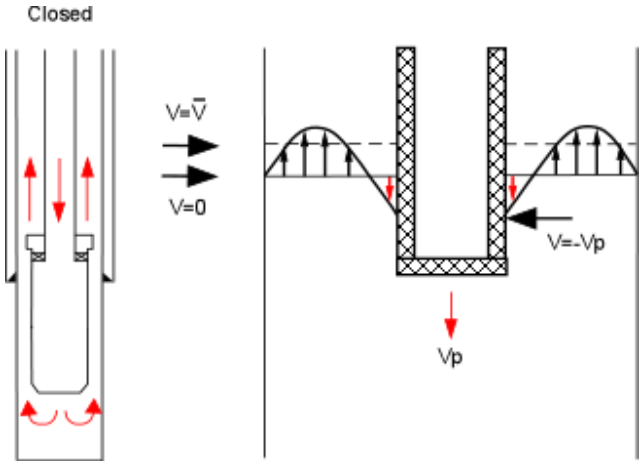

Figure 9 Mud-velocity profile during casing reciprocation for a closed casing (Liu, 2001).

Open casing

If the casing is open ended, a portion of the flow goes into the annulus and casing interior (Chambre Syndicale de la Recherche et la Production du Petrole et du Gaz Naturels, 1982). The equivalent velocity of the mud can be estimated as

$$Ve = Vp\left[\frac{D_1^2 - D^2}{D_2^2 - D_1^2 + D^2} + \kappa\right],$$

[12]

where D is the inner casing diameter.

Open casing with auto-fill

The difference between auto-fill float equipment and fully open casing is due to the additional pressure drop across the orifices on the former. The actual equivalent velocity should be between those of closed casing and fully open casing (Liu, 2001).

Casing with flow diverter

This tool, used in conjunction with auto-fill float equipment, has ports open to the casing annulus to allow the fluid trapped in the casing to escape to the larger annulus between the casing and the formation. A system equipped with this tool has two places for fluid to flow between the casing interior and the annulus: one at the bottom of the casing (the auto-fill float tool) and the other at the top (circulation sub). This device helps to reduce the equivalent velocity of the mud.

2.5 Geomechanical Damage

Geomechanical damage includes any stress-induced changes to the hydraulic-conductivity properties of materials within the wellbore system: casing, annular cement, near-wellbore formation region, and all interfaces between these components. Such changes are the result of permanent

alterations in material fabric associated with pore collapse and particle rearrangement (Dusseault and Gray, 1992, and Thallack et al., 1993).

2.5.1 Near-wellbore region

Drilling a well in a formation changes the initial stress state and causes a redistribution of stresses within the rock at the borehole wall. This redistributed stress state may exceed the strength of the formation, resulting in its failure (Nguyen et al., 2000, Chen et al., 2002, Al-Ajmi and Zimmerman, 2006). The extents of the broken zone are usually controlled by a combination of two groups of factors: uncontrollable and controllable (Zheng, 1982, Cheatham, 1984, Dusseault and Gray, 1992, Rawlings et al., 1993, McLellan and Wang, 1994, Morita and Whitebay, 1994, Jones and Barree, 1996, McLellan, 1996, Chen et al., 1998, McLellan and Hawkes, 1999, Hawkes et al., 2002, Jamshidi and Amani, 2014). The uncontrollable factors can, in turn, be divided into rock properties (rock strength and post-failure behaviour, anisotropy, bedding planes and natural fractures, permeability, porosity, stiffness, dilation) and boundary conditions (pore pressure, temperature, magnitude of vertical and horizontal in situ Earth stresses).

Controllable factors include mainly wellbore-fluid properties (circulation rate, density, rheology, fluid pressure, mud chemical composition) and mechanical conditions (hole trajectory, size and deviation; drill string

vibration; tripping speed). Controllable factors can be managed by selecting the proper method of excavation.

The causes of wellbore instability can be classified into mechanical and chemical effects (McLean and Addis, 1990a, McLean and Addis, 1990b, Sommerville and Smart, 1991, Rawlings et al., 1993, and Nguyen et al., 2000, Javaheri and Rahmannejad, 2012). Instability is often the result of a combination of both types of effect. Mechanical instability is linked to stress changes associated with the formation's response to borehole creation and usually occurs instantaneously at the time of drilling. Chemical instability refers to the interaction between the drilling mud and the formation, and occurs after a period of time (Mohiuddin et al., 2001). Mechanical effects, as well as time-dependent effects resulting from pore-fluid migration and temperature difference between the formation and the drilling fluid, are discussed in this section. Chemical interaction between wellbore fluid and the walls of the hole is considered in the 'Chemical failure' section.

Mechanical failure

As drilling progresses, pre-existing stresses are redistributed around the borehole wall (Abulhadi et al., 2011, Weijermars, 2013). This new stress field can be considered to consist of four parts: the virgin stress in the rock, the change in this stress field caused by creating the opening, the

fluid pressure inside the well, and the pressure caused by the flow of fluid towards or away from the borehole (Daemen and Fairhurst, 1970). If these induced stresses exceed the strength of the rock, it will yield and possibly detach or converge.

Mechanical failure can be tensile or compressive (Cheatham, 1984, and McLean and Addis, 1990a), and its onset will depend on the magnitude of the stresses in the immediate vicinity of the hole. Tensile failure occurs when hydraulic pressure of the mud becomes too high, causing formation stress at the borehole wall to go into tension and exceed the tensile strength of the rock (Nicolas-Lopez et., 2012). This type of fracturing generally causes lost circulation. Conversely, if the mud pressure is too low, compressive stress at the borehole wall increased until it reaches a certain critical value, at which point some pre-existing cracks start to grow and eventually cause separation from the rock mass (shale caving or hard-rock break-out). This process is known as compressive failure.

Compressive failure can be further divided into four possible mechanisms, based on whether the intermediate stress is tangential, axial or radial (Maury, 1994, and Chen et al., 1998):

- Break-out
- Toric failure
- Helical shear

- Elongated shear

The first three failure modes only consider the radial stress to be either the intermediate or the minor principal stress. These modes occur when in situ stresses are higher than internal pressure (mud pressure does not provide enough support to wellbore). Conversely, elongated shear failure occurs when the radial stress becomes the major principal stress (i.e., when the mud pressure is excessively high; Maury and Sauzay, 1987). Figure 10 depicts the different failure modes in relation to the principal stresses imposed on the material.

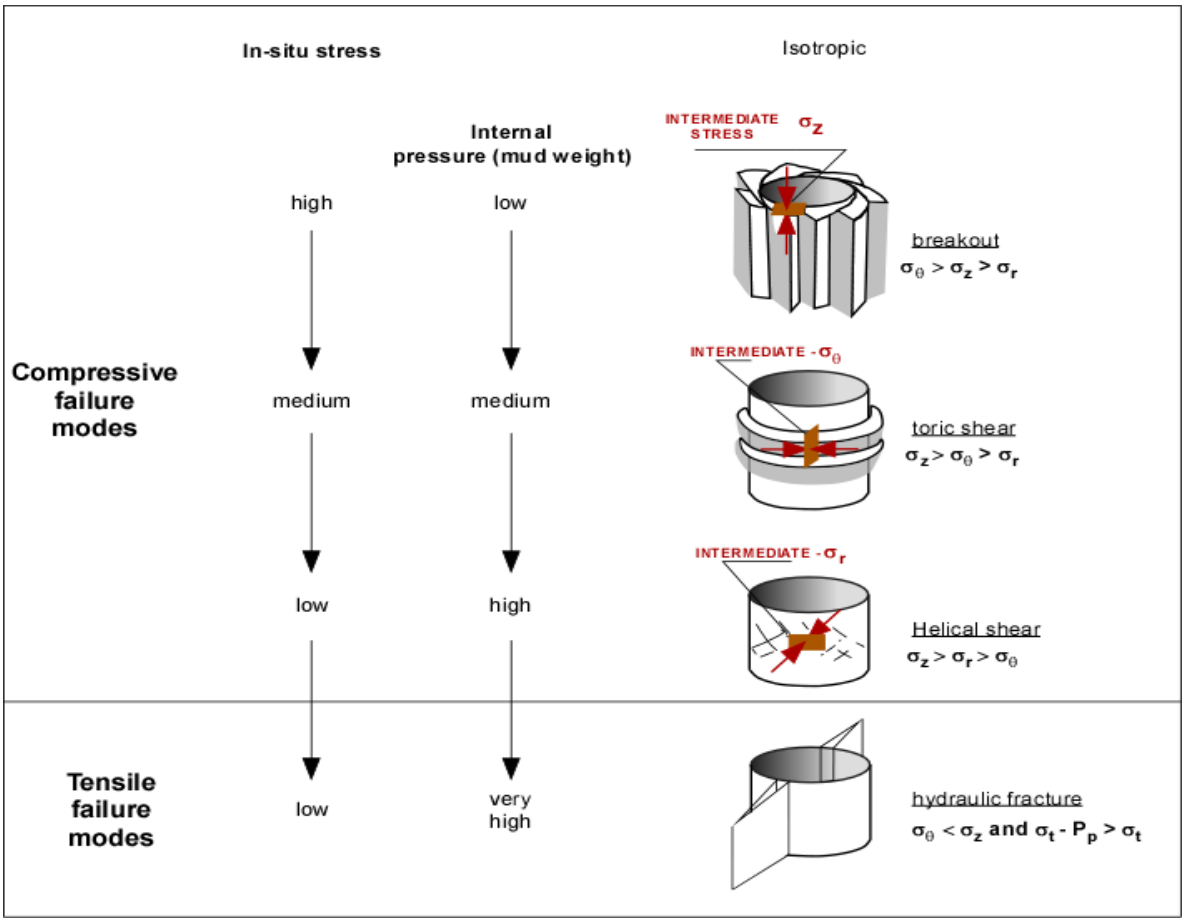

Figure 10 Types of mechanical failure mode (modified from Maury and Sauzay, 1987)

Compressional behaviour of geomaterials

Post-failure behaviour of rock is crucial to wellbore stability because it controls the extent of the damaged zone (Zhang et al., 2010). Two types of rock encountered in petroleum engineering are of interest: brittle (limestone, sandstone) and ductile (clay, chalk, cohesionless sand). The main differences between these two lie in the microscopic mechanism of their irreversible deformation (Figure 11). A rock is considered as brittle if the macroscopic failure takes place under small intensities of strain (less than 1%), with drastic reduction of elastic constants and large volumetric dilatancy (Dusseault and Gray, 1992, Shao and Khazraei, 1994, and Charlez, 1997). Rupture is due to progressive opening and propagation of existing flaws parallel to the direction of major principal stress, and subsequent coalescence of these microcracks. These rocks tend to be of low porosity and well cemented. However, a brittle rock may fail in a ductile manner under high stress or at elevated temperature (Dusseault and Gray, 1992). A detailed description of the mechanism of borehole instability due to crack propagation in brittle rocks is beyond the scope of this thesis. The reader is referred to the quantitative description of the mechanism of rock fracture near a free surface developed by Germanovich et al. (1994) and the description of physical mechanisms observed during borehole breakout by Crook et al. (2003).

		Brittle	Ductile
	Porosity	low < 30% solid matrix with randomly embedded inclusions	high > 30% granular assemblages where contact stiffness play major role
	Bond strength (cohesion)	high	low
Failure modes	Deviatoric loading	microfissuring	sliding between grains
		axial splitting sub-parallel to the bore-hole wall (extensive breaking)	fracture zones that follow trajectories of high shear (narrow band of break activity)
	Hydrostatic loading	crack closure during elastic phase	pore collapse
	Strain at failure	< 1%	1 - 10%
	Volume change at failure	dilatant	contractant

Figure 11 Modes of material behaviour

On the other hand, ductile rocks will yield only after a large plastic strain (several per cent), and failure occurs without any macroscopic rupture. From a structural viewpoint, ductile rocks are differentiated from brittle rocks by high porosity and small cohesion. Under hydrostatic loading, ductile rocks strain plastically, with an irreversible reduction of the porosity by collapse of the pore structure (purely contractional volumetric strain). Three phases can be observed during plastic collapse: an initial phase of progressive rupture of bonds, followed by pore collapse, and finally consolidation. Some ductile materials, such as cohesionless rocks, do not exhibit these three phases. Because they have no bonding between

grains, only the consolidation stage can occur. A detailed description of the plastic collapse mechanism is presented by Charlez (1997). Under deviatoric loading, these materials fail by frictional processes and plastic sliding between grains, which are very often localized into shear bands.

In each case (brittle and ductile), the strength of the rock mass, generally measured by the unconfined compressive strength (UCS), can give an estimation of its post-failure characteristics. Although, there are no definite rules for classifying the average post-peak deformation characteristics, Figure 12 can used as a starting point.

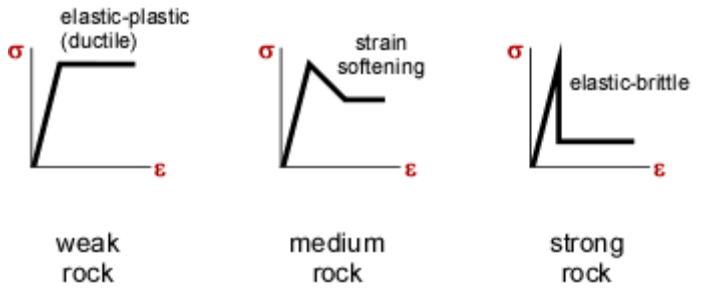

Figure 12 Post-failure behaviour for rock masses of differing competency (modified from Hoek)

Discontinuities

Drilling through some thousands of metres implies crossing various types of discontinuities (fractures, faults, bedding joints) that can be present in rock masses (Liu et al., 2013, Yan et al., 2013). Several experimental studies and numerical analyses that investigated the behaviour of fractured rock masses have shown that these rocks exhibit anisotropic behaviour under shearing loads. Strength anisotropy caused by

discontinuities is the main cause of rock failure, with collapse in most cases occurring in the form of shear failure along these planes. The effect of strength anisotropy varies with stress state, rock strength, and wall conditions (Chen et al., 1998, and Yamamoto et al., 2002, Younessi and Rasouli, 2010).

In general, the observed shear strength along the joint is weaker than that in the perpendicular direction. Thus, it is not surprising that the severity of wellbore instability also varies with joint orientation (strike and dip). Failure along discontinuities increases when the strike of the joint is parallel to the wellbore axis (i.e., less than 20° different; Labenski et al., 2003). It is maximized when the dip of the discontinuity departs from the maximum principal stress axis, and is minimized when the approaches to the minimum stress direction (Yamamoto et al., 2002).

Pore pressure

Some additional mechanisms must be considered when predicting the mechanical behaviour of porous rocks. One of the most profound modifiers of rock behaviour is pore water. Most of the voids within porous rocks are interconnected and thus subject to penetration by migrating fluids (Hawkes and McLellan, 1996, Mendoza-Amuchastegui, 2009, Li et al, 2012, Sun et al., 2013). The penetrating fluid exerts pressure on the pores, thereby reducing the effective contact pressure between grains,

which modifies the behaviour expected for a dry rock. The effect of pore-fluid pressure on rock behaviour can be predicted using the concept of effective stress (Bouteca and Gueguen, 1999). The effective stress concept (as defined by Terzaghi) postulates that the total stress within a soil or rock is shared by the soil grains (effective stress) and the water held within the pores (pore pressure). Thus, the total stress can be defined as

$$\sigma_T = \sigma' + u \qquad \textbf{[13]}$$

Where σ is the total stress, σ' the effective stress, and u the pore pressure. The magnitude and effect of pore-pressure changes will be a function of the porosity and associated permeability of the rock. In the case of rocks with high to medium porosities and permeabilities, mud invasion increases pore pressure, reducing the effective stress. Rupture can result if the induced tensile radial stress exceeds the tensile strength of the rock. Conversely, in rocks of very low permeability, loading results in an excess of pore pressure induced by deformation of the rock and high bulk modulus of the pore fluid (undrained response). This excess pore pressure reduces the confining pressure applied on the rock, which can lead to wellbore failure (Tan and Willoughby, 1993, Maury, 1994, and Chen et al., 1998).

Filter Cake

Pore-pressure effects are reduced and, in some cases, eliminated when a filter cake is formed on the wellbore walls. A mud cake prevents pore-pressure build-up in the formation and increases the amount of support pressure that is transmitted to the borehole wall (Morita and Whitebay, 1994).

The effectiveness of a mud cake (h) can be measured in terms of pressure drop at the cake (p_w - p_a) and far-field formation pressure (u) using the following equation

$$h = \frac{p_w - p_a}{p_w - u}$$

[14]

In the case of an effective filter cake, mud pressure does not penetrate the formation, resulting in the pore pressure at the wall of the wellbore (p_a) being equal to the far field pore pressure (u). Conversely, for the case of an ineffective filter cake or if there is no filter cake, the wellbore fluid will penetrate the formation and the pore pressure at the wall (p_a) is raised to wellbore fluid pressure (p_w). The value of h ranges from 0 for ineffective filter cake to 1 for a perfect one (Deily and Owens, 1969, Tan and Willoughby, 1993, Morita and Whitebay, 1994, and McLellan and Wang, 1994).

Thermal failure

Thermal effects are very seldom considered in wellbore stress analysis. Mud circulation, detachment of rock, and mud invasion can alter the temperature near the wellbore. Temperature differences between the mud and the wall of the borehole of 25°C are common when drilling at depths of 2000–3000 m, and can reach 60°–70°C in deeper holes. A temperature difference of this order of magnitude can induce stresses of several tens of megapascals, according to the thermal expansion of the rock. This radially varying thermal-stress field around the borehole disturbs the pre-existing equilibrium conditions and can eventually lead to wellbore failure (Maury, 1994, Brudy and Zoback, 1999, Khurshid et al., 2013).

The bottom-hole mud is generally cooler than the formation, whereas top-hole mud is warmer than formation (Tang and Luo, 1998). The redistribution of stresses at the borehole wall, observed from the heating effect of the circulation of hot mud, is fundamentally different from those induced when the circulated mud is colder than the initial temperature of the rock. Consequently, the geomechanical consequences in terms of wellbore stability are significantly different. A rise in wellbore temperature results in an increase in tangential stress, increasing the possibility of shearing; conversely, tensile tangential stress is generated by a temperature decrease, promoting hydraulic fracturing. Whereas heating of the formation reduces wellbore stability, a temperature decreases tends

to increase stability (Maury and Sauzay, 1987, Dusseault and Gray, 1992, Tang and Luo, 1998, Choi and Tan, 1998, Gelet et al., 2012).

In addition to purely mechanical effects, temperature also affects the pore-pressure magnitude, particularly under the undrained conditions associated with low-permeability rocks. Heating by 50°C corresponds to pore pressure of approximately 10 MPa (Roegiers, 2002). Thus, thermal effects deserve greater attention in stress analysis (Maury and Sauzay, 1987, Maury, 1994, and Tang and Luo, 1998).

Chemical failure

Shales account for more than 75% of the formations drilled and are responsible for about 80–90% of drilling problems (Santarelli, 1992, VanOort et al., 1996, and Manohar, 1999, Qiang et al., 2010, Wang et al., 2014), with lost-time and trouble costs for the drilling industry conservatively estimated at $500 million/year (VanOort et al., 1996). These problems can be related to mechanical and chemical instabilities. This section describes the chemical factors affecting borehole stability. Chemical instability is the result of shale sensitivity to certain drilling constituents, particularly water, a complicating factor that distinguishes it from other rocks (Manohar, 1999, Whitteveen et al., 2013). The chemical-instability problem is time dependent, unlike mechanical instability that

occurs as soon as the well is drilled. As drilling fluid contacts the shale formation, the resulting interactions can be categorized as follows:

- **Osmosis:** This an induced hydraulic pressure resulting from a chemical-potential differential between the drilling fluid and shale native pore fluid (Al-Bazali et al., 2011, Roshan and Rahman, 2013). This pressure (osmotic) can be given by

$$\Delta Pm = \frac{RT}{V} \ln\left(\frac{a_{sh}}{a_{df}}\right) \times \sigma ,$$

[15]

where V represents the partial molar volume of water, R is the gas constant, T is temperature, and a_{sh} and a_{df} denote activity of the shale pore fluid and the drilling fluid, respectively. This disturbance will propagate through the shale like any other pore-pressure disturbance, with the same consequences (fluid flow). Flow (into or out of the shale) will proceed from the fluid containing the lower concentration (high activity) of solute into the fluid of higher solute concentration (low activity; Zeynaly-Andabily et al., 1996).

Due to a combination of fine pore sizes and the negative charge of clay on pore surfaces, the shale behaves as a semipermeable membrane: it is permeable to the solvent (uncharged water) but not to the solute (cations and anions in the mud filtrate). An ideal semipermeable

membrane is characterized by a 100% efficiency, which means that all solute is reflected by the membrane and only water can pass (VanOort et al., 1996). In non-ideal (leaky) membranes, typical of most shales, solutes can cross the membrane because it has a range of pore sizes, including wide pore throats that constitute preferential flow paths. The solutes transferred across the membrane system will reduce membrane efficiency and create a chemical-potential difference between the drilling fluid and the shale native pore fluid (Zeynaly-Andabily et al., 1996, Tan et al., 1998, and Tan et al., 2002). This ultimately means that the hydrostatic pressure generated by osmosis is different than that predicted by equation [15]. No osmosis will occur in high-permeability shales ($\sigma = 0$). Most of these systems have dual permeability, with microfractures that result in significant permeability to solutes and therefore bypass the selective shale matrix (VanOort et al., 1996, and Tan et al., 1998).

Osmotic induced instability can be managed by selection of the proper mud formulation. Various additives to control excess pore pressure have been proposed to solve this problem. They can be categorized into three types based on their capability to increase membrane efficiency: inhibitive, plugging, and high capillary entry (Carminati et al., 2000, and Schlemmer et al., 2002). Inhibitive additives work by lowering the activity of the drilling fluid, thus inhibiting the diffusion of

solute through the pores. This inhibition contributes to a membrane effect by increasing efficiency. For inhibitive additives, drilling-fluid and pore-fluid chemistry, as well as filtrate viscosity and clay type, all contribute to the improvement of membrane efficiency. Unlike inhibitive additives, plugging additives depend not on chemical interactions but on the precipitation of a relatively impermeable layer onto the shale matrix. Silicate-based and some aluminum-based fluids are examples of typical plugging additives. High-capillary-entry additives are associated with invert emulsion-based drilling fluids and do not depend on a deposited or precipitated solid film (Schlemmer et al., 2002). These fluids act through the capillary entry mechanism, which prevents them from invading the shale.

In addition to the initial osmotic effect, the slope of the pressure-development curve will gradually change over time or not change at all, depending on the type of membrane that is formed. Generally, one can expect 1) the slope of an inhibited membrane to become negative after a period of equilibration, 2) a zero slope and constant osmotic pressure with a plugging membrane, and 3) a positive slope of increasing pressure with a high-capillary-entry membrane (Schlemmer et al., 2002, and Schlemmer et al., 2003). A rising osmotic pressure indicates improving membrane efficiency.

- **Swelling:** This is a direct result of the increase in interparticle spacing between clay particles because of an increase in moisture content and a change in pore-fluid properties (Fam and Dusseault, 1998, and Civan, 2000, Al-Bazali, 2011, Roshan and Fahad, 2012).

  The swelling potential of shale depends on the type of layered structure in the clay minerals (Fam and Dusseault, 1998, and Civan, 2000). Clay minerals can be classified into three main groups: kaolinite, illite, and montmorillonite. Kaolinite is a two-layered mineral with K^+ as the exchange cation. Kaolinitic shale is generally considered non-swelling. Illite is a low-expanding layered mineral with the interlayer space being occupied mainly by poorly hydrated K^+ ions. Montmorillonite is a very soft mineral with a three-layered structure and a high–base-exchange capacity, all of which results in a degree of swelling that is considerably greater than the other clays.

  The amount of expansion also depends on the type and amount of exchangeable cations contained in the rock. For example, the presence of Na^+ as the predominant exchangeable cation in montmorillonite can result in swelling several times greater than Ca-montmorillonite. This can be attributed to Ca^{++} being bonded to the clay surface more strongly than Na^+ (Civan, 2000). Based on their replaceability, the most common cations in clays can be ordered, from

most to least easily bonded, as $Li^+ > Na^+ > K^+ > Rb^+ > Cs^+ > Mg^{++} > Ca^{++} > Sr^{++} > Ba^{++} > H^+$ (Civan, 2000).

The swelling potential of shale can be evaluated using laboratory methods; however, they are quite costly because elaborate test procedures are required (Cokca, 2002, and Chiappone et al., 2004). Therefore, simple indirect techniques have been developed to meet the need for faster and cheaper methods for the characterization of shale. One of these techniques is the methylene-blue test, a standard technique in the oil industry. This test determines the ionic absorption potential of shale by measuring the amount of methylene-blue dye solution absorbed by a sample. The amount is usually measured by determining with a colorimeter the amount remaining in solution. The measured ionic absorption depends on the surface area of the clay particle, which is a function of clay type, and an indicator of the percentage for water absorption. Thus, testing with methylene blue can be considered to give a measure of the swelling potential of shale when hydrated. The methylene-blue test is usually reported in meq/100 g and is called the cation exchange capacity (CEC). The value of the CEC varies considerably with clay-mineral type, as shown in Table 2. Clay such as montmorillonite, which has a high cation-exchange capacity, swells considerably; in contrast, clay with a low exchange capacity (e.g., kaolinite) will be relatively inert.

Table 2 Cation-exchange capacities of clay minerals

Mineral	CEC (meq/100g)
Kaolinite	3 - 15
Illite	10 - 40
Montmorillonite	70 - 130

Two swelling mechanisms can be observed in shale: crystalline and osmotic. Crystalline swelling occurs when clay is exposed to concentrated brine or aqueous solutions containing similar cationic load from divalent or multivalent ions. Osmotic swelling is the increase in volume caused by exposure of clay to dilute solutions (Manohar, 1999, and Civan, 2000). Volume changes resulting from crystalline swelling are relatively small. Osmotic swelling, on the other hand, can be very large, usually exceeding several times its original volume. It should be noted that the osmosis discussed earlier is associated with water migration between the drilling fluid and the pore water, whereas osmotic swelling is directly related to water migration between pore water and clay surfaces.

Since shale hydration is the main cause of swelling, considerable effort is devoted to controlling it (Erkekol et al., 2006, Friedheim et al., 2011). The introduction of inhibitive additives was the first attempt to do so.

Since then, numerous types of formulation have been designed, oil muds with concentrated brines as the internal phase being the most successful at preventing hydration (Darley and Gray, 1988). The interaction of drilling fluids with shale can be categorized, in terms of increasing ability to control shale-swelling, as Type I, II or III (modified from Van Oort, 2003).

Type I: non-dispersed, dispersed water-base muds (WBM)

This is the least effective fluid for shale-swelling control. Over time, pore and swelling pressures will increase at the wellbore wall, resulting in the progressive enlargement of wellbores. Lignite, lignosulfonate and freshwater muds are probably the best-known examples of this type of fluid.

Type II: inhibited WBM

This has been for decades the standard oil-field solution to shale-swelling problems. Inhibited muds control swelling by reduction of drilling-fluid activity or by cation exchange. Lowering the activity of the water, by adding soluble salts, stimulates osmotic backflow of shale pore water towards the wellbore, hence reducing shale hydration. Nevertheless, maintaining a balanced water activity of shale with mud everywhere in a well is not a practical proposition, as shale activity is not known and varies with depth and mineralogy. Cation exchange, on

the other hand, can usually provide an adequate degree of shale-swelling control, usually by replacing less inhibitive, more hydrated ions at the clay surface with K^+ ions. The K^+ ion is more effective because of its low hydration energy and its small size, which enables it to better fit in the clay crystal lattice, hence reducing interlayer swelling (Van Oort, 2003).

The number of commercial shale inhibitors is impressive; thus, rather than discussing each of them individually, they are grouped by type:

- Salts, probably the best known inhibitors in this group, are potassium chloride (KCl) and sodium chloride (NaCl). They derive their effectiveness from cation exchange and high osmotic pressure, respectively. Other common inhibitors are calcium/magnesium/zinc chloride/bromide ($CaCl_2$, $CaBr_2$, $ZnCl_2$, $MgCl_2$, $MgBr_2$, $ZnBr_2$), and formate and acetate salts. Two factors make them suitable for shale drilling: they generate very large osmotic pressures, and they have elevated filtrate viscosities (Van Oort, 2003).
- Polymers with special shale affinity are multivalent functional groups that can attach onto the clay surface at multiple sites. These fluids have been developed as alternatives to KCl, which can only exchange K^+ ions at single clay sites. The inhibitive

action of KCl also applies, to a large extent, to these polymers (Van Oort, 2003).

- Sugar and sugar derivatives are low-molecular-weight viscosifiers that have the advantage of lowering water activity and therefore generate osmotic pressure. These systems are sensitive to biological degradation, which makes preservation of the mud difficult. Most of these problems are solved by the use of methyl glucoside, a system less vulnerable to attack by biological organisms (Van Oort, 2003)

Type III: non-invading WBM/oil-base muds (OBM)

This is a solution that neatly sidesteps the physicochemical-force complications. Mud invasion and associated swelling are prevented by reducing the permeability of the shale (e.g., by forming a permeability barrier at the shale's surface or within microfractures; Van Oort, 2003). These drilling fluids act through two mechanisms that prevent them from invading shales: pore plugging and high-capillary-entry pressure. Pore-plugging works by depositing a relatively impermeable precipitate external to the shale matrix; this type of fluid system is typical of silicate- and glycol (TAME)–based muds. High-capillary-entry fluids are associated with all-oil–synthetic systems, in which invasion is restricted by high-capillary-entry pressure (Van Oort, 2003, and Schlemmer, 2002).

2.5.2 Annular cement

Annular oil-well cement can be damaged by mechanical or thermal loading. An abrupt change in the casing temperature or a variation in the internal casing pressure can induce cracking of the cement sheath (Ferla et al., 2009, Yuan et al., 2013, Ardakani and Ulm, 2014).

Brittleness of cement has been noted by several authors (Tasdemir and Karihaloo, 2000, Tandon and Faber, 1999, and Li and Maalej, 1996). It is generally accepted that every material has a certain amount of imperfections that, according to Griffith theory, act as crack initiators. In a hardened cement paste, such defects stem from imperfections in the mixing process, whereby large air bubbles and packing defects are introduced into the mixture (Li and Maalej, 1996, Ridha et al., 2013). However, these crack-like pores contribute only about 10% to the total volume fraction of pores. Hence, they do not affect toughness or modulus, which are known to be a function of the gel to pore space ratio, but affect fracture initiation (Li and Maalej, 1996). The relationship between bond force and interatomic spacing indicates that the interatomic bond (cohesion) must be stretched to cause fracture. Thus, for tensile fracture to occur under compressive loads, a local tensile stress is required to break interatomic bonds in the material (Wang and Shrive, 1995).

Crack observations done on rocks are consistent enough to suggest that fracture mechanisms on cement can be described by the ones observed in rocks. There are many models of crack formation, but they belong to two main categories (Hoxha and Homand, 2000): continuum damage and micromechanical damage modelling. Although continuum mechanics is able to describe any changes in stress state, it has difficulty in describing cracking in detailed terms (i.e., crack density, crack width, etc.). In contrast, micromechanical models generally provide a clear physical meaning of their hypothesis and variables (Hoxha and Homand, 2000). In terms of wellbore and cement-stability evaluation, continuum-damage models are able supply the information needed at a low cost in terms of computer resources. A thorough description of typical models for brittle failure in compression can be found in Wang and Shrive (1995).

Crack-evolution mechanisms have been studied by microscopic cracking or by sonic-activity measurements (Martin et al, 1994). These workers observed that an increase in crack level is closely related to the level of the deviatoric stress and a general tendency for the cracks to align in the direction of the major compressive strength. It is widely recognized that a brittle material undergoing a compression triaxial test goes through different phases (Bieniaski, 1967). A first stage, in which any existing microfissures are closed, is followed by the development of small cracks, which are tensile and originated at those points were local stresses are

amplified and thus overcame the local tensile strength. As the loading increases, the rate of crack evolution increases, following the direction of the maximal compressive stress. As stress approaches the level at which failure occurs, crack density reaches at a level at which individual cracks begin to coalesce and crack propagation is no longer stable (Martin et al., 1994, Bieniaski, 1967). Thus, the dominant mechanism of brittle fracture in compression is basically Mode I cracking, the same as in tension (Wang and Shrive, 1995).

Apparent shear displacement sometimes occurs after vertical cracking parallel to the direction of uniaxial compressive load has taken place. This postcracking effect can be misleading. As noted by Wang and Shrive (1995), longitudinal splitting is common if steps are taken to eliminate friction between loading platens and specimen; Picandet et al. (2001) reached the same conclusion. In compact tension tests done on cement pastes, Tandon and Faber (1999) concluded that fracture toughness is independent of loading rate. This is contrary to the findings in the same testing on concrete and mortar samples, where shielding processes during fracture increases the toughness. This mechanism derives from the presence of sand and aggregate particles, where microcracks developed ahead of the crack tip lower the effective elastic modulus of the undamaged material. This generally results in a reduction in the crack-tip

stress-intensity factor, so the material appears to be tougher than the original undamaged material (Li and Maalej, 1996).

In fractured cement, the opening, the length, and the connectivity of the cracks become important and lead to an increase in the longitudinal permeability (Burloin et al., 2003). However, high confining pressures lead to a partial closure of microcracks, thus decreasing permeability. Conversely, the beneficial effect of a confining pressure has been reported to be low when there is no significant presence of cracks (Burloin et al., 2003).

2.5.3 Wellbore Interfaces

Flow paths for migration can be created when the bond between the casing and the cement, or between the cement and the formation, is broken (Zou and Wojtanowicz, 2009, Newell and Carey, 2013). One common source of bonding failure is the development of mud-cake layers stuck to the inner and outer walls of the annulus during the drilling process. Two major problems result from the existence of mud cake in finished wellbores. First, if this cake is not removed prior to cementing, the bond between the cement and the formation may not develop. This zone of weakness can result in development of a micro-annulus that will allow gas to migrate to the surface or to other zones (Bourgoyne et al., 2000). Second, the residual cake degrades with time and allows a porous

conduit to develop in the annulus (Frigaard et al., 2001). Several studies have recognized that a mud cake is difficult to completely remove, despite the use of chemical washes, spacers and mechanical scrapers (Ravi et al., 1992, Haberman et al., 1992, Dacord and Baret, 1994, Dillenbeck and Simpson, 1999, and Ladva et al., 2004).

Cement hydration during the setting process can also affect the quality of the cement's bond with the annular interfaces. Hydration of cement is an exothermic process connected with a reduction in slurry volume (shrinkage). During this period, while the paste is undergoing autogenous shrinkage, external interfaces provide an active restraint to the system that resists this deformation and reduces the measured physical shrinkage. However, when stresses generated at these boundaries are high enough to overcome the tensile strength of the interface, debonding of the surfaces occurs. Such debonding can cause problems, such as wellbore microannuli and fluid migration (Bentz et al., 2001).

Finally, even a flawless primary cementing job can be damaged by different types of operations occurring after the cement has set (Lecampion et al., 2013). This damage can result in formation of a micro-annulus that will allow gas flow to the surface or to other zones.

- First, weakening of the casing-cement bond can occur through tripping drill collars, stabilizers and other equipment because of the mechanical impacts generated during tubular travelling.
- Second, dramatic and sudden changes in pressure can lead to expansion of the casing and cement sheath. When the pressure inside the casing is released, the cement may not fully recover, resulting in separation of the casing from the cement (Bourgoyne et al., 2000). Transient increases in the internal casing pressure can occur as a result of common completion activities (e.g., casing-pressure tests routinely conducted to confirm the competency of each string). Pressure tests are also performed prior to perforating and fracturing, and after setting packers or bridge plugs. High pressures are also experienced during acidifying, fracturing, and cementing operations.
- Third, a micro-annulus can be created by the radial displacement of the casing as a result of temperature or/and pressure reduction common during completion and production operations. Cool fluid injection, underbalanced perforation, reduction in reservoir pressure due to depletion, or change in mud weight once the cement has set are all good examples of casing contraction (Nelson, 1990, Dusseault and Gray, 1992, Baumgarte et al., 1999, and Bourgoyne et al., 2000).

2.6 Deterioration Damage (Aging)

In the case of a perfect seal, the cement grouting, as a porous material with extremely low porosity and permeability, allows the transfer of fluids from the reservoir at an extremely low rate. However, as cement degrades over time, usually from chemical alteration, its transport properties are enhanced, thus altering its sealing quality. Typical chemical-alteration mechanisms of cement include carbonation, sulphate attack, and acid attack and leaching. The effect of each of these mechanisms on the transport properties of cement will vary. Whereas acid attack and carbonation modify cement permeability by increasing its porosity, sulphate attack changes its permeability through cracking.

2.6.1 Carbonation

It is known that carbonation affects the microstructure of cement, both its porosity-permeability and its compressive strength (Carey et al., 2007, Carey et al., 2010, Liteanu and Spiers, 2011, Xu et al., 2011, Nasvi et al., 2013, Wolterbeek et al., 2013, Verba et al., 2014). The CO_2 reactivity of cement is characterized not only by its chemical composition, but also by the properties of the CO_2 medium itself (i.e., partial pressure, temperature and relative humidity; Onan, 1984). It is known that, although the ultimate effect of carbonation is dependent on the chemical nature of the cement hydration products, the actual rate of carbonation is influenced more by porosity and water content of the exposed cement surface (Walsh et al., 2013). Some water is necessary to initiate a reaction, but excessive

moisture restricts the carbonation reaction due to the ample blockage of the sample pores.

2.6.2 Sulphate attack

Sulphates transported into the cement from the environment can result in cracking and scaling of the cement surface, thus changing the permeability properties of the cement. Expansion caused by ettringite formation is the mechanism of sulphate attack most widely recognized in the literature. However, loss of adhesion and strength from decomposition of dominant phases in hydrated Portland cement (i.e., calcium hydroxide [CH] and calcium silicate hydrates [C-S-H] gel) should also be considered an integral part of the sulphate attack (Wang, 1994).

Two types of sulphate can attack cement: sodium and magnesium sulphate (Santhanam et al., 2003). Attack by sodium sulphate (Na_2SO_4) can be divided into five characteristic stages:

1) the cementitious specimen comes into contact with the Na_2SO_4 solution, which usually has a pH of 6–8;
2) gypsum and ettringite start forming close to the surface of the cement, and the expansion rate increases;

3) the unaltered zone tries to resist this expansion by generating an opposing force; when tensile stress is high enough, cracks begin to form in the interior of the cement;

4) when the solution reaches these cracks, it reacts with the hydration products and deposits inside them; and

5) as more reaction products are generated, tensile stress is again generated inside the unaltered cement and a new cycle of cracking begins.

Attack by magnesium sulphate ($MgSO_4$) can be divided into four typical stages:

1) the cementitious specimen comes into contact with the $MgSO_4$ solution, which has a pH of 7–8;

2) a layer of brucite (magnesium hydroxide, $Mg(OH)_2$) rapidly forms on the surface due to the reaction of calcium hydroxide ($Ca(OH)_2$, abbreviated as CH) with the solution; at the same time, a layer of gypsum forms inside the brucite layer; due to the impervious nature of brucite, further sulphate penetration is possible only by diffusion; when the solution reaches the sound cement, gypsum and ettringite start forming, thus leading to an expansion;

3) as the cement tries to expand, the unaltered zone will try to resist this expansion by generating an opposing force; when tensile stress is high enough, cracks begin to form in the interior; and

4) when the brucite layer breaks due to expansion of the cement, flow channels are established and a direct attack of the C-S-H can occur; the C-S-H reaction produces M-S-H and, as a consequence, strength and integrity will be lost.

In an attempt to limit the effect of sulphate attack on cement, the C_3A content has been adjusted according to the degree of sulphate exposure. However, cement composition will not ensure sulphate resistance; thus, ion ingress should be minimized by decreasing the permeability (by altering the water to cement [w/c] ratio). Permeability is considered the key to the durability of cement in various aggressive environments, since the sulphate ions must first diffuse into the concrete and subsequently react with the cement portion of the concrete. The physical resistance of the cement can be related to its permeability, and the chemical resistance of the cement is dependent on the type of binder (Khatri et al., 1997). For moderate conditions (up to 1 500 mg/l sulphate in water), type II Portland cement (less than 8% C_3A) can perform satisfactorily if the w/c ratio is below 0.50. In severe conditions (1 500–10 000 mg/l sulphate in water), a type V cement and w/c ratio below 0.45 are recommended. For very

severe attack (greater than 10 000 mg/l in water), type V cement plus a pozzolanic admixture should be used, with a w/c ratio less than 0.45.

Researchers have attempted to study the effects of sulphate attack using diffusion-based models. However, the rates of damage associated with sulphate attack defy the predictions made from such models (Santhanam et al., 2003). In an initial appraisal of the likely alteration of structural concrete in a repository situated below the water table in the United Kingdom it was concluded that, in many potential repository locations, reaction with sulphate in the local groundwater is the process that will most probably lead to eventual loss of the concrete's mechanical integrity. The following empirical expression was derived (Atkinson and Hearne, 1990) from a survey of results from accelerated tests and long-term field experiments

$$R(\mathrm{mm\,y^{-1}}) = 5.5 C_A(\%) c_0(\mathrm{M}), \quad \textbf{[16]}$$

where R is the degradation rate, C_A is the tri-calcium aluminate content of the cement and c_0 is the sum of the concentrations of sulphate and magnesium ions in the groundwater. However, as noted by Atkinson and Hearne (1990), this approximation cannot be used to calculate degradation rates over periods longer than 40 years. Additionally, rates seem to be underestimated when the tri-calcium aluminate content of the cement is low. This is because the assumption that only C_3A contributes to

the expansion reaction is incorrect, as demonstrated in the experiments reported by Atkinson and Hearne (1990). Several other authors (Kurtis et al., 2000, and Cao et al., 1997) have reached the same conclusion.

In a later study, Atkinson and Hearne (1990) incorporated expansion data from sulphate-attack experiments into a mechanistic model for sulphate degradation in which the criterion for disruption was the accumulation of a critical amount of stored elastic energy in the reaction zone. This energy comes from the constrained expansion of the reacted zone due to the existence of an unreacted zone. It is this stress that eventually leads to mechanical rupture and loss of the reaction zone by spalling at some critical condition (Atkinson and Hearne, 1990). After spalling, a new reaction zone builds up and the cycle repeats itself. The degradation rate can be given by

$$R(mmy^{-1}) = \left(\frac{E\beta^2 c_0 C_E D_i}{\alpha\gamma(1-\upsilon)} \right)$$

[17]

The work of Atkinson and Hearne (1990) has been the basis for various sulphate-attack models to predict the service life of concrete structures exposed to sulphate attack (e.g., CONCLIFE software developed at the National Institute of Standards and Technology).

Kurtis et al. (2000) proposed a model based on an extensive database of experimental results. They performed a statistical analysis of expansion data collected from a long-term experiment and developed a model that could predict the damage (in terms of expansion) due to sulphate attack based on the chemistry (C_3A content) and the characteristics of the mixture. These test data are important because no comprehensive database has yet been compiled for cement exposed to typical field concentrations of sulphate over such a long period with such a wide variety of mixture parameters (Kurtis et al., 2000). Because of the disparity in the performance between samples produced from cements with low (<8%) and high (>10%) C_3A contents, two models were proposed and derived from the analysis of the testing data (Kurtis et al., 2000). However, due to the low C_3A content of typical oil-well cement, only the equation applicable to C_3A contents less than 8% is of interest here

$$EXP = 0.0246 + 0.0180(T * w/c) + 0.00016(T * C_3A), \quad \textbf{[18]}$$

where expansion (EXP) is expressed as a percentage, C_3A content of the cement is expressed as a percentage, w/c is the water to cement ratio, and T is time in years. Nevertheless, according to these investigators, this model should be considered valid for w/c values in the range 0.37–0.71 and for severe sulphate exposure over periods of up to 40 years.

2.6.3 Acid attack and leaching

During the lifetime of the well, cement is subjected to the risk of water intrusion, which can lead to leaching of the calcium solid matrix (Matteo and Scherer, 2012). Although the kinetics of leaching is very slow, it can be a risk over the long term. Thus, leaching of cement by water should be considered among the possible degradation scenarios for cement (Kamali et al., 2003, and Heukamp et al., 2003).

Leaching mechanisms

Calcium leaching occurs when cementitious materials, which are stable at approximately pH 13, are exposed to water with calcium concentrations below the equilibrium concentration. Leaching occurs as a coupled diffusion-dissolution process involving sharp dissolution fronts that propagate through the cement structure. The diffusion-dissolution transport process of the species in the interstitial solution can be attributed to the gradient present in the solution between the surface and the core of the cement. This concentration gradient is created when the interstitial solution contained in the porous structure of a cement paste, which is highly charged with alkaline Na^+ and K^+ ions in particular, as well as OH^- and Ca^{2+} ions, comes in contact with an aqueous solution of low mineral content (Faucon et al., 1998). On the other hand, the sharp dissolution fronts are due to the locally quasi-instantaneous dissolution. In other words, when the diffusion kinetics is slower than the kinetics of reaction inside the paste, it can be considered that the dissolution occurs almost

instantaneously. The time of the leaching process is governed by the diffusion properties of the material and will obey a square root of time law (Kamali et al., 2003, Heukamp et al., 2001, Eijk and Brouwers, 1998, Faucon et al., 1998, and Revertegat et al., 1992).

Calcium leaching of cement-based materials produces a new material composed of C-S-H with low calcium/silicate (C/S) ratio (approximately 1) and an extremely porous material generated by the dissolution of Portlandite (CH) crystals. Portlandite (CH) is dissolved first, followed by C-S-H decalcification; this creates a new pore-size family, with microporosity for the former and macroporosity for the latter (Carde and Francois, 1999, and Revertegat et al., 1992). The visible pore-size range in the leached cement-paste matrix will vary from 0.1 to 10 μm. The lower value is comparable to the typical pore size of macropores (0.1 μm) in intact cementitious materials at the same w/c ratio. The higher value corresponds approximately to the typical size of calcium hydroxide clusters in intact cementitious materials (Heukamp et al., 2003).

Total leaching of the calcium hydroxide will lead to a porosity increase of about 13%, whereas the increase due to the decalcification of the C-S-H is 8% (Carde and Francois, 1999).

Effect of w/c ratio on Ca leaching

The kinetics of diffusion-dissolution mechanisms during leaching is closely related to the characteristics of the material and environmental conditions. The kinetics of leaching increases with the ionic diffusivity through the material, which is known to increase with the w/c ratio (Slamecka and Skvara, 2002, Garboczi and Bentz, 1999, and Beaudoin et al., 1994).

Effect of pH on Ca leaching

It is widely recognized that the pH of the pore solution of traditional cement-based materials is about 13 (Kamali et al., 2003, Cao et al., 1997, Khatri et al., 1997, and Revertegat et al., 1992). Because of the highly basic nature of the pore solution of the cement, acids and even neutral groundwater can substantially lower the pH of the pore solution. This leads to the progressive dissolution of calcium from two distinct sources: calcium hydroxide and calcium silicate hydrates (C-S-H) from the cement-paste matrix (Revertegat et al., 1992). Calcium hydroxide (CH) is the first to be destabilized at pH 11.5, followed by C-S-H decalcification. Once dissolved, these species will generally diffuse from the interior of the cement toward the exposed surface. The lower the pH of the aggressive water and the higher the concentration gradient, the more significant the leaching will be, due to faster transfer kinetics (Revertegat et al., 1992).

Temperature effect on Ca leaching

The rule that temperature accelerates diffusion and dissolution kinetics is often true but cannot be generalized. Calcium hydroxide (CH) belongs to the group of rare compounds whose solubility decreases with increasing temperature (Kamali et al., 2003). However, the effect of temperature on leaching kinetics has not been extensively studied. For instance, Kamali et al. (2003) showed that the higher the temperature, the higher the leaching kinetics.

Leached permeability

Few test data are available in the literature on the properties of leached cement. Given this restriction, these properties must generally be estimated. This is usually done through models that relate porosity and permeability. Studies of cement-paste permeability have indicated the existence of this relationship (Powers et al., 1955), but its rational quantification has been rather difficult due to the fact it is influenced by parameters such as pore size, pore shape, and the tortuosity of the pores. In spite of this difficulty, a number of empirical and numerical models have been built.

Research on this subject started as early as 1955, when the first model was presented by Powers et al. (1955). Based on the results of experiments on the permeability to water of cement paste, they proposed a power-law relationship between permeability and porosity.

Then, in 1986, Katz and Thompson developed a model to relate permeability to pore structure of cementitious materials. This equation is expressed as

$$kd = \frac{1}{226} l_c^{\,2} * 0.18 * (n - n_c)^2,$$

[19]

where l_c is the critical pore diameter of the cementitious material, defined as the diameter of the pore that completes the first connected pore pathway; and n_c is the critical value of capillary porosity for percolation (Garboczi and Bentz, 1998).

Finally, in the 1990s, permeability versus porosity models were reinvestigated, resulting in two notable improvements. The first was presented by Lerman in 1998. He performed theoretical studies with channel networks of different geometries. This work resulted in an equation where permeability is modelled as a function of the pore size rather than only porosity (n)

$$kd = \frac{n^3}{(1-n)^2} \frac{(d/2)^2}{45}$$

[20]

The second notable improvement was provided by Udegbunam et al. (1999). In order to develop a simple model, the open pores in the medium

were idealized as a network of cylindrical pores through which fluids are transported. The flow through such a tube of unit length is given by the Hagen-Poiseuille equation

$$Q = \frac{\pi d^4}{128\eta}\frac{\Delta P}{\Delta L},$$

[21]

where Q is flow rate, $\Delta P/\Delta L$ is the pressure gradient, η is the fluid viscosity and d is the average pore diameter. By considering a unit volume of hardened cement paste with 'N' cylindrical pores and assuming a paralell orientation between them, an expression for permeability as a function of porosity was proposed

$$kd = \frac{nd^2}{32}$$

[22]

3 Framework of Leakage Assessment Methodology

3.1 General

Leakage through wells has been reported as one of the more likely pathways for CO_2 to reach the surface; however, determination of actual flow rates has been a difficult task. Any quantitative estimation of CO_2 leakage from standard numerical simulation approaches requires the assignment of accurate transport-property parameters. This section provides a detailed overview of the methodology developed to identify the main leakage paths within the wellbore system, and the processes that affect the transport properties of those paths. The challenges associated with integrating real operational data into the performance assessment are discussed within the context of the performance-assessment methodology.

3.2 Conductivity of the Wellbore-System

The methodology requires some basic wellbore information, so the first step was data acquisition. Wellbore information can be collected from two main sources: 1) wellbore microfiche, which are the records stored at the relevant energy resources department, and 2) database files provided by the well owner. Generally speaking, the same information should be found in both places; however, in some cases, more detailed information could be available in the database files.

In general, information for wellbores drilled in the last decade is more detailed and complete than that available for wells drilled during the early development of the fields. Information for wellbores drilled in 1930s to 1950s is usually limited to geometry of the wellbore (diameter, length), description of the casing (diameter, length, grade), and cement type and volume. On the other hand, information available for a typical wellbore perforated in the 1990s is, in most cases, very detailed and complete.

Cementing records usually include cement type, volume, depth set, circulation pressures, spacer volume, and casing reciprocation stroke length and time. Casing information includes length, grade, and number and spacing of accessories. Finally, daily drilling reports include such information as drilling mud density and volume, pressure, and daily drilling advance.

Families of wellbores, each well having the same geometry and similar drilling and completion characteristics, need to be identified. In most cases, each wellbore family will be associated with a different development stage of an oil field. A more detailed definition of wellbore geometry can be found in Section 3.5.

With the typical well families defined, the conductivity of the major components of the wellbore system can be assigned: the casing can be

regarded as an impervious element, cement (annular) as a low-permeability element (with a value of 1 x 10^{-18} m^2), and aquitards and aquifers as low- and high-permeability elements, respectively. Assuming good bonding quality, interfaces between these components can be considered as no-flow regions.

Finally, the effect of the four major alteration mechanisms on the intact conductivity properties of the wellbore-system elements is assessed and their values modified accordingly. This is discussed in more detail in the next section.

3.3 Conductivity-Alteration Mechanisms

A detailed review of available literature reveals that a wide variety of mechanisms can modify the transport properties of the wellbore system. Based on the physics involved in these conductivity-alteration mechanisms, a four-group classification is proposed: geomechanical damage, hydrochemical damage, mud removal, and deterioration damage (cement). These mechanisms can occur during the various phases of a well life, namely drilling, completion, operation, and abandonment. A process-flow–type diagram of the entire methodology is illustrated in Figure 13, and the approach used within each group to assess hydraulic integrity of the wellbore system is discussed in the following sections.

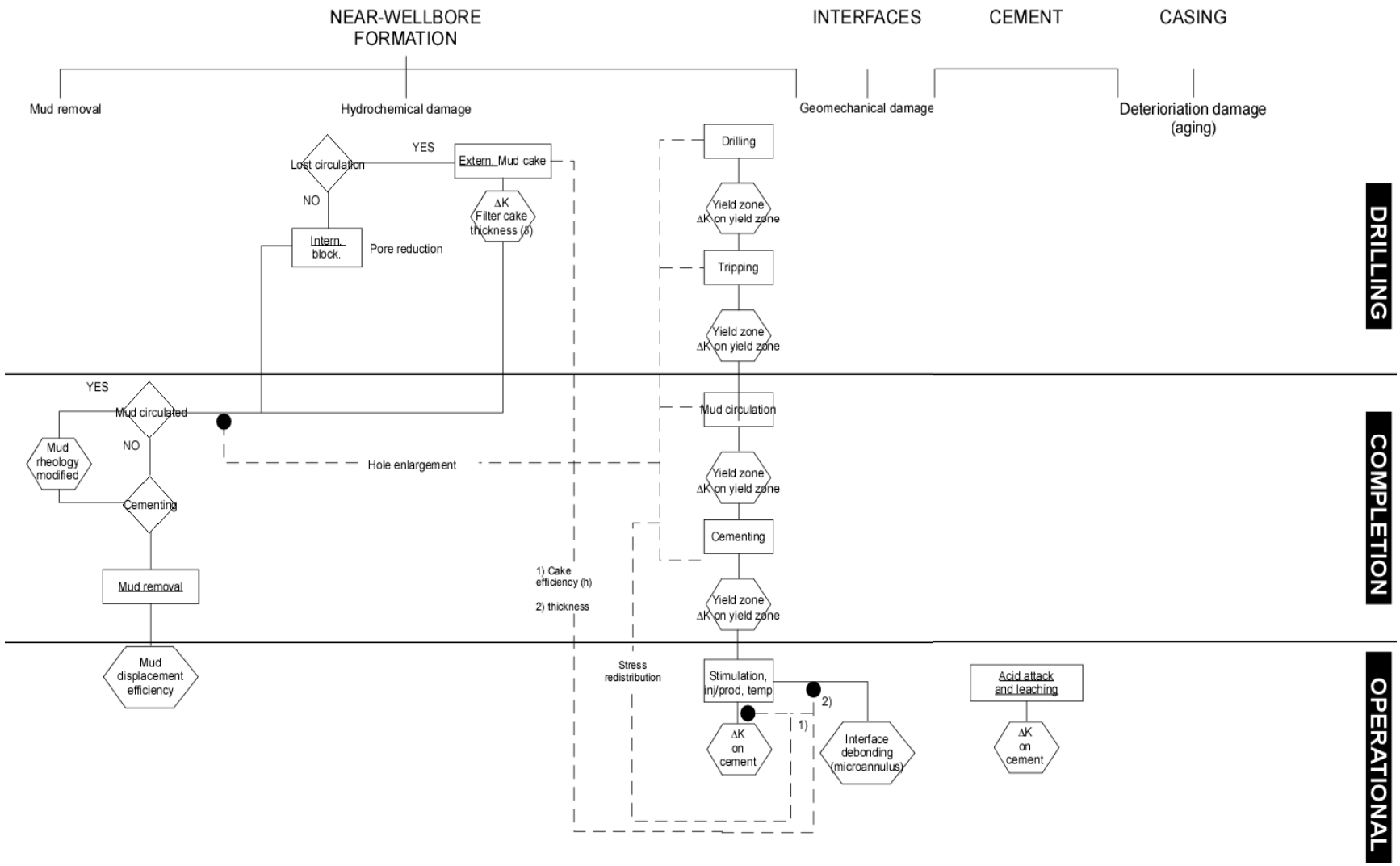

Figure 13 Methodology for assessment of transport properties.

3.4 Hydrochemical Damage

The method developed to quantitatively estimate hydrochemical damage is described in this section. It assumes that damage is caused mainly by particle-invasion processes as a result of exposure of the permeable rock to mud fluids during drilling. The different particulate processes are classified in two groups: internal and external. Internal processes occur in the porous medium in the form of gradual pore reduction, whereas external processes occur over the formation face (i.e., filter cake). The complete method integrates the many factors that affect damage through every phase of well drilling. These include particle size, mud type, temperature, pressure and pump rate.

The first step is to identify the types of particulate processes that can occur. To achieve this, a problem-diagnostic protocol was developed (Figure 14). This diagnostic tool identifies the most probable type of particulate process by asking the user a series of questions. With the type of process identified, the appropriate steps can then be followed to assess its consequences and severity. Most of these steps are almost intuitive, but a structured approach is required for success.

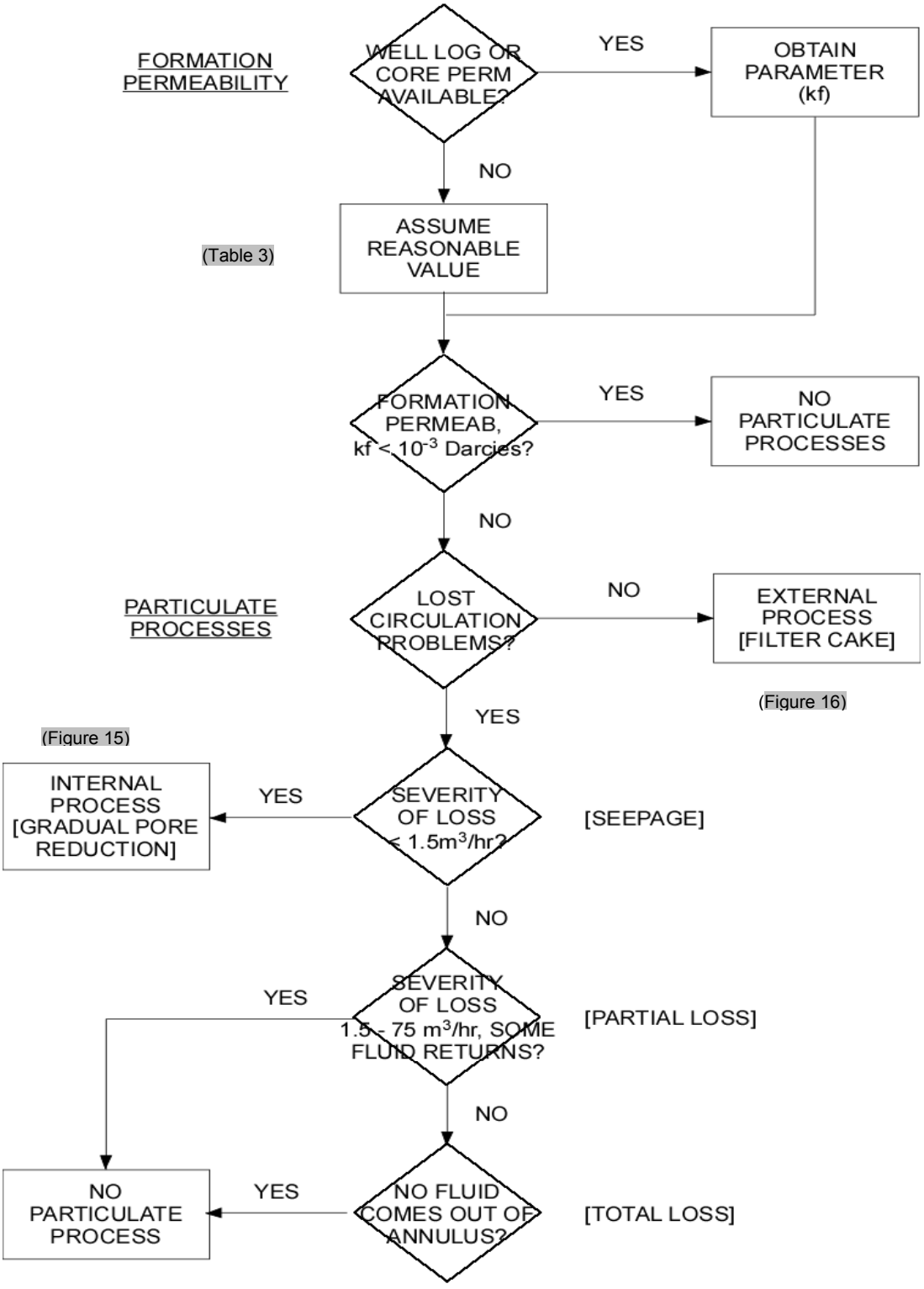

Figure 14 Problem-diagnostic protocol to identify type of particulate process.

Table 3 Typical rock permeabilities.

Formation type	kf (D)
Unconsolidated sands	$> 10^2$ to 10^0
Consolidated sands	10^0 to 10^{-3}
Siltstone	10^{-3} to 10^{-6}
Shale	10^{-6} to 10^{-9}
Limestone (Vuggy)	10^1 to 10^{-2}
Limestone (Microporosity)	10^{-5} to 10^{-2}

From Hawkes and McLellan 1996, Garg 1980, Darvish and Mattar 2001, Howard 1991, Alexander, Dong et al 2007, Saller et al. 1999, Aston 2002 [selecting right drill fluid]

3.4.1 Internal processes

Permeability impairment by gradual pore reduction can be assessed from Figure 15. These charts were constructed using the diagnostic equations developed in the thin-slice algebraic model. This model has an advantage over the other models discussed in Section 2.3 in that it can evaluate the effect of gradual pore reduction as the main mechanism acting during external particle invasion. Given the high concentration of solids normally found during drilling, only the case where particles originate from external sources is considered.

As seen on Figure 15, the gradual pore-reduction mechanism is indicated by slow, parabolic-type permeability reduction and deep particle invasion (Wojtanowicz et al., 1988). It is important to recognize, however, that gradual reduction of the pore size will continue until a critical value is

reached, after which pore-throat plugging and subsequent cake formation will prevail (Wojtanowicz et al., 1988). Thus, at most one order of magnitude in permeability reduction should only be considered.

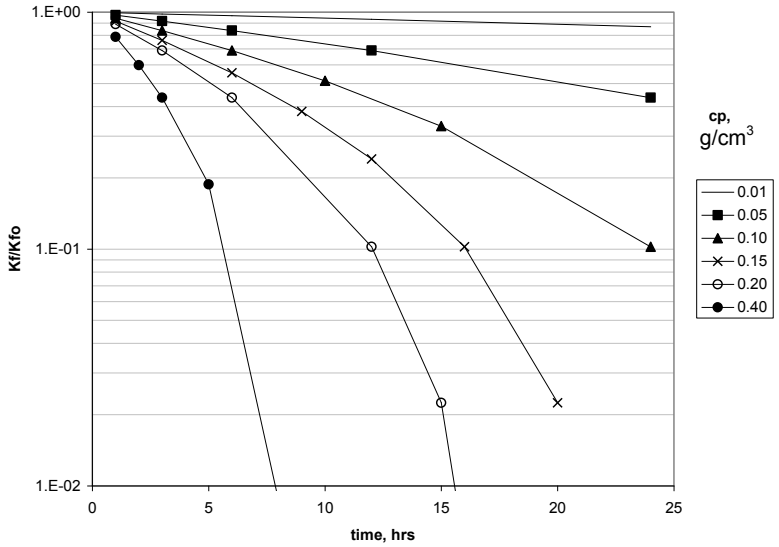

(a)

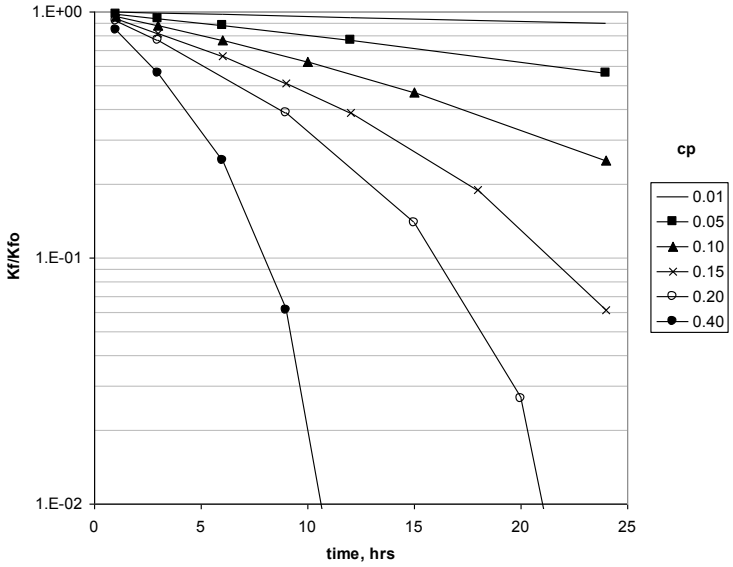

(b)

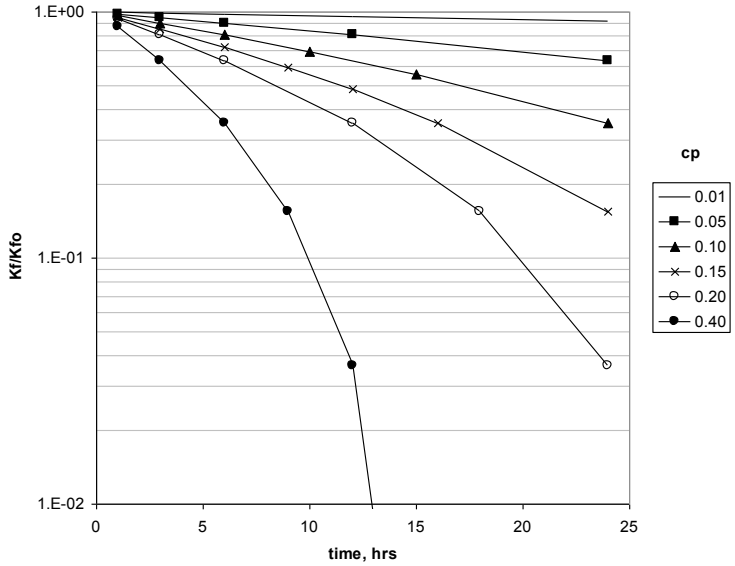
1.E+00
1.E-01
1.E-02
Kf/Kfo
0
5
10
15
20
25
time, hrs
cp
0.01
0.05
0.10
0.15
0.20
0.40

(c)

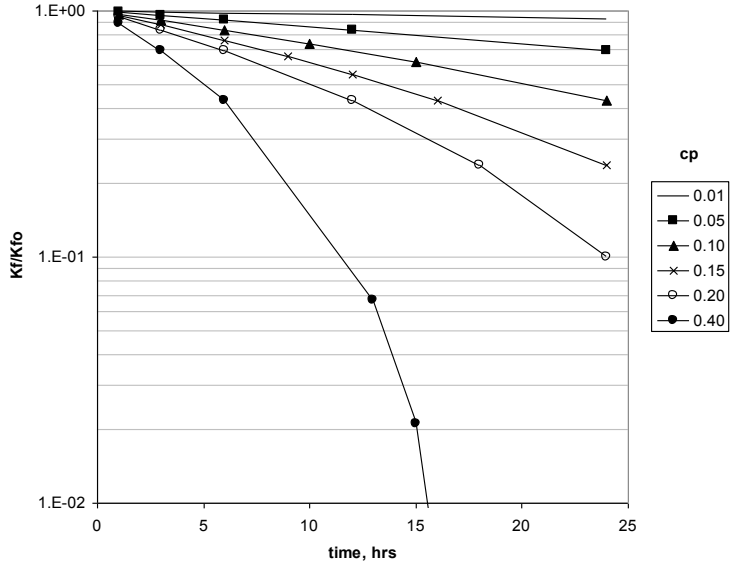
1.E+00
1.E-01
1.E-02
Kf/Kfo
0
5
10
15
20
25
time, hrs
cp
0.01
0.05
0.10
0.15
0.20
0.40

(d)

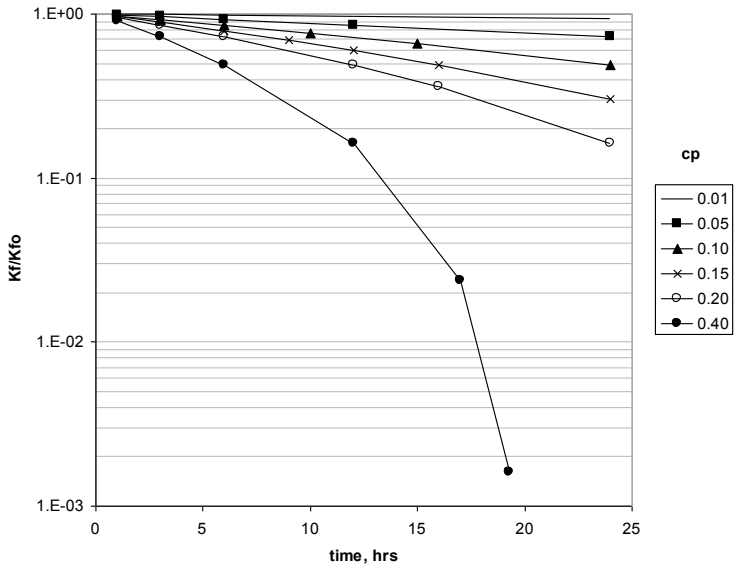

(e)

Figure 15 Permeability decline due to gradual pore reduction for formation porosities of 10% (a), 15% (b), 20% (c), 25% (d), and 30% (e), and various mass concentrations of particles in flowing suspension (cp).

3.4.2 External processes (filter cake)

Two parameters are of interest when assessing the impact of filter cake on wellbore-transport properties: cake thickness and permeability. A process-flow–type procedure is proposed to predict the values of cake permeability and thickness (Figure 16). This approach assumes that a mud cake can only be present adjacent to permeable zones (10^{-3}–10^{1} D).

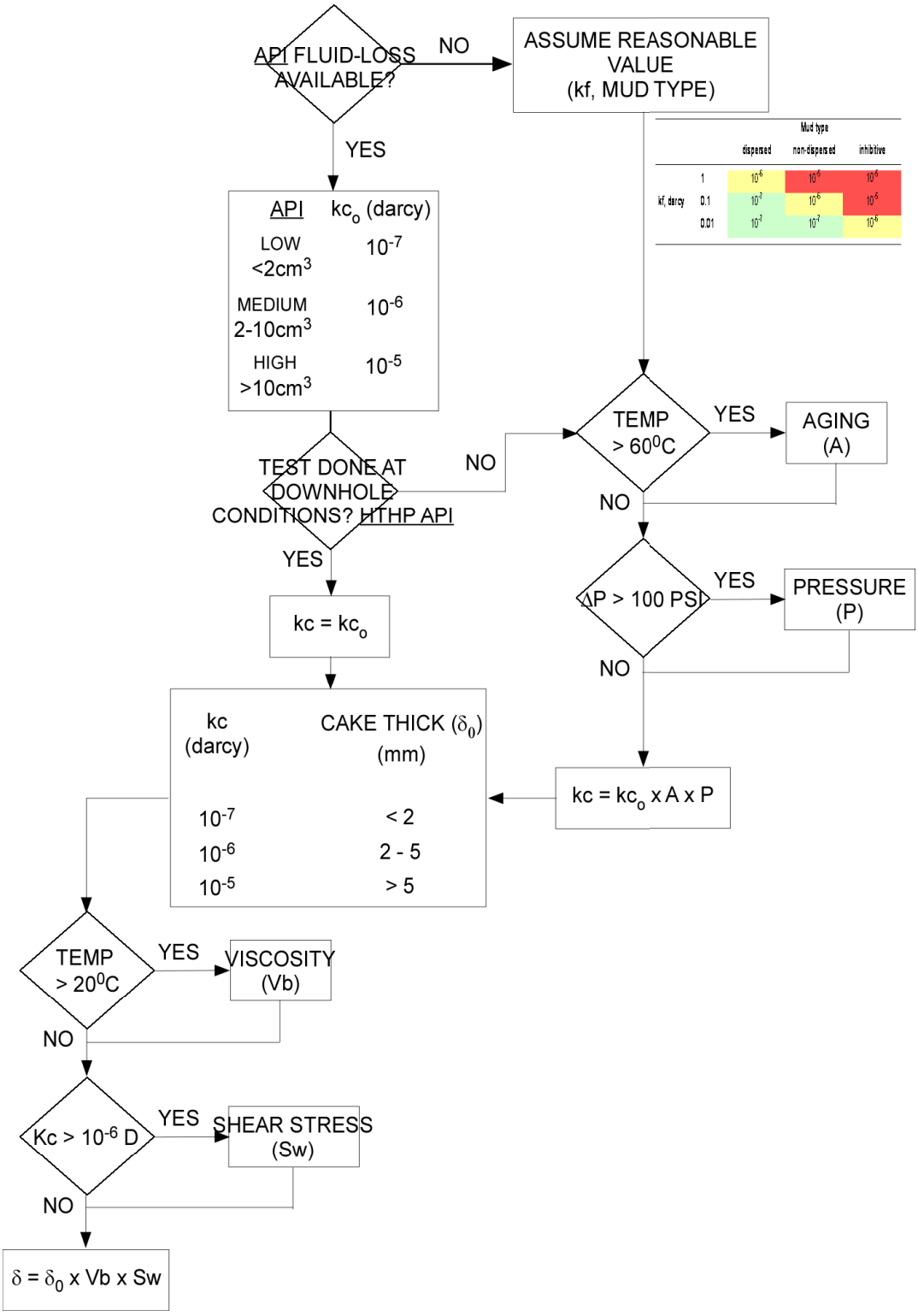

Figure 16 Flowchart for particulate processes.

Cake permeability

Cake permeability can be expressed as

$$kc = kc_o \times A \times P ,$$

[23]

where kc_o is uncorrected cake permeability (D), and A (aging due to temperature) and P (differential pressure between borehole and formation) are weight-independent functions. Each function corresponds to the influence of temperature and differential pressure with cake permeability.

The functions A and P were built using the experimental database from the literature presented in Section 2.2. In order to build the weight functions, a reference condition was defined. In this reference condition, the value of the various weight functions is equal to one. The procedure used during the API fluid-loss test was chosen as the reference protocol (mud is filtered at a differential pressure of 100 psi and maintained at 20˚C).

Uncorrected cake permeability kc_o

Despite its shortcomings, the API static-fluid-loss test is still the only practical and widely test used to estimate the filtration properties of a fluid at the well site. This is based on the generally accepted assumption that the behaviour of the fluid, when pushed against a filter paper, is at least qualitatively the same as in real rock (Santos et al., 1999). Consequently,

the API test result can be used to calculate uncorrected cake permeability (Table 4). Typical cake-permeability values for this table were obtained from an extensive literature review spanning more than two decades of research (Ershaghi and Azari, 1980b, Hassen, 1980, Peden et al., 1982, Courteille and Zurdo, 1985, Hartmann et al., 1988, Chesser et al., 1994, Li et al., 1994, Fraser et al., 1995, Isambourg et al., 1999, Santos et al., 1999, Zain and Sharma, 1999, Amanullah and Tan, 2000, Proett et al., 2001, Proett et al., 2002, and Martins et al., 2004). These values were then associated with API fluid loss using correlations developed in the laboratory. These relationships establish that high values of fluid loss are related to high-permeability cakes and low fluid loss with low-permeability cakes.

Table 4 Uncorrected cake permeability as a function of values obtained using the API fluid-loss test.

API	kc_o (D)
Low (< 2 cm^3)	10^{-7}
Medium (2 – 5 cm^3)	10^{-6}
High (> 5 cm^3)	10^{-5}

Note The practice of estimating the 30 minute API fluid loss value from the 7 ½ minute value should be avoided as this can lead to serious errors (Arthur and Peden, 1988)

When the API fluid-loss value is not available, cake permeability can be estimated as a function of two main contributing factors, namely rock

permeability (kf) and mud type, the contribution of each evaluated using a consequence matrix (Table 5).

Rock permeability plays an obvious role in determining the bridging size of the cake during the filtration process. High-permeability formations will capture particles larger than those bridged at low-permeability formations. This will result in cakes with higher permeabilities (Ershaghi and Azari, 1980b, Hassen, 1980, Peden et al., 1982, Courteille and Zurdo, 1985, Hartmann et al., 1988, Chesser et al., 1994, Li et al., 1994, Fraser et al., 1995, Isambourg et al., 1999, Santos et al., 1999, Zain and Sharma, 1999, Amanullah and Tan, 2000, Proett et al., 2001, Proett et al., 2002, and Martins et al., 2004).

On the other hand, the electrochemical conditions prevailing in the mud (mud type) are also a major factor in determining the permeability of its filter cake. As a generalization, flocculated muds have high cake permeabilities. Conversely, deflocculation of a mud by addition of a thinning agent causes a decrease in cake permeability (Darley and Gray, 1988).

Table 5 Uncorrected cake permeability

		Mud type		
		dispersed	non-dispersed	inhibitive
kf (D)	1	10^{-6}	10^{-5}	10^{-5}
	0.1	10^{-7}	10^{-6}	10^{-5}
	0.01	10^{-7}	10^{-7}	10^{-6}

The most commonly used drilling fluids are summarized and classified by their degree of flocculation (mud type) in **Error! Reference source not found.**.

Cake permeability (kc_o) is now corrected to account for down-hole temperature and filtration-pressure conditions (weighting functions A and P). The procedure to quantitatively assess their effect is discussed in detail in the following sections. No correction is needed if filtration measurements were taken at simulated bottom-hole temperature and filtration pressure (High-Temperature-High-Pressure [HTHP] API filtration test).

Modelling the influence of temperature

Temperature effects can be categorized into two groups, one allowing for the effects on mud of intermediate temperatures (60–90˚C) and the other considering the effects of high temperatures (>100˚C) (Darley and Gray,

1988, Hartmann et al., 1988, Chesser et al., 1994, and Liu and Civan, 1995). In the first group, the dominant mechanism is flocculation and dehydration of the bentonite with an associated change in cake permeability. In the second group, degradation (aging) of the mud constituents occurs, resulting in a dramatic increase in cake permeability. Table 6 shows the effect of aging the weighting multiplier A as a function of the above temperature ranges

Table 6 Aging the weighting multiplier A as a function of annular mud temperature (Ta).

Ta (°C)	Cause	A
< 60	reference protocol	1
60 – 90	clay flocculation some additive degradation	1.2 – 1.5
> 100	additive degradation	10 - 15

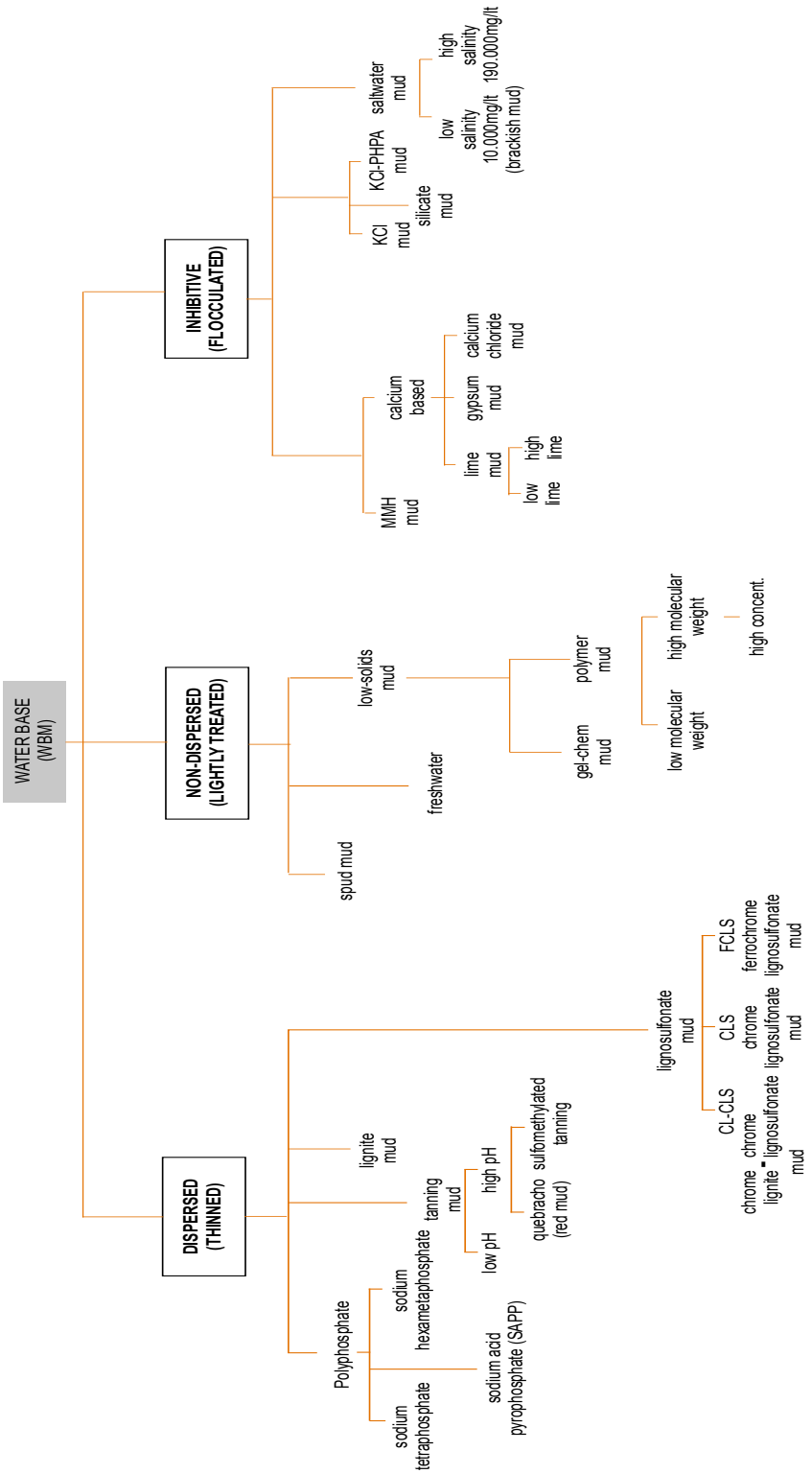

Figure 17 Classification of drilling muds according to flocculation degree (mud type).

Modelling the influence of differential pressure

Figure 18 shows the differential-pressure weighting function P. This chart was constructed by using the equation proposed by Courteille and Zurdo (equation [4]; 1985).

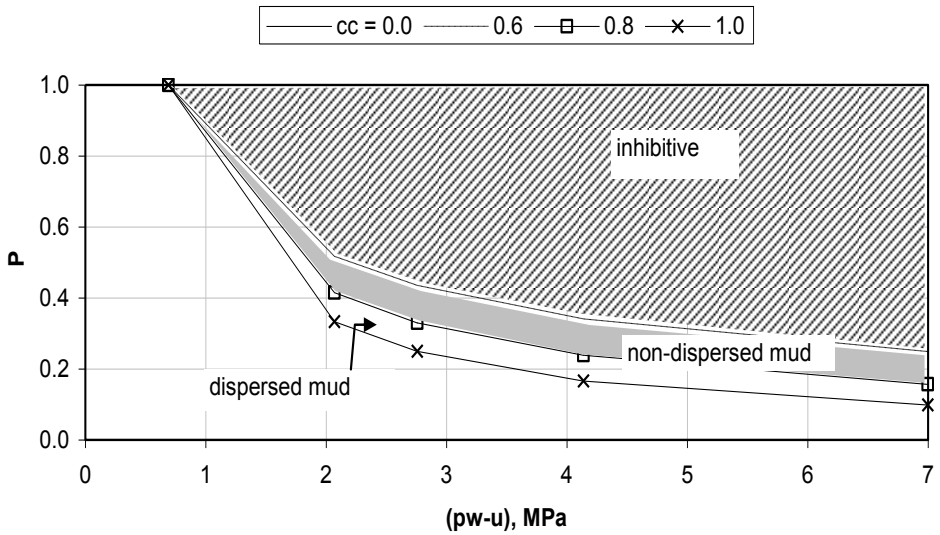

Figure 18 Differential-pressure weighting function (P).

The use of the weighting function (P) requires access to basic information on fluid properties, none of which may be available. Basic properties include cake compression, formation pore pressure, and internal support pressure. Recommendations for obtaining these values are discussed below.

Cake compressibility can be obtained from Table 7.

Table 7 Cake compressibility index (cc).

Mud type	Compressibility index (cc)	Description
Dispersed	0.8 – 1.0	
Non-dispersed	0.6 – 0.8	contain a number of materials that give cake higher compressibility[1]
Inhibitive	0 – 0.6	stronger structure and greater resistance to pressure[2]

[1] Chesser et al., 1994
[2] Darley and Gray, 1988

Values of formation pore pressure (u) can be obtained directly from formation-integrity or hydraulic-fracturing test results. Indirect measurement of pore pressures can be made through borehole-logging techniques. When no measurements are available, the pore pressure can be estimated from the values suggested in Table 8.

Table 8 Guidelines for assessment of formation pore pressure.

Formation pressure class	Pressure gradient kPa/m	u/Po	Description
Underpressured	< 9.8	< 0.45	Formations that have had hydrocarbon production
Normal	9.8 - 11.7	0.45 - 0.5	Any formation not fitting the underpressured and overpressured descriptions
Overpressured	> 11.7	0.5 - 0.9	Low kf formation w/ restricted pore-fluid release during burial • Thick shale formation • Sand body interbedded w/ shale • Isolated sand body

The internal support pressure (pw) can be obtained from drilling reports. In their absence, pw can be evaluated considering typical mud-density ranges (1200–2400 kg/m^3). In either case, overbalance pressure, (pw - u) should be of the same order of magnitude as the typical pressure difference maintained between the drill mud and the formation pressure, which usually ranges from 0.5 to 7 MPa (Fam and Dusseault, 1998).

Cake thickness

A simplified procedure is proposed to predict the value of cake thickness as a function of cake permeability (kc). Additional correction factors are used to account for changes in wellbore fluid properties (base fluid viscosity) due to temperature, and wellbore hydraulic conditions (shear stress on the filter cake surface). Cake thickness is expressed as

$$\delta = \delta_0 \times V_b \times S_w ,$$

[24]

where δ_0 is uncorrected cake thickness (mm) as a function of cake permeability (kc), and V_b (base fluid viscosity change due to temperature variation) and S_w (shear stress on the filter cake) are weight-independent functions. Each function corresponds to the influence of fluid viscosity and shear stress with cake thickness.

The functions Vb and Sw were built using relationships from the literature previously presented in Chapter 3. In order to build the weight functions, reference conditions were defined. In these reference conditions, the value of the various weight functions is equal to one.

Uncorrected cake thickness

Table 9 shows uncorrected cake thickness as a function of cake permeability.

Table 9 Uncorrected cake thickness as a function of cake permeability.

kc (D)	Cake thickness (δ_o), mm	API fluid-loss
10^{-7}	< 2	Low
10^{-6}	2 – 5	Medium
10^{-5}	> 5	High

These values were defined based on the relationship that exists between cake thickness and cake permeability. These correlations establish that high cake permeabilities result in thick filter cakes (Darley and Gray, 1988).

Modelling the influence of temperature

Temperature increase can produce a significant reduction in fluid viscosity. This will affect the filtration process in the form of an increased fluid loss. Temperature effects on fluid loss can be evaluated using the expression proposed by Larsen (Larsen, 1938), and then correlated with cake thickness using the linear relationship known to exist between them (Darley and Gray, 1988). Cake thickness was then normalized as a percentage of the cake thickness at the reference temperature of 20°C ($\delta/\delta_{20°C}$) and plotted against mud temperature (Figure 19).

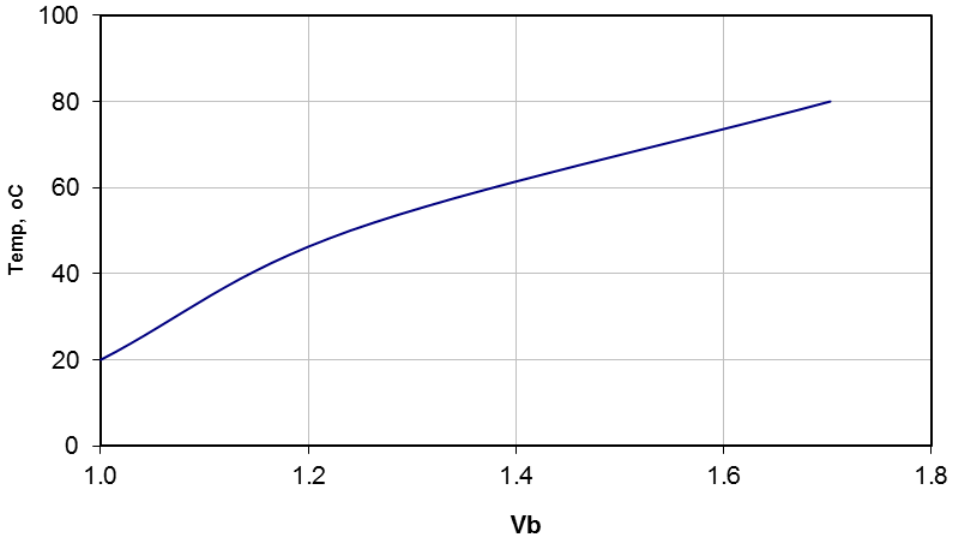

Figure 19 Weighting multiplier Vb as a function of mud temperature (Ta).

Modelling the influence of shear stress (annular velocity)

Dynamic filter cakes differ from static cakes in that the soft surface layers are not present due to the erosive action of the mudstream (Darley and Gray, 1988). When mud circulation is stopped, cake growth is not restricted since no erosion takes place (static filtration). Because, in practice, the evaluation of the filtration properties of a drilling fluid is based in static tests, a weighting function (Sw) was introduced to account for erosion of the filter during mud circulation.

The value of the function Sw was established by evaluating when the shear stress at the wall exceeds the cake yield strength (cake erosion). Shear stress at the wall (τ_w) was calculated based on the typical fluid rheologies and flow rates commonly used. These values were obtained after an extensive literature review spanning almost four decades of published data (Brice and Holmes, 1964, Parker et al., 1964, McLean et al., 1967, Childers, 1968, Clark and Carter, 1973, Zuiderwijk, 1974, Haut and Crook, 1979, Peden et al., 1982, Peden et al., 1984, Wojtanowicz et al., 1987, Arthur and Peden, 1988, Fordham et al., 1988, Longeron et al., 1988, Lockyear and Hibbert, 1989, Lockyear et al., 1990, Nelson, 1990, Smith, 1990, Fisk and Shaffer, 1991, Jones et al., 1991, Brady et al., 1992, Jiao and Sharma, 1992, Ravi et al., 1992, Fraser et al., 1995, Griffith and Osisanya, 1995, Longeron et al., 1995, Arginier et al., 1997, and Isambourg et al., 1999).

Cake yield strength (τ_c) was calculated using the equation of Ravi et al. (1992), for which they assumed that the particles are connected by van der Waals forces of molecular attraction

$$\tau_c = \frac{1}{4r_c^{\,2}} \frac{H \times d_c}{12 \times l^2} \times 1.99x10^{24}, \quad \textbf{[25]}$$

where τ_c is the calculated shear strength of the filter cake (in lb./100 sq. ft.), r_c is the average particle radius (in μm), H is the Hamaker coefficient (3 x 10^{-20} joules), and l is the separation distance between particle surfaces (in μm). Cake particles are assumed to be ⅓ of the formation pore size, as this is the size required to bridge the formation. Thus, for typical formation permeabilities ranging from 10^{-3} to 10^{1} D, the average cake-particle diameter (d_c) ranges from 40 to 1 μm.

A comparison of cake yield strength and shear stress at the wall reveals that the effect of annular velocity on the cake can be divided into two groups (Figure 20), one for cakes formed with coarse particles (>10^{-6} D) and a second for finer cakes (<10^{-6} D). For the first group, shear stress at the wall exceeds the cake yield strength at all times and complete erosion of the cake will take place. For the second group, cake yield strength is not, in theory, exceeded; however, some erosion will still occur (of the soft upper layers). No cake erosion (Sw = 0) will take place if the mud was not

circulated prior to cementing or there was a long period of time between circulation and cementing.

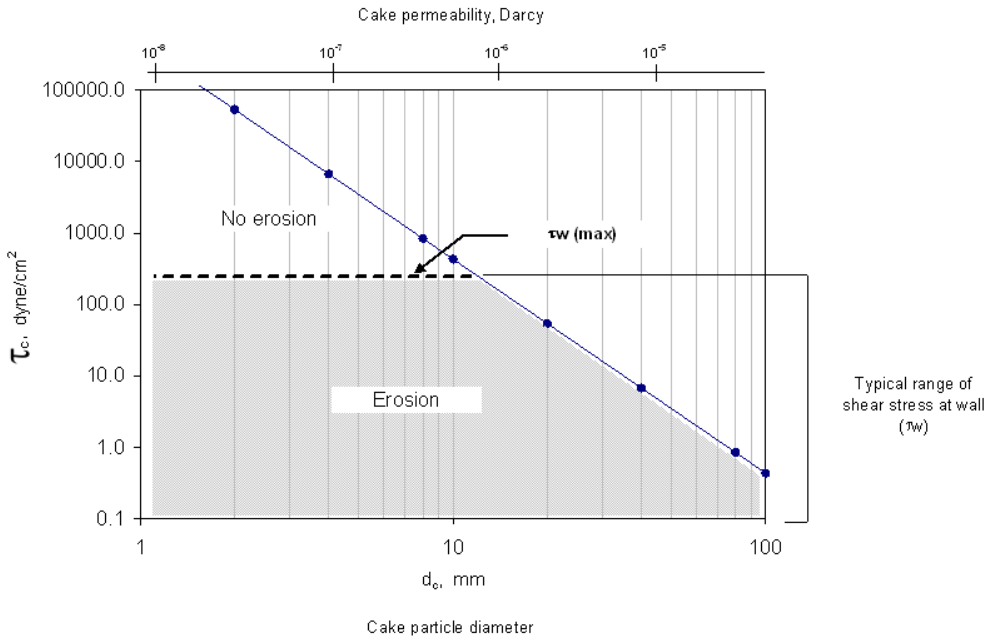

Figure 20 Cake yield strength versus shear stress at the wall.

Table 10 shows the shear-stress weighting multiplier (Sw) as a function of cake permeability.

Table 10 Shear-stress weighting multiplier (Sw) as a function of cake permeability.

Cake permeability kc (D)	Erosion level	Sw
$< 10^{-6}$	partial ($\tau w < \tau c$)	0.6
$> 10^{-6}$	total ($\tau w < \tau c$)	0.0

3.5 Mud Removal

Displacement efficiency of mud can be evaluated based on the ratio between the interface velocity on the narrow side and the average velocity in the annulus (Figure 21).

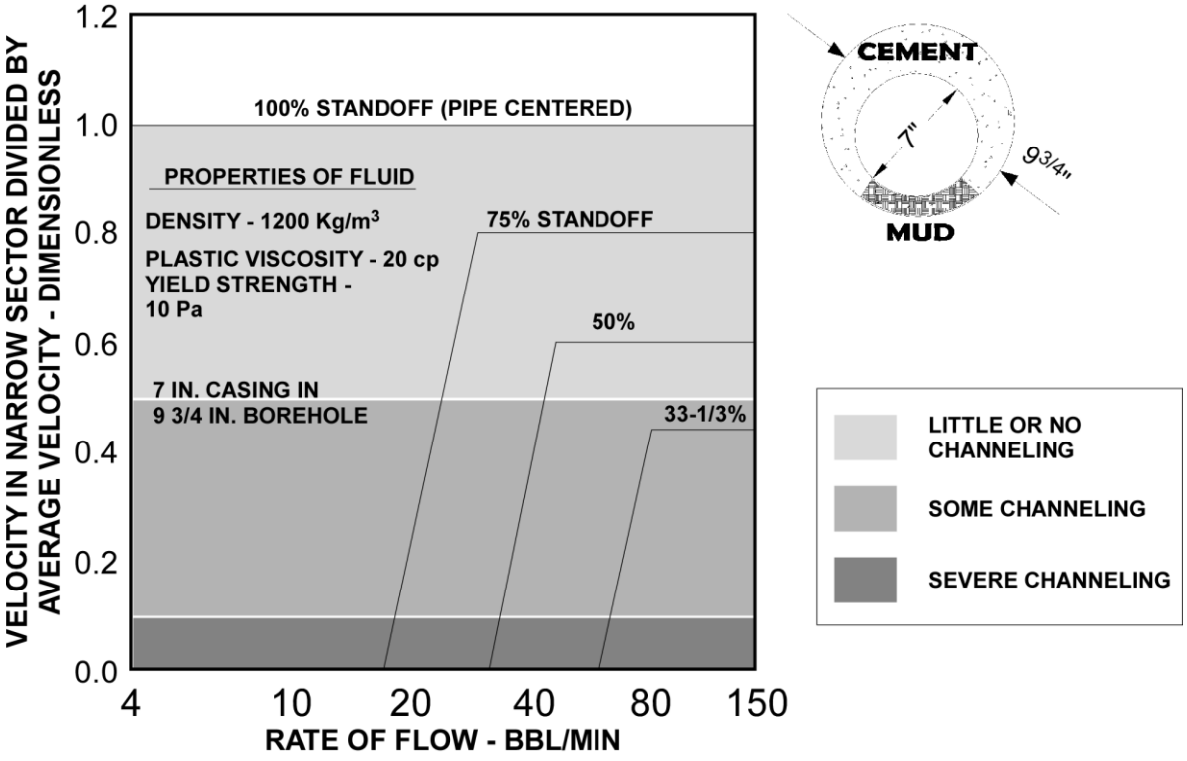

Figure 21 Typical chart of Velocity in narrow sector versus average velocity for several standoffs (STO).

Based on this ratio, there are three scenarios for displacement efficiency of mud. A Class I scenario indicates that a continuous mud channel is present in the annulus. This will offer a preferential route for gas migration that has a permeability usually on the order of several darcies (Bonett and Dafitis, 1996). A mud channel will also be present in a Class II scenario,

but it will not be continuous. A Class III scenario indicates that mud has been effectively displaced, so no mud channel is expected to exist.

Table 11 Displacement categories (Dc; from Lockyear et al., 1990).

Class	V_{narrow}/V_{avg}	Description
I	< 0.1	Severe channelling
II	0.1 - 0. 5	Some channelling
III	> 0.5	Little or no channelling

The annular mud-velocity ratio (V_{narrow}/V_{avg}) charts were developed based on the slot approach to modelling laminar flow of non-Newtonian fluids, as described by McLean et al. (1967). Thus, if the turbulent-flow technique was used, higher-than-predicted displacement efficiencies should be expected. This can be attributed to erosive and dispersive processes over the displaced fluid promoted by turbulence. Since the amount of erosion is difficult to assess, the suggested approach is to compare the actual contact time with the recommended practice of 10 minutes contact time. If actual contact time is higher than 10 minutes, one can expect erosion and dispersion to significantly contribute to mud displacement and the displacement category should therefore be increased one level. If the actual contact time is less than 10 minutes, no additional benefit is obtained from the erosive action of turbulent eddies.

Contact time can be expressed as

$$\text{Contact} \cdot \text{time} = \frac{V_T}{5.61 \times Q},$$

[26]

where contact time is expressed in minutes, V_T volume of turbulent flow fluid in cu. ft., and Q flow rate in barrels/min (Brice and Holmes, 1964). The positive effect of contact time on displacement efficiency should only be taken into account when the displacing fluid is completely in turbulence all around the annulus.

Use of this methodology requires access to relatively detailed basic information on wellbore geometry, fluid properties, and the conditions of displacement, none of which may be available. Thus, the procedure described in the following sections is suggested to assess these properties (Figure 22).

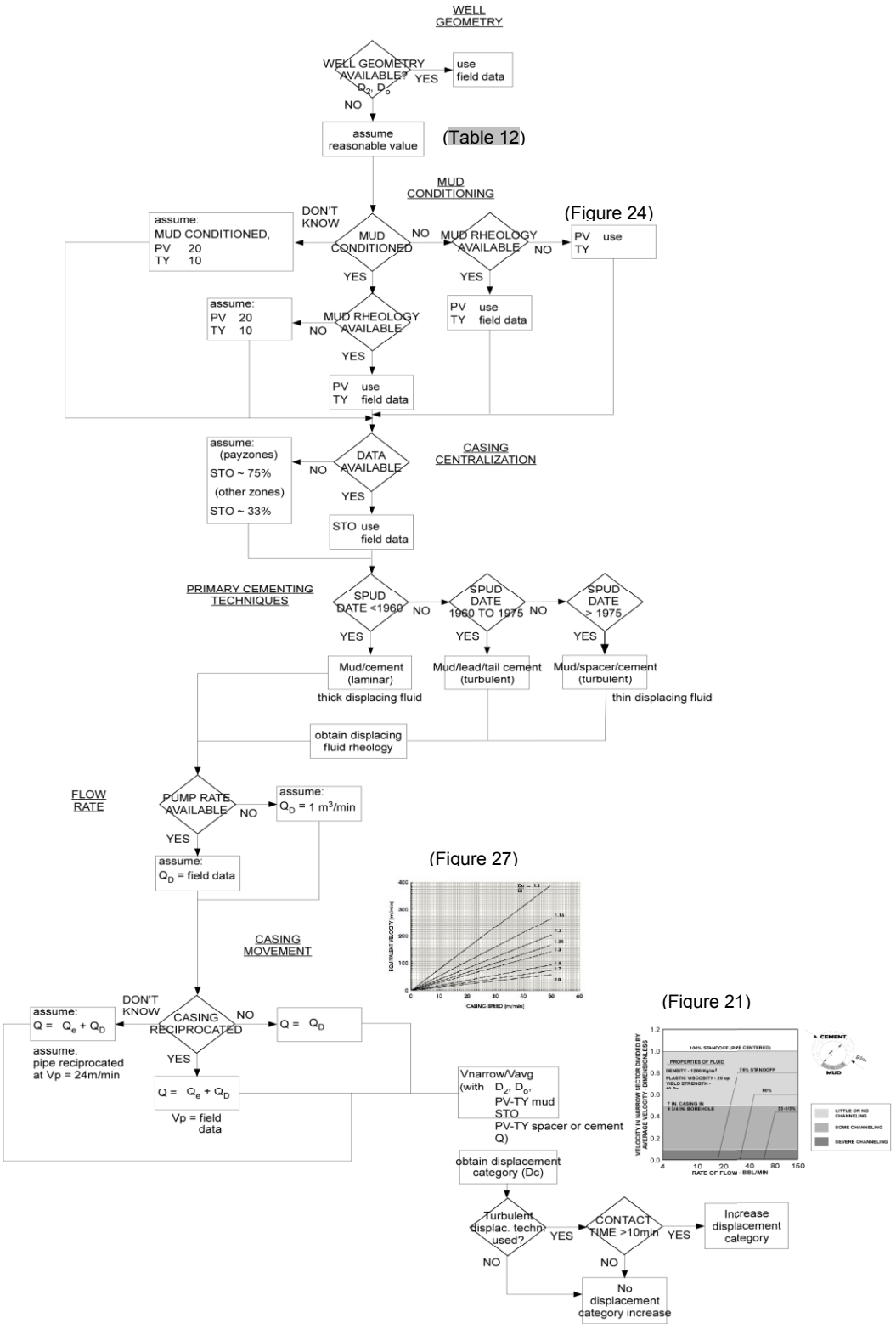

Figure 22 Procedure for evaluating efficiency of mud removal.

3.5.1 Well geometry

Open-hole size (D_2) should be obtained from wireline caliper logs. These logs have varying degrees of accuracy, depending upon the type of tool used (two-pad caliper, three-pad caliper, etc.). The four-arm caliper log will provide the most accurate representation of the actual borehole geometry. In the many areas where caliper logs are not available, hole size can be determined from wellbore-stability analyses.

Casing size (D_o) should be obtained from completion records. Use Table 12 as a guideline when casing records are not available.

Table 12 Casing size (D_o).

Type	Size	Cement column
Intermediate	6 5/8 – 13 3/8	Usually up to surface[1]
Production	4 ½ - 9 5/8	Across producing zone only[1]

[1] Nelson, 1990
Note Generally speaking, annular space ($D_2 – D_o$) ranges between 40 to 75 mm (Brady et al., 1992)

3.5.2 Mud conditioning

Mud-displacement efficiency is dependent upon the relative properties of the fluids involved, so the rheological properties of the drilling fluid prior to cementing are needed. These properties can be evaluated by following the procedure outlined in Figure 23. In the absence of data, mud can be assumed as fully circulated and thinned to the rheological properties

outlined in Table 1. The validity of this assumption is based on the fact that these practices have been accepted as sound since research in displacement mechanics was first done in 1940 (Haut and Crook, 1981).

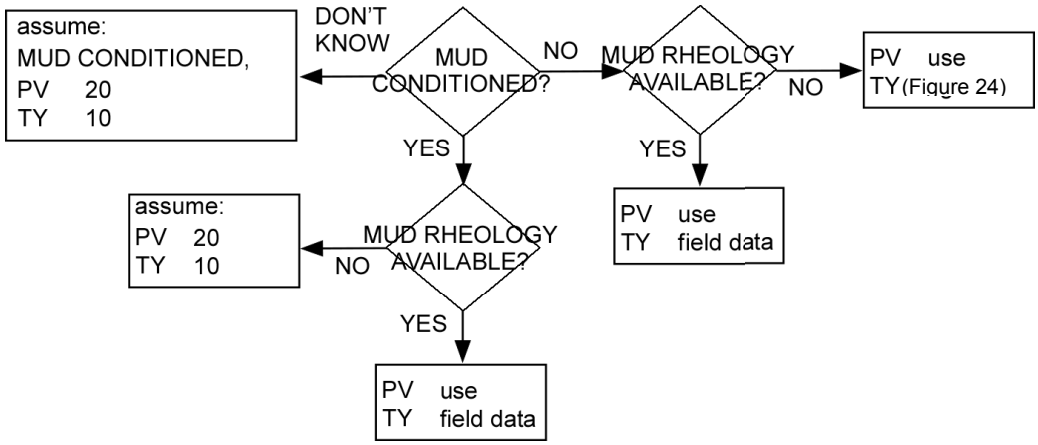

Figure 23 Procedure for determining mud-conditioning and drilling-fluid rheological properties.

Figure 24 shows typical rheological properties of water-based dispersed drilling fluids.

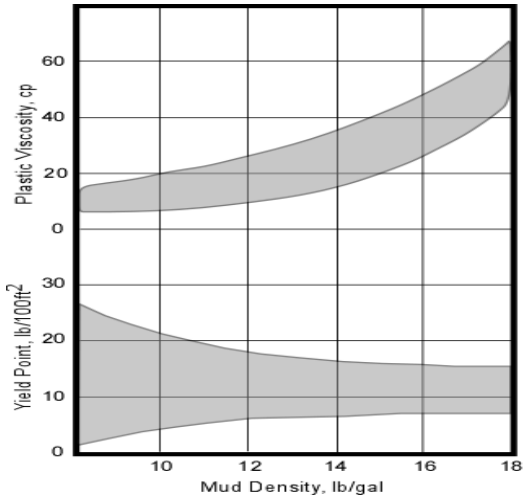

Figure 24 Range of plastic-viscosity and yield-point values for dispersed water-base muds (from Chambre Syndicale de la Recherche et la Production du Petrole et du Gaz Naturels, 1982).

3.5.3 Casing centralization

Casing centralization is defined using the common parameter in the oil industry, casing standoff (STO). This parameter is defined by the formula

$$STO = 100 \times \left[1 - \frac{\delta_T}{R_2 - R_o} \right],$$

[27]

where R_2 and R_o are the hole and casing radius respectively, and δ_T is the total casing deflection.

Total casing deflection (δ_T), is composed of casing deflection (δ_{cg}) and casing-centralizer deflection (δ_c - Juvkam-Wold and Wu, 1992), is expressed as

$$\delta_T = \delta_{cg} + \delta_C$$

[28]

Casing deflection can be calculated based on the mathematical model described by Juvkam-Wold and Wu (1992). This model takes into account such relevant factors as the lateral force at any given location based on borehole geometry, buoyed string weights, and tension forces. The model was developed based on Timoshenko's formula for a bi-fixed end pipe with an axial force (Timoshenko, 1983)

$$\delta_{cg} = \left(\frac{N_e * s^3}{384 E_t I} \right) \left(\frac{24}{u^4} \right) \left(\frac{u^2}{2} - \frac{u * \cosh u - u}{\sinh u} \right)$$

and

$$u = \left(\frac{T_e s^2}{4 E_t I} \right)^{\frac{1}{2}},$$

[29]

where s is centralizer spacing and E = 206.8 x 10^3 MPa. The effective load (Ne) is defined as the root mean square of the gravitational and axial-load forces

$$N_e = \left[W_e{}^2 + T_e{}^2 \right]^{\frac{1}{2}}$$

$$W_e = F_b * W_s * s * \sin\theta$$

and

$$T_e = 2T \sin\beta$$

[30]

The buoyancy factor is calculated as

$$F_b = 1 - \frac{\rho_m}{\rho_s},$$

[31]

where ρ_s is about 7836 kg/m^3 and ρ_m is the mud density.

Axial tension (T) is calculated by means of the equations presented in American Petroleum Institute (API) Specification 10D, which summarizes the axial tension that acts on the casing as

$$T_i = T_{i-1} + Ws \times \cos\theta,$$

[32]

where Ws is the casing weight, T_{i-1} is the axial tension on the casing below element i, and θ hole inclination angle at the centralizer. Table 13 gives typical casing weight for different casing sizes. Centralizer spacing (s) is assumed to be one per casing joint throughout pay zones, with a maximum standoff of 75%, when no data are available.

Table 13 Casing weight for different casing sizes.

Casing size (in.)	Casing weight (lb/ft)	Casing weight (kg/m)
4 - 1/2	13 - 18	19 - 26
5	13 - 23	19 - 34
5 - 1/2	17 - 23	25 - 34
7	20 - 46	29 - 68
7 - 5/8	26 - 51	30 - 75
8 - 5/8	28 - 58	41 - 86
9 - 5/8	36 - 70	53 - 104
10 - 3/4	40 - 85	59 - 126

In addition to casing deflection (δ_{cg}), the casing centralizers will also contribute to total casing deflection in the borehole because of their lateral compressive displacement (Juvkam-Wold and Wu, 1992). This displacement is a function of type, fit, and strength of the centralizer, and it can be calculated using the equation

Spring-bow centralizer $\delta_C = \frac{N_e}{Ks}$

Rigid centralizer $\delta_C = 0$,

[33]

where Ne is the lateral load on the centralizer and Ks the centralizer stiffness. Lateral load (Ne) will have the same expression as equation [30] when the centralizers are uniformly spaced. If the centralizer spacing changes, use the average of the total lateral loads from each of the adjacent of the two adjacent casing spans (Juvkam-Wold and Wu, 1992). The centralizer stiffness is calculated using the results (load-displacement curve) of the restoring-force test performed on the centralizer in question according to API Specification 10D. This API specification defines the capability of a spring-bow centralizer to push the pipe radially away from the borehole wall (restoring force) as

$$Ks = \frac{RF_{67\%}}{D_2 - D_o},$$

[34]

where D_2 is the hole diameter, D_o is the diameter of the casing on which the centralizer is mounted, and $RF_{67\%}$ is the restoring force provided by the manufacturer. Unless noted on wellbore records, the restoring force can be obtained from API Specification 10D for restoring forces (Table 14).

Table 14 Dimension and performance data for casing centralizers (API, 1986).

Casing size (in.)	Hole size (in.)	Restoring force (Lbs) API ($RF_{67\%}$)
4 - 1/2	6	464
4 - 1/2	6 - 1/4	464
4 - 1/2	6 - 1/2	464
4 - 1/2	7 - 7/8	464
5	6 - 1/4	520
5	6 - 1/2	520
5	7 - 7/8	520
5	8 - 1/2	520
5 - 1/2	7 - 7/8	620
5 - 1/2	8 - 1/2	620
5 - 1/2	8 - 3/4	620
5 - 1/2	9 - 7/8	620
5 - 1/2	12 - 1/4	620
7	8 - 1/2	1040
7	8 - 3/4	1040
7	9 - 7/8	1040
7 - 5/8	9 - 7/8	1056
8 - 5/8	11	1440
8 - 5/8	12 - 1/4	1440
9 - 5/8	12 - 1/4	1600
10 - 3/4	12 - 1/4	1020
10 - 3/4	13 - 1/2	1020
10 - 3/4	14 - 3/4	1020

The decision on which type of centralizer was used depends on several factors, including borehole condition. Use Table 15 to determine the type of centralizer used if no records are available.

Table 15 Selection criteria for centralizer type (from Kinzel and Koithan, 1997).

Hole condition	Spring-bow	Rigid
Gauge	excellent	excellent
Oversized	excellent	not advisable
Undergauged	good	cannot be used
High build-up	good	not advisable

Placement of centralizers is often avoided, usually because of experiences with centralizers being destroyed and fouling the running of the casing (Sauer, 1987). Therefore, field records must be carefully examined to determine if this was a common practice.

Figure 25 and Figure 26 provide an example of a casing standoff (STO) chart for an openhole diameter of 14 ¾" through the range of dogleg factors $\beta = 0.01$ to 4. Appendix A provides the remainder of the casing standoff charts for openhole diameters from 13 ½" down to 6 ¼". The results provide accurate estimation of the casing deflection in a slightly inclined wellbore ($\theta < 2^\circ$) for a wide range of dogleg values (β) and with significant axial tension (T).

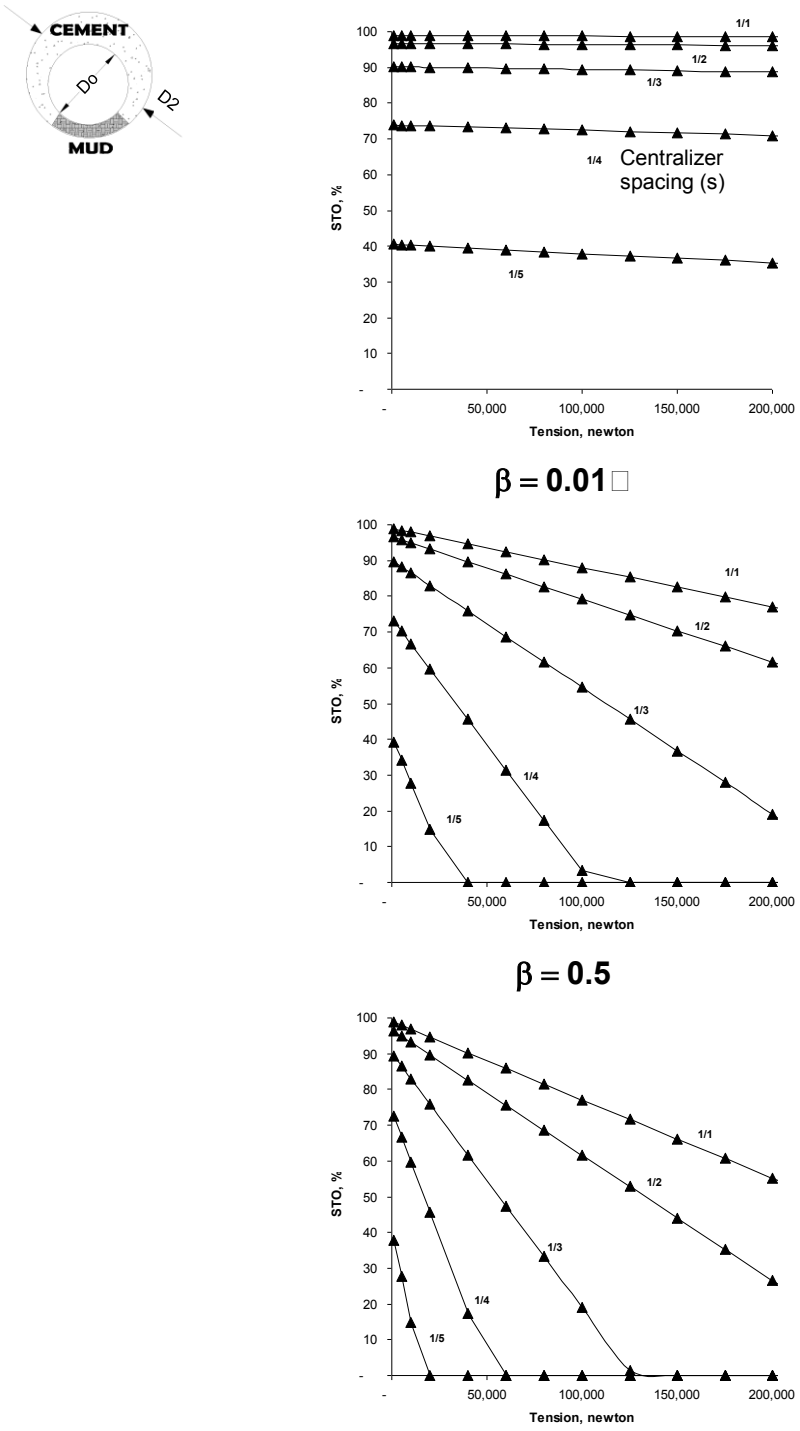

Figure 25 Casing standoff (STO) for a straight, inclined wellbore with axial tension. D_2 =14 ¾" and D_0 = 10 ¾".

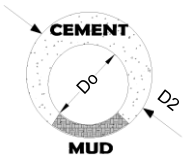

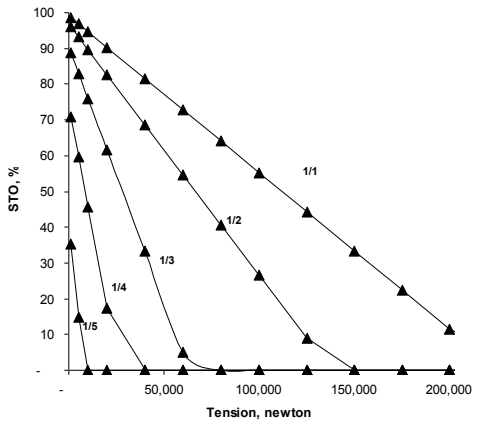

$\beta = 2$

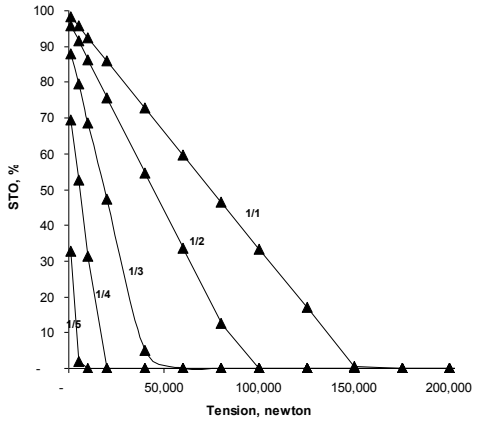

$\beta = 3$

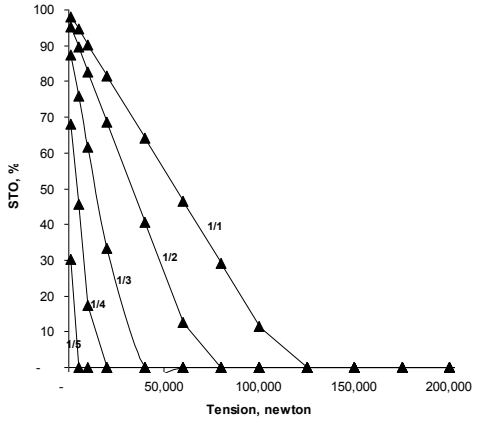

$\beta = 4$

Figure 26 Casing standoff (STO) for a straight, inclined wellbore with axial tension. D_2 =14 ¾" and D_0 = 10 ¾".

3.5.4 Primary cementing techniques and fluid velocity (pump flow rate)

The process to determine the cementing practices most likely employed is based on the assumption that the recommended cementing practices at the time of wellbore construction were followed. Thus, if the age of the wellbore is known, a complete picture of the displacement process can be obtained.

Table 16 gives recommended practices for improved mud displacement and cementing.

Table 16 Recommended cementing practices.

Period	Standard practice
< 1960	Mud/cement (Laminar flow)
1960 - 1975	Mud/lead/tail cement (Turbulent flow)
>1975	Mud/spacer/cement (Turbulent flow)

Flow rate (Q_D) on cementing jobs has historically been approximately 1 m^3/min (6.3 bbl/min). However, pumping and related surface equipment have been modified to accommodate higher cement-displacement rates, so displacement rates as high as 3 m^3/min (18.9 bbl/min) are currently not uncommon (Smith, 1990). Whenever possible, the pumping rate during cementing should be obtained from field records. In many cases,

however, the consistency and quality of record keeping for drilled wells varies considerably, from excellent to nonexistent, particularly for older wells. Under such circumstances, flow rate can be assumed to be 1 m^3/min.

3.5.5 Pre-flushes

When pre-flushes (wash, spacer, etc) are known to have been used during cementing, their rheological characteristics are of interest because their properties relative to that of the mud will have a great impact on displacement efficiency. Field data must be used whenever possible, however fluid rheology is often not available. In such cases, assume that recommended practices have been used. Table 17 lists properties of some pre-flushes that are recommended for optimization of the primary cementing job. In general, they should have the lowest plastic viscosity/yield point ratio acceptable for the system (Nelson, 1990).

Table 17 Properties of recommended pre-flushes (from Nelson, 1990).

Property	Wash	Spacer	Lead slurry
Yield point (lb./100 sq. ft.)	0	1	5
Plastic viscosity (cp)	1	10	15

The type of pre-flush that was used must be known in order to select the proper fluid rheology. Since fluid description is generally limited to the

name of the product use Table 18 to determine the type of pre-flush (washer or spacer) used during cementing.

Table 18 Spacers and chemical washers (modified from WorldOil.com)

Type	Subtype	Description	Product
Chemical wash (not weighted)	Well drilled with water-based mud	Reactive: containing sodium silicate	Flowcheck, floguard, superflush, thix-seal flush, zonelock
		Aqueous: containing surfactants and solvents	Mudclean, MRS-2, mudflush, nowflush6, CW-7
		Aqueous: containing surfactants and solvents plus agents to reduce fluid loss	Mudsweep, ultraflush, alpha pre-flush, CW-100
		Nonaqueous: containing surfactants and solvents in hydrocarbon carrier fluid	N-Ver-Sperse
	Well drilled with oil-based mud		Alpha pre-flush, nowflush6, CW-8
	Cold environments	Aqueous: containing freeze-point depressant	
Spacer (weighted)	Aqueous	Formulated for turbulent-flow regime at low pump rates	MCS-2, Ultraflush II, turbloflo3, dual spacer, sdspacer, mudpushXT
		Formulated for laminar-flow regime under most cementing conditions	Tunned spacer, supersweep, mudpushXL
		Formulated for a non-specific regime	Alphaspacer, mudpushWHT
	Emulsion	Water continuous (external) phase	APS-1, mudpushXEO
		Oil continuous (external) phase	OB-1, RSB, SAM-4
		Solvent continuous (external) phase	Turbo solvent

	Well drilled with oil-based mud	MCS-3, RSB, turbosolvent, dualspacer, alphaspacer, SAM-4, nowflush5, mudpushXLO
	Compatible with high salt concentrations	Dual spacer, dual spacerE, mudpushXS

3.5.6 Casing movement

The effect of casing movement on mud-displacement efficiency can be calculated provided the type of movement is known. There are two basic types of casing movement: reciprocation and rotation. Although casing rotation is used in some parts of the world, reciprocation is most common, so only the effect of this type of movement is considered here.

Efficiency increase during reciprocation is related to a displacement-velocity increase (fluid relative to pipe) equal to the speed of the downstroke. This equivalent displacement velocity (Ve) depends on the casing end, but it is only significant for closed-end casing; thus, only this case is considered.

Equivalent velocity (Ve) can be calculated from the mathematical model described in equation [11]. This equation was derived by Liu (2001) and used to generate Figure 27. The effect of alternation of standoff, as the pipe translates laterally due to side thrust from moving centralizers and

collars across wellbore irregularities, is not considered (McLean et al., 1967, Childers, 1968, and Clark and Carter, 1973).

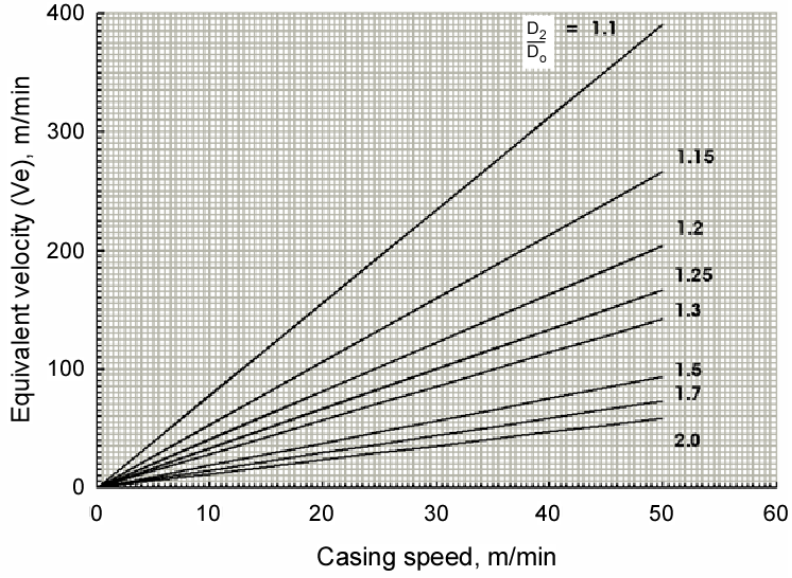

Figure 27 Equivalent mud velocity during movement of closed-end casing.

As an alternative to limited data on casing movement, typical velocities employed for casing reciprocation can be used: a full cycle completed in 1–2 minutes and a stroke length generally of about 1–2 joints (6–12 m), which is approximately equal to a casing speed ranging from 12 to 24 m/min. This is based on guidelines that have been developed over the years for improving cementing in the industry (Sauer, 1987, Nelson, 1990, and Smith, 1990).

With the equivalent mud velocity (Ve) and the annular space geometry (D_2, D_o), an equivalent mud-flow rate (Qe) can be calculated and added to the displacement mud-flow rate (Q_D).

3.6 Geomechanical Damage

Rock-mass classification schemes for tunnelling and underground mining have been developing during the past 100 years. Among the most popular schemes used are the tunnelling quality index (Q-Value; Barton et al., 1974) and the rock mass rating (RMR; Bieniawski, 1976). Although these schemes were developed for civil engineering problems and work appropriately for their application, they are not readily adaptable for wellbore-integrity applications because they do not take into consideration such factors as post-failure behaviour of the rock, filter-cake efficiency, and temperature.

A general method for providing a quantitative estimate of damage on the near-wellbore rock, annular cement and wellbore interfaces was developed and described in the following three sections. This methodology follows the same logic involved in developing the rock-mass classification schemes used for tunnels, in that it assigns a rating to each of the components affecting wellbore integrity.

3.6.1 Near-wellbore region

A well-stability rating (Nw) is proposed for the determination of the quality of the rock and to provide information on deformation properties of the

rock mass. This system takes some of the basic elements of the RMR and Q systems (as defined by Bieniaswki and Barton, respectively) and adjusts them to account for support pressure, filter-cake efficiency, and the effects of temperature. The result is a six-parameter description of rock masses, each parameter having several ratings of importance. The proposed parameters are stress-reduction factor, discontinuity spacing, discontinuity orientation, rock strength, support pressure, and temperature. This well-stability rating system is presented in Table 19, which gives the ratings for each of the six parameters. These ratings are then summed to give a value of Nw.

This method was developed through exhaustive analysis of more than one hundred computer simulations and case records. Several months were spent on their evaluation and development of improved numerical scales, until a consistent picture of rock-mass quality was obtained.

The range of possible rating values (approx. 0–100) encompasses the entire spectrum of wellbore-system quality, from highly deteriorated up to a completely intact system.

Table 19 Well-stability rating (Nw).

1 Stress reduction factor	SRF				
a. competent rock [stress problem]					
Stress level (Po/UCS)	> 0.05	0.05 - 0.1	0.1 - 0.5	0.5 - 1	1 - 3
Rating	27	20	18	12	7
b. incompetent rock [squeezing problem]					
Squeezing level (Po/UCS)				3 - 5	> 5
Rating				4	2
c. Swelling rock [chemical problem]					
Swelling activity (Sa)[1]				mild	high
Rating				4	2
[1] Use Figure 36 for detailed assessment					
A. Stress anisotropy					
Anisotropy ratio (σ_1/σ_3)			1	1 - 2	2 - 5
Rating			1	0.8	0.6

Note i) For anisotropic virgin stress field reduce compressive strength (UCS) by using correction factor
ii) σ_1 and σ_3 are the major and minor principal stresses in the plane of the borehole

2 Discontinuity spacing	Js				
Range of values	> 0.3m	0.3 - 0.1	0.1 - 0.05m	0.0 - 0.025m	< 0.025m
Rating	10	7		2	-4

3	Discontinuity dip	Jd			
	Range of values		flat	dipping	vertical
	Rating		-5	-5	0

Note i) Dip: flat 0 - 20°; dipping: 20 - 50°; and vertical: 50 - 90°

4	Uniaxial compressive strength	UCS				
	Range of values	> 100 MPa	100 - 50 MPa	50 - 20 MPa	20 -5 MPa	< 5 MPa
	Rating	10	8	4	1	0

5	Support pressure $h^*(p_w-u)/Po$	Jp				
	Range of values	> 0.8	0.8 - 0.5	0.5 - 0.2	0.2 - 0.05	< 0.05
	Rating	27	21	16	9	6
	B. Cake efficiency					
	Class			> 0.5	0.5 - 0.2	< 0.2
	Rating			10	7	5

Note i) Support pressure: h cake efficiency (); pw drill fluid pressure (drill report/assume value); u pore pressure (Table 8); Po mean stress

6 Temperature		Jt				
Range of values, ΔT		-40 °C	-20 °C	0 °C	+20 °C	+40 °C
Rating	UCS, MPa < 20	6	3	1	-2	-4
	20 - 75	8	6	4	3	1
	75 - 120	16	13	9	8	7

Note i) ΔT = Ta-To
Where Ta = Temperature of mud in annulus Equation [35]
To = Original formation temperature Equation[38]

Based on the value of Nw, the rock mass can be classified as good, fair, poor and very poor. These classes can be related to the degree of damage and alteration of flow properties in the near-wellbore region. Table 20 gives the ranges of Nw for the rock-integrity classes.

Table 20 Definition of rock-integrity classes.

Class number	I	II	III	IV
Rating	100 ← 61	60 ← 41	40 ← 21	< 21
Description	Good	Fair	Poor	Very poor
Well condition[1]	No breakout	Breakout ≤25% of well diameter	Breakout ≥ 25% of well diameter	Squeezing (large convergency)
		No impac□ on drilling	Impact on drilling (washing)	Impact on drilling (tight hole)
Flow properties[2]				
Rock post-failure characteristics				

- Brittle	Intact properties	Increase	I□crease	Decrease (1–2 orders of magnitude)
- Ductile		Decrease	Decrease	

Notes: i) Total or partial breakout detachment for the case of brittle rocks.
ii) Permeability increase in brittle rocks of 1–3 orders of magnitude.
iii) Permeability decrease in ductile rocks of 1–2 orders of magnitude.

[1] modified from Tan and Willoughby, 1993
[2] from Charlez, 1997, McLennan and Abou-Sayed, 2002, and Soares and Ferreira, 2002

Table 20 provides a very simple way of immediately identifying the general behaviour of the rock mass in the near-wellbore region. The general shape of the damaged region associated with every rock class is depicted in Figure 28.

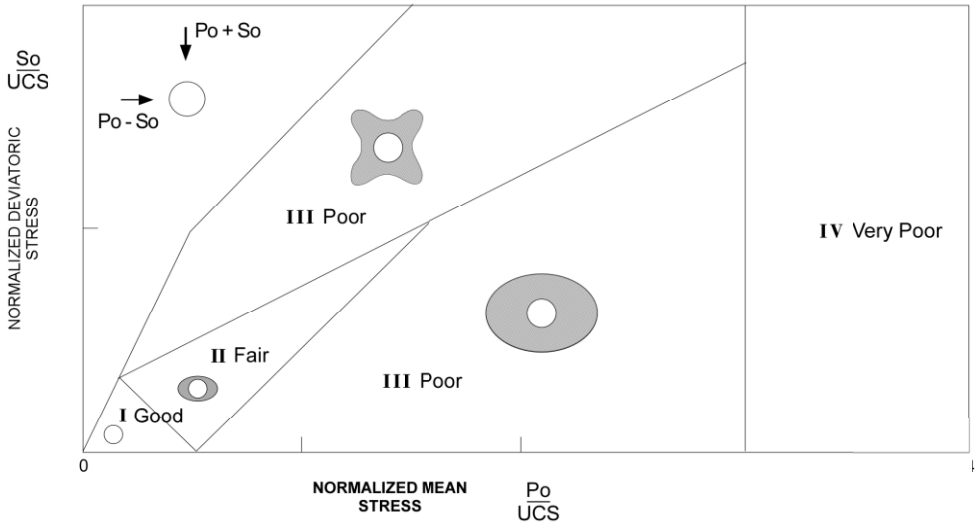

Figure 28 Size and shape of failed rock regions based on rock-integrity classes.

Figure 29 shows the standard procedure developed to calculate the well-stability rating (Nw). An assessment of the required input parameters is followed by calculation of the corresponding ratings.

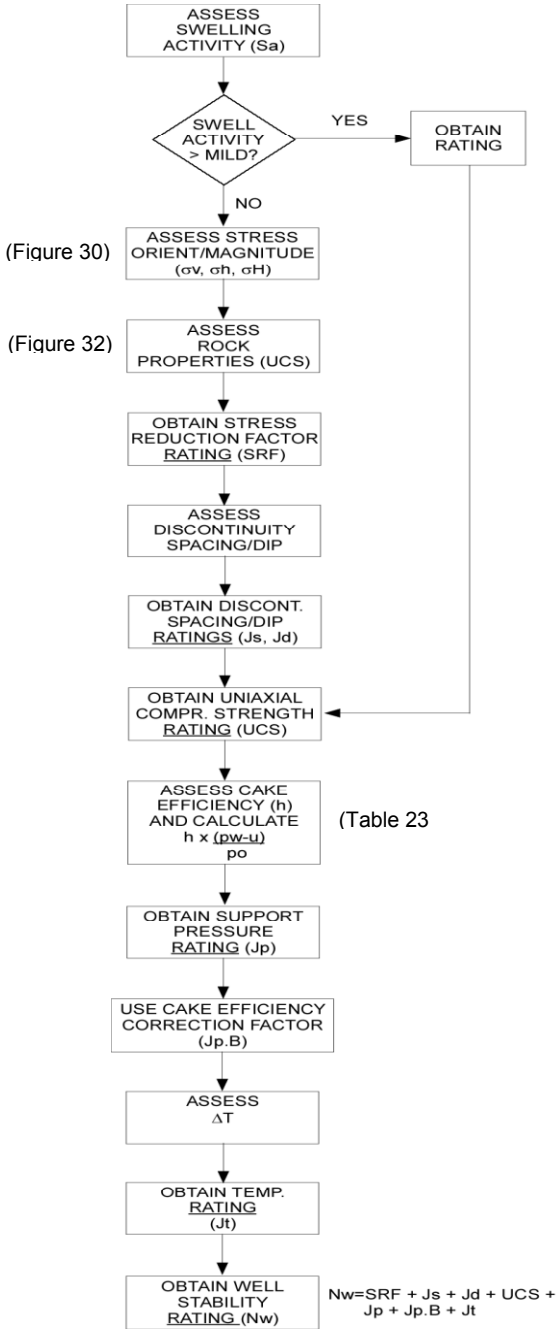

Figure 29 Flow chart for calculating the wellbore-stability rating (Nw).

This process starts by flagging the type of wellbore instability present: mechanical and chemical. If chemical instability occurs, then the key task is to assess swelling potential and osmotic pressures. On the other hand, if mechanical instability is the most likely scenario, then a different set of factors that contribute to bad hole must be considered. These include in-situ stress/ rock strength ratio, discontinuity spacing and dip, support pressure, and temperature.

The approach suggested for evaluating mechanical instability is presented in the next section. The complete process for assessing chemical instability is deferred to a later section.

Mechanical failure

Some detailed basic information (i.e. in situ stress, pore pressure, rock strength) is needed to determine the relative influence of the various factors that contribute to mechanical failure. Some can be measured directly, others can be derived from known quantities, but some must be estimated based on correlations.

Stress reduction factor (SRF - Stress Problem) –

The key parameters for evaluating this factor are simply the principal components of earth stress (assumed to be the vertical and horizontal stresses) and rock strength. Earth stresses can be assessed following the

suggested procedure outlined in Figure 30. Vertical stress, σV, can be obtained by integrating the density through the overburden. However, when logging is not available – such as the case of shallow formations, an exponential extrapolation of vertical stress can be used to model the unlogged region. The minimum horizontal stress, σh, can be obtained based on the known relationship that exists between stress and depth. Three cases are defined:

- Case I $\sigma V < \sigma h < \sigma H$

- Case II $\sigma h < \sigma V < \sigma H$

- Case III $\sigma h < \sigma H < \sigma V$

Case I represents shallow basins, while Case II is characteristic of ultra-deep reservoirs. Case III represents most of the completions in the oil and gas industry (Gil and Roegiers, 2002).

The maximum horizontal stress, σ_H, cannot be determined directly, so stress magnitude must be evaluated from local or regional databases or theoretical correlations (i.e. Shorey's equation, 1994).

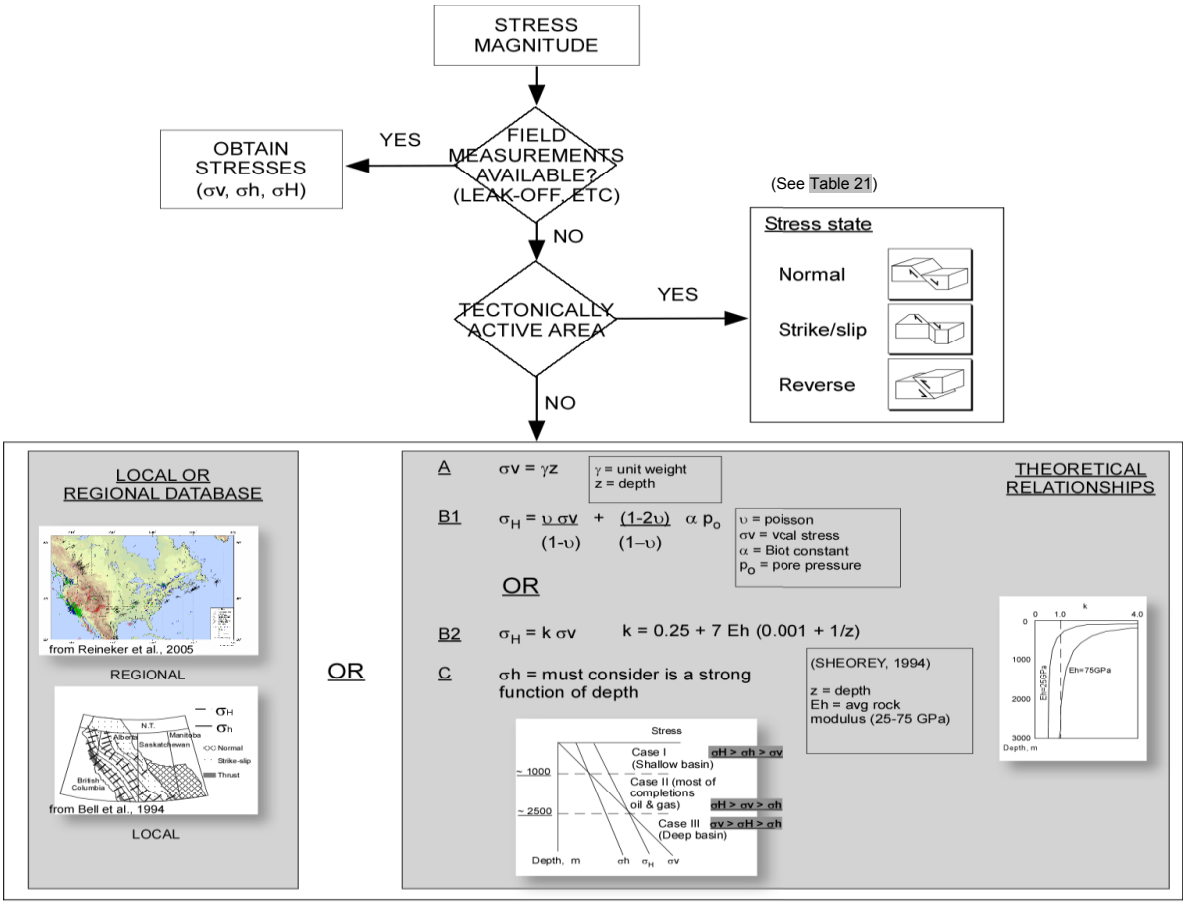

Figure 30 Procedure to facilitate prediction of in situ stress orientation and magnitude.

Stress estimation is based on the assumption that the principal in-situ stresses consist of a vertical stress, which is equal to the overburden weight, and two unequal horizontal stresses, which are a strong function of depth. However, in tectonically active areas, the magnitude of local stresses may be altered. In this case, bounds on the in-situ stress state will be a function of the tectonic condition (normal, strike/slip, reverse). General expressions for the different tectonic cases are available in Table 21.

Table 21 In situ stress bounds[1]

Stress state	Upper bound	Lower bound
Normal	$\frac{\sigma_h}{\sigma_v} = 1, \quad \sigma_h = \sigma_H$	$\frac{\sigma_h}{\sigma_v} = 0.5$
Strike/slip	$\frac{\sigma_H}{\sigma_v} \le \frac{A - C}{B}$	$\frac{\sigma_H}{\sigma_v} \ge 1$
Reverse	$\frac{\sigma_h}{\sigma_v} \le 1$ $\frac{\sigma_H}{\sigma_v}, \frac{\sigma_h}{\sigma_v} \le \frac{A - C}{B}$	$\frac{\sigma_h}{\sigma_v} \ge \frac{B + C}{A}$ $\frac{\sigma_h}{\sigma_v}, \frac{\sigma_H}{\sigma_v} \ge 1$

$A = 7 - \sin\phi \qquad B = 5 - 3\sin\phi \qquad C = \frac{[2p_o(1+\sin\phi) + 2(ds - c\cos\phi)]}{\sigma_v}$

[1] modified from Aadnøy and Hansen (2005)

Rock strength magnitude can be measured using different techniques (Figure 31).

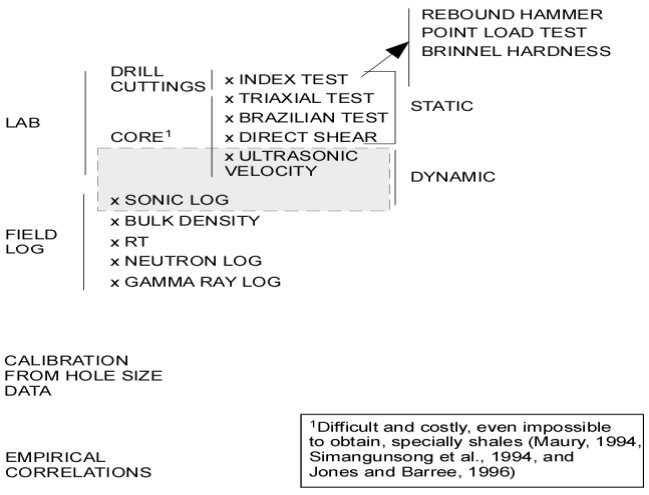

Figure 31 Techniques for measuring or estimating rock mechanical properties.

One is through destructive testing of core samples. In the absence of cores, rock strength can be estimated from open-hole size data (Figure

32a). Rock strength can also be estimated from porosity correlations (Figure 32b).

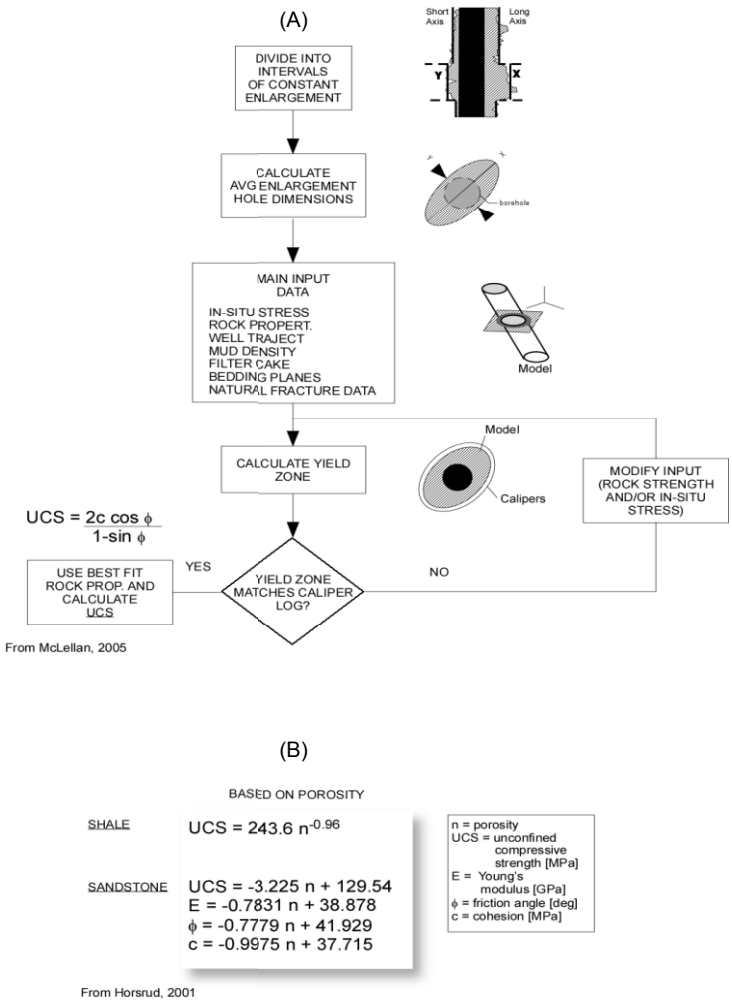

Figure 32 Procedure to facilitate prediction of rock mechanical properties from empirical correlations (porosity), index testing on drill cuttings, or calibration from hole size.

A more common method of measuring rock strength is through Young's modulus recorded by acoustic logs. However, there is a difference this dynamic Young's modulus and the static Young's modulus in a test core material. Thus, to use this information to obtain rock strength, two

correlations are used. First in the conversion from dynamic modulus to static modulus, then in the transformation from static modulus to unconfined compressive strength (UCS - Figure 33).

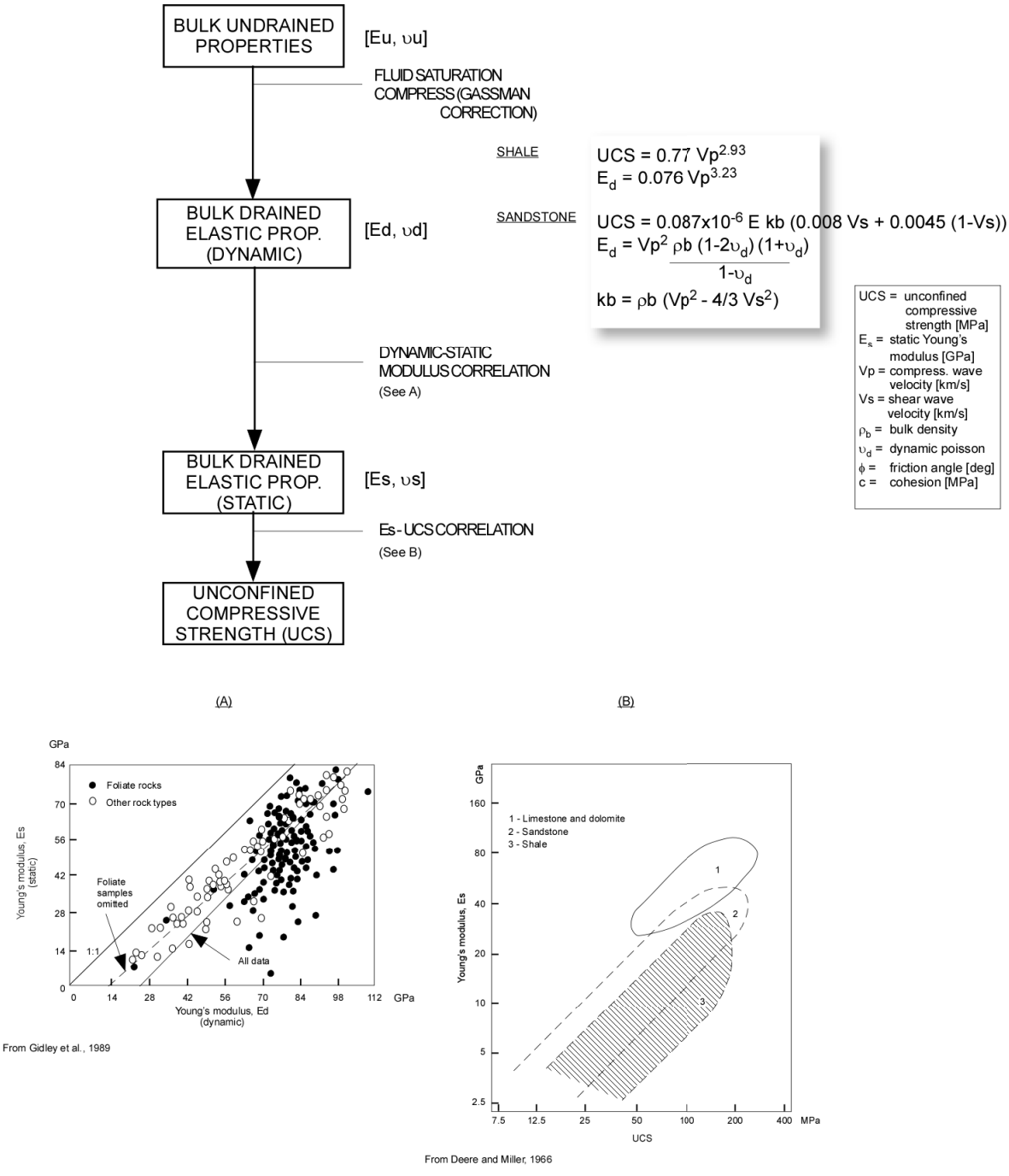

Figure 33 Procedure to facilitate prediction of static elastic properties of rock from ultrasonic measurements.

Discontinuity spacing and dip – Several techniques can be used to evaluate fractures. They include:

- Ultrasonic borehole imager (UBI),

- Formation micro-imager (FMI),

- Azimuthal resistivity imager (ARI), and

- Core analysis.

The UBI, FMI and ARI tools produce high-resolution images of the formation. These images can show different fracture attributes, often allowing discrimination between open and closed fractures, and even between natural and hydraulically induced fractures. Therefore, making them ideal for fracture detection. Core samples offer a direct way to evaluate fractures, however, in some cases, they might available only at some depths, or not available at all. In such situations, UBI, FMI and ARI data will be needed to supplement fracture information.

Support pressure – The key parameters for evaluating this factor are simply the internal support pressure (pw), the pore pressure (u), in-situ stresses (Po), and filter cake efficiency (h). Internal support pressure (pw), and formation pore pressure (u) can be determined through the methods already discussed in section 3.4.2. In-situ stresses can be determined using the flow chart from Figure 30.

Filter cake efficiency is evaluated following a two-step process. The first step is to determine cake efficiency class (Table 22).

Table 22 Filter-cake efficiency classes for formations of high (10^{-3} to 10^{-1} D) and low (10^{-9} to 10^{-3} D) permeability.

Formation permeability (kf, D)		Mud type WBM				OBM
		No additives	Additives A	Blocking B	Blocking C	
		Efficiency Class				
High (10^{-3} to 10^{1})		Low	n/a	High to intermediate [1]	High	n/a
Low (10^{-9} to 10^{-3})	Unfractured	Low	n/a	n/a	High	High
	Fractured	Low	Low	High to Low	High	Low

[1] use Figure 34 for detailed assessment
A, cementituous
B, undeformable (flaky, fibrous, granular)
, deformable (resin, high molecular weight)

Three efficiency classes are possible: high, intermediate, and low. Efficiency class will be a function of mud type (oil-base, water-base) and formation permeability. For oil-base muds (OBM), fluid invasion is prevented by high capillary entry. Thus, OBM are more suitable for reducing pore pressure penetration in low permeability formations (unfractured shales). For water-base muds, fluid invasion is prevented by pore plugging. A great variety of plugging additives can be used, but in general, they can be divided into three categories: cementitious,

undeformable and deformable. Cementitious additives are commonly used in low permeability fractured formations, but are not very efficient at preventing pore pressure build up in the formation. Conversely, deformable additives are used in any type of formation (high and low permeability), providing an impervious wall coating to fluid invasion. Undeformable additives are also used in any type of formation, being the only additive that will form a filter cake. Efficiency for this type of additive ranges from low to high and it will be a function of filter cake to formation permeability ratio (kc/kf - Figure 34)

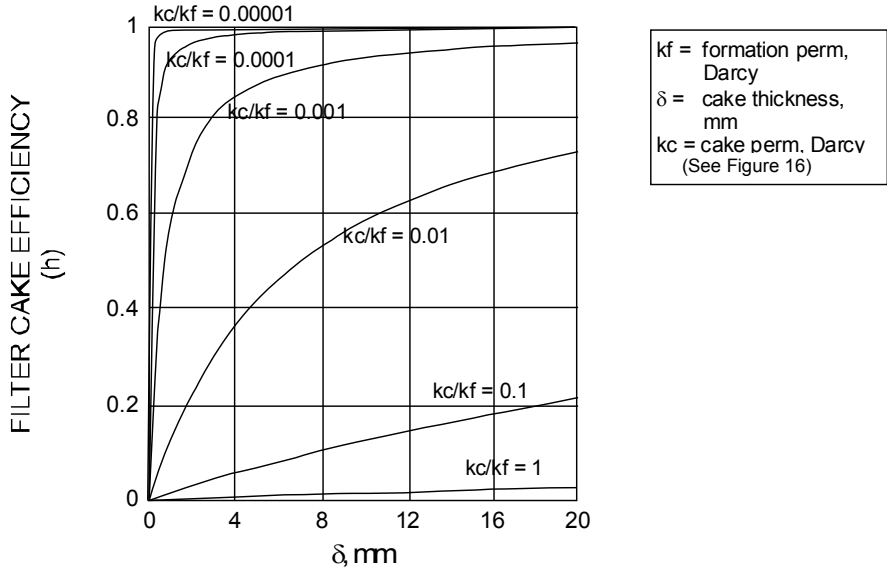

Figure 34 Filter-cake efficiency for undeformable cake additives on permeable formations (10^{-3} to 10^{1} D), from McLellan and Wang, 1994.

With the cake efficiency class defined, the next step is to determine its efficiency factor (h)

Table 23 Filter-cake efficiency factor (h) as a function of efficiency class.

Efficiency class	Cake efficiency factor (h)
High	> 0.5
Intermediate	0.5 - 0.2
Low	< 0.2

Thermal failure

Temperature factor (Jt) –The effect of drilling-fluid temperature on wellbore-stability can be calculated using the difference in temperature between annular mud (Ta) and the surrounding formation (To). Annular mud temperature is easy to calculate using the relationship established by Tang and Luo (1998).

$$\text{if } z \le \tfrac{2}{3}L: \qquad T_a = T_i + Gm_1 \times z$$

$$\text{if } z > \tfrac{2}{3}L: \qquad T_a = T_i + Gm_1 \times \frac{2}{3}L + Gm_2 \times (z - \frac{2}{3}L),$$

[35]

where Ti is the inlet mud temperature, L is well depth, z is depth and Gm is the mud-temperature gradient. This expression assumes that mud has been circulated for more than the theoretical time (6 hours) to reach dynamic thermal equilibrium; thus, it will only provide values at steady state circulation conditions.

Two distinct of mud-temperature gradients can be identified (Figure 35): one extending from surface to about two-thirds of the well length (Gm_1), the depth at which mud starts to cool off , and the second for greater depths (Gm_2).

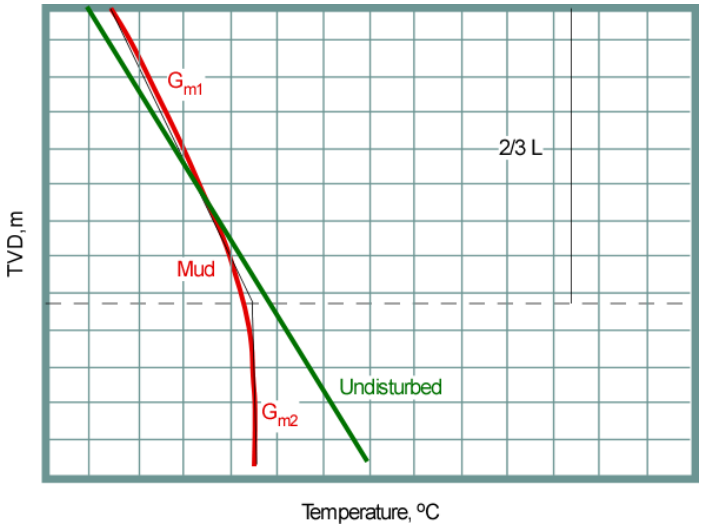

Figure 35 Typical mud-temperature profile.

Based on this the general equation for mud-temperature gradient can be written as:

$$Gm_i = 0.019 \times F_{Qi} \times F_{\rho mi} \times F_{cmi} \times F_{Gti} \times F_{Li},$$

[36]

where F_{Qi}, $F_{\rho mi}$, F_{cmi}, F_{Gti}, F_{Li} are weight independent functions; Q is mud-flow rate, ρm is mud density, cm is mud specific heat, Gt is geothermal gradient, and L is well length; and i = 1, 2. Each function corresponds to the influence of one mud-flow rate, mud density, mud specific heat,

geothermal gradient and well length with temperature gradient. The various functions were built from the equation

$$T_a = \beta_1(B\varsigma_1 + 1)e^{\varsigma 1 \times Z} + \beta_2(B\varsigma_2 + 1)e^{\varsigma 2 \times Z} + Gt \times Z + T_s + T_{mf}$$

[37]

All the constants in this equation and the method to derive its analytical solution are presented in Tang and Luo, 1998. In order to build the weight functions, a reference value was defined. In these reference conditions, the value of the various weight functions is equal to one. Values of the various functions are given in Tables 27 and 28.

Table 24 Functions that define the mud-temperature gradient Gm_1.

1	Flow rate	F_{Q1}		
	Range of values (m^3/min)	3	1	0.5
	Rating	0.40	1.00	1.25

2	Mud density	$F_{\rho m1}$		
	Range of values (kg/m^3)	1000	1300	2000
	Rating	1.21	1.00	0.65

3	Mud specific heat	F_{cm1}		
	Range of values (J/kg.°C)	1600	1700	2500
	Rating	1.05	1.00	0.70

4	Geothermal gradient	F_{Gt1}		
	Range of values (°C/m)	.015	.019	.030
	Rating	0.85	1.00	1.35

5	Well depth	F_{L1}		
	Range of values (m)	1000	4500	5000
	Rating	0.30	1.00	1.05

Table 25 Functions that define the mud-temperature gradient Gm_2.

1	Flow rate	F_{Q2}		
	Range of values (m^3/min)	3	1	0.5
	Rating	0.10	1.00	1.70

2	Mud density	$F_{\rho m2}$		
	Range of values (kg/m^3)	1000	1300	2000
	Rating	1.3□	1.00	0.50

3	Mud specific heat	F_{cm2}		
	Range of values (J/kg.°C)	1600	1700	2500
	Rating	1.05	1.00	0.50

4	Geothermal gradient	F_{Gt2}		
	Range of values (°C/m)	.015	.019	.030
	Rating	0.85	1.00	1.45

5	Well depth	F_{L2}		
	Range of values (m)	1000	4500	5000
	Rating	0.20	1.00	1.05

The original formation temperature at any depth is described by

$$T_o = T_s + Gt \times z,$$

[38]

where T_s is the surface formation temperature, z is depth, and Gt is the geothermal gradient. The geothermal gradient varies considerably with tectonic setting and the thermal properties of the rock, but gradients typically vary from 15 to 30°C/km for tectonically stable Precambrian shield areas and passive sedimentary basins (Cengage, 2003).

Once the details of well temperature are known, the effect of the thermal stress, occurring during heating or cooling, on wellbore stability can be computed from the relationship between ΔT and the rock modulus E (Table 19).

Chemical failure

Stress reduction factor (SRF – chemical problem) – The problems of wellbore chemical instability in shales can be classified into two groups: swelling and osmotic pressure.

Swelling

Many factors contribute to swelling; however, they can be categorized into mud- and shale-related factors. The first category includes salt type and

concentration (mud type). The second category includes specific surface and cation-exchange capacity (clay composition). Since swelling is a complex problem, some simplifications had to be made in order to develop a procedure capable of providing a qualitative assessment of this phenomenon (Figure 36).

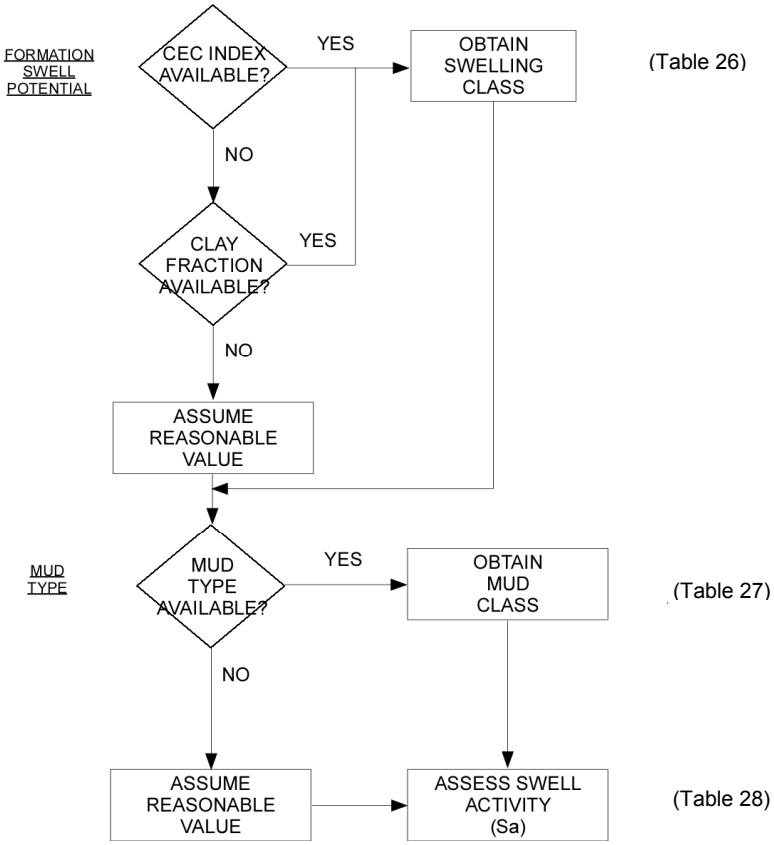

Figure 36 Procedure to facilitate prediction of swelling activity.

The first step is to determine the swelling class (Table 26). Three classes are possible: low, moderate, and high, and it will depend on the type of clay present (clay ffraction). When direct measurement of this quantity is

not available, swelling class can be determined from methylene blue test data. This test is usually reported as the cation exchange capacity (CEC).

Table 26 Guidelines for assessment of shale-swelling class (modified from Kariuki et al, 2003).

Swelling class	Activity index (meq/100 g)	Clay fraction
Low	< 10	Kaolinite (> 50)
Moderate	10 - 40	Illite (> 25)
High	> 40	Smectite (> 50)

The second step is to determine mud class. Based on its shale-swelling control ability, mud can be classified in: type I, type II and type III fluids (Van Oort, 2002). Their ability to stabilize swelling increases with type, so type III fluids are best able to prevent swelling (Table 27).

Table 27 Guidelines for assessment of mud class (modified from Van Oort, 2002).

Mud class	Mud system	
Type I	Non-dispersed	Lignite
	Dispersed	Lignosulfonate
		Spud
		Freshwater
		Gel-chem
		Polymer
Type II	Inhibitive	KCl
		KCl - PHPA

Type III	Non-invading -Plugging -High capillary entry	$CaCl_2/MgCl_2$ Saccharide Gypsum Lime mud Tame (Glycol) Silicate Invert emulsion Oil Synthetic

With the swelling and mud class defined, the final step is then to evaluate the swell activity (Sa - Table 28).

Table 28 Guidelines for assessment of swelling activity (Sa).

		Swelling class		
		Low	Moderate	High
Mud class	Type I	Mild	High	High
	Type II	Low	Mild	High
	Type III	Low	Low	Mild

Osmotic pressure

Osmosis is the process whereby water can migrate through porous media due to a chemical imbalance between drilling fluid and the native pore fluid in the shale. Typically, in the absence of any other external force, water flows from less saline to more saline fluid (Van Oort et al., 1996, Fam and

Dusseault, 1998, and Schlemmer et al., 2002). When the water activity of the drilling fluid (a_{df}) is higher than the shale activity (a_{sh}), an osmotic flow of drilling fluid into the formation will increase the pore pressure near the wellbore wall, causing a loss of support pressure for the formation and aggravating instability. On the other hand, if fluid flux is out of the formation ($a_{df} < a_{sh}$), the pore pressure near the wellbore wall will decrease. If the osmotic backflow is greater than the flow due to hydraulic gradient (Darcy's flow), there will be a net flow of water out of the formation into the wellbore. This will result in a lowering of the pore pressure below the in situ value and dehydration of the formation. This is beneficial because it increases the effective support of the drilling fluid on the borehole wall (Tan et al., 1998, Manohar, 1999, Fjaer et al., 2002, and Schlemmer et al., 2002). Therefore, the maximum osmotic pressure of a specific shale is an important factor in borehole stability and must be assessed (Fam and Dusseault, 1998).

The change in pore pressure caused by the difference in chemical potential (osmosis) can be calculated using

$$\Delta Pm = \frac{RT_a}{V} \ln\left(\frac{a_{df}}{a_{sh}}\right) \times \sigma ,$$

[39]

where V represents the mean partial molar volume of water on either side of the membrane, R is the gas constant, T_a is mud temperature, and a_{df}

and a_{sh} denote activity of the drill fluid and shale pore fluid, respectively. The coefficient σ represents the efficiency of the osmotic process and is usually expressed as a membrane efficiency. This coefficient depends on many factors: shale type, clay content, pore size, and in situ stresses. Use Table 29 when measured membrane-efficiency values are not available.

Table 29 Membrane types (modified from Schlemmer et al., 2002).

Membrane type	Mud system	σ	ΔPm (MPa)
Low permeability			
I	Non-dispersed/dispersed	0	0
II	Inhibitive	< 0.2	6.9
IIIa	Non-invading -Plugging	> 0.5	27.6
IIIb	- High capillary entry	1	8.3
High permeability			
Dual-permeability systems with (micro)-fractures that constitute preferential flow paths for convection, bypassing the selective shale matrix (Van Oort, 1996)		0	0

Shales are extremely difficult to characterize on a practical basis; as a result, very often little information is available on their chemical properties. In these cases, one can make a reasonable assumption about the magnitude of the generated osmotic pressure based on engineering judgment and information from other sources, such as the property correlations provided in Table 29 (Tan et al., 1998).

The alteration in the near-wellbore pore pressure caused by osmosis can then be integrated into calculation of the support-pressure factor (h (p_w-u)/Po). This is done by offsetting of virgin pore pressure (u) by the change in osmotic pressure (ΔP_m).

3.6.2 Annular cement

Casing support and zonal isolation are the most critical functions of annular cement. These are achieved when the drilling fluid is completely removed from the annulus and replaced with competent cement. This cement should have the mechanical properties to withstand stresses from various down-hole operations during the life of the well.

Conventional calculations of cement integrity, which use only compressive strength as the quality indicator, are both practical for day-to-day use and accurate enough if the cement is not subjected to a large stress change. However, recent studies (Thiercelin et al., 1998, Bosma et al., 1999, and

Ravi et al., 2002) have shown that, when the change in stress is significant, the integrity of cement depends on other mechanical properties, such as tensile strength and Young's modulus.

High pressure- or temperature-induced stresses are most often caused by operations inherent in the well's economic life, such as completion, pressure testing, injecting, stimulating, and producing. These large changes and their subsequent effect on the cement are not taken into account when cement is selected (Bosma et al., 1999). However, recent experience has shown that cement could lose its ability to provide zonal isolation after such operations. This failure can create a path for formation fluids to enter the annulus.

Mechanical failure

Clearly, the ability to predict these effects is critical to the successful assessment of cement integrity. A systematic approach (Figure 37) takes into account the two major phases that are vital for the integrity of the cement: drilling and operation. This is done by first assessing the stability of the borehole and then evaluating the integrity of the cement during the subsequent operational loading.

Stability of the borehole can be evaluated by the wellbore-stability rating (Nw), as discussed in Section 3.6.1. Two different borehole scenarios can be presented: stable and unstable.

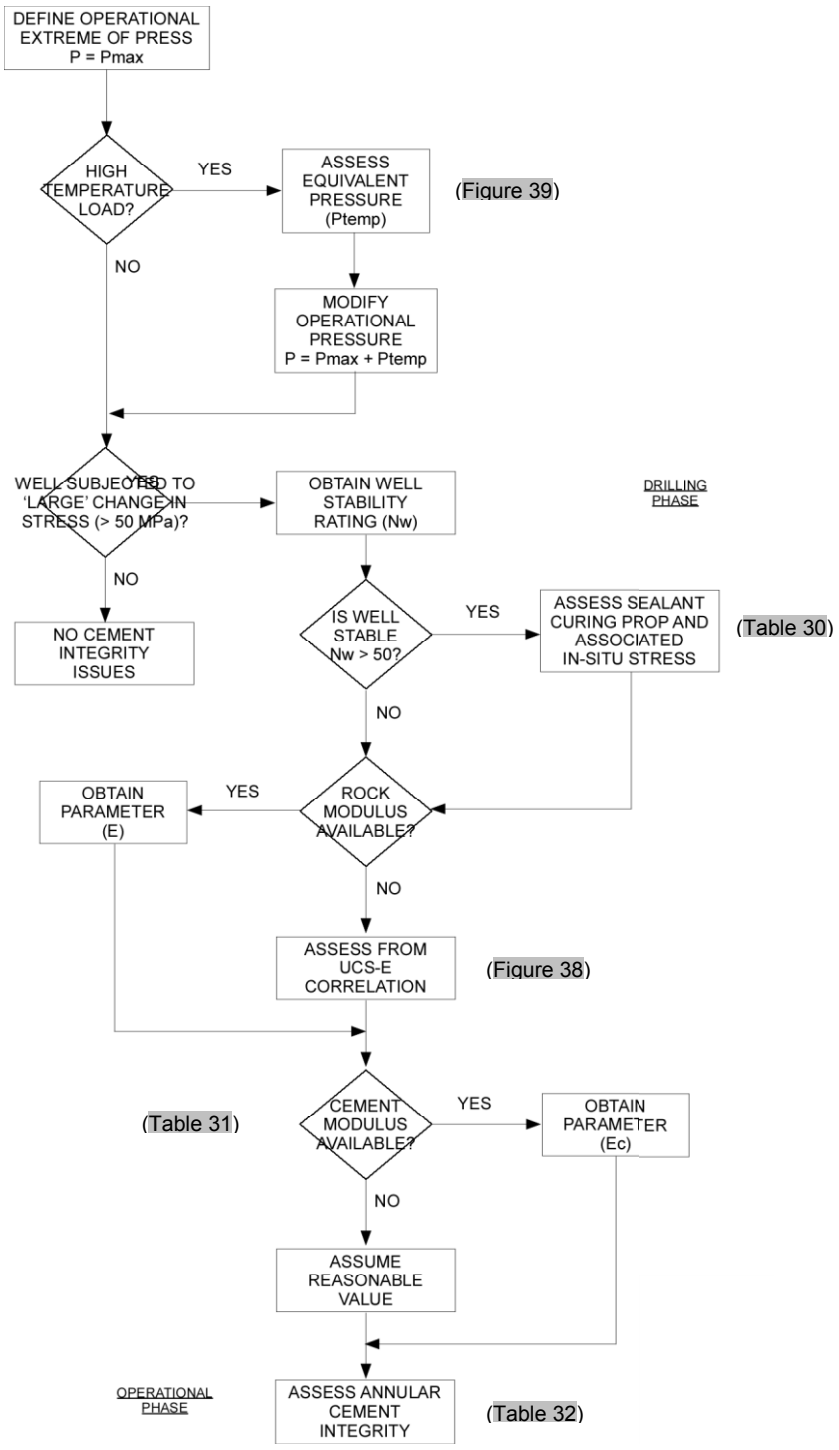

Figure 37 Procedure for prediction of annular cement integrity.

If the borehole is stable, then the resultant in situ stresses in the cement are important because they determine the predominant failure scenario of the cement (Bosma et al., 1999). The in situ stress condition in the cement depends on cement curing characteristics, which can be categorized into the three types as shown in Table 30

Table 30 Cement-curing properties and associated in situ stress (from Bosma et al., 1999).

Type	In situ stress
Shrinking	0
Zero net effect	σs
Expansive	$\sigma s + \sigma e$

Notes: i) σs hydrostatic pressure
ii) σe restrained expansion

If the wellbore is unstable, then it will transmit stresses to the cement. This will result in essentially the same stress condition in the cement sheath, regardless of the curing conditions (Bosma et al., 1999).

The next step is to evaluate the effect of changes in pressure and temperature on the integrity of the well cement during well operation. To fully describe this problem, it is necessary to define the properties of the rock and cement, and the operational details for stimulation, production, and injection. Ideally, the extremes in pressure (P_{max}) and temperature

(T_{max}) should be identified when the operational envelope for the well is being drafted.

Rock and cement properties are normally measured from uniaxial-compression or triaxial-compression loading. However, if cores are unavailable, these properties must be estimated. One technique is to assume a reasonable range of strength properties from correlations such as those provided in Figure 38 for rock and Table 31 for cement.

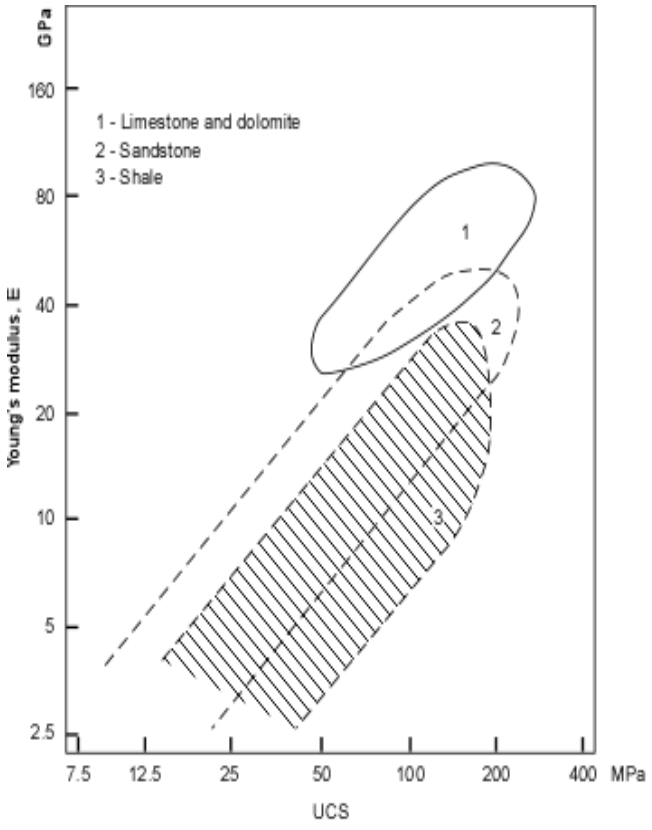

Figure 38 Elastic modulus–compressive strength (UCS) for intact sedimentary rocks (from Deere and Miller, 1966).

Table 31 Elastic modulus for cement.

Type	Elastic modulus (GPa)
Shrinking	6 - 10
Zero net effect	1 - 4
Expansive	2 - 6

Baumgarte et al., 1999, Bosma et al., 1999, LeRoy-Delage et al., 2000, Lullo and Rae, 2000, and Boukelifa et al., 2005

Thermal failure

Increases in temperature can produce significant expansion of the casing. This can result in cracking of the annular cement in much the same manner as excessive inner casing pressure (Goodwin and Crook, 1992). Because of this analogy, the effect of change in temperature of the casing on cement integrity can be evaluated in terms of an equivalent internal pressure (Figure 39).

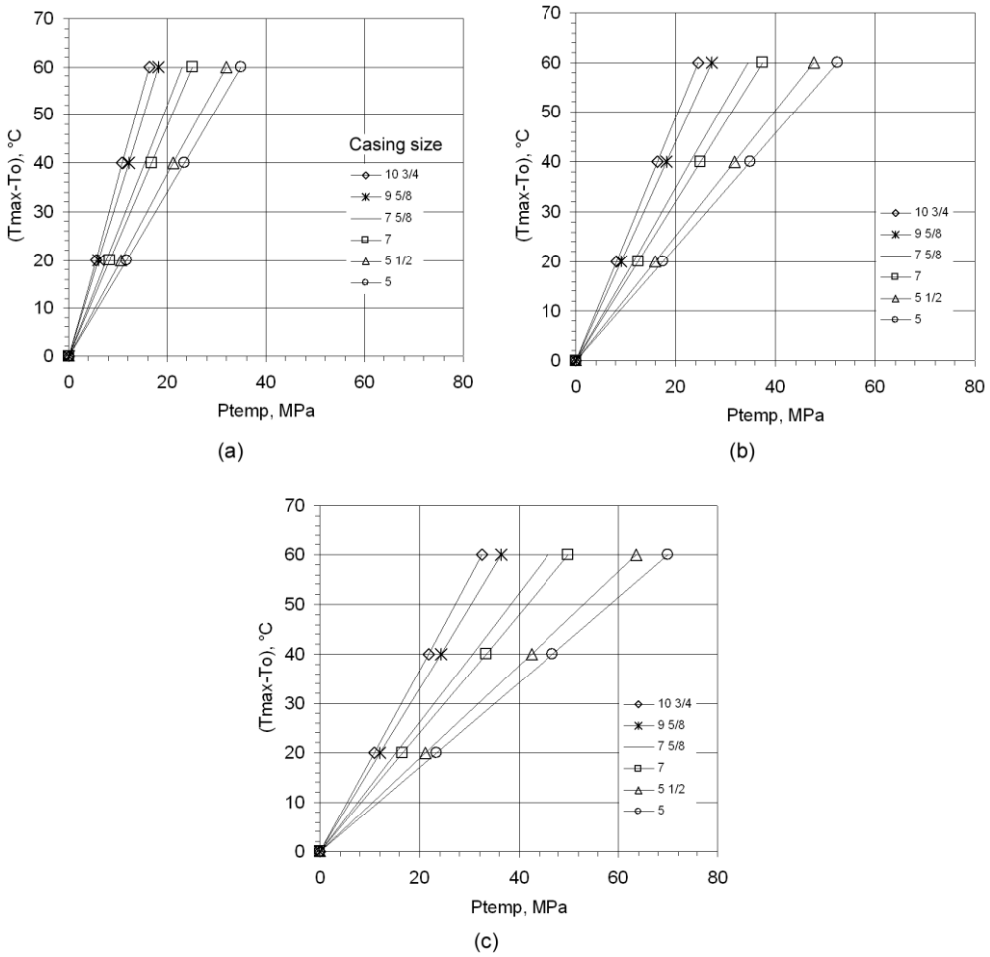

Figure 39 Equivalent internal pressure (Ptemp) as a function of annular temperature differential (Tmax – T_0) for casing thicknesses of a) 10 mm, b) 15 mm, and c) 20 mm.

The values in this figure were generated by calculating the casing expansion due to a differential in temperature (Δd_o), according to

$$\Delta d_o = (Tmax - T_0) \times \Omega \times d_o ,$$

[40]

where casing expansion is set equal to the casing pressure expansion and the equation is then solved for the change in pressure required to produce an equivalent expansion value

$$\Delta P = \frac{\Delta d_o \times E_t \times h_c}{d_o^{\,2}} = P_{temp},$$

[41]

where Δd_o is change in casing outer diameter, T_o is the far-field formation temperature, Ω is the thermal volumetric expansion of steel (2.07 x 10^{-5} in/in 1/°F), E_t is Young's modulus for steel, and h_c is the casing-wall thickness. Equations [40] and [41] are available in Goodwin and Crook (1992).

With all factors now defined, the solution procedure shown in Table 32 is used to study sealant integrity.

Table 32 Sealant-failure mechanism (from Bosma et al., 1999).

Stable	Shrinking	Zero net effect	Expansive
Ec > E	Tensile	Tensile	Tensile
Ec ≈ E	Tensile	Shear	Shear
Ec < E			Shear

Unstable	All cement types
Ec > E	shear
Ec ≈ E	shear
Ec < E	shear

Cement curing characteristics (potential for volumetric change during hydration) for oil-well cements most commonly used are available in Figure 40.

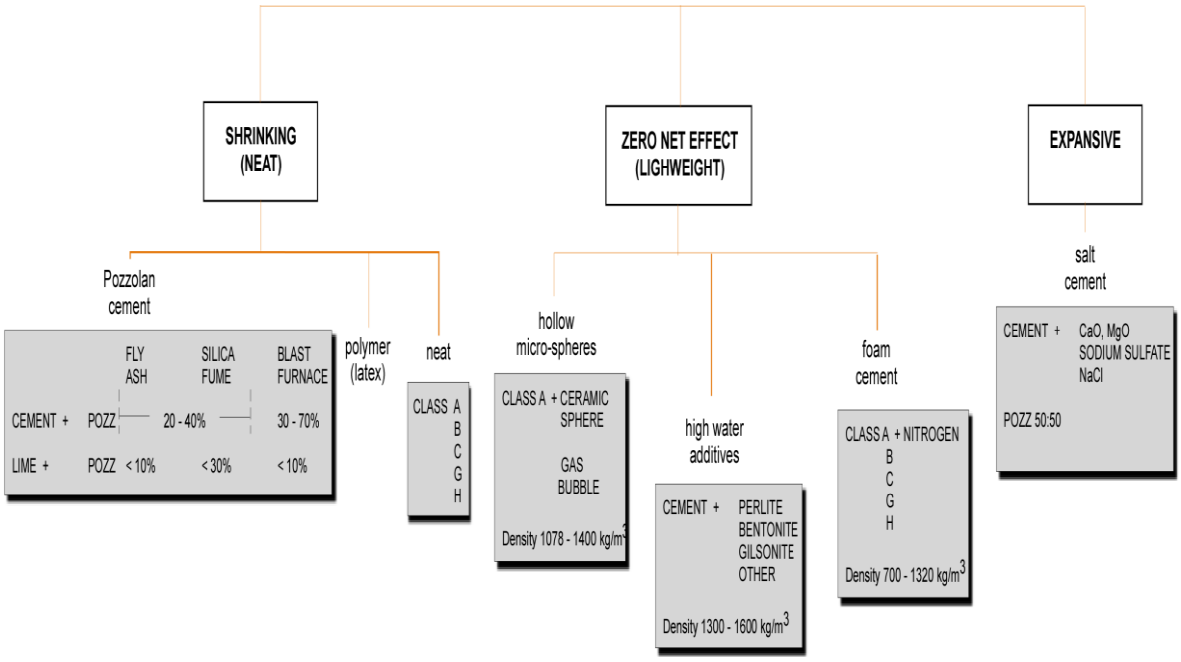

Figure 40 Classification of oil-well cements according to potential for volumetric change during hydration.

3.6.3 Wellbore Interfaces

Modelling debonding at interfaces is difficult because it represents a series of complex physical processes. In spite of this, a methodology has been developed to assess the risk of micro-annulus formation (Figure 41). This simple method uses well data, filter-cake conditions and cement characteristics to estimate micro-annulus formation.

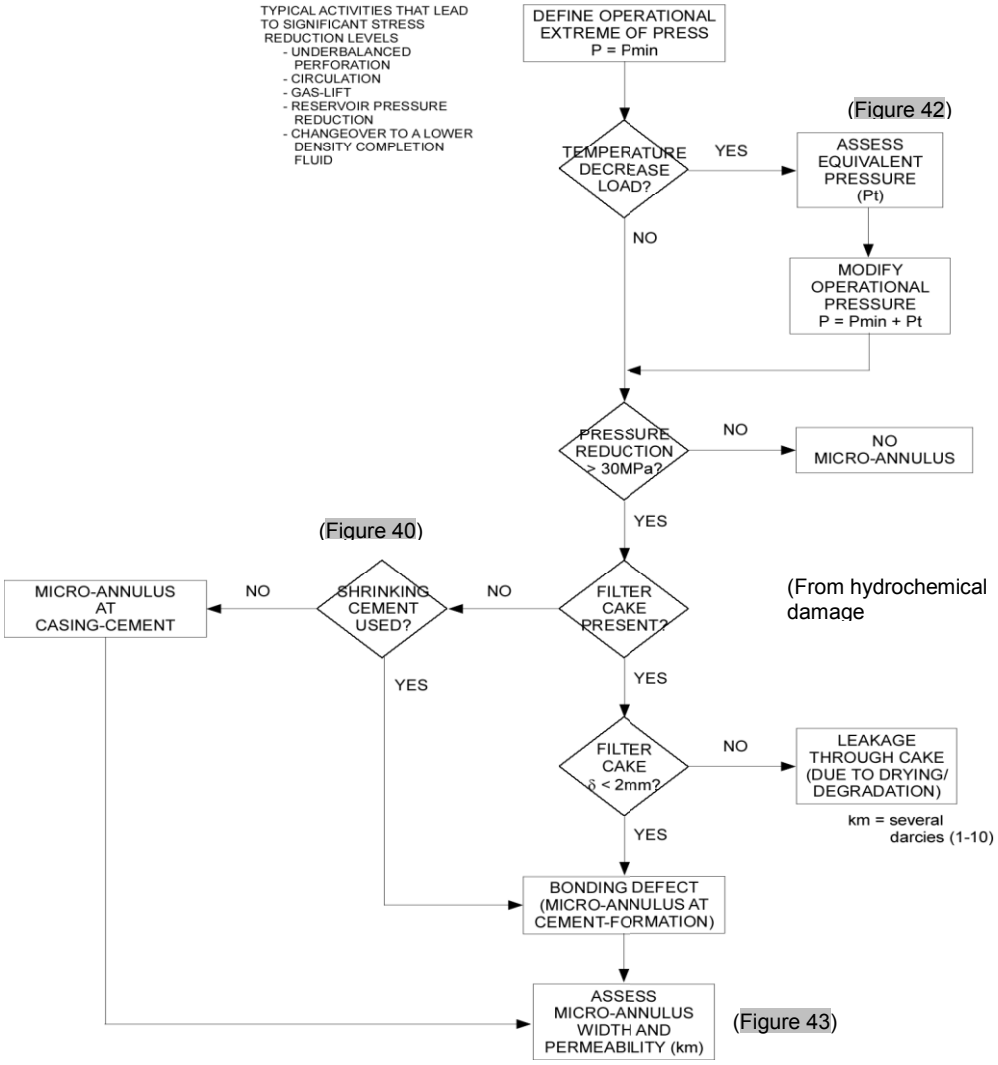

Figure 41 Procedure for predicting micro-annulus development.

The first step in assessing the potential for micro-annulus formation is to define the operational details in terms of pressure and temperature reduction. Ideally, the extremes in pressure (Pmin) and temperature (Tmin) reduction should be identified when the operational envelope for the well is being drafted. The effect of change in temperature of the casing on interface integrity can be evaluated in terms of an equivalent internal pressure (Figure 42).

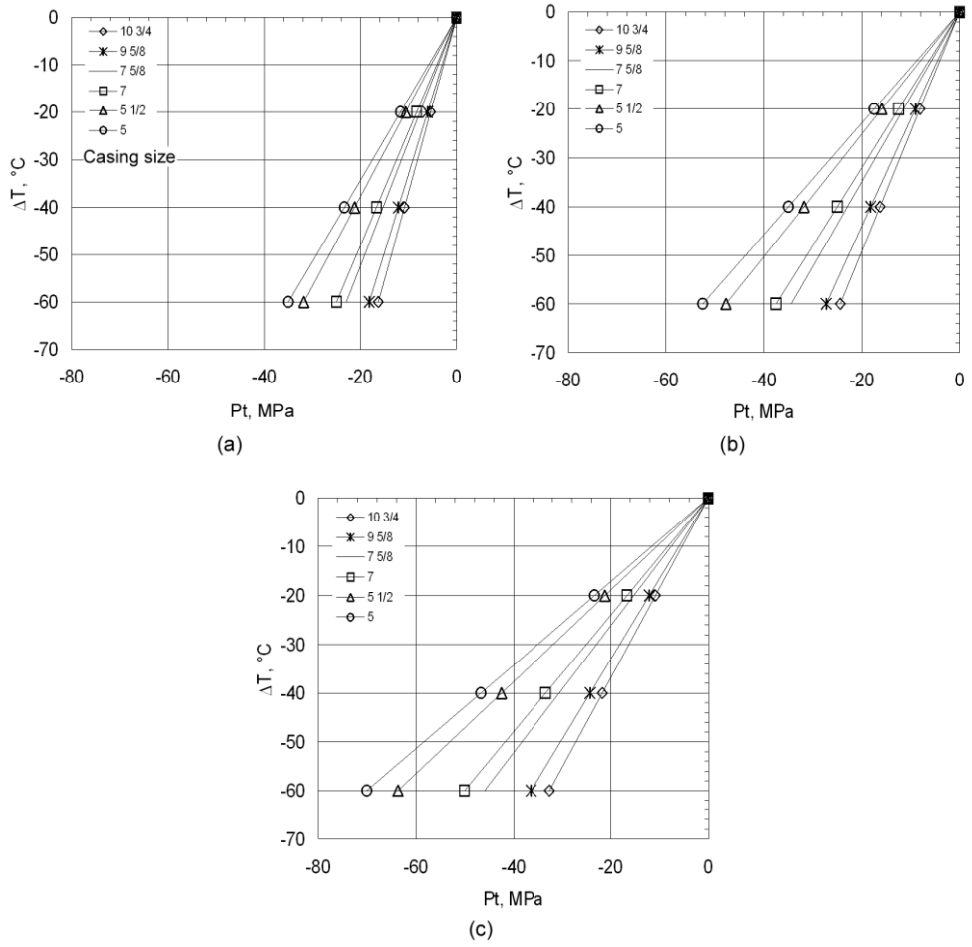

Figure 42 Equivalent internal pressure (Pt) as a function of annular-temperature differential (ΔT) for casing thicknesses of a) 10 mm, b) 15 mm, and c) 20 mm.

These figures were generated using the same assumptions employed during construction of the plots in Figure 39. Other relevant information, such as casing size and thickness, is also collected. Much of the information comes from drilling reports. Such supplementary data may be difficult to find because data-acquisition programs in the past were focused only on logging primarily production. In these cases, Table 12 provides guidance for selection of casing size (Do).

With pressure and casing properties defined, it is possible to make predictions about micro-annulus formation. Determining the precise type of micro-annulus is often difficult, although they can be divided into three primary categories: filter-cake leak, cement-casing and cement-formation micro-annulus.

First, the filter cake is characterized in terms of thickness, resulting in two scenarios: no cake and cake present. A filter cake in the annulus results in two scenarios: thin and thick cake. A thick filter cake (>2 mm) may present a serious sustained casing-pressure problem. Flow to surface through the cake occurs as the filter cake dehydrates after cement sets, and a micro-annulus forms at the cement-formation interface. This results in a preferential route for gas migration that has a permeability on the order of several darcies. A thin cake (<2 mm) results in the development of some local bonding defects.

If no cake is present, good bonding at the cement-formation interface can be initially assumed. However, in spite of complete cake removal, bonding defects can still develop at this interface. One of the most common causes for bond-strength reduction is shrinkage within the cement matrix due to hydration (Stewart and Schouten, 1988). This occurs because the volume of the hydrated phases is less than that of the initial reactants (Nelson, 1990). This reduction of volume is typically found in neat cement slurries (Figure 40).

Although cement shrinkage or a thin cake (<2 mm) leaves partially unbonded areas, it does not by itself lead to the development of a micro-annulus. Development of a micro-annulus more likely results from a decrease of internal casing pressure or temperature, a consequence of activities commonly found during completion and production operations (Nelson, 1990, and Bourgoyne et al., 2000). On the other hand, a micro-annulus between casing and cement will tend develop if no cake is present or a non-shrinking cement was used.

Experiments to examine the effect of decreasing internal casing pressure showed that a micro-annulus develops and remains active whenever internal casing pressure is dropped more than 30 MPa (McElfresha and Boncan, 1982, Seidel and Greene, 1985, Mathew and Copeland, 1986,

Perry and Henry, 1986, and Nelson, 1990). The micro-annulus expected from this pressure change is >20 μm (0.001 in.), a void sufficient to give gas a flow path, albeit at a low rate. Such events may take weeks or months to manifest themselves as measurable phenomena at surface. With the operational (pressure) and interface conditions (cake, no cake) defined, the final step is to evaluate micro-annulus width and permeability (Figure 43).

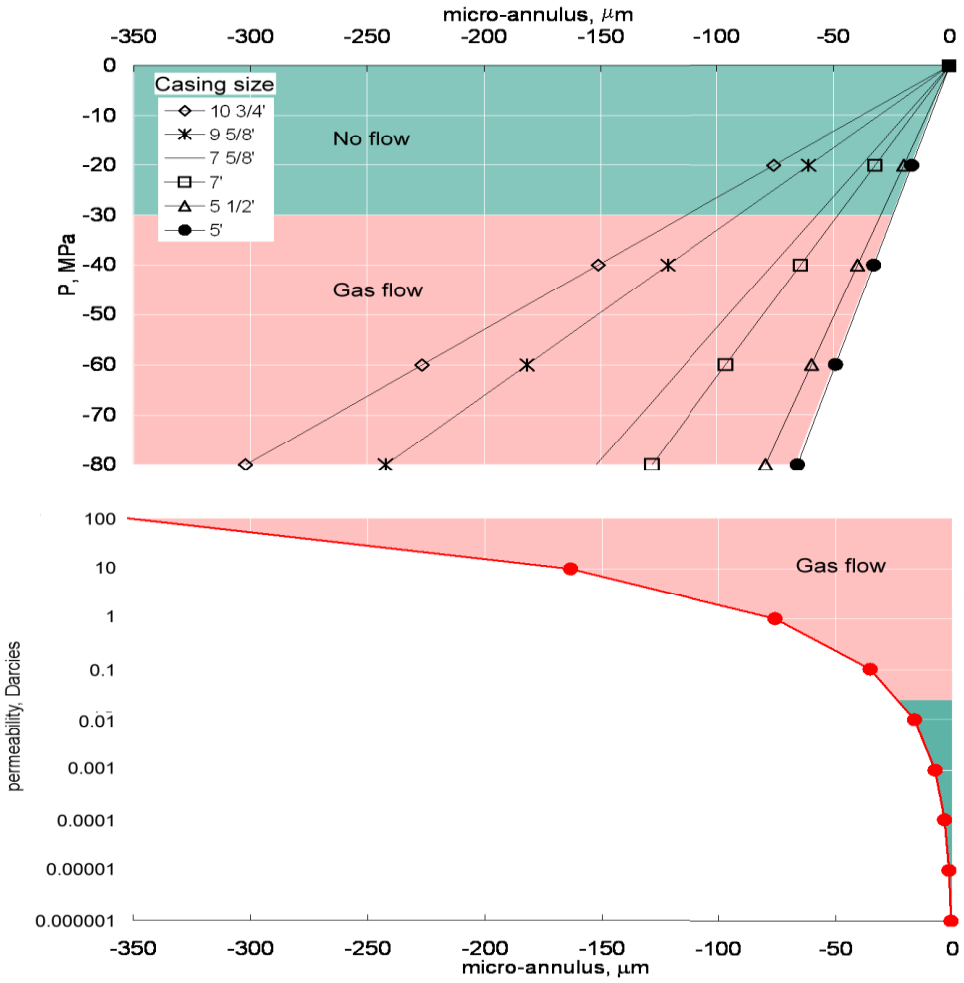

Figure 43 Micro-annulus width and equivalent permeability as a function of reduction in internal casing pressure (P) for various casing sizes.

To calculate the micro-annulus width, the radial contraction of a casing due to a reduction in internal pressure equation was used.

$$\Delta R = \frac{\Delta P \times D^2}{4.7Et},$$

[42]

Where

ΔR = change in casing radius (microannulus width),

D = casing mean diameter,

t = casing wall thickness,

E = modulus of elasticity of steel, and

ΔP = change in internal pressure.

Micro-annular permeability was calculated using the equation for a micro-fracture.

$$kA = \frac{2}{3} \times \frac{W \times B^3}{8},$$

[43]

Where

W = fracture length,

B = fracture thickness,

A = flow area.

3.7 Deterioration Damage (Aging)

Leakages during the operational phase are generally associated with improper mud removal and gas-invasion control, and cement cracking due to overstressing. In the long term, however, the main leakage

mechanisms will change and eventually chemical degradation of cement will play a major role.

Cement degradation can result in a significant permeability increase. This will affect the flow process in the form of increased leakage (Heukamp et al., 2003). Degradation processes can be classified as 1) sulphate attack, 2) carbonation, 3) chloride attack, and 4) calcium leaching. Each mechanism will have a different impact on the transport properties of cement; however, only calcium leaching is of interest under down-hole conditions, (Kathri et al., 1997).

Two parameters are of interest when assessing the effect of calcium leaching on wellbore transport properties: leaching time and leached-cement permeability. The procedure to assess these properties is presented in the next two sections.

3.7.1 Degradation (leaching) time

The leaching times for cement pastes with various annular thicknesses are presented in Figure 44 and Figure 45. These charts were constructed using the simplified procedure proposed by Kamali et al. (2003), whose model predicts degradation time as a function of cement parameters (water to cement [w/c] ratio, silica fume content) and environmental conditions (temperature, pH) in the form of the following equation

$$L_d = a \times t^{1/n},$$

[44]

where L_d is annular cement thickness; t is degradation time; a is a constant parameter modelled as a function of w/c, silica fume content, pH and temperature; and n = 1 or 2 for degradation in the presence or absence, respectively. of an electric field.

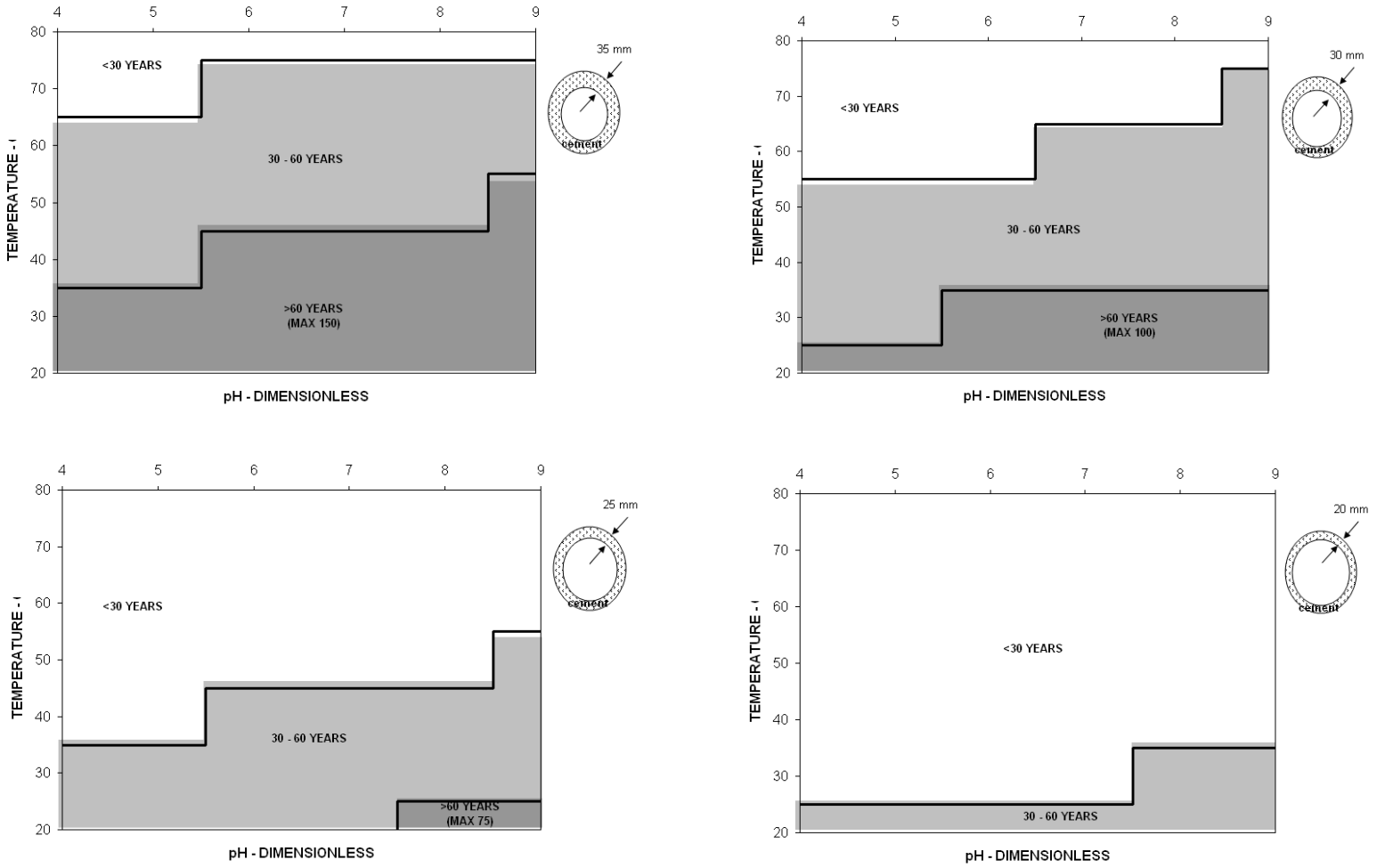

Figure 44 Leaching time for neat cement.

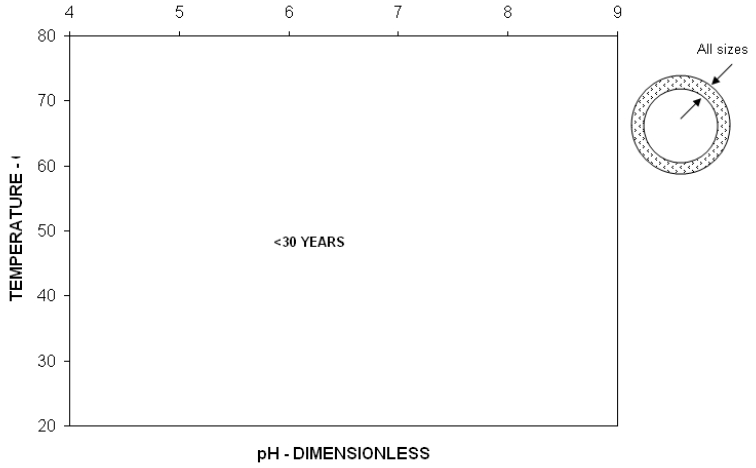

Figure 45 Leaching time for lightweight cement.

The degradation times in Figure 44 and Figure 45 are given for two cement systems, neat cement and lightweight cement, with different w/c ratios. A neat cement paste will usually have a w/c ratio of 0.4. Lightweight cements, on the other hand, will generally have a w/c ratio of 0.9 or higher (Halliburton, 2006). Degradation of new ultra-lightweight cements is not considered here; these cements are made by adding hollow microspheres, such as gas bubbles (boron or sodium silicate) or ceramic bubbles (Smith, 1984).

Well geometry (annular thickness), formation temperature, and type of cement must be defined before these charts can be used. The flow chart in Figure 46 enables the numerous factors involved in cement aging to be addressed quantitatively.

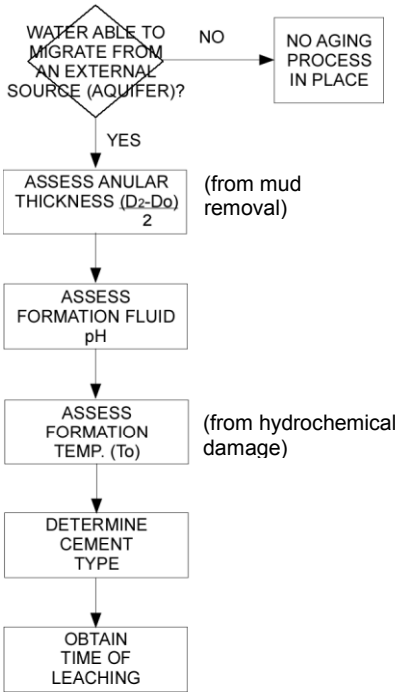

Figure 46 Protocol to assess leaching time for annular cement.

3.7.2 Permeability of intact and leached cement

Two cement systems are considered: low permeability (such as neat cement) and a high permeability (such as lightweight cement). **Error! Reference source not found.** gives typical intact and leached transport properties of these two cement systems.

Intact properties were determined from an extensive data set of experimental measurements found in the open literature (Powers et al., 1955, Hughes, 1985, Cui and Cahyadi, 2001, Galle and Daian, 2000, and Halliburton, 2006).

On the other hand, few laboratory data on leached-cement properties are available in the literature. Thus, these properties had to be estimated. Several values of leached permeability were calculated using various models available in the literature to assess permeability (Katz and Thompson, 1986, Lerman A., 1988, and Udegbunam et al., 1999). These results were then averaged.

Table 33 Permeabilities of intact and leached cement (from Wilkins and Free, 1982, and Sabbins and Wiggings, 1994).

Cement type	Permeability (m^2 *[D]*	
	Intact	Leached
Shrinking, expansive	1×10^{-19}	1×10^{-17}
	[1×10^{-7}]	*[1×10^{-5}]*
Zero net effect	1×10^{-16}	1×10^{-14}
Lightweight	*[1×10^{-4} to 1 $\times 10^{-3}$]*	*[0.01 – 0.1]*

To use these models, leached porosity and pore diameter had to be determined. Porosity was chosen from measured porosities of degraded Portland cement samples reported in literature (Carde and Francois, 1999, Goueygou et al., 2001, and Marchand et al., 2001). Leached pore diameter was obtained from pore-size distributions measured on intact cement samples with similar high porosities (Cook and Hover, 1999).

4 The Weyburn Project: Application of the Methodology to Real Field Data

4.1 Project Description

Although carbon dioxide (CO_2) has been used for enhanced oil recovery for decades, its capture and long-term storage in geological reservoirs as a viable means of climate-change mitigation was not evaluated until very recently. Through the dedicated work of scientists and the support industry, several large-scale projects are underway or in the planning stages. An example of this type of project is the Weyburn-Midale CO_2 Monitoring and Storage Project. This carbon-capture and -storage (CCS) project is a collaborative endeavour to investigate the technical and economic feasibility of CO_2 storage in a partially depleted oil reservoir. Specifically, the International Energy Agency's Weyburn Project aims to comprehensively monitor and verify the progress of the CO_2 flood and establish the likelihood of safely storing the CO_2 in the reservoir for the long term (White et al., 2004). Initiated in 2000, the project is supported by Encana Corporation (now Cenovus), Saskatchewan Industry and the International Energy Agency Greenhouse Gas R&D Programme (IEAGHG).

Located in the southeastern corner of the province of Saskatchewan in Western Canada, within the north-central Williston Basin, the Weyburn unit is a 180 km^2 oil field discovered in 1954 (Figure 47). It is estimated

that this field hosts approximately 1.4 billion barrels of oil. Primary production within the field continued until 1964, when the initiation of waterflood resulted in oil production peaking at 46,000 barrels/day in 1965. Waterflood has continued since then, with significant field development, including horizontal infill drilling commencing in 1991.

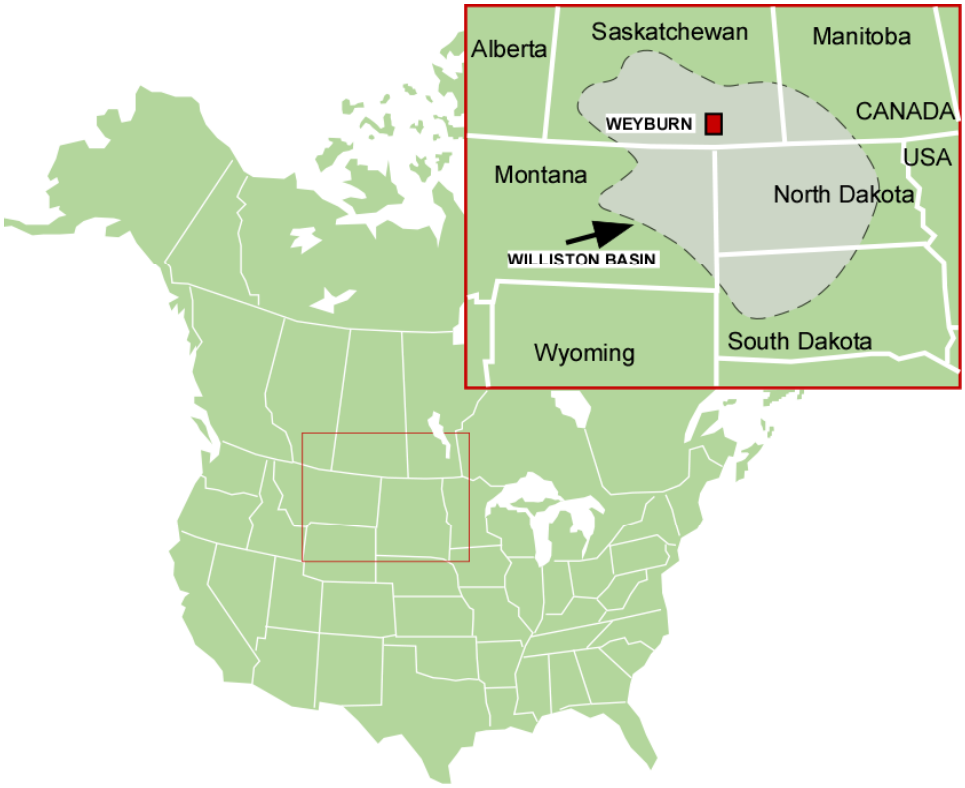

Figure 47 Location of the Weyburn field in southeastern Saskatchewan. Inset shows the location of the study area within the Williston Basin (White et al, 2004).

Oil in the Weyburn field is at an average depth of 1.5 km, within a thin zone (maximum thickness of 30 m) of fractured carbonates in the Midale beds (Figure 48) of the Mississippian Charles Formation, which were deposited in a shallow carbonate-shelf environment. The two main

reservoir layers in the Midale beds are: an upper dolostone unit (0–10 m thick), the Marly; and a lower limestone unit (0–20 m thick), the Vuggy. These units are sealed by anhydritic dolostones and anhydrites of the Midale Evaporite.

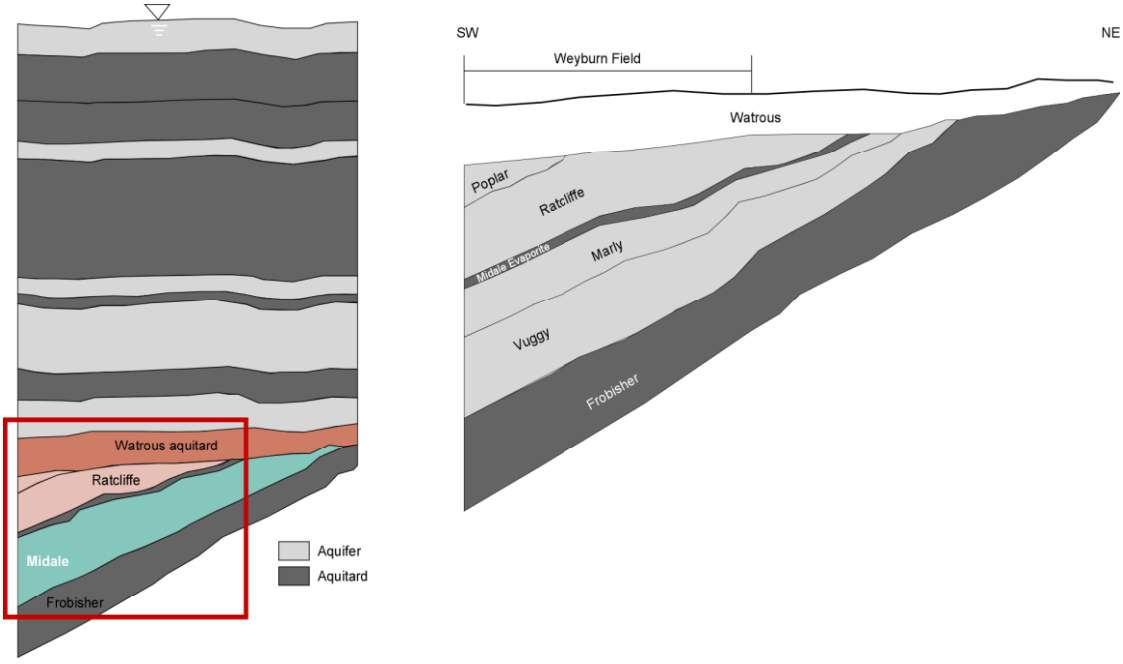

Figure 48 (left) Cutaway block diagram showing simplified regional hydrostratigraphy above the Weyburn project; layers in light grey are aquifers, those in dark grey are aquitards. (right) Generalized southwest–northeast cross-section through the Weyburn pool, showing the two major reservoir units (Modified from White et al., 2004).

The Midale Marly has relatively high porosity (16%–38%) and low permeability (1 to >50 mD), whereas the Midale Vuggy has relatively lower porosity (8%–20%) and higher permeability (10 to >300 mD) (White et al., 2004, and Whittaker, 2004). Most oil production from the Weyburn field prior to the CO_2-miscible flood was from the Vuggy beds, because of the

high permeability of this unit (White et al., 2004). The Marly beds are less permeable; thus, CO_2 is being injected into this unit as an effective method of extracting the oil.

The CO_2-based enhanced oil recovery (EOR) scheme was initiated in September of 2000 in 18 inverted 9-spot patterns (Phase 1A) of the EnCana (now Cenovus) Weyburn unit at an initial injection rate of 2.69 million m^3/day (Figure 49).

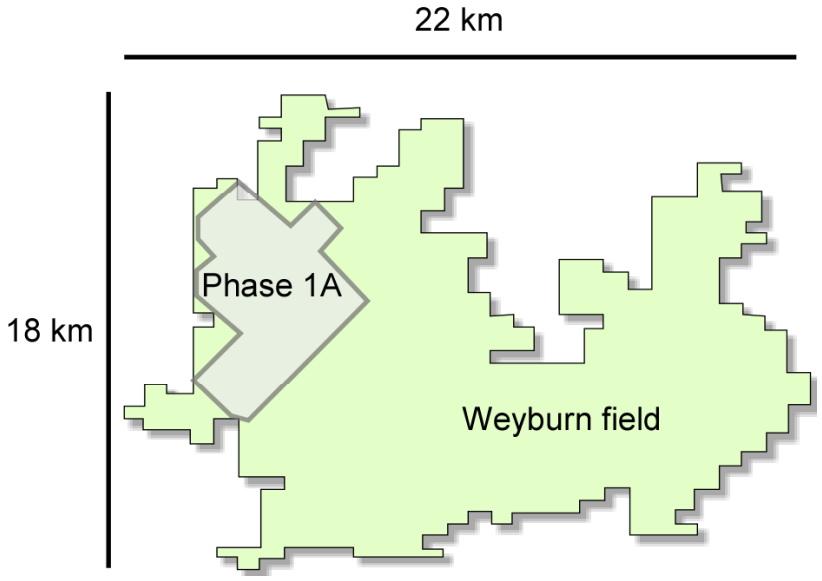

Figure 49 Weyburn oil field; the grey area in the west indicates the Phase 1A area.

The CO_2 flood has been extended in a southeasterly direction and the ultimate aim is to expand gradually over a period of 15 years into a total of 75 patterns. The expectation is that approximately 10.8 billion m^3 (or ~20 million tonnes) of CO_2 will be injected into the reservoir over the lifetime of the project (White et al., 2004). The CO_2, which is approximately 95%

pure, is a purchased byproduct from the Dakota Gasification Company's synthetic fuel plant located in Beulah, North Dakota. Approximately 5000 tonnes/day CO_2 are purchased and transported through a 320 km pipeline to the Weyburn field (Whittaker, 2004).

4.2 Data Interpretation and Results

In order to use the methodology, one must start by selecting a set of basic wellbore information, which includes well geometry (diameter, length), casing (diameter, thickness, grade), and cement type and volume. Wellbore information on the Weyburn field came from two main sources: older data obtained from historical well files transferred to microfiche (records stored with the Saskatchewan Ministry of Energy and Resources) and newer data obtained from internal well files (in paper and electronic format) provided by Encana (now Cenovus). Generally the same information was found in both places, but substantially more detailed data were available in the newer, electronic well-file records. Furthermore, the quality of the records is related to age. Data for wellbores drilled in the last decade are more detailed and complete than those available for wells drilled during the early development of the Weyburn field.

Information on wells drilled in the 1950s is generally limited to registries for geometry of wellbore (diameter, length), casing (diameter, length, grade), and cement type and volume. On the other hand, information available for

a typical wellbore perforated in the 1990s is very detailed and complete. Cementing data include records of cement type, volume, depth set, circulation pressures, spacer volume, and casing reciprocation stroke length and time. Casing data include casing length, grade, accessories number, and spacing. Daily drilling reports provide a detailed information such as mud density, volume, pressure, and daily drilling advance.

Figure 50 illustrates a selected range of statistics for the wells within Phase 1A of the Weyburn Project. This figure shows that, in general, wellbores can grouped into four types, each one associated with the age of drilling. However, for purposes of illustrating the well-assessment methodology, this chapter will concentrate on a comprehensive review of wellbores drilled only in the period of 1956 - 1967.

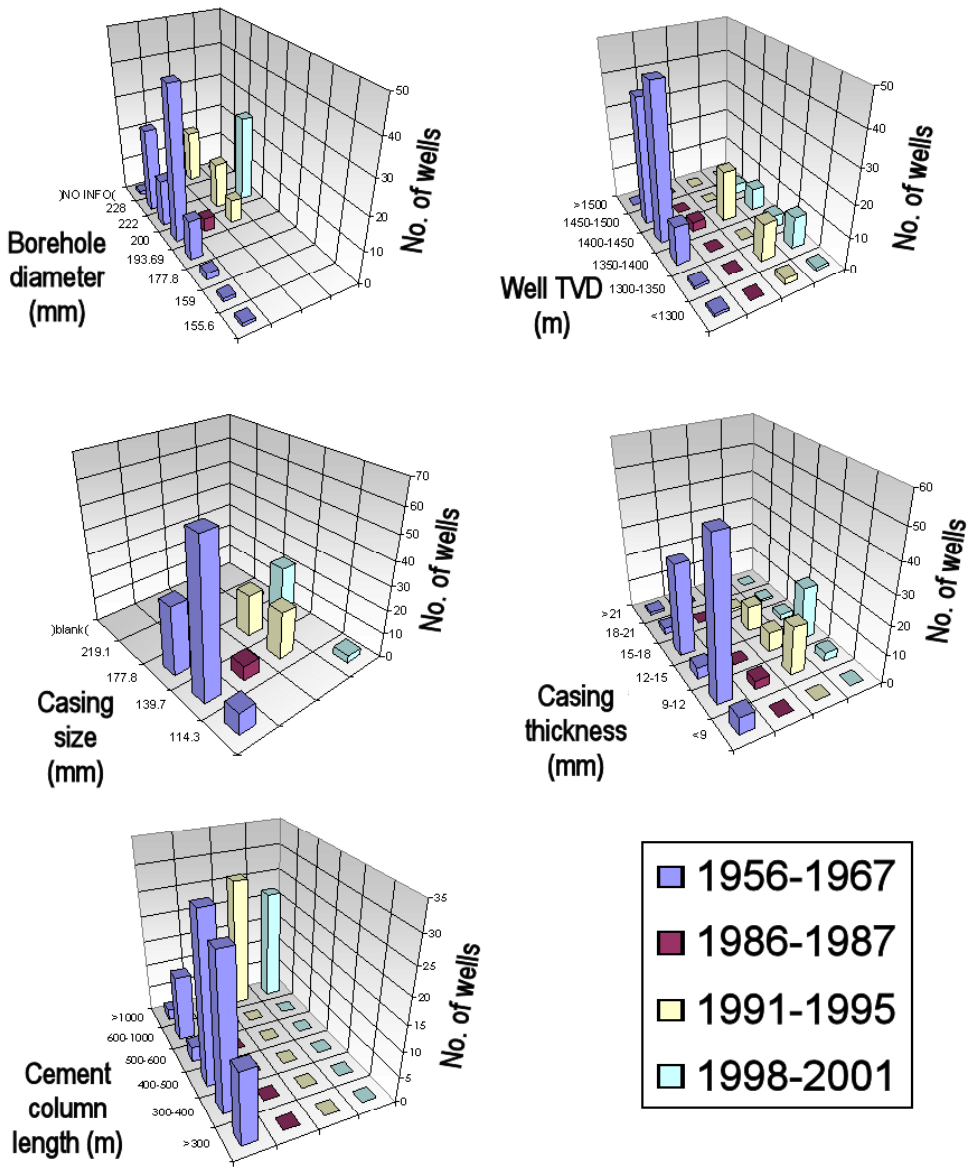

Figure 50 Wellbore statistics for the lower portion of wells within the Phase 1A area of the Weyburn Project.

Figure 51 shows the typical geometry of a vertical wellbore drilled in the 1950s at the Weyburn field. These boreholes were drilled in two segments, a surface section (90–170 m long) and an intermediate-hole section (1300–1500 m long). The upper section consists of a 10¾-in. (273 mm) casing centralized in a 13 ¾-in. (350 mm) hole. The intermediate

section consists of a 5 ½-in. (139.7 mm) OD pipe inside a 7⅞-in. (200 mm) hole.

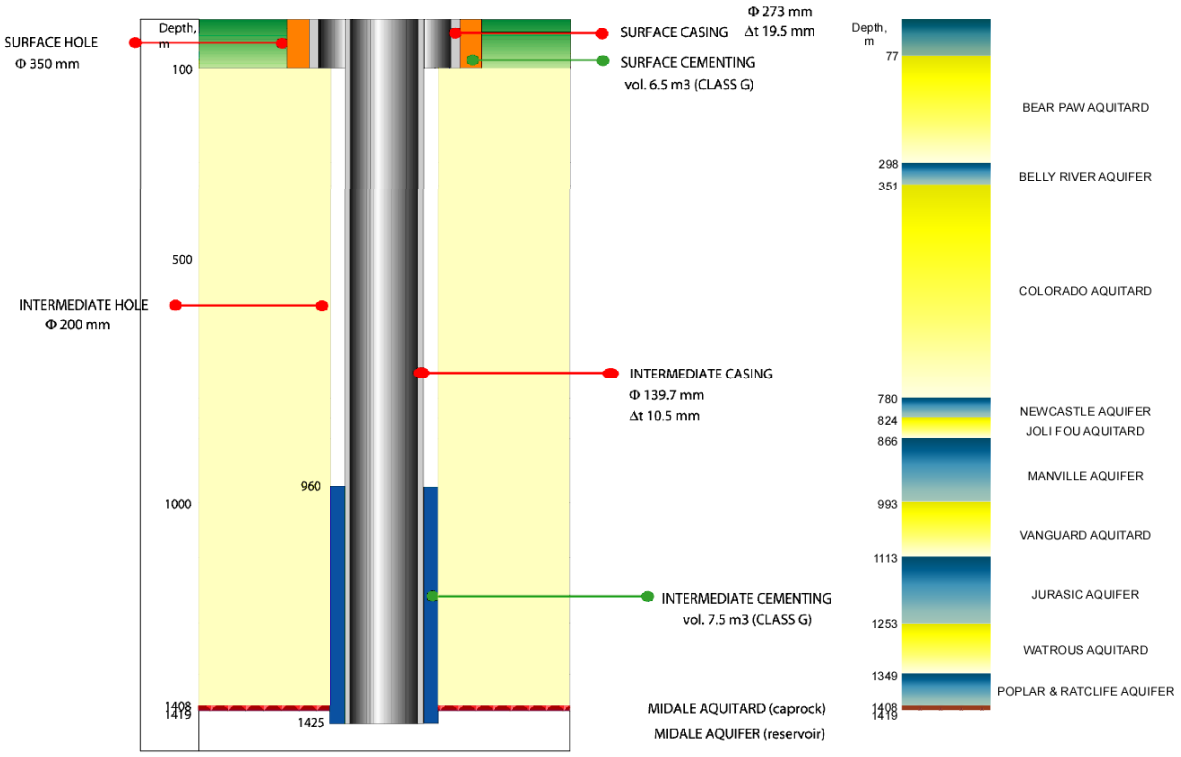

Figure 51 Typical geometry of a vertical wellbore in the 1950s at the Weyburn field (left) and simplified hydrostratigraphy above the Midale reservoir (right).

Surface casing was usually cemented with class G cement and the cementation went right to the surface. The production casing was cemented with one cement system: class G slurry with an average density of 1.45 kg/L. The top of the cement is, on average, 400 m above the caprock. This is enough to isolate the two low-pressure water zones (consolidated sandstone) intercalated with low-permeability shaly siltstone

beds at that level. Horizons that are isolated include the Jurassic aquifer, the Watrous aquitard, the Ratcliffe aquifer, and the Midale caprock.

With the typical wellbore geometry defined, the next step is to set up a conceptual model. In this model, the well is treated as a cylindrical column of length L and is divided into a number of sections, each of which is analyzed separately. The boundaries of the sections coincide with major features, which include potential fluid pathways (aquifers) or trapping mechanisms (aquitards) within the stratigraphic column. Thus, a typical wellbore drilled in the 1950s can be partitioned into four sections, each one corresponding to one of the formations isolated by the cement column—Jurassic, Watrous, Ratcliffe, and Midale.

Within each section, the transport properties of the major components of the wellbore system need to be established. The casing can be identified as an impervious element and the cement (annular and abandonment plug) as a low-permeability element. Aquitards are major flow barriers and are assumed to be impermeable, and aquifers are systems with high permeabilities and fast-flowing formation waters. Assuming good bonding quality, interfaces between these components can initially be considered as no-flow regions.

The conductivity properties in each of these components are then modified by considering and evaluating the effects of the four major permeability-disturbance groups: hydrochemical damage, mud removal, geomechanical damage, and deterioration damage. Use of the methodology to assess the effects of the four major permeability-disturbance groups is illustrated in the following sections. For simplicity, only a typical well section bounded by an aquifer (Ratcliffe) is evaluated.

4.3 Hydrochemical Damage

An evaluation of the hydrochemical damage begins with the determination of the formation permeability. Every pertinent data source is used, from well logs and tests in wells to lab testing of core. The Ratcliffe aquifer has a relatively high porosity (10%–30%) and high permeability (0.1–2 D). Once permeability has been assessed, damage potential is investigated. Any formation with permeability $>10^{-3}$ D will suffer from some type of particulate-damage process. The high-permeability Ratcliffe aquifer clearly has high potential for particulate damage (Figure 52). From drilling reports, one can further conclude that the particulate process in operation is of the external type (filter cake).

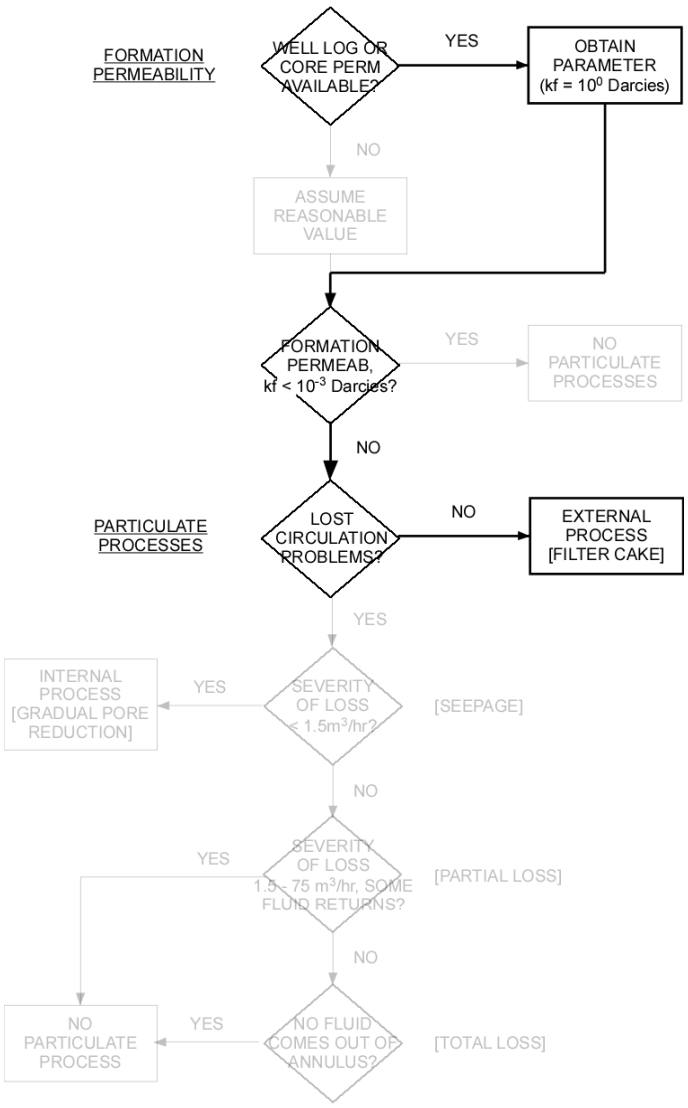

Figure 52 Problem diagnostic protocol to identify type of particulate process (aquifer).

With the type of particulate process identified, the external-process flow chart provides the basis for modelling of filter-cake properties (Figure 53). The use of this figure is discussed next. In this example, a gypsum mud weighted to 1200 kg/m^3 was used to drill in Weyburn, where the expected bottom-hole temperature is 55°C.

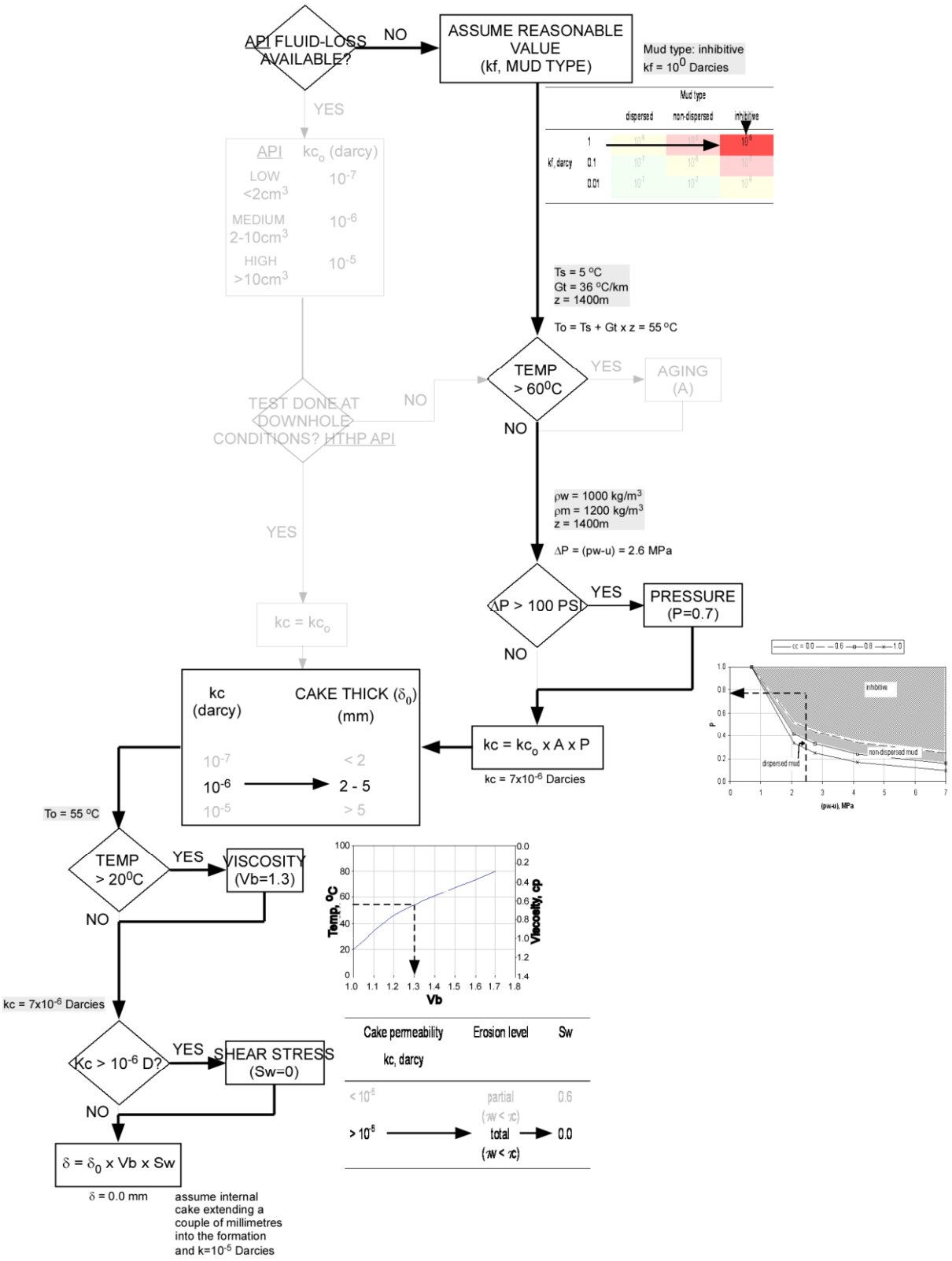

Figure 53 Flow chart for external-processes flow chart (aquifer).

This mud can be classified as an inhibitive fluid (Figure 54). The mud was kept overbalanced at all times, with differential pressures up to 2.6 MPa. The porosity and permeability of the filter media (Ratcliffe aquifer) were previously indicated.

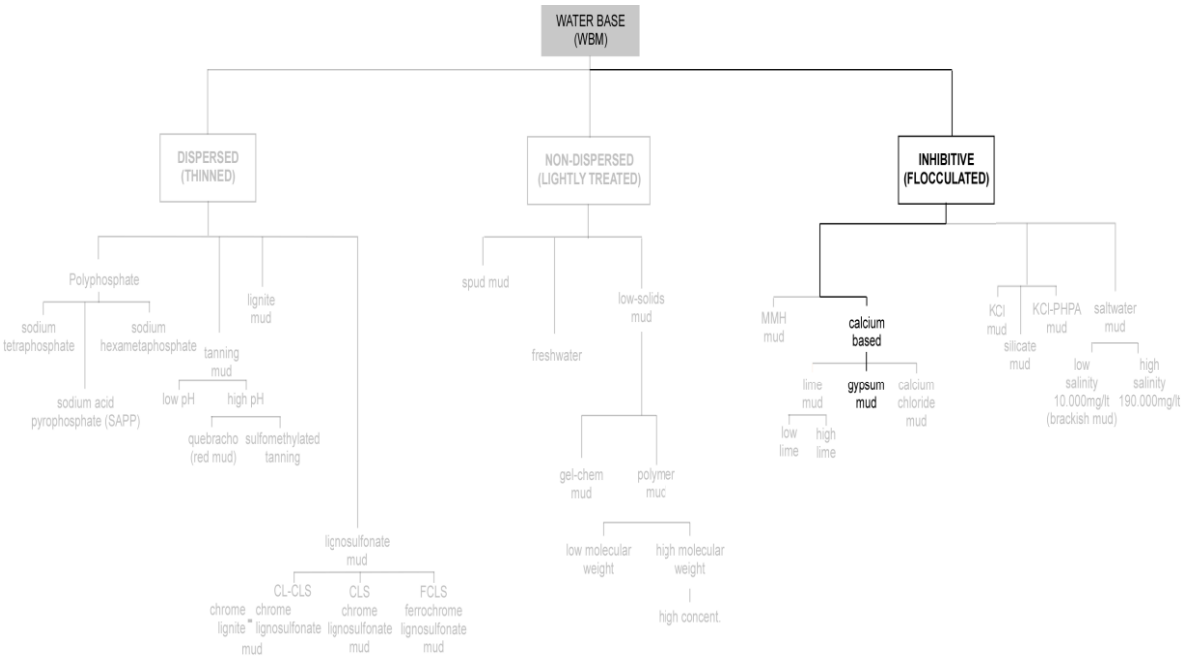

Figure 54 Obtaining mud type based on degree of flocculation (aquifer).

With no API fluid-loss value available, formation permeability and type of mud are then used to determine cake permeability (kc). In this case, an average value for cake permeability of 10^{-5} D will be used. Table 6 shows that, for a bottom-hole temperature of 55°C, the aging weighting multiplier (A) is 1. For a filtration pressure of 2.6 MPa and an inhibitive mud, Figure 18 gives a differential-pressure weighting function (P) of 0.7. Using these values gives

$$kc = 10^{-5} \times 1 \times 0.7 = 7 \times 10^{-6} \text{ D}$$

Cake permeability is then related to thickness. Table 9 gives cake thickness (δ_0) of 2 – 5 mm. Additional correction factors are calculated to account for changes in wellbore-fluid properties (base-fluid viscosity) due to temperature, and wellbore hydraulic conditions (shear stress on the filter-cake surface). From Figure 19, for a bottom-hole temperature of 55°C, the weighting multiplier (Vb) is 1.3. Table 10 shows that a kc value of 7×10^{-6} D gives a Sw value of 0, which means complete erosion of the filter cake.

4.4 Mud Removal

Figure 55 illustrates the method of estimating mud-removal efficiency. To use this method, the following information is required:

- Well geometry
- Fluid rheology
- Casing centralization (STO)
- Displacement technique
- Pump rate
- Pipe movement

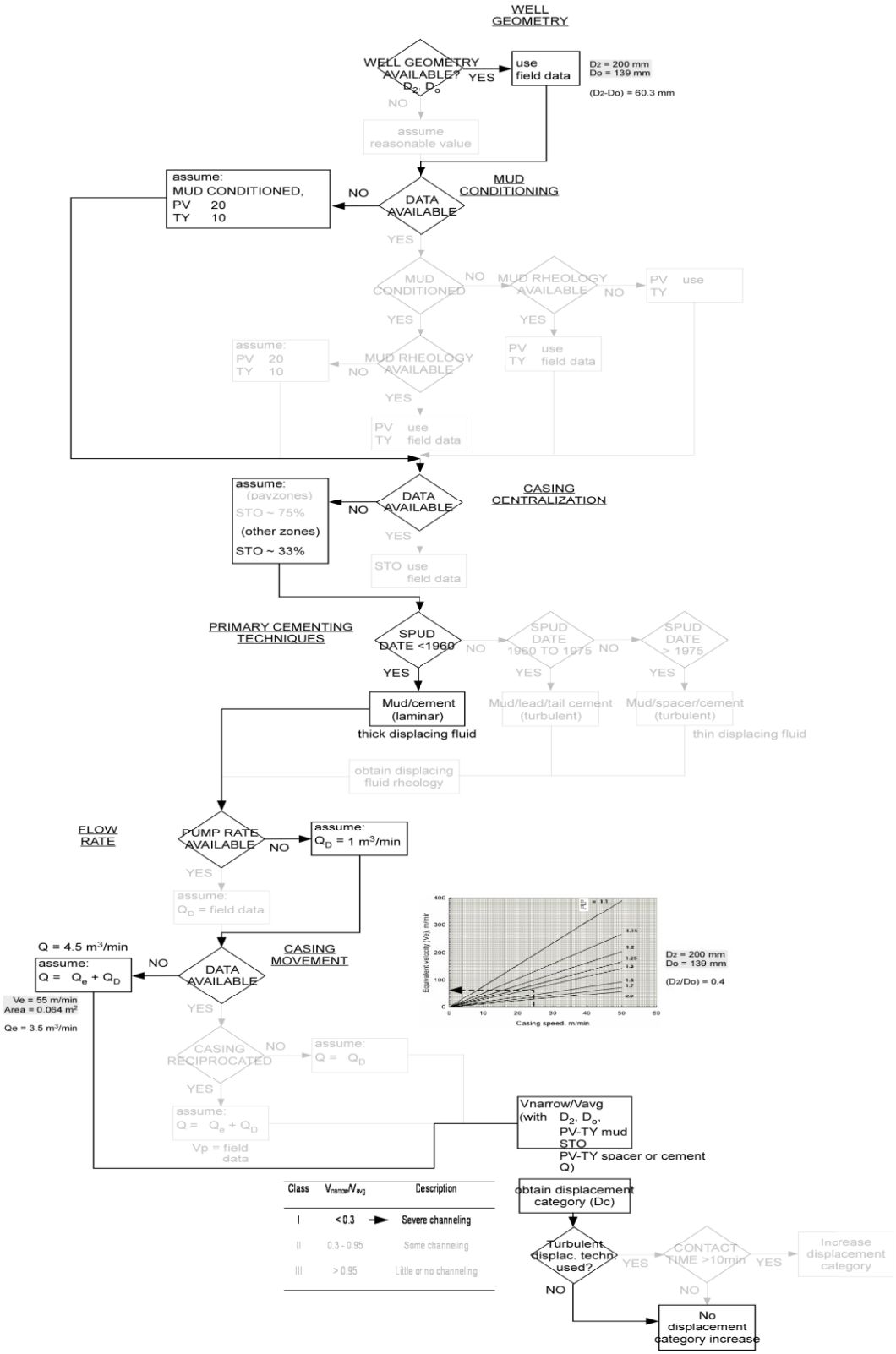

Figure 55 Flow chart for mud removal and cementing (aquifer).

Well geometry can be estimated from drilling reports. Completions in the Weyburn field for the time interval investigated here typically include a 5½-in. (139.7 mm) casing inside a 7⅞-in. (200 mm) hole. Caliper logs indicate a fairly gauge section at the Ratcliffe level.

The drilling fluid used was a water-based gypsum mud with a density of 1200 kg/m^3. Measured rheological properties of this drilling mud were not available, so they had to be estimated. One technique is to assume that optimal properties were employed. Assuming that the recommended drilling-fluid properties were used gives values of PV = 20 cp and TY = 10 lb./100 sq. ft.

To calculate the standoff, the centralizer-placement spacing must be determined. Since this information is not available, the approach was to use the accepted industry practice, a maximum standoff ratio of 33% across non-producing horizons. Another key parameter in the mud-removal process is the displacement technique used. For wells drilled in the 1950s, the standard practice was to use cement as the displacing fluid, at a low displacement rate (laminar flow). For this flow regime, the corresponding recommended fluid rate (Q_D) is 1 m^3/min.

No data were reported on pipe movement, so an assumption was made that casing was reciprocated, the usual type of pipe movement, with

typical amplitude on the order of 12 m and a full cycle completed in 1 minute (24 m/min). From the casing speed and the borehole to casing diameter ratio (D_2/D_o), the corresponding equivalent mud velocity (Ve) is calculated on the design chart (Figure 27).

With a Ve value of 55 m/min and the annular-space geometry (D_2, D_o), the equivalent mud-flow rate (Qe) is calculated as 3.5 m^3/min. This value is then added to the mud-flow rate (Q_D) to get an actual flow rate value (Q) of 4.5 m^3/min.

Once the parameters that contribute to proper mud displacement are known, an approximate value of the displacement efficiency (V_{narrow}/V_{avg}) is easily calculated (Figure 21). From Table 11, a value for V_{narrow}/V_{avg} of <0.1 places displacement efficiency (Dc) in class I, which indicates a high tendency for cement to bypass mud. The positive effect of turbulent eddies can be ignored, as displacement was done under laminar-flow conditions only. This preferential flow path for gas has a permeability on the order of several darcies.

4.5 Geomechanical Damage

4.5.1 Near-wellbore region

To assess well-stability rating (Nw), some relatively detailed basic information on in situ stress is needed. Figure 56 helps to illustrate this

process. A normal fault regime exists in the Weyburn field, with $\sigma v \approx \sigma H \approx \sigma h$. The vertical stress at the Ratcliffe level due to the lithostatic load is ~31 MPa, as estimated from a density log.

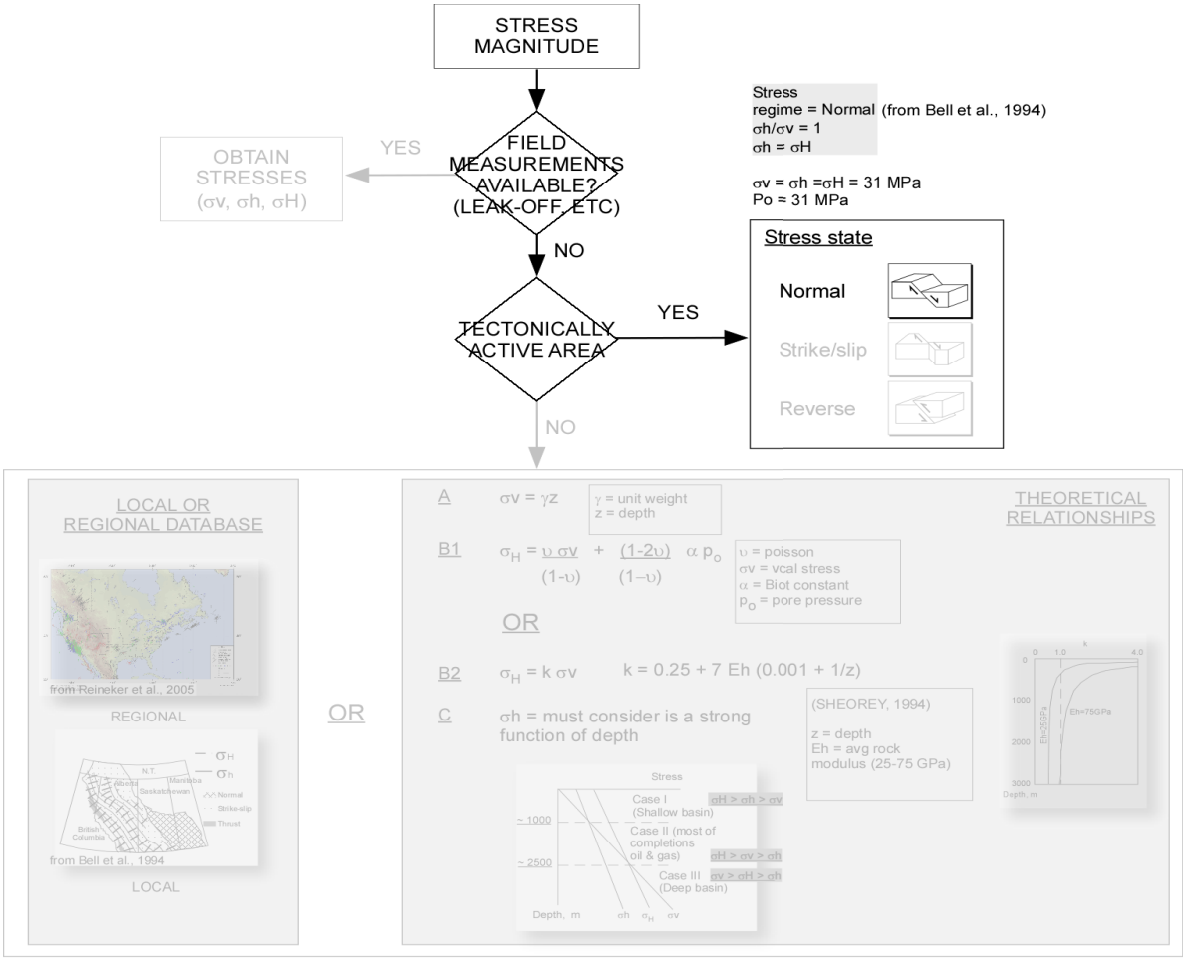

Figure 56 Procedure for predicting in situ stress (aquifer).

Borehole-stability predictions also require knowledge of the mechanical properties of the formations. Since laboratory test results on cores are not available (Figure 57), empirical correlations were used to predict these properties.

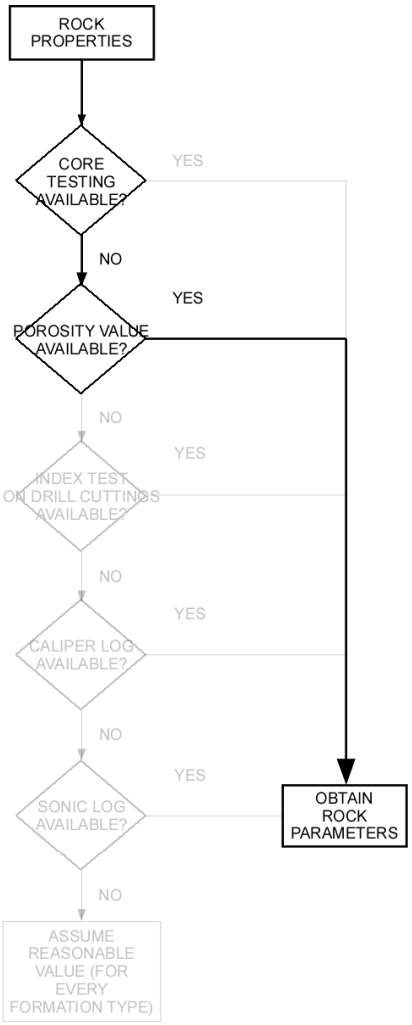

Figure 57 Procedure for predicting rock-mechanical properties (aquifer).

The correlations use porosity as the primary input parameter (Figure 58); thus, various sources of porosity, such as sonic wireline and acoustic measurements on cuttings, were used to obtain a somewhat continuous estimate of rock-mechanical properties. For carbonates in the Ratcliffe aquifer, porosity is relatively high, with 20% being an average value. Using this value, the computed rock strength (UCS) is 65 MPa.

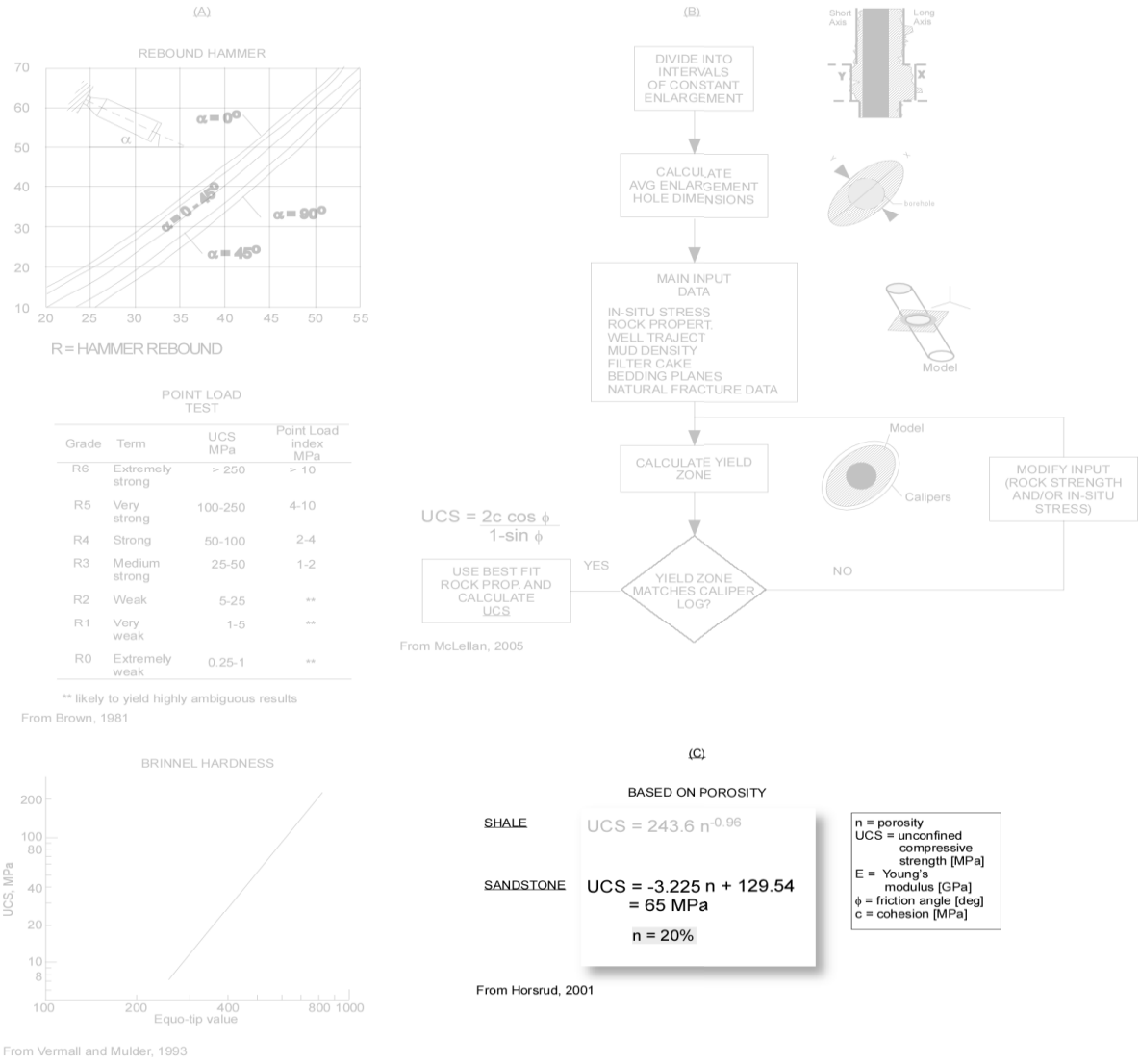

Figure 58 Procedure for predicting rock-mechanical properties from empirical correlations, index testing on drill cuttings, or calibration from hole size (aquifer).

Another property that is important in the determination of potential borehole stability is filter-cake efficiency. Figure 59 show the method followed to assess this. The method starts by recognizing formation permeability (kf) because, by knowing this value, the proper correlations can be applied. Thus, for a kf of 10^0 D and a drilling mud that uses undeformable blocking additives, the efficiency class of the filter cake falls

between the high and intermediate classes (Table 22). The most likely value of filter-cake efficiency (h) is then calculated using the correlations shown in Figure 34. Cake thickness (δ) is assumed to be 2 mm. No direct measurement of the cake permeability (kc) is available, but it is understood that predicted values of 10^{-5} D occur in this formation (Section 4.3). Thus, the cake to formation permeability ratio (kc/kf) is 10^{-5}.

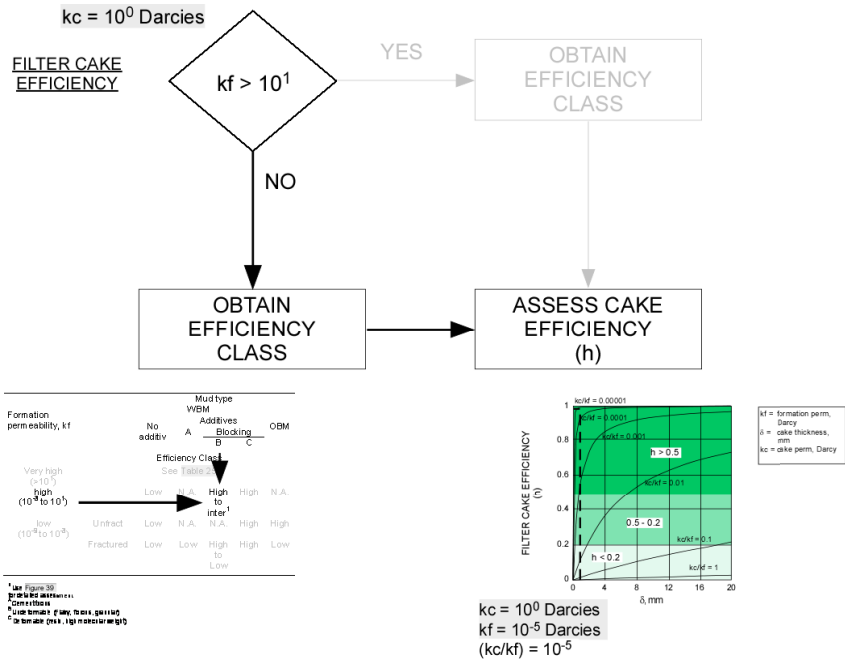

Figure 59 Procedure for predicting the filter-cake efficiency factor (h).

Taking into consideration the effect of temperature requires calculating the temperature change at the wellbore wall. This value requires a more refined numerical analysis using equations [35] and [36]. All input parameters are shown in Table 34.

Table 34 Data for calculating temperature change near the wellbore.

Far-field temperature	To	55°C
Inlet-mud temperature	Ti	10°C
Depth	z	1300 m
Well length	L	1400 m
Mud-flow rate	Q	1 m^3/min
Mud density	ρm	1200 kg/m^3
Mud specific heat	cm	1700 J/kg °C
Geothermal gradient	Gt	0.036 °C/m

Figure 60 shows the calculation of the temperature change.

$$Ta = 10 + 0.012 \times 2/3 \times 1400 + 0.006\ (1300 - 2/3 \times 1400)$$
$$= 23.4°C$$

$$Gm_1 = 0.019 \times F_{Q1} \times F_{\rho m1} \times F_{cm1} \times F_{Gt1} \times F_{L1}$$
$$= 0.019 \times 1.0 \times 1.14 \times 1.0 \times 1.54 \times 0.38$$
$$= 0.012$$

F_{Q1}	= 1.0 (Q = 1.0 m^3/min)
$F_{\rho m1}$	= 1.14 (ρm = 1200 kg/m^3)
F_{cm1}	= 1.0 (cm = 1700 J/kg °C)
F_{Gt1}	= 1.54 (Gt = 0.036 °C/m)
F_{L1}	= 0.38 (L = 1400 m)

$$Gm_2 = 0.010 \times F_{Q2} \times F_{\rho m2} \times F_{cm2} \times F_{Gt2} \times F_{L2}$$
$$= 0.010 \times 1.0 \times 1.23 \times 1.0 \times 1.69 \times 0.29$$
$$= 0.006$$

F_{Q2}	= 1.0 (Q = 1.0 m^3/min)
$F_{\rho m2}$	= 1.23 (ρm = 1200 kg/m^3)
F_{cm2}	= 1.0 (cm = 1700 J/kg °C)
F_{Gt2}	= 1.69 (Gt = 0.036 °C/m)
F_{L2}	= 0.29 (L = 1400 m)

$$\Delta T = Ta - To$$
$$= -31.6\ °C$$

Figure 60 Calculation of temperature change at a depth of 1300 m (Ratcliffe aquifer).

Having calculated all the key parameters of the rating system (Nw), the next step is to obtain ratings for each one of them. These ratings are summed to give a value of Nw. The values of stress level (Po/UCS), discontinuity spacing (Js), discontinuity dip (Jd), uniaxial compressive strength (UCS), support pressure ([pw – u] / Po), cake efficiency (h), and temperature (Jt) are given in Table 35.

Table 35 Data for well-stability rating (Nw).

Property		Value
Stress level	(Po/UCS)	0.47
Discontinuity spacing	Js	none
Discontinuity dip	Jd	none
Uniaxial compressive strength	UCS	65 MPa
Support pressure	(pw-u)/Po	0.084
Cake efficiency	h	0.99
Temperature	ΔT	-31.6 °C

Figure 61 gives the classification of individual key parameters used to obtain the well-stability rating for the near-wellbore rock mass. This figure shows that, for a stress level of 0.47, the stress reduction factor (SRF) is 18. For no discontinuities, Figure 61 gives a discontinuity spacing (Js) of 10, and a discontinuity dip (Jd) of 0. The uniaxial compressive strength factor (UCS) is 8 for a rock with a strength of 65 MPa. For a support pressure of 0.084, the pressure factor rating (Jp) is 9. Since cake efficiency is 0.99, this gives a rating of 10. Figure 61 shows that, for a

temperature change of –31.6°C and a medium strength rock (20–75 MPa), the temperature factor rating (Jt) is 7. Summing these values gives

$$Nw = 18 + 10 + 0 + 8 + 9 + 10 + 7 = 62$$

1 Stress reduction factor SRF

a. competent rock [stress problem]

Stress level (Po/UCS)	> 0.05	0.05 - 0.1	0.1 - 0.5	0.5 - 1	1 - 3
Rating	27	20	18	12	7

b. incompetent rock [squeezing problem]

Squeezing level (Po/UCS)			3 - 5	> 5
Rating			4	2

c. Swelling rock [chemical problem]

Swelling activity (Sa)[1]			mild	high
Rating			4	2

A. Stress anisotropy

Anisotropy ratio (σ_1/σ_3)		1	1 - 2	2 - 5
Rating		1	0.8	0.6

Note i) For anisotropic virgin stress field reduce compressive strength (UCS) by using correction factor
ii) σ_1 and σ_3 are the major and minor principal stresses

2 Discontinuity spacing Js

Range of values	> 0.3m	0.3 - 0.1m	0.1 - 0.05m	0.05 - 0.025m	< 0.025m
Rating	10	7	3	-2	-4

3 Discontinuity dip Jd

Range of values		flat	dipping	vertical
Rating		-5	-5	0

Note i) Dip: flat 0 - 20°; dipping: 20 - 50°; and vertical: 50 - 90°

4 Uniaxial compressive strength UCS

Range of values	> 100 MPa	100 - 50 MPa	50 - 20 MPa	20 -5 MPa	< 5 MPa
Rating	10	8	4	1	0

5 Support pressure $h^*(p_{xy}-u)/Po$ Jp

Range of values	> 0.8	0.8 - 0.5	0.5 - 0.2	0.2 - 0.05	< 0.05
Rating	27	21	16	9	6

B. Cake efficiency

Class			> 0.5	0.5 - 0.2	< 0.2
Rating			10	7	5

Note i) Support pressure: h cake efficiency (Figure 38); pw drill fluid pressure (drill report/assume value); u pore pressure (Table 8); po mean stress

6 Temperature Jt

Range of values, ΔT		-40 °C	-20 °C	0 °C	+20 °C	+40 °C
	UCS, MPa					
	< 20	6	3	1	-2	-4
Rating	20 - 75	8	6	4	3	1
	75 - 120	16	13	9	8	7

Figure 61 Wellbore-stability rating (Nw) for a 1950s well in the Weyburn field.

The Nw value of 62 indicates that the rock mass is in the 'good rock' category. This suggests a wellbore in good condition with no breakout present (gauge hole - Figure 62). No permeability or hole-size corrections are needed in this case.

Rating	100 ← 61	60 ← 41	40 ← 21	< 21
Description	Good rock	Fair rock	Poor rock	Very poor
Well condition[1]	no breakout	Breakout ≤ 25 % well diameter	Breakout ≥ 25 % well diameter	Squeezing (large converg.)
		no impact on drilling	Impact on drilling (washing, tight hole)	Impact on drilling (tight hole)

[1] Modified from SPE 26325

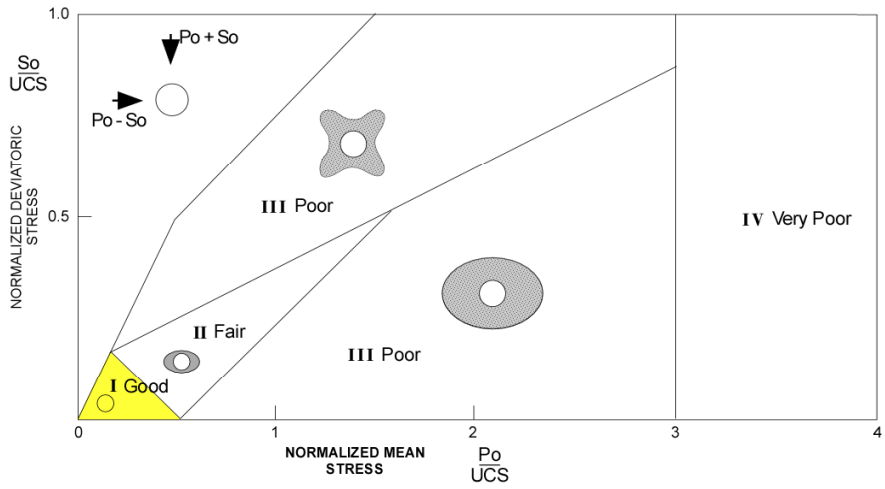

Figure 62 Wellbore rock classes (aquifer).

4.5.2 Annular cement

Failure of the cement sheath is most often due to stresses induced by changes in pressure and temperature resulting from operations during the

well's economic life. However, the need to consider properties of the cement sheath for long-term integrity is critical only if the well is subjected to "large" changes in stress level (Ravi et al., 2002). Examples of wells in which the cement may be subjected to a significant stress level are

- high-pressure and/or high-temperature (HP, HT, and HPHT) wells,
- deepwater wells,
- gas-storage wells,
- wells in weak unconsolidated formations,
- steam-injection wells, and
- producing wells converted into water injectors.

Maximum pressure at the Weyburn field is in the range 14–28 MPa. Reservoir pressures were extracted from a history-match analysis of pre-CO_2 production. This range is substantially below pressure levels encountered in most HP wells (>50 MPa), resulting in conditions where annular cement can easily retain zonal isolation (Figure 63).

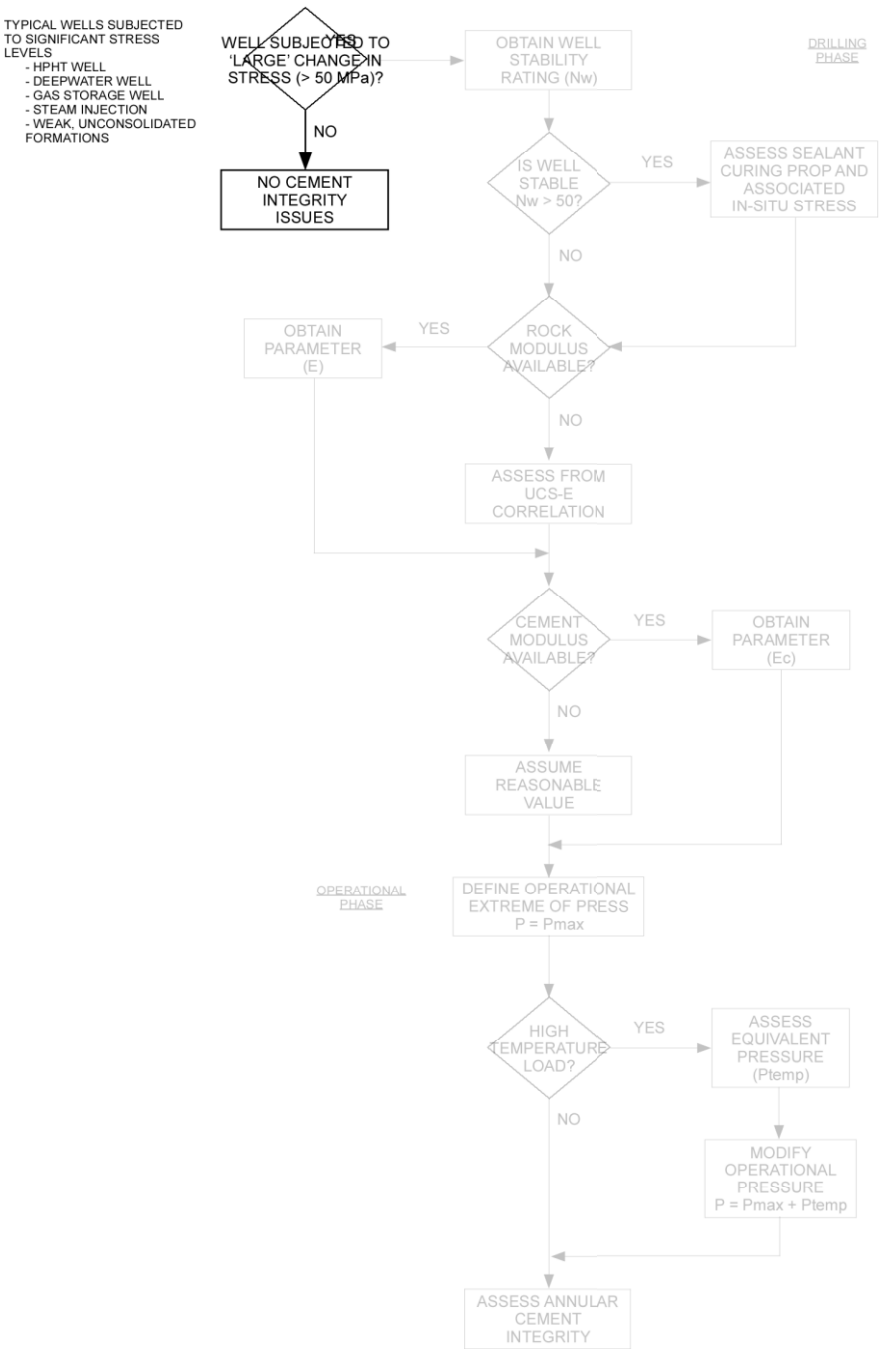

Figure 63 Procedure for predicting annular cement integrity (aquifer).

4.5.3 Wellbore interfaces

Figure 64 illustrates the method of estimating the potential for micro-annulus development.

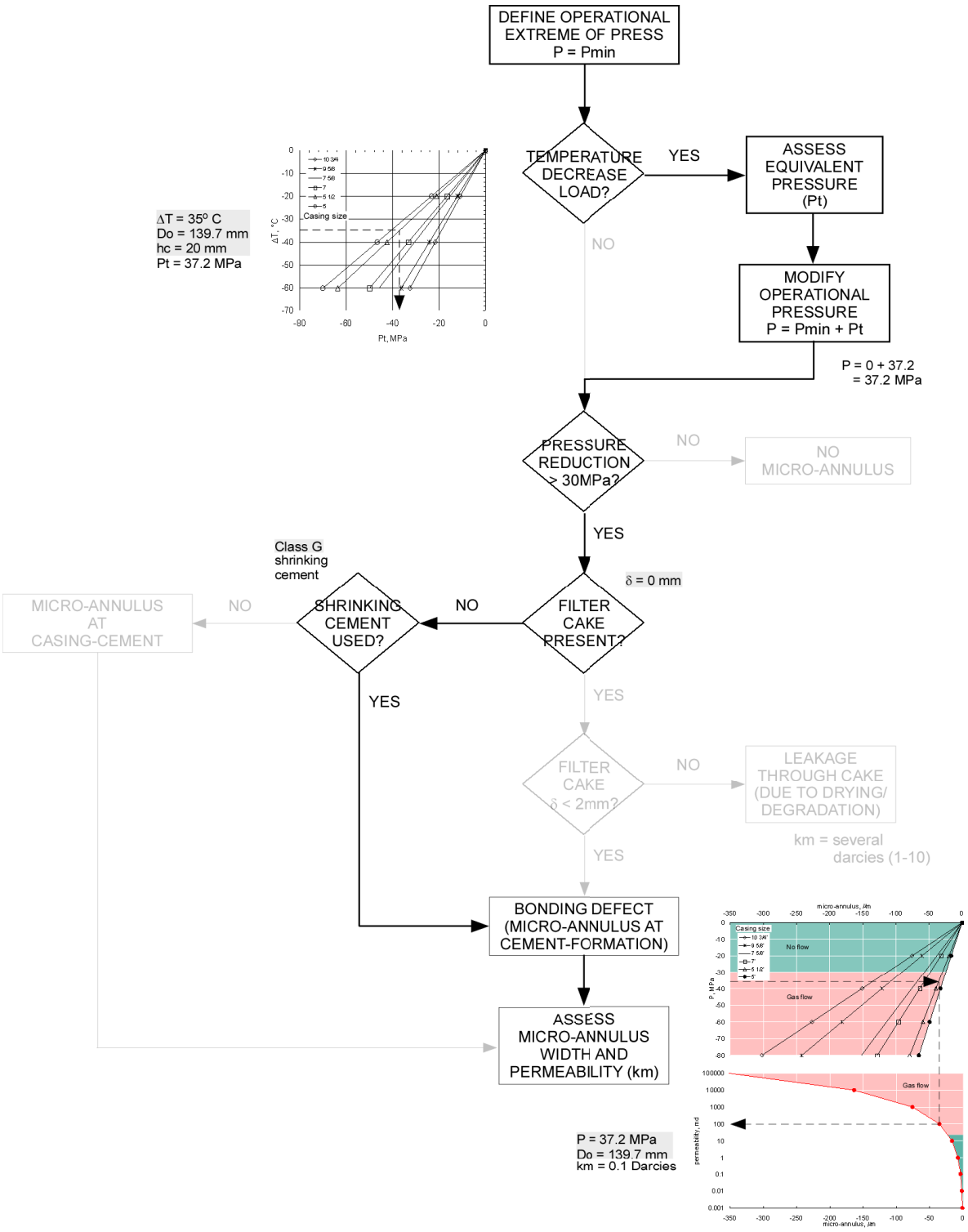

Figure 64 Procedure for predicting micro-annulus development (aquifer).

In the Weyburn field, most completion operations were performed at low pressure. Therefore, micro-annulus formation due to decrease in internal casing pressure is not a significant concern. On the other hand, the effect of temperature on wellbore interfaces integrity is a concern in those wellbores where cool-fluid injection is common. At Weyburn, cool-fluid injection is seen on water-alternating-gas (WAG) injectors and CO_2 injectors.

Geothermal temperatures have been measured in the Weyburn field, but temperatures of down-hole fluid are currently unknown and a subject of debate. Therefore, a conservative temperature difference of –35°C was chosen. The equivalent internal-casing pressure (Pt) resulting from a temperature decrease of this magnitude is 37.2 MPa (Figure 42). This is greater than what is considered an acceptable pressure loading (30 MPa), so a micro-annulus can be expected. Properties of casing are given in Table 39.

Table 36 Data for calculation of equivalent internal-casing pressure.

Casing diameter	Do	5 ½ in
Casing-wall thickness	hc	20 mm

The next step is to evaluate where the micro-annulus is created. As the condition at the wellbore wall affects the type of micro-annulus formed, it is necessary to consider filter-cake thickness. Based on the methodology for

estimating this parameter (Figure 53), it is concluded that most of the filter cake was removed. Consequently, no debonding is expected at the interface between the cement and the formation due to filter cake.

However, even a flawless primary cementing job can be damaged by the shrinking nature of cement. Shrinking cement leads to a bonding defect at the cement-formation interface. Most cement slurries used in the Weyburn field during the 1950s can be classified as a shrinking cement; thus, a large interface debonding can be expected at the cement-formation boundary. Due to the level of temperature decrease, the casing contraction results in micro-annuli at this interface. The ultimate micro-annulus condition is then determined (Figure 43).

4.6 Deterioration Damage (Cement Aging)

Aging processes will occur only if a fluid (such as water) is able to migrate from an external source (such as from an aquifer) towards annular cement. If water is not freely available (i.e., across shale sections), aging will be effectively reduced. For the section evaluated (Ratcliffe aquifer), water is freely available. Formation water pH is 7 and temperature is 55°C. Annular cement is class G slurry and, based on Figure 40, considered as neat cement. The corresponding annular thickness is 30 mm.

From these data (Figure 65), the expected time of leaching ranges from 30 to 60 years (Figure 44). **Error! Reference source not found.** gives the rating of leached permeability for this type of cement as 10^{-5} D.

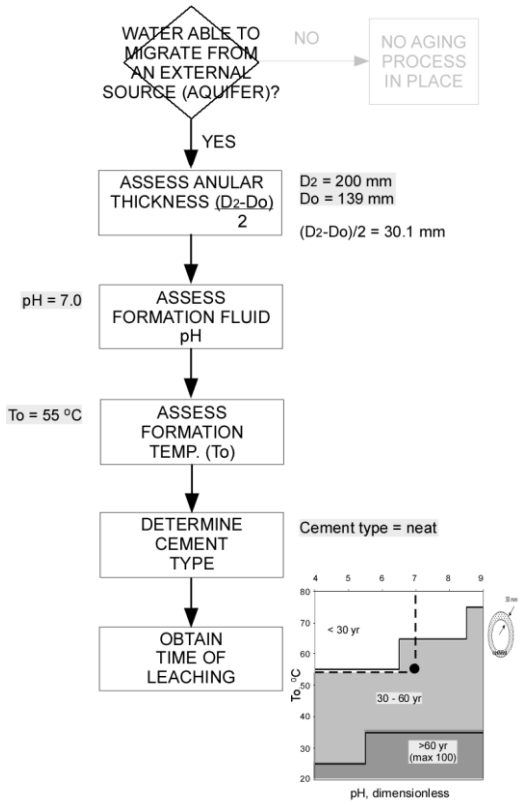

Figure 65 Protocol to assess time of leaching for annular cement (aquifer).

With the transport properties of the wellbore defined, a cross-section can now be presented Figure 67. Here, mud has formed a channel that the cement was unable to displace. This bypassed mud represents a potential fluid pathway. The section also involves an aquifer with a reduced permeability at the wellbore wall.

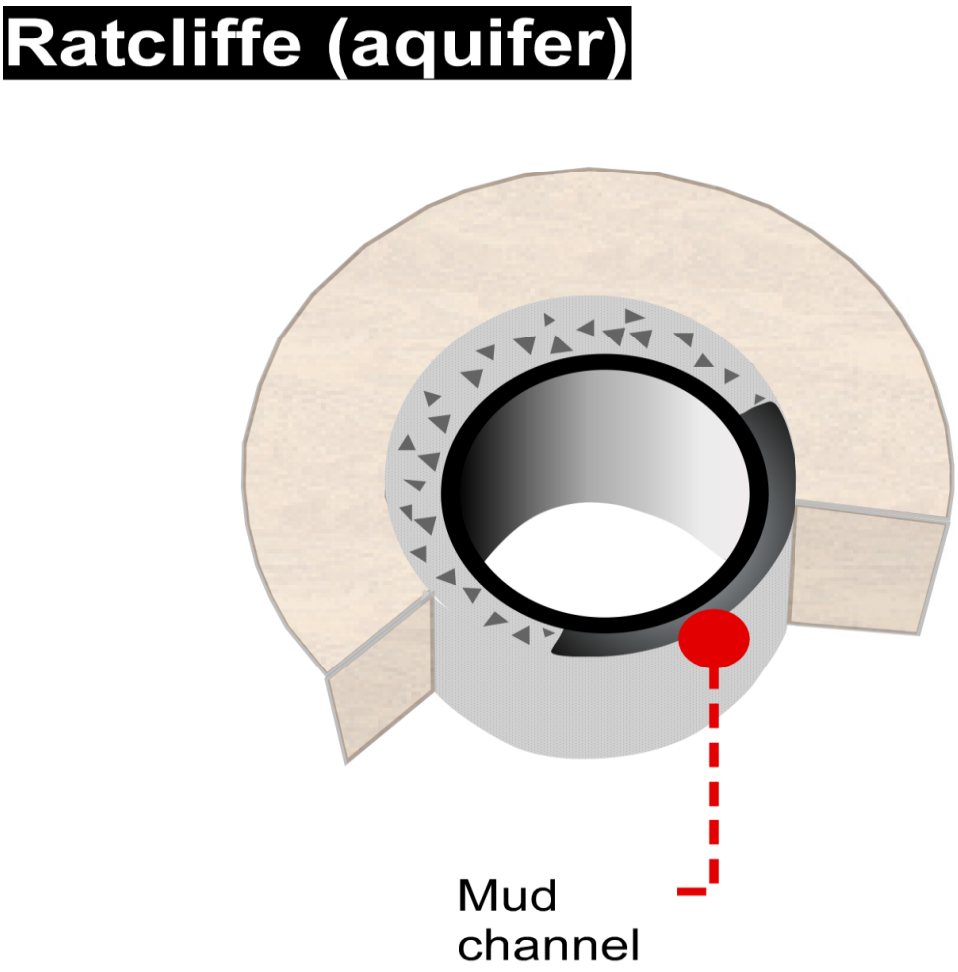

Figure 66 Typical wellbore condition at Ratcliffe section (aquifer).

Finally, the methodology is repeated with the other sections, and their transport properties computed. The resulting wellbore system is shown in Figure 67.

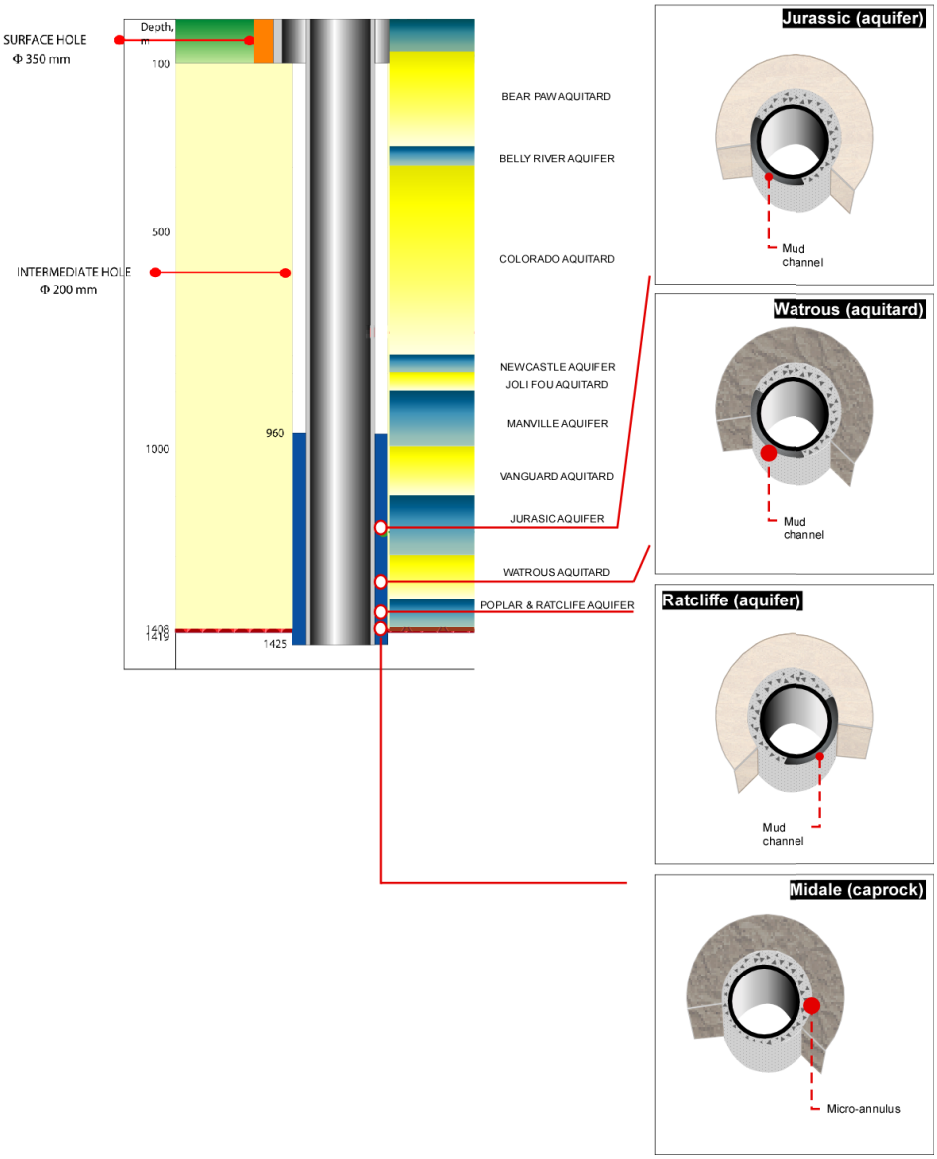

Figure 67 Description of a multilayered aquifer-aquitard system penetrated by a well in the Weyburn field.

5 Annular gas flow modelling

After completion of enhanced oil recovery (EOR) by CO_2 flooding in the Weyburn field, the injected CO_2 is expected to stay in the reservoir before slowly dispersing into the geosphere due to stratigraphic and hydrological trapping mechanisms. During this period, the only potential leakage pathways for the injected CO_2 will be through abandoned wells.

The question is: "How important is the leakage to the overall performance of CO_2 storage in the Weyburn reservoir?" With detailed characterization of the wellbore-system model completed, the answer to this question can now be investigated. As discussed at Section 4.2, the wellbore conceptual model was subdivided into hydrostratigraphic units (two aquitards and two aquifers); the mean thickness and permeability of these units are provided in Table 37. The data for these units were extracted from the methodology for assessment of transport properties developed in Chapter 3.3. Equivalent permeability for each sector was obtained using the expression for flow parallel across individual layers (equation [45]).

$$k_l = \frac{\sum_{i=1}^{n} hi * ki}{H_T}$$

[45]

Table 37 Wellbore transport properties.

	Cement	Micro-annulus	Mud channel
Midale (aquitard)			
hi, m	0.03	0.00003	
ki (D)	1×10^{-7}	0.1	
$k_l = 1x10^{-4}$ D			
Ratcliffe (aquifer)			
hi, m	0.39		0.13
ki (D)	1×10^{-7}		10
$k_l = 2.4$ D			
Watrous (aquitard)			
hi, m	0.39		0.13
ki (D)	1×10^{-7}		10
$k_l = 2.4$ D			
Jurassic (aquifer)			
hi, m	0.39		0.13
ki (D)	1×10^{-7}		10
$k_l = 2.4$ D			

The mechanics of CO_2 discharge through a wellbore by simulating a very simple and idealized problem can then be explored. It is considered that the annulus has been in contact with CO_2 long enough that the gas will have penetrated into the annulus by dissolution and advection sufficiently that advection is occurring at steady state. The reader is referred to the

work of Pruess and Garcia (2002) for a detailed review of the fundamental dynamics of transient CO_2 flow behaviour in a well.

The model can be divided into three broad components, based on their function within the model: 1) the reservoir; 2) multiple aquifers and aquitards above the reservoir; and 3) the well, which penetrates all of these formations. The system is further simplified by assuming one-dimensional flow geometry and neglecting gravity, isothermal, and non-inertial effects. It is also assumed that constant pressure and phase composition (single-phase gas) exist at the top and bottom of the well. The temperature of the flow system is constant throughout. Migration into the surrounding formations is conservatively neglected.

Much of the information for one-dimensional model equations can be found in basic texts on flow in porous media, such as Nelson (1990). The equation that can be used to estimate the flow rate of gas through the annulus to the surface is

$$q = k_{ll} \times \pi\left(R_2{}^2 - R_o{}^2\right)\frac{1}{1424\mu z T_r}\frac{\Delta P^2}{\Delta L},$$

[46]

where q is the flow rate (Mscf/D), z is the gas deviation factor, and T is the reservoir temperature (°R).

Using this equation, the CO_2 flow rate through the wellbore can be estimated for various values of equivalent permeability. Table 38 contains some typical values from reservoir and well data. Figure 68 is a plot of the steady-state gas-flow rate for a range of permeabilities, calculated using the data in Table 38. As can be seen from this figure, the flow rate of gas bled from a wellbore can vary from very slight to thousands of standard cubic feet per day (Mscf/D).

Table 38 Well and reservoir data for gas flow along the annulus.

Wellbore radius	R_2	0.652 ft
Casing radius	Ro	0.458 ft
Reservoir pressure	ΔP	3000 psi
Well length	ΔL	1000 ft
Gas viscosity	μ	0.03 cp
Gas deviation factor	z	0.95
Reservoir temperature	Tr	560°R

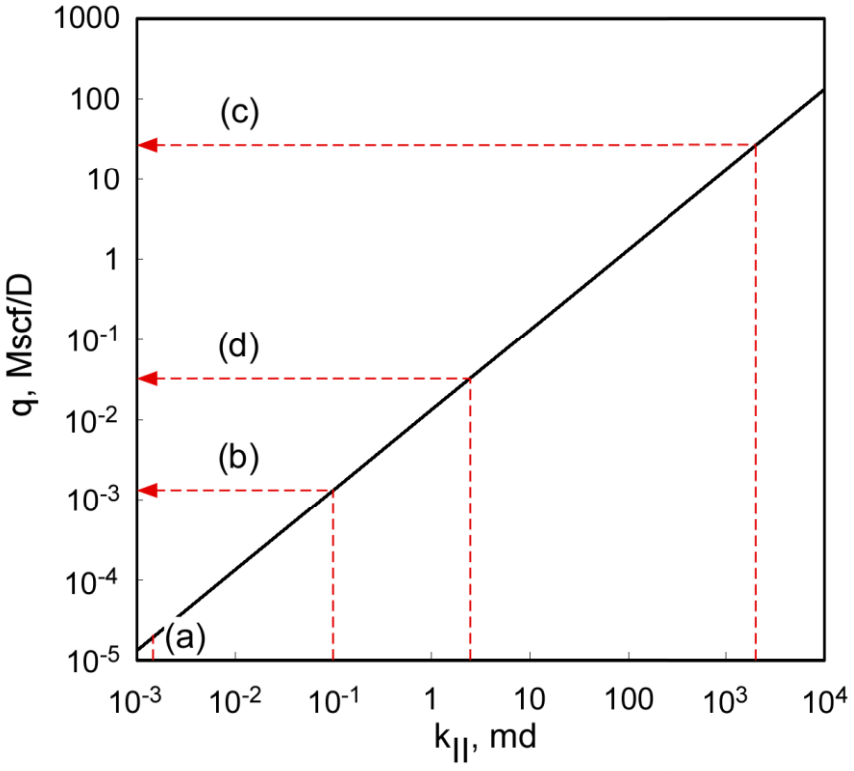

Figure 68 Rate of gas flow along the annulus for a range of equivalent annular permeabilities. Red dashed lines indicate the flow rate for cases of a) tight wellbore, b) wellbore with a micro-annulus, c) wellbore with a continuous mud channel, and d) typical multilayered well.

Figure 68 is used to discuss the relationship between these equivalent permeability values and zonal isolation, and what this represents within the context of CO_2 geological storage at Weyburn. For a tight wellbore (perfect annular cement sheath), only the innate matrix permeability of the cement sheath needs to be considered. Typical Portland cement systems used at Weyburn usually exhibit extremely low matrix permeability, with this property being less than 1 μD. In such cases, flow through the annulus will be very small and probably not detectable by logging, and zonal isolation very high.

However, the presence of a small micro-annulus might result in an increased equivalent permeability. As can be seen in the Midale section (Table 37), even a seemingly small micro-annulus width results in an increased equivalent permeability (0.1 mD). This conductive channel might become a flow path for gas migration, and because of this, the well may not provide complete isolation.

The existence of a continuous mud channel can further aggravate this situation. For a typical equivalent permeability of 2.4 D resulting from the presence of a mud channel (Figure 68), the flow rate is several thousand standard cubic feet per day (Mscf/D). It is important to point out that such flow is several orders of magnitude larger than the flow for a tight wellbore, and would probably result in loss of zonal isolation.

Nevertheless, it should be remembered that a typical wellbore is a multilayered system, so the resistance to flow in the well becomes a function of the resistance contribution from each sector. Figure 69 shows a typical wellbore with gas migration occurring vertically through the entire system. Owing to wellbore-history specifics, the coefficient of permeability of each wellbore sector may vary.

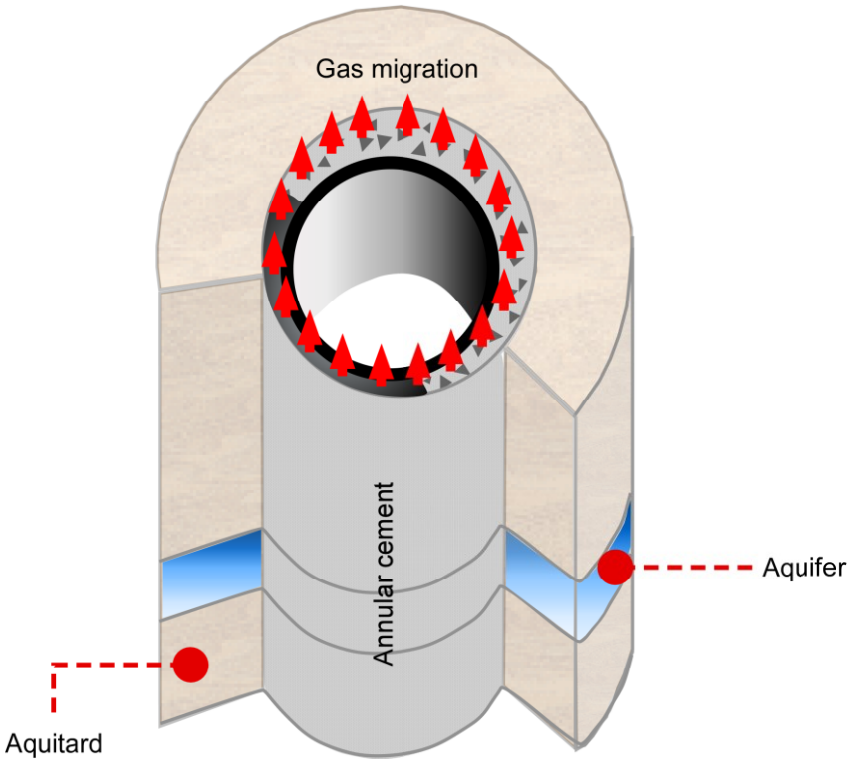

Figure 69 Vertical gas migration in wellbore.

For an assumption of essentially vertical flow, the discharge velocity is the same for all layers. So,

$$V = V_1 = V_2 = V_3 = \ldots = V_n,$$

[47]

where V, V_1, V_2, V_3, …, are the discharge velocities in layers 1, 2, 3, …, respectively. Substitution of Darcy's law into equation [47] yields an expression of equivalent permeability for the entire system

$$k_{II} = \frac{H_T}{\sum_{i=1}^{n} \frac{hi}{ki}},$$

[48]

where k_{ll} is effective coefficient of permeability for flow in the vertical direction, hi is the thickness of each section, and H is the total thickness ($H_T = h_1 + h_2 + h_3 + \ldots + h_n$).

For the example considered here, the wellbore system involves four sections. Using the data in Table 37 and equation [48], an equivalent permeability (k_{ll}) of 2.7 x 10^{-3} D is computed. For this case, the total leakage rate is close to 0.01% of the leakage rate observed in a well with a continuous mud channel (Figure 68). This means that even a single thick, tight (impervious) section may be optimal for minimization of distributed leakage through the wellbore.

A field program, conducted as a component of the IEAGHG Weyburn–Midale CO2 Monitoring and Storage Project, was undertaken to assess wellbore integrity in a 54-year old vertical well. Field measurements of equivalent wellbore annular permeability within the Watrous Formation suggest that the permeability of the cemented annulus is very low, falling somewhere in the 7 – 80 μD range (Hawkes and Gardner, 2013).

Equivalent wellbore annular permeability of the tested well was assessed using the proposed methodology. The well investigated had been drilled to a depth of 1471 m (4824 ft), cased with 139.7 mm (5.5 in.) production casing and cemented with a 1-to-1 blend of Portland cement and

pozzolan. Cased-hole logging indicates that the top of the cemented annulus is located approximately 500 m (1640 ft) above total depth of the well, and that production casing is centralized throughout the cemented annulus (Hawkes and Gardner, 2013). The well had been drilled as an oil producer in 1957, and is located in an area that had been under CO_2 flood for approximately 5 years priors to testing. However, this well was not used for injection of CO_2.

As indicated in Chapter 4, equivalent wellbore annular permeability is evaluated considering the effects of the four major permeability-disturbance groups: hydrochemical damage, mud removal, geomechanical damage, and deterioration damage.

Evaluation of the hydrochemical damage involves identifying the type of particulate processes that can occur. To achieve this, a problem-diagnostic protocol can be used (Figure 70). For a typical Watrous Formation permeability of 0.01 μD, the potential for hydrochemical damage is very low.

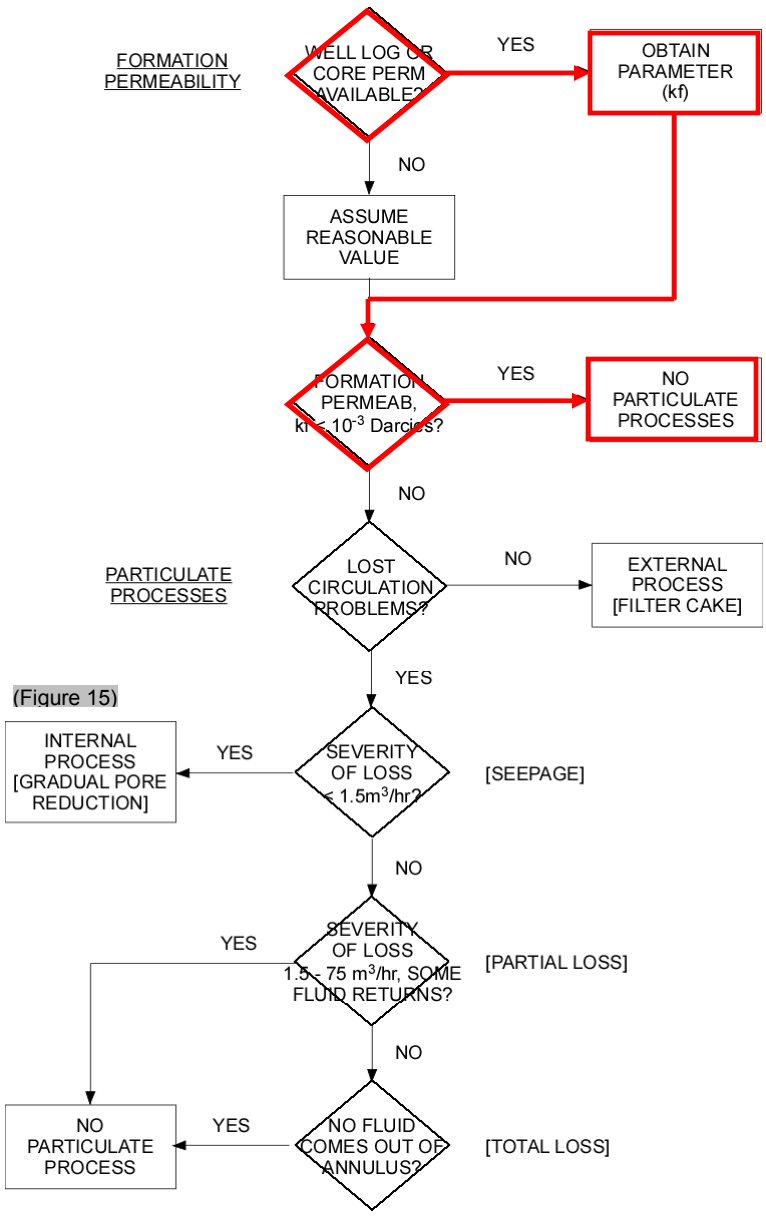

Figure 70 Problem-diagnostic protocol to identify type of particulate process.

Mud removal (displacement) efficiency can be evaluated based on the ratio between the interface velocity on the narrow side and the average velocity in the annulus. Using the values obtained in Section 4.4, and considering the fact that the production casing was centralized (STO >

75%) it can be seen that mud was effectively removed (Figure 71). This result is consistent with cased-hole logging results.

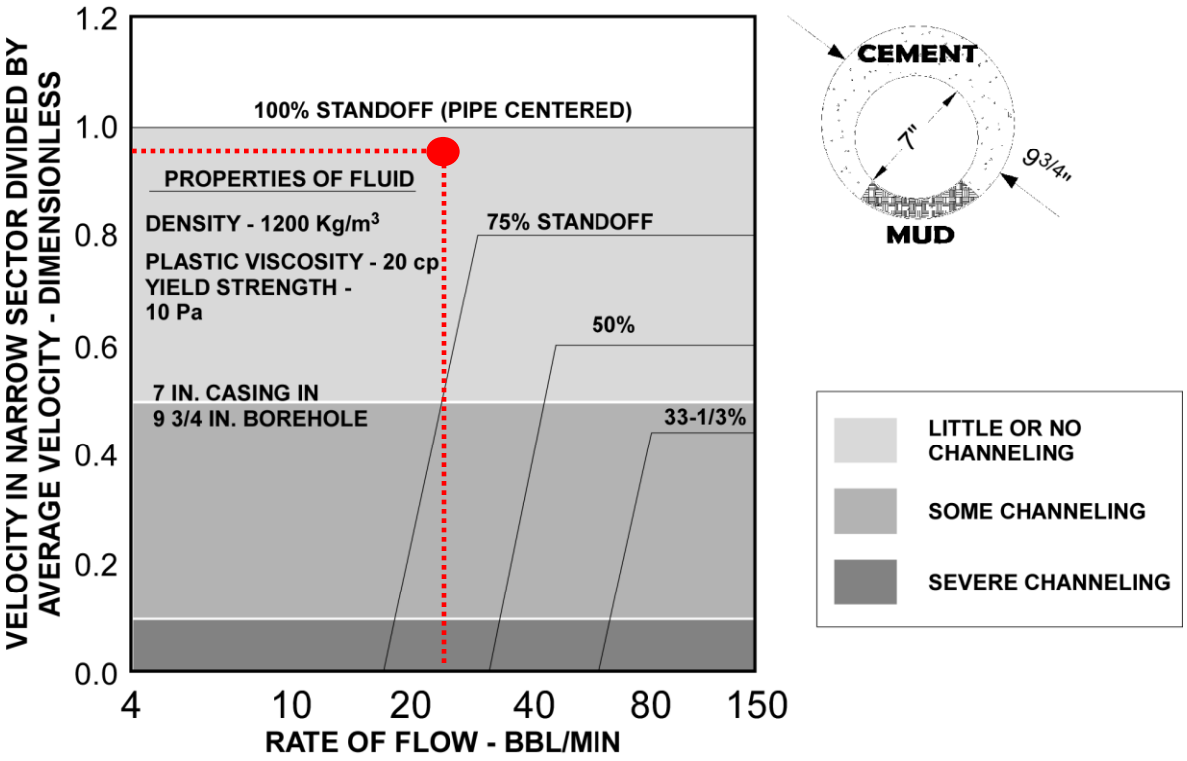

Figure 71 Typical chart of Velocity in narrow sector versus average velocity for several standoffs (STO).

Geomechanical damage involves the quantitative assessment of damage on the near-wellbore formation, the annular cement, and the wellbore interfaces. For the case being investigated here, the 54-year wellbore have similar properties and boundary conditions than those assessed for a typical well drilled in the 1950s (section 4.5.1 and 4.5.2). This suggests a near-wellbore region in good condition with no breakout present (gauge hole) and an annular cement capable of retaining zonal isolation.

The potential for development of a micro-annulus was evaluated using the protocol provided in Figure 72. As this well was not used for CO_2 injection, it is not expected that a micro-annulus will develop.

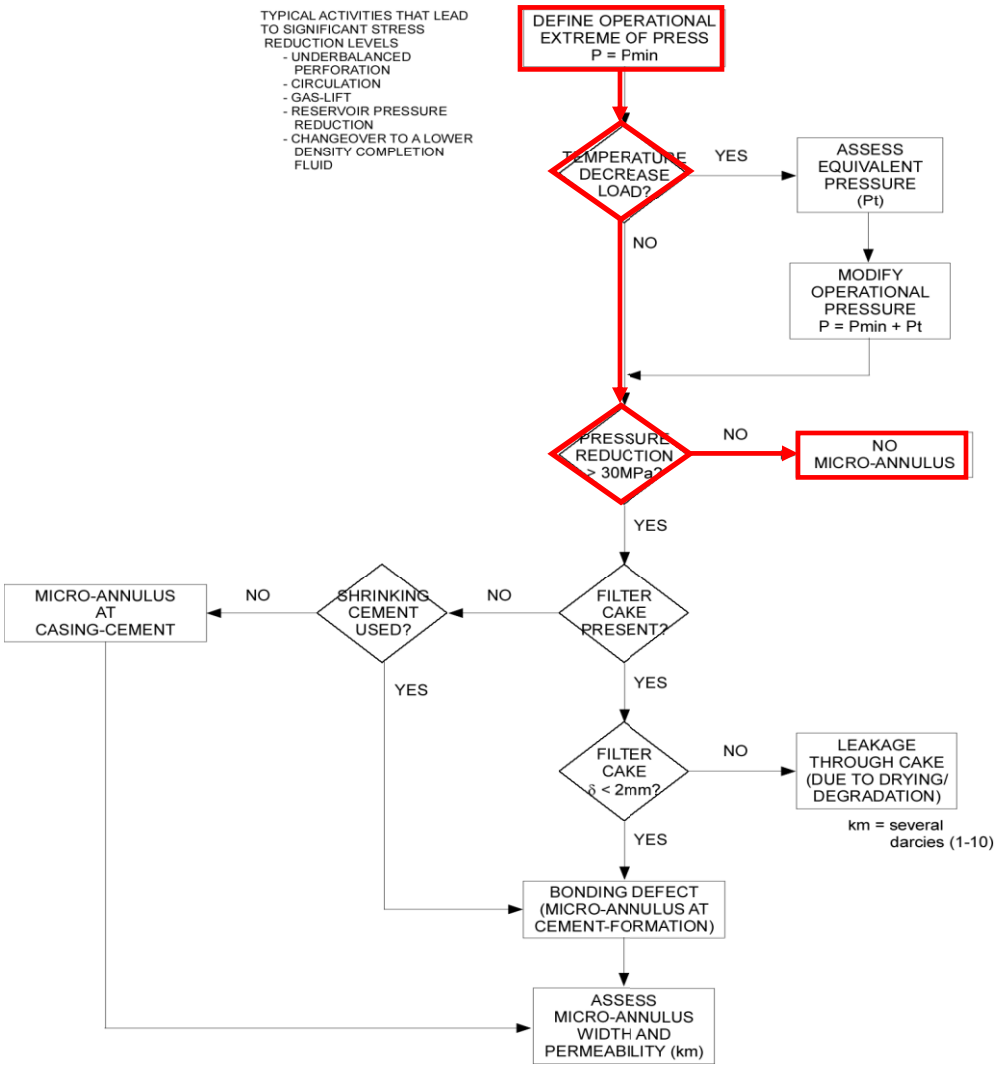

Figure 72 Procedure for predicting micro-annulus development.

Aging processes will occur only if a fluid (such as water) is able to migrate from an external source (such as from an aquifer) towards annular cement. If water is not freely available (e.g., across shale sections), aging

will be effectively reduced. For the section evaluated (Watrous aquitard), water is not freely available, thus, aging will be in the range of hundreds of years.

With detailed characterization of the wellbore-system model completed, the equivalent wellbore annular permeability within the Watrous Formation can be calculated (equation [45]). As the results from the methodology indicate that neither a micro-annulus nor a mud channel exists in the wellbore, the equivalent annular permeability will be that of the annular cement. Nelson and Guillot (2006) suggest that matrix permeabilities for Portland–pozzolan mixtures tend to be less than 1 μD. This result is consistent with field measurements; which suggest that equivalent permeability of the cemented annulus is in the 7 – 80 μD range (Hawkes and Gardner, 2013).

By way of comparison, vertical permeabilities in the 1–10 md range were interpreted by Crow et al. (2010) for the cemented annulus of a 30-year old well in a natural CO_2 reservoir in the United States. These results are roughly two orders of magnitude greater than those obtained by Hawkes and Gardner (2013). Unfortunately, there is not enough information about this wellbore to use the methodology to assess the equivalent permeability. However, the permeability range interpreted by Crow et al.

(2010) suggests that a preferential flow path may exist, possibly in the form of a micro-annulus (Figure 68).

6 Conclusions and Recommendations

6.1 General

A methodology to assess the transport properties of wells used in the geological storage of CO_2 has been presented. This methodology systematically evaluates the effect of each physical and chemical process that arises during the life of a well (drilling, completion, production) on its transport properties. Based on the physics involved in these permeability-alteration mechanisms, a four-group classification was proposed: geomechanical damage, hydrochemical damage, mud removal, and deterioration damage (cement and casing). This routine is flexible enough to allow the addition of new mechanisms as they are found to have an impact on well conductivity. Challenges associated with integrating real operational data into the performance assessment were discussed within the context of the performance-assessment methodology

The ability to capture the 'exact' state of all wellbores is extremely difficult. In order to quantify the main processes associated with the hydraulic integrity of the wells, the methodology implemented 'integrity indices' as a tool to assess the most likely future performance of wellbores. These integrity indices will permit the identification of possible high-risk areas associated with the CO_2 injection and will allow focused effort in those areas to refine the elements associated with the leakage risk.

The approach adopted within each group to assess transport properties of the wellbore system and a comprehensive review of their effects on the leakage flux of CO_2 are provided here.

6.2 Hydrochemical damage

The method developed to quantitatively estimate hydrochemical damage assumes that damage is caused mainly by particle invasion processes as a result of exposure of the permeable rock to mud fluids during drilling. The various particulate processes are classified in two groups: internal and external. Internal processes occur in the porous media in the form of gradual pore reduction, whereas external processes occur on the face of the formation (i.e., filter cake).

The method integrates the many factors that cause damage through every phase of well drilling. These include particle size, mud type, temperature, pressure, and pump rate. The method starts by flagging the type of particulate process that can occur, using a problem-diagnostic protocol that was developed for the project. This diagnostic tool identifies the most probable type of particulate process by asking the user a series of questions. With the type of process identified, the appropriate steps can then be followed to assess its consequences and severity. Most of the steps are almost intuitive, but a structured approach is required for success.

The modelling results presented show that, in all cases, the various particulate processes associated with the flow of high-particle-content mud will lead to an order-of-magnitude decrease in hydraulic conductivity of permeable formations.

6.3 Mud removal

A model was developed for evaluating the efficiency of mud removal. This model allows the simulation of mud displacement for vertical or near-vertical wells only. Mud-removal efficiency is calculated in terms of the ratio between the interface velocity on the narrow side and the average velocity in the annulus. Results show that efficiency is strongly dependent upon the relative properties of the fluids involved, casing centralization, and displacement rate.

Incomplete mud displacement can manifest as a continuous mud channel that forms on the narrow side of the eccentric annulus. This residual mud dehydrates as the cement sets and allows a porous conduit to develop in the annulus, thereby favouring gas migration. This flow path, and its effective width, correspond to a permeability that is far greater than the intrinsic permeability of undisturbed set cement. The permeability of this preferential route for gas migration should be of primary concern when

evaluating the flow rate through the annulus. Surprisingly, only a cursory treatment of the subject is found in literature.

Scratchers, scrapers, or cable wipers, when used during casing movement, have been shown to mechanically erode the filter cake and therefore considerably improve the displacement process. However, there is currently a lack of data on the effects of these mechanical devices on mud circulation.

Very little work has been done on the pressure and temperature dependence of the rheological properties of drilling muds. Most drilling fluids are water-based; thus, in view of the low compressibility and viscosity-pressure dependence of water, the effect of pressure on their flow properties has usually been considered negligible. This is likely the case for most drilling systems, but the effect could be considerable in those systems exhibiting high solid to liquid ratios. On the other hand, temperature can have a drastic effect on fluid rheology, but the extent of this is highly dependent on the drill system. Thus, more attention should be paid to the complete characterization of drilling fluids when used at high temperatures and pressures, and the effect of drilling-fluid properties on mud-removal efficiency.

6.4 Geomechanical damage

Assessment of any alteration of flow properties due to geomechanical damage covers the evaluation of stress redistribution at the wellbore wall, development of mechanical cracking of the cement annulus, and debonding of the casing-cement and formation-cement interfaces.

In assessing wellbore instability, stresses induced at the borehole wall and the interaction mechanisms between drilling fluid and the formation were proven critical for determining whether drilling will induce instability. Results show that, in either case, the extent of the damaged zone and the change in permeability is strongly dependent on the post-failure behaviour of the rock (brittle or ductile). Brittle rocks generally exhibit elevated permeability associated with dilatant deformation. Some or all of this damaged zone will break to the point where rock particles are detached from the well (collapse). In contrast, the collapse mechanism in ductile rocks corresponds to a convergence of the wellbore and an irreversible reduction of permeability (Charlez, 1997, McLennan and Abou-Sayed, 2002, and Soares and Ferreira, 2002).

The development of mechanical cracking of annular cement was also investigated. It was shown that cement integrity depends on mechanical properties, such as Young's modulus, and on the stability condition of the well. It was found that, in the case of a stable well, the dominant failure mechanism is dependent on the type of cement used and the relative

Young's modulus values of the cement and rock. On the other hand, it was seen that annular cement, irrespective of the volumetric behaviour of cement, is forced into shear damage due to displacements originating from an unstable wellbore.

Finally, a method was developed to estimate the potential for debonding at the casing-cement and formation-cement interfaces. It takes into account Earth stresses around the wellbore, as well as the bonding condition at the wall. For the purposes of gas-leakage estimation, interface debonding can be divided into three types: casing-cement interface, formation-cement interface, and cake leakage.

The presence of a micro-annulus has a considerable impact on the simulated leakage of gas. However, as discussed earlier, micro-annulus conductivity is an equivalent value resulting from the well-known expression of permeability for the flow through a slot. This relationship can be used as an approximation only; significant deviations from this value can be found and often attributed to the imperfect geometry of the micro-annulus. The permeability of the micro-annulus should be of primary concern, so a more comprehensive investigation of the subject is needed.

The effects of volumetric change during cement hydration at the cement-casing and cement-formation interfaces have long been a subject of debate because research studies show conflicting results. Some investigators concluded that volumetric shrinkage of cement would result in a micro-annulus (Baumgarte et al., 1999, Bentz et al., 2001, and Ladva et al., 2004). Others showed that shrinkage of cement is probably too small to induce a significant continuous micro-annulus; instead, some local bonding defects can result (Wu et al., 1983). Given that a consensus does not yet exist, this subject undoubtedly requires additional investigation.

6.5 Deterioration damage

A simple method has been developed to predict the degradation time of cement. Time-dependent data generated by this method show that significant deterioration due to the interaction between cement and groundwater may take as long as 150 years. On the other hand, high-water-content cements (lightweight) can rapidly degrade, in some cases in less than 30 years. However, these degradation times can be regarded as conservative values. The model used to estimate them does not take into consideration the natural calcium content of the groundwater. In addition, the use of high-particle-concentration mud and fluid-loss additives can alter the conductivity properties of the surrounding permeable formations (internal cake), thus modifying the calcium flux rate from cement. Further

studies that take into consideration this possible scenario and its effect on degradation rates are advised.

The value chosen as the intact permeability of cement was based on data available from the public literature, the measurements having been made on cement samples under laboratory conditions. However, previous research on cement durability has demonstrated the importance of the curing conditions. Among the many variables that affect the hydration of cement paste and its initial conductivity are temperature and water changes due to exposure to the ambient environment. High temperature produces a porous material and a sealed curing condition (e.g., cement in contact with a shale section) can create greater shrinking of the cement than a saturated condition (e.g., cement in contact with an aquifer). However, studies on the effect of the ambient environment on the curing of oil-well cement are not available. It is expected that research in this area will have to expand quickly to address the many outstanding questions regarding long-term sealing capability of wellbores. Furthermore, an extensive literature review shows that measurements of the increase in permeability of oil-well cement with age have not been made, so work is also needed in this area.

When a well is abandoned, cement is poured inside the casing. As the slurry sets, adhesion between cement and casing provides sealing

capabilities. From the perspective of long-term assessment, the cement plug will provide a potential independent pathway for CO_2. Hence, migration of the injected CO_2 in the reservoir through an abandoned well can occur via

1) the annular space, and
2) the cement plug

The length of the sealing column in an abandoned well is determined according to local regulations. The seal usually consists of a series of cement plugs, with the remaining space usually left open and/or filled with formation waters at deeper depths. Because leakage through the plugs depends on the combined effects of well-abandonment techniques, cement degradation and CO_2 migration, a full understanding of this mechanism is needed. However, no solutions have yet been developed that can analyze practical leakage problems involving cement plugs. Thus, this subject requires further investigation.

References

Aadnoy, B.S., and Hansen, A.K. (2005): Bound on in-situ magnitudes improves wellbore stability analyses; paper SPE 87223.

Abdulhadi, N. O., Germaine, John T., and Whittle, A. J. (2011): Experimental Study of Wellbore Instability in Clays; Journal of Geotechnical and Geoenvironmental Engineering, v 137, n 8, p 766-776.

Adamson, K., Birch, G., Gao, E., Hand, S., McDonald, C., Mack, D., and Quadri, A. (1998): High-pressure, high-temperature well construction; Oilfield Review, summer, 14 p.

Amanullah, Md., and Tan, C.P. (2000): Anon-destructive method of cake thickness measurement; paper SPE 64517.

Amanullah, Md., and Tan, C.P. (2001): A field applicable laser-based apparatus for mud cake thickness measurement; paper SPE 68673.

Al-Ajmi, A.M., and Zimmerman, R.W. (2006): Stability analysis of vertical boreholes using the Mogi-Coulomb failure criterion; International Journal of Rock Mechanics and Mining Sciences, v 43, n 8, p 1200-1211.

Al-Bazali, Talal M. (2011): Role of anions on shale stability: The neglected phenomenon; Special Topics and Reviews in Porous Media, v 2, n 3, p 237-247.

AL-Bazali, T. M. (2011): The consequences of using concentrated salt solutions for mitigating wellbore instability in shales; Journal of Petroleum Science and Engineering, v 80, n 1, p 94-101.

API. (1986): Spec 10 D, Casing Centralizers, third edition; 10, p. 12-13.

Ardakani, S., and Ulm, F. (2014): Chemoelastic fracture mechanics model for cement sheath integrity; Journal of Engineering Mechanics, v 140, n 4.

Arceneaux, M.A., and Smith, R.L. (1986): Liner rotation while cementing: an operator's experience in South Texas; paper SPE 13448.

Argillier, J-F., Audibert, A., and Longeron, D. (1997): Performance evaluation and formation damage potential of new water based drilling formulations; paper SPE 38152.

Arthur, K.G., and Peden, J.M. (1988): The evaluation of drilling fluid filter cake properties and their influence on fluid loss; paper SPE 17617.

Atkinson, A., and Hearne, J.A. (1990): Mechanistic model for the durability of concrete barriers exposed to sulphate-bearing ground waters;

Materials Research Society Symposium Proceedings, v. 176, p. 149-156.

Bailey, L., Way, P., and L'Alloret, F. (1998): Filter cake integrity and reservoir damage; paper SPE 39429.

Barton, N.R., Lien, R., and Lunde, J. (1974): Engineering classification of rock masses for the design of tunnel support; Rock Mechanics, v. 6, 4, p. 189-239.

Baumgarte, C., Thiercelin, M., and Klaus, D. (1999): Case studies of expanding cement to prevent microannular formation; paper SPE 56535.

Beaudoin, J.J., Feldman, R.F., and Tumidajski, P.J. (1994): Pore structure of hardened Portland cement paste and its influence on properties; Advanced cement Based Materials, v. 1, p. 224-236.

Bell, J.S., Price, P.R., and McLellan, P.J. (1994): Geological Atlas of the Western Canada Sedimentary Basin -In-situ stress in the Western Canada Sedimentary Basin, Canadian Society of Petroleum Geologists and Alberta Research Council, Edmonton, p. 439-446.

Bellabarba, M., Bulte-Loyer, H., Froelich, B., Le Roy-Delage, S., Van Kuijk, R., Zeroug, S., Guillot, D., Moroni, N., Pastor, S., and Zanchi, A. (2008): Ensuring zonal isolation beyond the life of the well; Oilfield Review, v 20, n 1, p 18-31.

Bentz, D.P., Jensen, O., Hansen, K.K., Olesen, J., Stang, H., and Haecker C.J. (2001): Influence of cement particle-size distribution on early age autogenous strains and stresses in cement-based materials; Journal of American Ceramic Society, v. 84, p. 129-135.

Bieniawski, Z.T. (1967): Mechanism of brittle fracture of rock; International Journal of Rock Mechanics Mining Science, v. 4, p. 407-423.

Bieniawski, Z.T. (1976): Rock mass classification in rock engineering; *in* Proceedings of the Exploration for Rock Engineering Conference, Cape Town, South Africa, p. 97-106.

Bo, M.K., Freshwater, D.C., and Scarlett, B. (1965): The effect of particle size distribution on the permeability of filter cakes; Transaction Chemical Engineering, v. 43, p. 228-232.

Bonett, A., and Pafitis, D. (1996): Getting to the root of gas migration; Oilfield Review, spring, 14 p.

Bosma, M., Ravi, K., Van Driel, W., and Schreppers, G.J. (1999): Design approach to sealant selection for the life of the well; paper SPE 56536.

Boukhelifa, L., Moroni, N., James, S.G., Le Roy-Delage, S., Thiercelin, M.J., and Lemaire, G. (2005): Evaluation of cement systems for oil- and gas-well zonal isolation in a full-scale annular geometry; paper SPE 87195.

Bouteca, M., and Gueguen, Y. (1999): Mechanical properties of rocks: pore pressure and scale effects; Oil and Gas Science and Technology, v. 54, 6, p. 703-714.

Brady, S.D., Drecq, P.P., Baker, K.C., and Guillot, D.J. (1992): Recent technological advances help solve cement placement problems in the Gulf of Mexico; paper SPE 23927.

Brice, J.W., and Holmes, B.C. (1964): Engineered casing cementing programs using turbulent flow techniques; paper SPE 742.

Brown, E.T. (1981): Rock characterization, testing and monitoring; ISRM Suggested Methods, Pergamon Press, Oxford, 654 p.

Brownie, S.V., and Smith, P.S. (1994): Mud cake cleanup to enhance productivity of high-angle wells; paper SPE 27350.

Brudy, M., and Zoback, M.D. (1999): drilling-induced tensile wall-fractures: implications for determination of in-situ stress orientation and magnitude; International Journal of Rock Mechanics and Mining Sciences, 36, p. 191-215.

Buckingham, J.C., Grimley, T.A., and Buckingham, J.P. (1994): Velocity and turbulence intensity profiles for Newtonian annular flows and the effect of mechanical aids on these profiles; paper SPE 28471.

Bourgoyne, A.T., Scott, S.L., and Manowski, W. (2000): A review of sustained casing pressure occurring on the OCS; US Minerals Management Service, 62 p., URL <http://www.mms.gov/tarprojects/008/008DE.pdf> [June, 2011].

Burloin, N., Skoczylas, F., Dubois, T. (2003): Induced anisotropy due to drying of concrete; Cement and Concrete Research, v. 33, p. 679-687.

Byck, H.T. (1939): Effect of temperature on plastering properties and viscosity of rotary drilling muds; Petroleum Technology AIME, p. 116.

Cao, H.T., Bucea, L., Ray, A., and Yozghatlian, S. (1997): The effect of cement composition and pH of environment on sulphate resistant of Portland cements and blended cements; Cement and Concrete composition, v. 19, p. 161-171.

Carde, C., and Francois, R. (1999): Modelling the loss of strength and porosity increase due to the leaching of cement pastes; Cement and Concrete Research, v. 21, p. 181-188.

Carey, J. , Wigand, M., Chipera, S., WoldeGabriel, G., Pawar, R., Lichtner, P. C., Wehner, S. C., Raines, M., Guthrie Jr., G. (2007): Analysis and performance of oil well cement with 30 years of CO2 exposure from the SACROC Unit, West Texas, USA; International Journal of Greenhouse Gas Control, v 1, n 1, p 75-85.

Carey, J., Svec, R., Grigg, R., Zhang, J., and Crow, W. (2010): Experimental investigation of wellbore integrity and CO2-brine flow

along the casing-cement microannulus; International Journal of Greenhouse Gas Control, v 4, n 2, p 272-282.

Carminati, S., Del Gaudio, L., and Brignoli, M. (2000): Shale stabilization by pressure propagation prevention; paper SPE 63053.

Cengage, G. (2003): Geothermal gradient; World of Earth Science, URL <http://www.enotes.com/earth-science/geothermal-gradient> [June, 2011].

Cerasi, P., Ladva, H.K., Bradbury, M-I L.L.C., and Soga, K. (2001): Measurement of the mechanical properties of filter cakes; paper SPE 68948.

Chambre Syndicale de la Recherche et la Production du Petrole et du Gaz Naturels (1982): Drilling mud and cement slurry rheology manual; Gulf Publishing Company, Houston, 107 p.

Charlez, P.A. (1997): The impact of constitutive laws on wellbore stability: a general review; paper SPE 28058.

Cheatham, J.B. (1984): Wellbore stability; paper SPE 13340.

Chen, X., Tan, C.P., and Haberfield, C.M. (1998): A comprehensive practical approach for wellbore instability management; paper SPE 48898.

Chen, X., Tan, C.P., and Haberfield, C.M. (2002): A comprehensive, practical approach for wellbore instability management; paper SPE 80146.

Chesser, B.G., Clark, D.E., and Wise, W.V. (1994): Dynamic and static filtrate-loss techniques for monitoring filter-cake quality improves drilling-fluid performance; paper SPE 20439.

Chiappone, A., Marello, S., Scavia, C., and Setti, M. (2004): Clay mineral characterization through the methylene blue test: comparison with other experimental techniques and applications of the method; Canadian Geotechnical Journal, v. 41, p. 1168-1178.

Childers, M.A. (1968): Primary cementing of multiple casing; paper SPE 1919.

Choi, S.K., and Tan, C.P. (1998): Modelling of effects of drilling fluid temperature on wellbore stability; paper SPE 47304.

Christanti, Y., Ferrara, G., Ritz, T., Busby, B., Jeanpert, J., Abad, C., and Gadiyar, B. (2011): A new technique to control fines migration in poorly consolidated sandstones - Laboratory development and case histories ; SPE - 9th European Formation Damage Conference 2011, v 1, p 602-614.

Christensen, B.J., Mason, T.O., and Jennings, H.M. (1996): Comparison of measured and calculated permeabilities for hardened cement pastes; Cement and Concrete Research, v. 26, 9, p. 1325-1334.

Civan, F. (2000): Reservoir formation damage: fundamentals, modelling, assessment, and mitigation, Gulf Publishing Company, Houston, 760 p.

Clark, C.R., and Carter, L.G. (1973): Mud displacement with cement slurries; paper SPE 4090.

Cocka, E. (2002): Relationship between Methylene blue value, initial soil suction and swell percent of expansive soils; Turkish Journal of Engineering and Environmental Science, v. 26, p. 521-529.

Cook, R.A., and Hover, K.C. (1999): Mercury porosimetry of hardened cement pastes; Cement and Concrete Research, v. 29, p. 933-943.

Corr, D.J., Monteiro, P., Kurtis, K., and Kiureghian, A. D. (2001): Sulphate attack of concrete: reliability analysis; ACI materials Journal, v. 98, p.99-104.

Courteille, J.M., and Zurdo, C. (1985): A new approach to differential sticking; paper SPE 14244.

Crook, T., Wilson, S., Yu, J.G., and Owen, R. (2003): Computational modelling of the localized deformation associated with borehole breakout in quasi-brittle materials; Journal of Petroleum Science and Engineering, 38, p. 177-186.

Crow, W., Carey, J.W., Gasda, S.E., Williams, D.B., Celia, M.A., (2010): Wellbore integrity of a natural CO_2 producer. International Journal of Greenhouse Gas Control 4, p. 186–197.

Cui, L., and Cahyadi, J.H. (2001): Permeability and pore structure of OPC paste. Cement and Concrete Research; v. 31, p. 277-282.

Daccord, G., and Baret, J.F. (1994): How fluid loss influences primary cementing: literature review and methodology; paper SPE 25150.

Daemen, J.J.K., and Fairhurst, C. (1970): Influence of inelastic rock properties on the stability of a wellbore; paper SPE 3032.

Darley, H.C.H., and Gray, G.R. (1988): Composition and properties of drilling and completion fluids; Gulf Publishing Company, Houston, 654 p.

Davidson, E., Mota, L., Mosley, N., Chimara, G., Morrison, A., and Archibald, I. (2012): New and effective filter cake removal optimizes water injectivity; Proceedings - SPE International Symposium on Formation Damage Control, v 2, p 608-618.

Deere, D.U., and Miller, R.P. (1966): Engineering classification and index properties for intact rock; Report No. AFNLK-TR-65-116, Air Force Weapons Laboratory, 277 p.

Deily, F.H., and Owens, T.C. (1969): Stress around a wellbore; paper SPE 2557.

Denney, D., Latorre, B., Bórquez, C., Delgado, J., and Lueje, A. (2009): Logistics and design considerations for cementing large casing strings in extended deviated wells: A case history; Journal of Petroleum Technology, v 61, n 11, p 60-61.

Dillenbeck, R.L., and Simpson, S. (1999): New downhole external casing mud removal technology improves primary cement results; paper SPE 53943.

Dusseault, M.B., and Gray, K.E., (1992): Mechanisms of stress-induced wellbore damage; paper SPE 23825.

Eijk, R.J., and Brouwers, H.J.H. (1998): Study of the relation between hydrated Portland cement composition and leaching resistance; Cement and Concrete Research, v. 28, p. 815-828.

El-Dieb, A.S., and Hooton, R.D. (1994): Evaluation of the Katz-Thompson model for estimating the water permeability of cement-based materials from mercury intrusion porosimetry data; Cement and Concrete Research, v. 24, 3, p. 443-455.

El-Sayed, M., Ezz, A., Aziz, M., Waheed, A. (2007): Successes in curing massive lost-circulation problems with a new, expansive LCM; Proceedings of the SPE/IADC Middle East Drilling Technology Conference and Exhibition, p 379-383.

Erkekol, S., Gucuyener, I. H., Kok, M.V. (2006): An experimental investigation on the chemical stability of selected formation and determination of the proper type of water-base drilling fluids. Part 2. Test results; Energy Sources, Part A: Recovery, Utilization and Environmental Effects, v 28, n 9, p 885-892.

Ershaghi, I., and Azari, M. (1980): A new approach to differential sticking; paper SPE 14244.

Ershaghi, I., and Azari, M. (1980b): Modelling of filter cake build-up under dynamic-static conditions; paper SPE 8902.

Fam, M.A., and Dusseault, M.B. (1998): Borehole stability in shales: a physico-chemical perspective; paper SPE 47301.

Faucon, P., Adenot, F., Jacquinot, J.F., Petit, J.C., Cabrillac, R., and Jorda, M. (1998): Long-term behaviour of cement pastes used for nuclear waste disposal: review of physico-chemical mechanisms of water degradation; Cement and Concrete Research, v. 28, p. 847-857.

Ferla, A., Lavrov, A., and Fjær, E. (2009): Finite-element analysis of thermal-induced stresses around a cased injection well; Journal of Physics: Conference Series, v 181, n 1, p 012051 (8 pp.).

Fisk, J.V., Shaffer, S.S., and Helmy, S. (1991): The use of filtration theory in developing a mechanism for filter-cake deposition by drilling fluids in laminar flow; paper SPE 20438.

Fjaer, E., Holt, R.M., Nes, O-M., and Sonstebo, E.F. (2002): Mud chemistry on time-delayed borehole stability problems in shales; paper SPE 78163.

Flumerfelt, R.W. (1975): Laminar displacement of non-Newtonian fluids in parallel plate and narrow gap annular geometries; paper SPE 4486.

Fordham, E.J., Ladva, H.K.J., Hall, C., Sherwood, J.D. (1988): Dynamic filtration of bentonite muds under different flow conditions; paper SPE 18038.

Francis, P., Eigner, M.R.P., Patey, I.T.M., and Spark, I.S.C. (1995): Visualization of drilling-induced formation damage mechanisms using reservoir conditions core flood testing; paper SPE 30088.

Francis, P. (1997): Dominating effects controlling the extent of drilling-induced formation damage; paper SPE 38182.

Fraser, L.J., Reid, P., Williamson, D., and Enriquez, F. (1995): Mechanistic investigation of the formation damaging characteristics of Mixed Metal Hydroxide drill-in fluids and comparison with polymer-base fluids; paper SPE 30501.

Fraser, L., Stanger, B., Griffin, T., Jabri, M., Sones, G., Steelman, M., and Valko, P. (1996): Seamless fluids program. A key to better well construction; Oilfield Review, Summer 1996, p. 42-56.

Testing and evaluation techniques for drilling fluids-shale interaction and shale stability Friedheim, J. , Guo, Q., Young, S., and Gomez, S. (2011): 45th US Rock Mechanics / Geomechanics Symposium.

Frigaard, I.A., Allouche, M., Gabard-Cuoq, C. (2001): Setting rheological targets for chemical solutions in mud removal and cement slurry design; paper SPE 64998.

Frigaard, I.A., and Pelipenko, S. (2003): Effective and ineffective strategies for mud removal and cement slurry design; paper SPE 80999.

Galle, C., and Daian, J.F. (2000): Gas permeability of unsaturated cement-based materials: application of a multi-scale network model; Magazine of Concrete Research, v. 52, 4, p. 251-263.

Garboczi, E., and Bentz, D.P. (1998): The microstructure of Portland cement-based materials: computer simulation and percolation theory; *in* Proceedings of the Material Research Society Symposium, v. 529, San Francisco, California, p. 89-99.

Garboczi, E., and Bentz, D.P. (1999): Computer simulation and percolation theory applied to concrete; Annual review of Computational Physics VII, p. 85-123.

Gdanski, R., and Bryant, J. (2011): Rheology measurements of concentrated broken gel for filtercake modeling; SPE - Hydraulic Fracturing Technology Conference 2011, p 165-180.

Gdanski, R.D., and Bryant, J.E. (2012): Observation of gel filter cake recovery by dissolution in flowback fluids ; Proceedings - SPE International Symposium on Formation Damage Control, v 1, p 366-387.

Gelet, R., Loret, B., and Khalili, N. (2012): Borehole stability analysis in a thermoporoelastic dual-porosity medium; International Journal of Rock Mechanics and Mining Sciences, v 50, p 65-76.

Germanovich, L.N., Roegiers, J.C., and Dyskin, A.V. (1994): A model for borehole breakouts in brittle rocks; paper SPE 28072.

Germanovich, L.N., Roegiers, J.C., and Dyskin, A.V. (1994): A model for borehole breakouts in brittle rocks; paper SPE 28072.

Gil, I., and Roegiers, J-C (2002): Borehole design: stability considerations; paper SPE 78182.

Goueygou, M., Lafhaj, Z., and Kaczmarek, M. (2001): Relationship between porosity, permeability and ultrasonic parameters in sound and damaged mortar; NDT, URL <http://www.ndt.net/article/ndtceo3/papers/v005/v005.html> [June, 2011].

Griffith, J.E., and Osisanya, S. (1995): Thickness optimization of drilling fluid filter cakes for cement slurry filtrate control and long-term zonal isolation; paper SPE 29473.

Guillot, D., Couturier, M., Hendriks, H., and Callet, F. (1990): Design rules and associated spacer properties for optimal mud removal in eccentric annuli; paper SPE 21594.

Guillot, D.J. , Froelich, B., Caceres, E., and Verbakel, R. (2008): Are casing centralization calculations really conservative?; SPE/IADC Drilling Conference, Proceedings, v 2, p 1076-1086.

Haberman, J.P., Delestatius, M., Hines, D.G., Baret, J.F. (1992): Downhole fluid-loss measurements from drilling and cement slurries; Louisiana; paper SPE 22552.

Halliburton (2006): eRed Book; <http://www.halliburton.com/esg/eredbook/erb_dnld.jsp> [June, 2011].

Hawkes, C.D., and McLellan, P. (1996): Modelling of yielded zone enlargement around a wellbore; *in* Proceedings of the 2nd North American Rock Mechanics Symposium, Montreal, Quebec.

Hawkes, C.D., Smith, S.P., and McLellan, P. (2002): Coupled modelling of borehole instability and multiphase flow for underbalanced drilling; paper SPE 74447.

Hawkes, C.D., and Gardner, C. (2013): Pressure transient testing for assessment of wellbore integrity in the IEAGHG Weyburn-Midale CO2 Monitoring and Storage Project; International Journal of Greenhouse Gas Control, v. 16, p. 50-61.

Hartmann, A., Ozerler, M., Marx, C., and Neumann, H-J. (1988): Analysis of mud cake structures formed under simulated borehole conditions; paper SPE 15413.

Hassen, B.R. (1980): New technique estimates drilling filtrate invasion; paper SPE 8791.

Haut, R.C., and Crook, J. (1979): Primary cementing: the mud displacement process; paper SPE 8253.

Haut, R.C., and Crook, J. (1981): Laboratory investigation of lightweight, low-viscosity cementing spacer fluids; paper SPE 10305.

Heukamp, F.H., Ulm, F.J., and Germaine, J.T. (2001): Mechanical properties of calcium leached cement pastes. Triaxial stress states and the influence of the pore pressures; Cement and Concrete Research, v. 31, p. 767-774.

Heukamp, F.H., Ulm, F.J., and Germaine, J.T. (2003): Poro-plastic properties of calcium leached cement-based materials; Cement and Concrete Research, v. 33, p. 1155-1173.

Hughes, D.C. (1985): Pore structure and permeability of hardened cement paste; Magazine of Concrete Research, v. 37, 2, p. 227-233.

Hoek, E. (2007): Practical rock science engineering; Evert Hoek Consulting Engineer Inc., 342 p., URL <http://www.rocscience.com/hoek/PracticalRcokEngineering.asp> [June, 2011].

Hosrud, P. (2001): Estimating mechanical properties of shale from empirical correlations; SPE Drilling and Completion Engineering Journal, p. 68-73.

Ives, K.J. (1985): Mathematical models and design methods in solid-liquid separation, Martinus Nijhoff Publishers, Houston, 331 p.

Irassar, E.F., Bonavetti, V.L., Gonzalez, M. (2003): Microstructural study on sulphate attack and limestone Portland cements at ambient temperature. Cement and Concrete Research, v. 33, p. 31-41.

Isambourg, P., Ottesen, S., Benaissa, S., and Marti, J. (1999): Down-hole simulation cell for measurement of lubricity and differential pressure sticking; paper SPE 52816.

Javaheri Ahghar, M., and Rahmannejad, R. (2012): Analysis of principal factors affecting wellbore stability; Journal of Mines, Metals and Fuels, v 60, n 1-2, p 23 -27.

Javora, P. H., Baccigalopi, G., Sanford, J., Cordeddu, C., Qu, Q., Poole, G., and Franklin, B. (2008): Effective high-density wellbore cleaning fluids: Brine-based and solids-free; SPE Drilling and Completion, v 23, n 1, p 48-54.

Jamshidi, E., and Amani, M. (2014): Numerical wellbore stability analysis using discrete element models; Petroleum Science and Technology, v 32, n 8, p 974-982.

Jiao, D., and Sharma, M.M. (1992): Formation damage due to static and dynamic filtration of water-based muds; paper SPE 23823.

Jones, J.F., and Barree, R.D. (1996): Mechanical stability analysis from drilling data alone; paper SPE 36443.

Jones, R.R., Carpenter, R.B., and Conway, M.W. (1991): A study of formation damage potential during cementing operations; paper SPE 22777.

Juvkam-Wold, H.C., and Wu, J. (1992): Casing deflection and centralizer spacing calculations; paper SPE 21282.

Kamali, S., Gerard, B., and Moranville, M. (2003): Modelling the leaching kinetics of cement-based materials-influence of materials and environment; Cement and Concrete Research, v. 25, p. 451-458.

Kariuki, P.C., and Van der Meer, F.D. (2003): Swelling clay mapping for characterizing expansive soils: results from laboratory spectroscopy and Hysens Dais analysis; *in* Proceedings of the 3rd EARSel Workshop on Imaging Spectroscopy, Oberpfaffenhofen, Germany.

Katz, A.J., and Thompson, A.H. (1986): Quantitative prediction of permeability in porous rock; Physical Review, v. 34, 11, p. 8179-8181.

Khatri, R.P., Sirivivatnanom, V., and Yang, J.L. (1997): Role of permeability in sulphate attack; Cement and Concrete Research, v. 27, p. 1179-1189.

King, R.W., and Adegbesan, K.O. (1997): Resolution of the principal formation damage mechanisms causing injectivity and productivity impairment in the Pembina Cardium reservoir; paper SPE 38870.

Kinzel, H., and Koithan, T. (1997): Planning the cementing job incorporates data management and technical expertise – A new software to calculate the optimum placement of mechanical cementing products; paper SPE 38130.

Krumbien, W.C., and Monk, G.D. (1943): Permeability as a function of the size parameters of unconsolidated sand; Transactions AIME, v. 151, p. 153-163.

Khurshid, I., Lee, K.J., and Choe, J. (2013): Analyses of thermal disturbance in drilling deep and high temperature formations; Energy Sources, Part A (Recovery, Utilization, and Environmental Effects), v 35, n 16, p 1487-97.

Kurtis, K., Monteiro, P., and Madanat, S.M. (2000): Empirical models to predict concrete expansion caused by sulphate attack; ACI Materials Journal, v. 97, p. 156-161.

Labenski, F., Reid, P., and Santos, H. (2003): Drilling fluids approaches for control of wellbore instability in fractured formations; paper SPE 85304.

Ladva, H.K.J., Craster, B., Jones, T.G.J., Goldsmith, G., and Scott, D. (2004): The cement-to-formation interface in zonal isolation; paper SPE 88016.

Landrum, W.R., Porter, J.E., and Turner, R.D. (1985): Rotating liners during cementing in the Grand Isle and West Delta areas; Louisiana; paper SPE 11420.

Larsen, H.D. (1938): Determining the filtration characteristics of drilling muds – Part 1; Petroleum Engineering, p. 1-42.

Lecampion, B., Bunger, A., Kear, J., and Quesada, D. (2013): Interface debonding driven by fluid injection in a cased and cemented wellbore: Modeling and experiments; International Journal of Greenhouse Gas Control, v 18, p 208-223.

Le Roy-Delage, S., Baumgarte, C., Thiercelin, M., and Vidick, B. (2000): New cement systems for durable zonal isolation; paper SPE 59132.

Lee, H.K., Smith, R.C., and Tighe, R.E. (1986): Optimal spacing for casing centralizers; paper SPE 13043.

Lerman, A. (1988): Geochemical processes: water and sediment environments; Krieger Publishing, Malabar, USA, 481 p.

Li, V.C., and Maalej, M., (1996): Toughening in cement based composites. Part I: cement, mortar and concrete; Cement and Concrete Composites, v. 18, p. 223-237.

Li, Y., Rosenberg, E., Argillier, J.F., Durrieu, J., and Montes, J. (1995): Correlation between filter cake structure and filtration properties of model drilling fluids; paper SPE 28961.

Liteanu, E., and Spiers, C.J. (2011): Fracture healing and transport properties of wellbore cement in the presence of supercritical CO2; Chemical Geology, v 281, n 3-4, p 195- 210.

Liu, G. (2001): Predicting surge pressures that result from running liners; World Oil, p. 1-4.

Liu, X., and Civan, F. (1995): Formation damage by fines migration including effects of filter cake, pore compressibility, and non-Darcy flow –A modelling approach to scaling from core to field; paper SPE 28980.

Liu, X., Zhu H., and Liang L. (2013): Research on fabric characteristics and borehole instability mechanisms of fractured igneous rocks; Petroleum Science, v 10, n 2, p 212.

Lockyear, C.F., and Hibbert, A.P. (1989): Integrated primary cementing study defines key factors for field success; paper SPE 18376.

Lockyear, C.F., Ryan, D.F., and Gunningham, M.M. (1990): Cement channelling: how to predict and prevent; paper SPE 19865.

Longeron, D., Argillier, J-F, and Audibert, A. (1995): An integrated experimental approach for evaluating formation damage due to drilling and completion fluids; paper SPE 30089.

Longeron, D., Alfenore, J., and Poux-Guillaume, G. (1998): Drilling fluids filtration and permeability impairment: performance evaluation of various mud formulations; paper SPE 48988.

Lullo, G., and Rae, P. (2000): Cements for long term isolation – Design optimization by computer modelling and prediction; paper SPE 62745.

Manohar, L. (1999): Shale stability: drilling fluid interaction and shale strength; paper SPE 54356.

Marchand, J., Bentz, D.P., Samson, E., and Maltais, Y. (2001): Influence of calcium hydroxide dissolution on the transport properties of hydrated cement systems; *in* Proceedings of the Workshop on the role of calcium hydroxide in concrete, Ana Maria Island, Florida, p. 113-129.

Martin, C.D., Martino J.B., and Dzik, E.J. (1994): Comparison of borehole breakouts from laboratory and field tests; paper SPE 28050.

Martin, M., Latil, M., and Vetter, P. (1978): Mud displacement by slurry during primary cementing jobs – Predicting optimum conditions; paper SPE 7590.

Martins, A.L., Waldmann, A.T.A., Aragao, A.F.L., and Lomba, R.F.T. (2004): Predicting and monitoring fluid invasion in exploratory drilling; paper SPE 86497.

Matteo, E., and Scherer, G. (2012): Experimental study of the diffusion-controlled acid degradation of Class H Portland cement; International Journal of Greenhouse Gas Control, v 7, p 181-191.

Matthew, S.M., and Copeland, J.C. (1986): Control of annular gas flow in the deep Anadarko Basin; paper SPE 14980.

Maury, V.M., and Sauzay, J.M. (1987): Borehole instability: case histories, rock mechanics approach, and results; paper SPE 16051.

Maury, V. (1994): Rock failure mechanisms identification: a key for wellbore stability and reservoir behaviour problem; paper SPE 28049.

McLean, M.R., and Addis, M.A. (1990a): Wellbore stability analysis: a review of current methods of analysis and their field application; paper SPE 19941.

McElfresh, P.M., and Boncan, V.C. (1982): Applications of foam cement; paper SPE 11203.

McLean, M.R., and Addis, M.A. (1990b): Wellbore stability: the effect of strength criteria on mud weight recommendations; paper SPE 20405.

McLean, R.H., Manry, C.W., and Whitaker, W.W. (1967): Displacement mechanics in primary cementing; paper SPE 1488.

McLellan, P., and Wang, Y. (1994): Predicting the effects of pore pressure penetration on the extent of wellbore instability: applications of a versatile poro-elastoplastic model; paper SPE 28053.

McLellan, P. (1996): Assessing the risk of wellbore instability in horizontal and inclined wells; Journal of Canadian Petroleum Technology, v. 35, 5, p. 21-32.

McLellan, P. (2005): Practical rock mechanics for drilling and completions; Advanced Geotechnology, Calgary, 240 p.

McLellan, P., and Hawkes, C. (1999): User-friendly borehole stability software for designing horizontal and deviated wells; *in* Proceedings of the CADE/CAODC Spring Drilling Conference, Calgary, Alberta.

McLennan, J.D., and Abou-Sayed, A.S. (2002): Some advances in near wellbore geomechanics; paper SPE 78194.

Mendoza-Amuchastegui, J., Vazquez-Jimenez, G., Espinosa-Ortega, M., Valle-Molina, C., Alvarado-Hernandez, E., Garcia-Herrera, M.G., and Nicolas-Lopez, R. (2009): Pore-pressure prediction and wellbore stability in the deep Mexican Gulf of Mexico; Leading Edge, v 28, n 6, p 702-6.

Mohiuddin, M.A., Awal, M.R., Abdulraheem, A., and Khan, K. (2001): A new diagnostic approach to identify the causes of borehole instability problems in an offshore Arabian field; paper SPE 68095.

Monteiro, P., and Kurtis, K.E. (2003): Time to failure for concrete exposed to severe sulphate attack; Cement and Concrete Research, v. 33, p. 987-993.

Moreno, F., Chalaturnyk, R., and Jimenez, J. (2004): Methodology for assessing integrity of bounding seals (wells and caprock) for geological storage of CO_2; *in* Proceedings of the 7th International

Conference on Greenhouse Gas Control Technologies (GHGT-7), Vancouver, British Columbia.

Morita, N., and Whitebay, L. (1994): Rock mechanics aspects of drilling and completing highly inclined wells in weak formations; paper SPE 27983.

Nasvi, M.C.M., Ranjith, P.G., Sanjayan, J., and Haque, A. (2013): Sub- and super-critical carbon dioxide permeability of wellbore materials under geological sequestration conditions: an experimental study; Energy, v 54, p 231-9.

Nelson, E.B. (1990): Well cementing, 2nd ed. Schlumberger, Sugar Land, Texas, 773 p.

Nelson, E.B., and Guillot, D. (2006): Well cementing, Schlumberger Educational Services, Sugar Land, Texas, 654 p.

Newell, D., and Carey, J. (2013): Experimental evaluation of wellbore integrity along the cement-rock boundary; Environmental Science and Technology, v 47, n 1, p 276-282.

Nguyen, P.D., Brumley, J.L., Dewprashad, B.T., Dusterhoft, R.G., and Weaver, J.D. (2000): Stabilizing wellbores in unconsolidated formations for fracture stimulation; paper SPE 66550.

Nicolás-López, R., Valdiviezo-Mijangos, O.C., Valle-Molina, C. (2012): A new approach to calculate the mud density for wellbore stability using the asymptotic homogenization theory; Petroleum Science and Technology, v 30, n 12, p 1239-1249.

Onan, D.D. (1984): Effects of supercritical carbon dioxide on well cements; paper SPE 12593.

Outmans, H.D. (1963): Mechanics of static and dynamic filtration in the borehole; paper SPE 491.

Parker, P.N., Ladd, B.J., Ross, W.M., and Wahl, W.W. (1965): An evaluation of a primary cementing technique using low displacement rates; paper SPE 1234.

Patnana, V.K., Karadkar, P.B.; Choudhary, Y.K. (2013): An environmentally acceptable and non-damaging diversion system for high-permeability formations; SPE - European Formation Damage Conference, Proceedings, EFDC, v 2, p 1111-1119, 2013.

Peden, J.M., Avalos, M.R., and Arthur, K.G. (1982): The analysis of the dynamic filtration and permeability impairment characteristics of inhibited water based muds; paper SPE 10655.

Peden, J.M., Arthur, K.G., and Avalos, M. (1984): The analysis of filtration under dynamic and static conditions; paper SPE 12503.

Perry, C., and Henry, K. (1986): Cement evaluation in the Gulf of Thailand; paper SPE 14606.

Picandet, V., Khelidj, A., and Bastian, G. (2001): Effect of axial compressive damage on gas permeability of ordinary and high-performance concrete; Cement and Concrete Research, v. 31, p. 1525-1532.

Plumb, R.A. (1994): Influence of composition and texture on the failure properties of clastic rocks; paper SPE 28022.

Powers, T.C., Copeland, L.E., Hayes, J.C., and Mann, H.M. (1955): Permeability of Portland cement paste; Journal of the American Concrete Institute, v. 51, p. 285-294.

Proett, M.A., Chin, W.C., Manohar, M., Sigal, R., and Wu, J. (2001): Multiple factors that influence wireline formation tester pressure measurements and fluid contact estimates; paper SPE 71566.

Proett, M.A., Chin, W.C., Manohar, M., Belanger, D., and Wu, J. (2002): Sample quality with integrated oil and water-based mud invasion; paper SPE 77964.

Pruess, K., and Garcia, J. (2002): Multiphase flow dynamics during CO2 disposal into saline aquifers; Environmental Geology, v. 42, 2-3, p.

Qiang, T., Jingen, D., and Baohua, Y. (2010): Wellbore instability and countermeasures in offshore bedding shale formations; Petroleum Science and Technology, v 28, n 16, p 1712-1718 282-295.

Rahmani, N.H.G., Gao, J., Ibrahim, M.N., Bou-Mikael, S., Al-Matar, B.S., Ruhaimani, F. (2009): Core flood investigation into asphaltene deposition tendencies in the Marrat reservoir, South East Kuwait; Proceedings - SPE International Symposium on Oilfield Chemistry, v 1, p 188-200.

Ravi, K.M., Beirute, R.M., and Covington, R.L. (1992): Erodability of partially dehydrated gelled drilling fluid and filter cake; paper SPE 24571.

Ravi, K.M., Bosma, M., and Gastebled, O. (2002): Safe and economic gas wells through cement design for life of the well; paper SPE 75700.

Rawlings, C.G., Barton, N.R., Bandis, S.C., Addis, M.A., and Gutierrez, M.S. (1993): Laboratory and numerical discontinuum modelling of wellbore stability; paper SPE 25869.

Revertegat, E., Richet, C., and Gegout, P. (1992): Effect of pH on the durability of cement pastes; Cement and Concrete Research, v. 22, p. 259-272.

Ridha, S., Irawan, S., and Ariwahjoedi, B. (2013): Strength prediction of Class G oilwell cement during early ages by electrical conductivity;

Journal of Petroleum Exploration and Production Technology, v 3, n 4, p 303-311.

Roshan, H., and Fahad, M. (2012): Chemo-poroplastic analysis of a borehole drilled in a naturally fractured chemically active formation; International Journal of Rock Mechanics and Mining Sciences, v 52, p 82- 91.

Roshan, H., and Rahman, S.S. (2011): Analysis of Pore Pressure and Stress Distribution around a Wellbore Drilled in Chemically Active Elastoplastic Formations; Rock Mechanics and Rock Engineering, v 44, n 5, p 541-52.

Roshan, H., and Rahman, S.S. (2013): The Effect of Water Content on Stress Changes Around a Wellbore Drilled in a Chemically Active Elastoplastic Formation; Petroleum Science and Technology, v 31, n 20, p 2118-2126.

Roegiers, J.C. (2002): Well modelling: an overview; Oil and Gas Science and Technology, v. 57, 5, p. 569-577.

Sabins, F., and Wiggings, M.L. (1994): Parametric study of gas entry into cemented wellbores; paper SPE 28472.

Santos, H. (2000): Differentially stuck pipe: early diagnostic and solution; paper SPE 59127.

Santarelli, F.J., Chenevert, M.E., and Osisanya, M.E. (1992): On the stability of shales and its consequences in terms of swelling and wellbore stability; paper SPE 23886.

Santhanam, M., Cohen, M.D., and Olek, J. (2002): Modelling the effects of solution temperature and concentration during sulphate attack on cement mortars; Cement and Concrete Research, v. 32, p. 585-592.

Santhanam, M., Cohen, M.D., Olek, J. (2003): Mechanism of sulphate attack: a fresh look. Part 2. Proposed mechanisms; Cement and Concrete Research, v. 33, p. 341-346.

Santos, H., Villas-Boas, M.B., Lomba, R.F.T., Sa, C.H.M., Oliveira, S.F., and Costa, J.F. (1999): API filtrate and drilling fluid invasion: is there any correlation?; paper SPE 53791.

Santos, H. (2000): Differentially stuck pipe: early diagnostic and solution; paper SPE 59127.

Sauer, C.W. (1987): Mud displacement during cementing: a state of the art; paper SPE 14197.

Savari, S., Kumar, A., Whitfill, D.L., Jamison, D.E. (2011): Improved lost circulation treatment design and testing techniques minimize formation damage ; SPE - 9th European Formation Damage Conference 2011, v 1, p 358-365.

Schlemmer, R., Friedheim, J.E., and Growcock, F.B. (2002): Membrane efficiency in shale – An empirical evaluation of drilling fluid chemistries and implications for fluid design; paper SPE 74557.

Schlemmer, R., Friedheim, J.E., Growcock, F.B., Bloys, J.B., Headley, J.A., and Polnaszek, S.C. (2003): Chemical osmosis, shale, and drilling fluids; paper SPE 86912.

Schlumberger (2005): Oilfield glossary, URL <http://www.glossary.oilfield.slb.com> [June, 2011].

Seidel, F.A., and Greene, T.G. (1985): Use of expanding cement improves bonding and aids in eliminating annular gas migration in Hobbs Grayburg-San Andres wells; paper SPE 14434.

Shao, J.F., and Khazraei, R. (1994): Wellbore stability analysis in brittle rocks with continuous damage model; paper SPE 28054.

Sheorey, P.R. (1994): A theory for in-situ stresses in isotropic and transversely isotropic rock; International Journal of Rock Mechanics and Mining Sciences, v. 31, 1, p. 23-24.

Silva, M.G.P., Martins, A.L., Barbosa, B.C., and Garcia, H. (1996): Designing fluid velocity profiles for optimal primary cementing; paper SPE 36136.

Simangunsong, R.A., Villatoro, J.J., and Davis, A.K. (2006): Wellbore stability assessment for highly inclined wells using limited rock-mechanics data; paper SPE 99644.

Slamecka, T., and Skvara, F. (2002): The effect of water ratio on microstructure and composition of the hydration products of Portland cement pastes; Journal of Ceramics, v. 46, p. 152-158.

Smith, T.R. (1990): Cementing displacement practices –Field applications; paper SPE 18617.

Smith, R.C. (1984): Successful primary cementing can be a reality; paper SPE 13498.

Soares, A.C., and Ferreira, F.H. (2002): An experimental study for mechanical formation damage; paper SPE 73734.

Sommerville, J.M., and Smart, B.G.D. (1991): The prediction of well stability using the yield zone concept; paper SPE 23127.

Soter, K. (2003): Removal of sustained casing pressure utilizing a work over rig; MsC Thesis, Department of Petroleum Engineering, Louisiana State University, 95 p.

Stewart, R.B., and Schouten, F.C. (1988): Gas invasion and migration in cemented annuli: causes and cures; paper SPE 14779.

Suri, A., and Sharma, M.M. (2004): Strategies for sizing particles in drilling and completion fluids; paper SPE 68964.

Swenson, E.G. (1968): Performance of concrete; University of Toronto Press, Toronto, 243 p.

Tallak, S.G., Holder, J., and Gray, K.E. (1993): Deformation effects on formation damage during drilling and completion operations; paper SPE 25430.

Tan, C.P., and Willoughby, D.R. (1993): Critical mud weight and risk contour plots for designing inclined wells; paper SPE 26325.

Tan, C.P., Rahman, S.S., Richards, B.G., and Mody, F.K. (1998): Integrated rock mechanics and drilling fluid design approach to manage shale instability; paper SPE 47259.

Tan, C.P., Amanullah, M., Mody, F.K., and Tare, U.A. (2002): Novel high membrane efficiency water-based drilling fluids for alleviating problems in troublesome shale formations; paper SPE 77192.

Tandon, S., and Faber, K.T., (1999): Effects of loading rate on the fracture of cementitious materials; Cement and Concrete Research, v. 29, p. 397-406.

Tang, L., and Luo, P. (1998): The effect of the thermal stress on wellbore stability; paper SPE 39505.

Tasdemir, M.A., and Karihaloo, B.L. (2001): Effect of aggregate volume fraction on the fracture parameters of concrete: a meso-mechanical approach; Magazine of Concrete Research, v. 53, p. 405-415.

Tehrani, A., Ferguson, J., and Bittleston, S.H. (1992): Laminar displacement in annuli: a combined experimental and theoretical study; paper SPE 24569.

Thiercelin, M.J., Baumgarte, C., and Guillot, D. (1998): A soil mechanics approach to predict cement sheath behaviour; paper SPE 47375.

Timoshenko, S. (1983): Strength of materials, Part II, Advanced theory and problems; Robert E. Krieger Publishing Company, Malabar, Florida, 510 p.

Tumidajski, P.J., and Lin, B. (1998): On the validity of the Katz-Thompson equation for permeabilities in concrete; Cement and Concrete Research, v. 28, No. 5, p. 643-647.

Udegbunam, O., Yaman, O., Aktan, O., and Hohm, T. (1999): Developing a rapid measurement of concrete permeability for use in QA/QC specifications; *in* Proceedings of the 78th Transportation Research Board Annual Meeting , Washington, D.C., p. 2-14.

Ulm, F.J., Heukamp, F.H., and Germaine, J.T. (2002): Residual strength of cement-based materials for nuclear waste storage systems; Nuclear Engineering and Design, v. 211, p. 51-60.

Van Oort, E., Hale, A.H., Mody, F.K., and Roy, S. (1996): Transport in shales and the design of improved water-based shale drilling fluids; paper SPE 28309.

Van Oort, E. (2002): On the physical and chemical stability of shales; Journal of Petroleum Science and Engineering, v. 38, p. 213-235.

Vargo, R.F., Jr., Heathman, J.F., Kellingray, D.S., Ward, M.D., and Lummus, J.M. (2007): Improved deepwater cementing practices reduce NPT; World Oil, v 228, n 9, p 71-80.

Vasquez, J., and Curtice, R. (2013): A porosity-fill sealant for water and gas shutoff: Case histories and lessons learned after more than 1,000 well interventions; SPE – European Formation Damage Conference, Proceedings, EFDC, v 1, p 98-112.

Verba, C., O'Connor, W., Rush, G., Palandri, J., Reed, M., and Ideker, J. (2014): Geochemical alteration of simulated wellbores of CO2 injection sites within the Illinois and Pasco Basins; International Journal of Greenhouse Gas Control, v 23, p 119-134.

Brine Walsh, S.D.C., Du Frane, W.L., Mason, H.E., Carroll, S.A. (2013): Permeability of Wellbore-Cement Fractures Following Degradation by Carbonated; Rock Mechanics and Rock Engineering, v 46, n 3, p 455-64.

Wang, J.G. (1994): Sulphate attack on hardened cement paste; Cement and Concrete Research, v. 24, p. 735-742.

Wang, E.Z., and Shrive, N.G., (1995): Brittle fracture in compression: mechanisms, models and criteria; Engineering Fracture Mechanics, v. 52, p. 1107-1126.

Wang, Y., Watson, R., Rostami, J., Wang, J., Limbruner, M., and He, Z. (2014): Study of borehole stability of Marcellus shale wells in long wall mining areas; Journal of Petroleum Exploration and Production Technology, v 4, n 1, p 59-71.

Waremburg, P.A., Kirksey, J.M., and Bannister, C.E. (1980): Improving cement bond in the Rocky Mountain area by the use of spacer, wash, and thixotropic cement; paper SPE 9031.

Weijermars, R. (2013): Mapping stress trajectories and width of the stress-perturbation zone near a cylindrical wellbore; International Journal of Rock Mechanics and Mining Sciences, v 64, p 148-159.

White, D.J., Burrowes, G., Davis, T., Hajnal, Z., Hirsche, K., Hutcheon, I., Majer, E., Rostron, B., and Whittaker, S. (2004): Greenhouse gas sequestration in abandoned oil reservoirs: The International Energy Agency Weyburn pilot project; GSA Today, v. 14, 7, 7 p.

Whitfill, D. (2008): Lost circulation material selection, particle size distribution and fracture modeling with fracture simulation software;

IADC/SPE Asia Pacific Drilling Technology Conference 2008 - "Drilling Technology to Access Future Energy Demand and Environmental Challenges", p 382-393.

Whittaker, S., Rostron, B., Khan, D., Hajnal, Z., Qing, H., Penner, L., Maathuis, H., and Goussev, S. (2004): IEA GHG Weyburn CO_2 monitoring and storage project, Summary Report - Geological characterization; *in* Proceedings of the 7th International Conference on Greenhouse Gas Control Technologies , Vancouver, British Columbia, p. 15-69.

Wilkins, R.P., and Free, D. (1989): A new approach to the prediction of gas flow after cementing; paper SPE 18622.

Wilson, M., and Monea, M. (2004): IEA GHG Weyburn CO_2 monitoring and storage project, Summary Report; *in* Proceedings of the 7th International Conference on Greenhouse Gas Control Technologies , Vancouver, British Columbia, p. 15-69.

Witteveen, P., Ferrari, A., and Laloui, L. (2013): An experimental and constitutive investigation on the chemo-mechanical behaviour of a clay; Geotechnique, v 63, n 3, p 244-55.

Wojtanowicz, A., Krilov, Z., and Langlinais, J.P. (1987): Study on the effect of pore blocking mechanisms on formation damage; paper SPE 16233.

Wojtanowicz, A., Krilov, Z., and Langlinais, J.P. (1988): Experimental determination of formation damage pore blocking mechanisms; Journal of Energy Resources Technology, v. 110, p. 34-42.

Wolterbeek, T., Peach, C., and Spiers, C. (2013): Reaction and transport in wellbore interfaces under CO2 storage conditions: Experiments simulating debonded cement-casing interfaces; International Journal of Greenhouse Gas Control, v 19, p 519-529.

Wu, J., Torres-Verdin, C., Sepehrnoori, K., and Proett, M.A. (2005): The influence of water-base mud properties and petrophysical parameters on mud cake growth, filtrate invasion, and formation pressure; Petrophysics, v. 46, 1, p. 14-32.

Xu, T., Zheng, L., and Tian, H. (2011): Reactive transport modeling for CO2 geological sequestration; Journal of Petroleum Science and Engineering, v 78, n 3-4, p 765-777.

Yamamoto, K., Shioya, Y., and Uryu, N. (2002): Discrete element approach for the wellbore instability of laminated and fissured rocks; paper SPE 78181.

Yan, J., Zili, Q., Mian, C., Fuxiang, Z., and Yunhu, L. (2013): Study on Mechanisms of Borehole Instability in Naturally Fractured Reservoir During Production test for Horizontal Wells; Petroleum Science and Technology, v 31, n 8, p 829-39.

Younessi, A., and Rasouli, V. (2010): A fracture sliding potential index for wellbore stability analysis; International Journal of Rock Mechanics and Mining Sciences, v 47, n 6, p 927-939.

Yuan, Z., Teodoriu, C., and Schubert, J. (2013): Low cycle cement fatigue experimental study and the effect on HPHT well integrity; Journal of Petroleum Science and Engineering, v 105, p 84-90.

Zain, Z.M., and Sharma, M.M. (1999): Cleanup of wall-building filter cakes; paper SPE 56635.

Zeynaly-Andabily, E.M., Chen, H., Rahman, S.S., Tan, C.P. (1996): Management of wellbore instability in shales by controlling the physical-chemical properties of muds; paper SPE 36396.

Zhang, L., Cao, P., and Radha, K.C. (2010): Evaluation of rock strength criteria for wellbore stability analysis; International Journal of Rock Mechanics and Mining Sciences, v 47, n 8, p 1304-1316.

Zheng, Z. (1998): Integrated borehole stability analysis – Against tradition; paper SPE 47282.

Zhou, D., and Wojtanowicz, A. K. (2009): Cement seal failure at casing shoe in shallow marine sediments; Journal of Energy Resources Technology, Transactions of the ASME, v 131, n 2, p 0231011-0231018.

Zuiderwijk, J.J.M. (1974): Mud displacement in primary cementation; paper SPE 4830.

Appendix A – Casing Standoff Charts

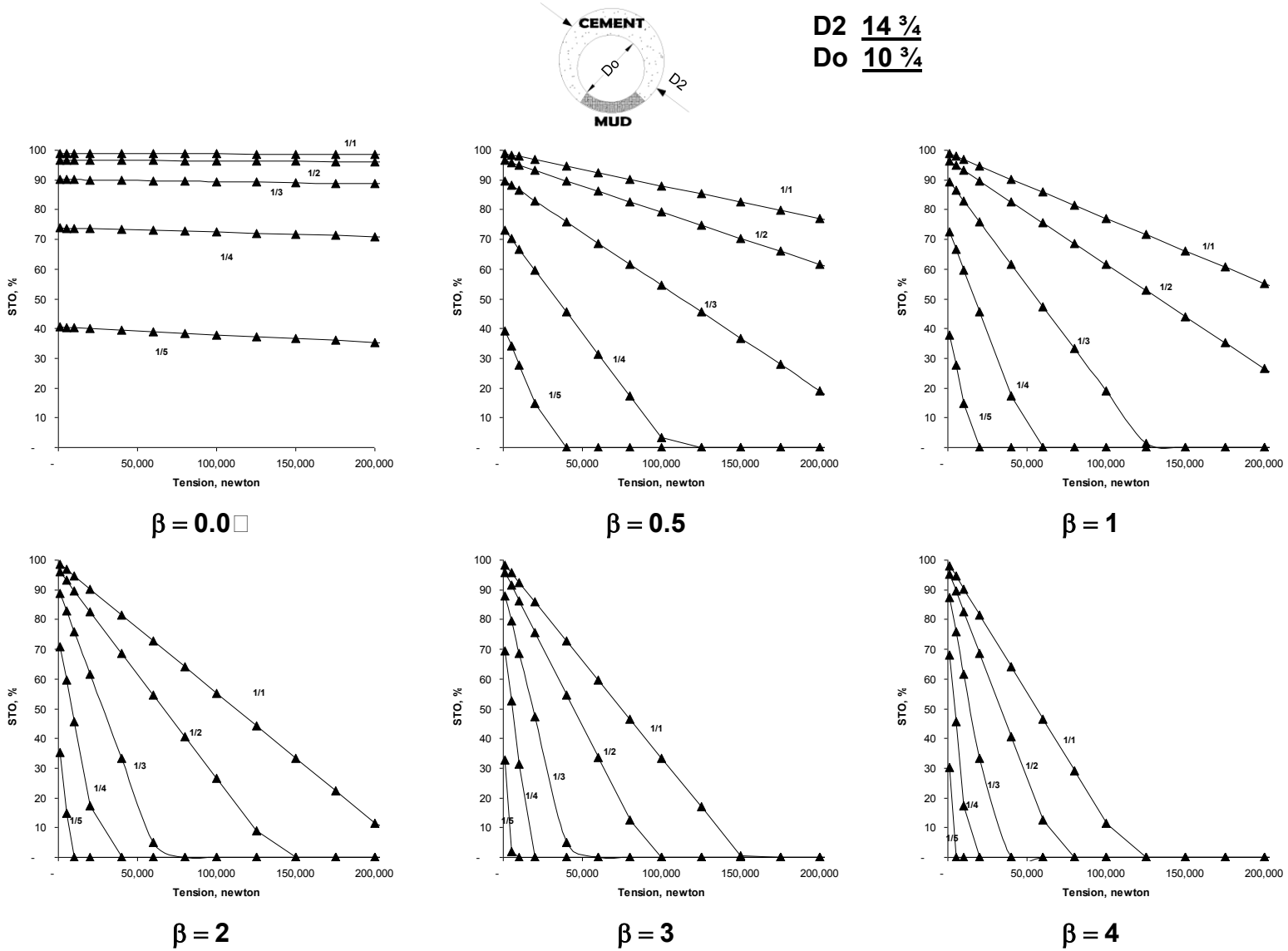

Figure 1a Casing standoff (STO) for straight, inclined wellbore with axial tension.

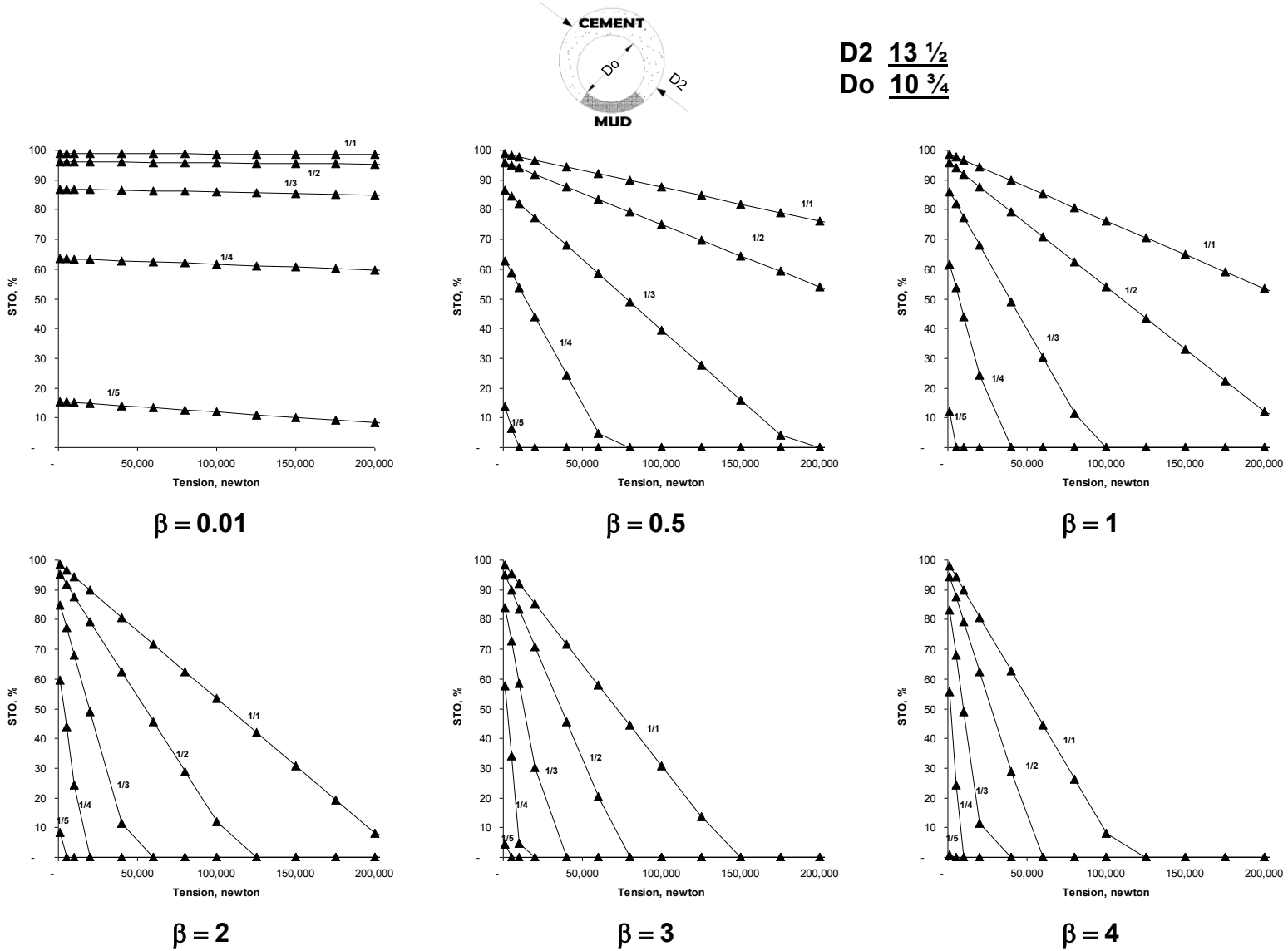

Figure 1b Casing standoff (STO) for straight, inclined wellbore with axial tension.

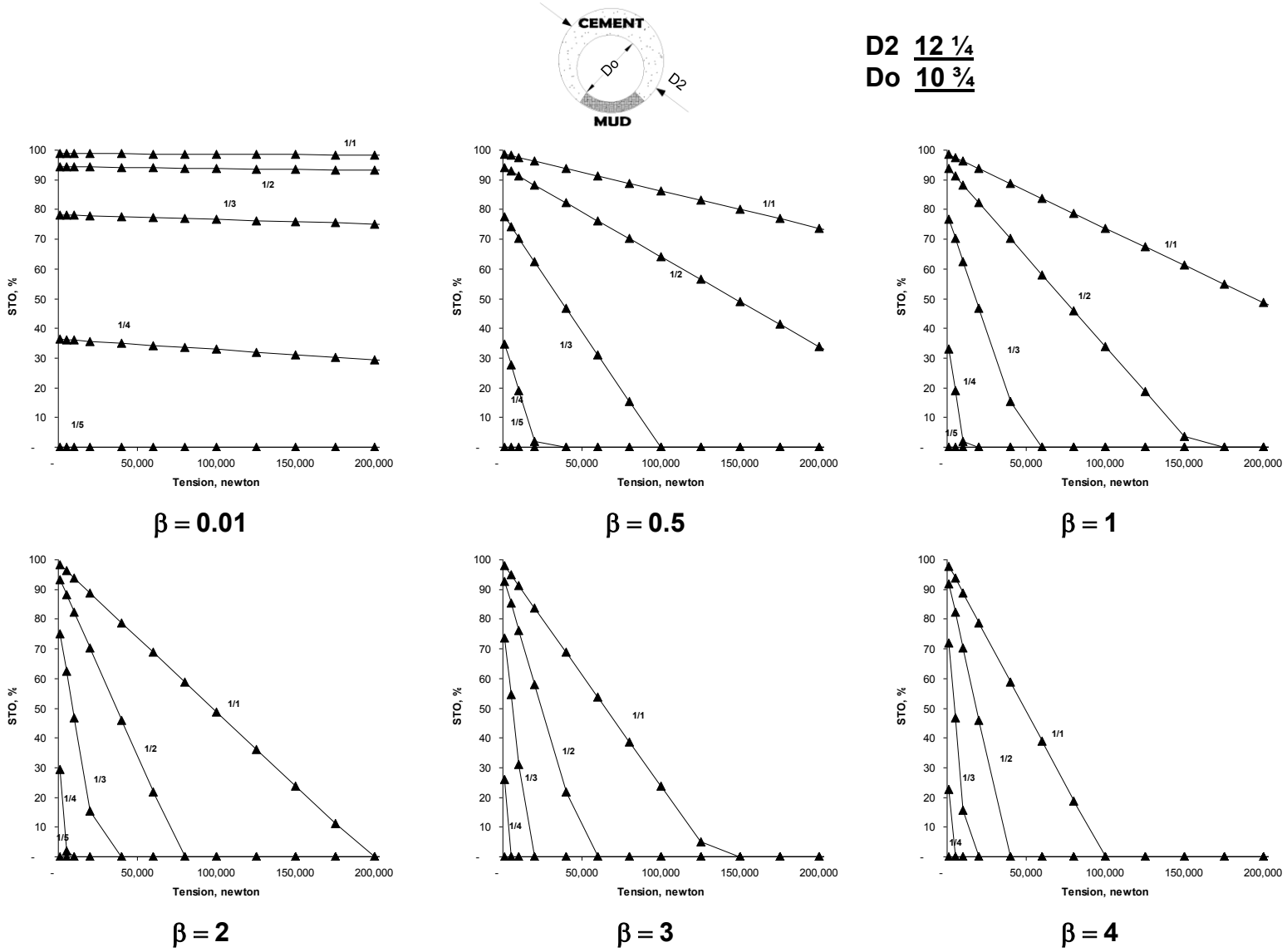

Figure 1c Casing standoff (STO) for straight, inclined wellbore with axial tension.

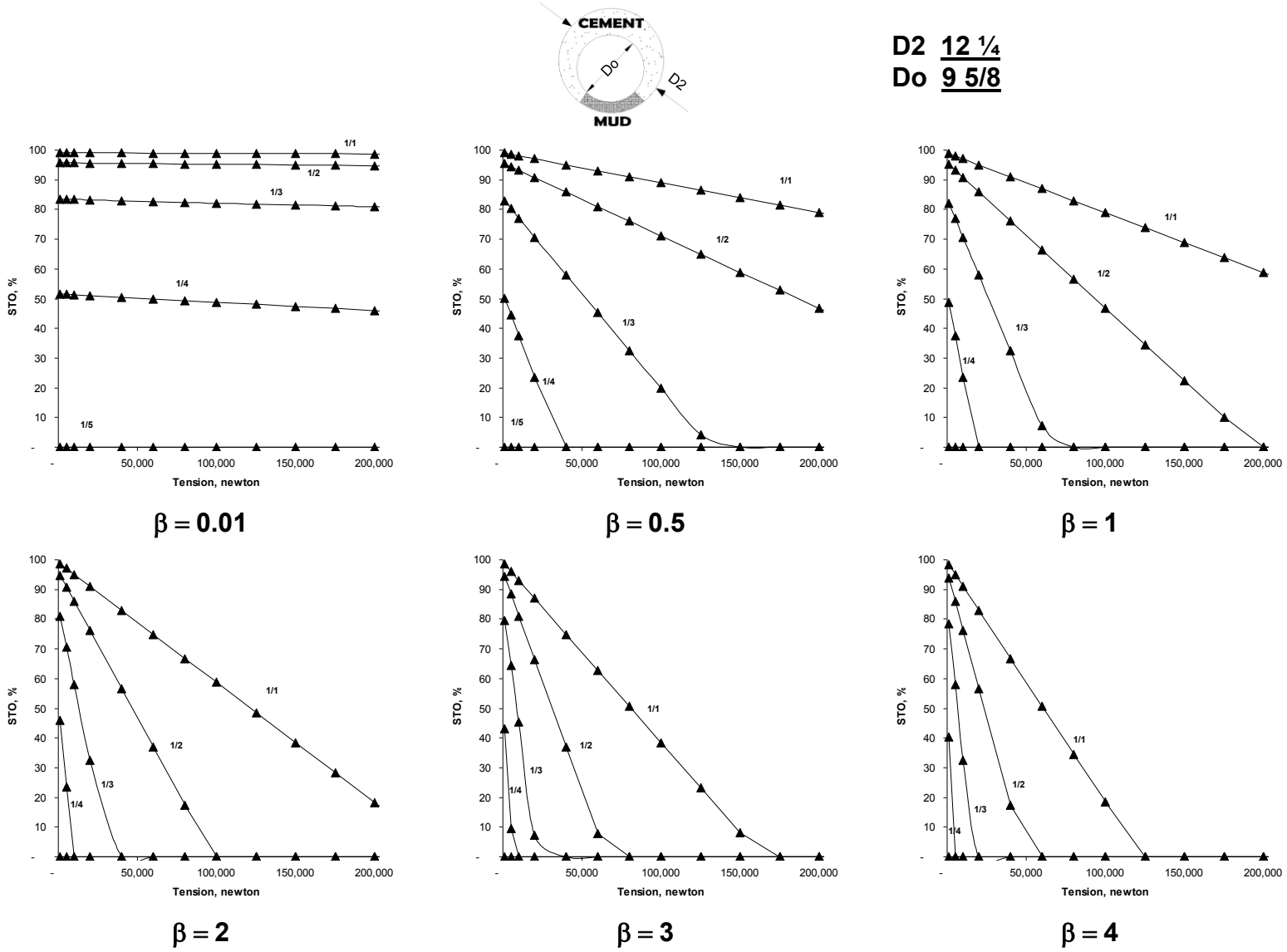

Figure 1d Casing standoff (STO) for straight, inclined wellbore with axial tension.

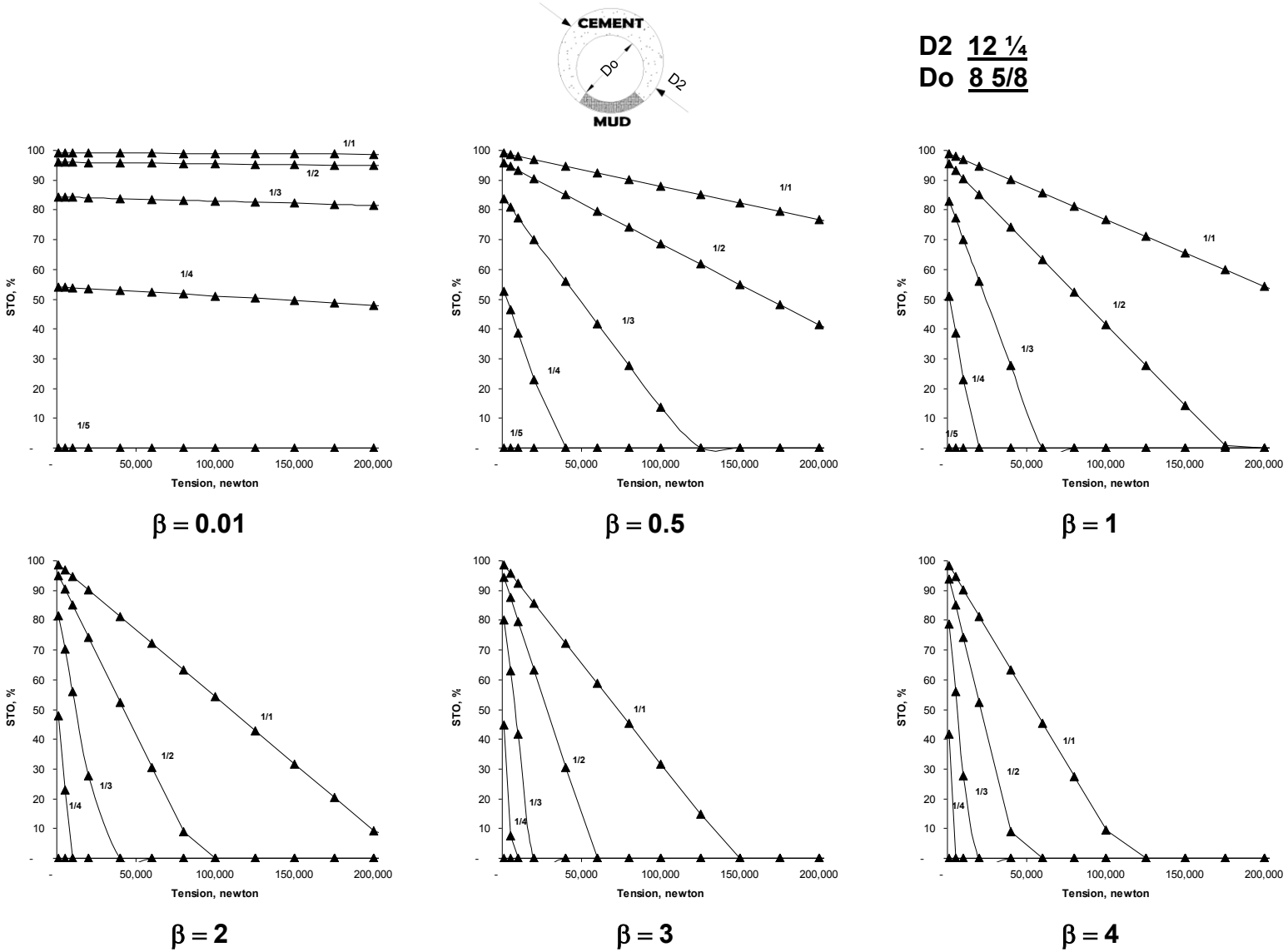

Figure 1e Casing standoff (STO) for straight, inclined wellbore with axial tension.

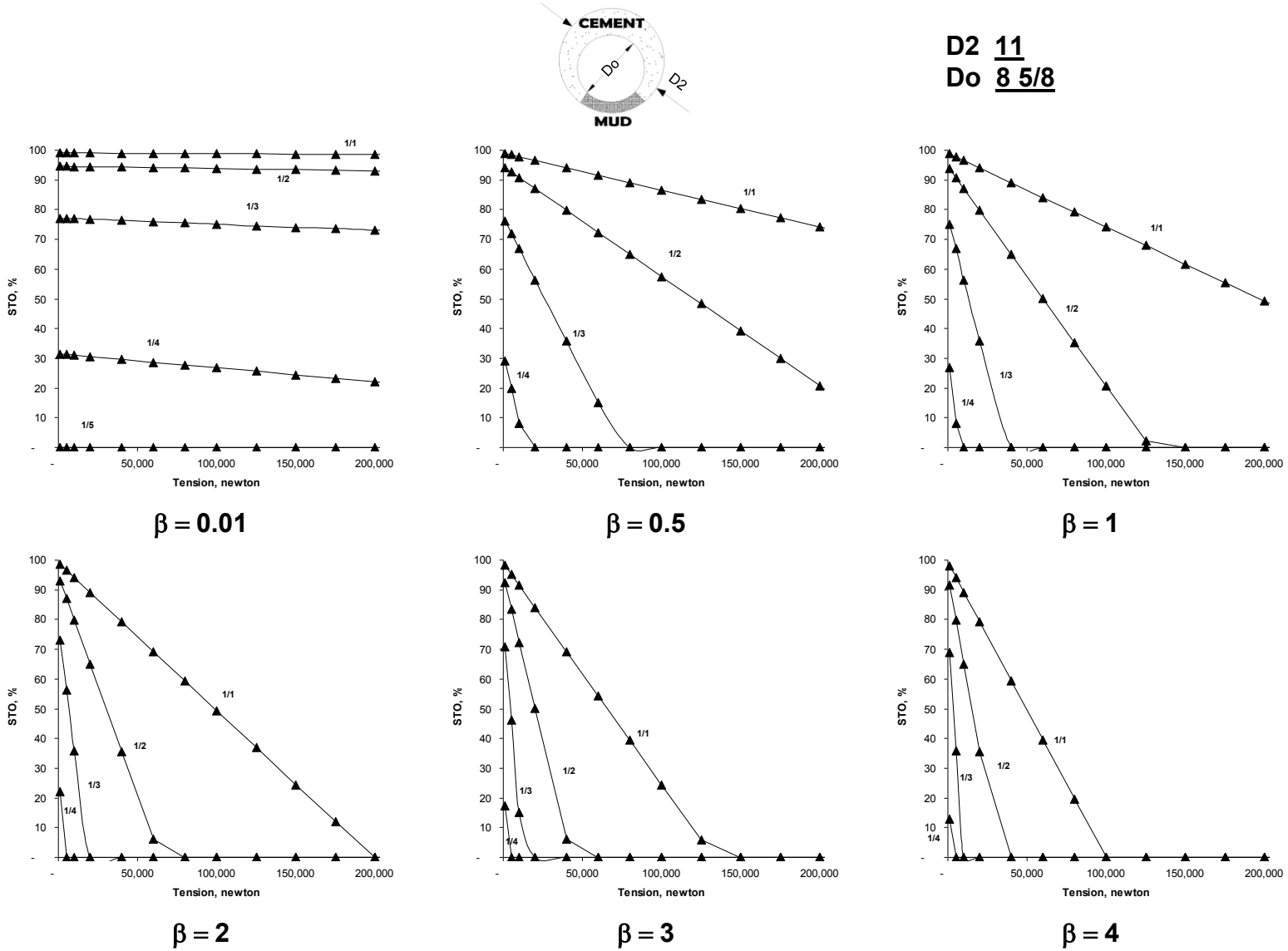

Figure 1f Casing standoff (STO) for straight, inclined wellbore with axial tension.

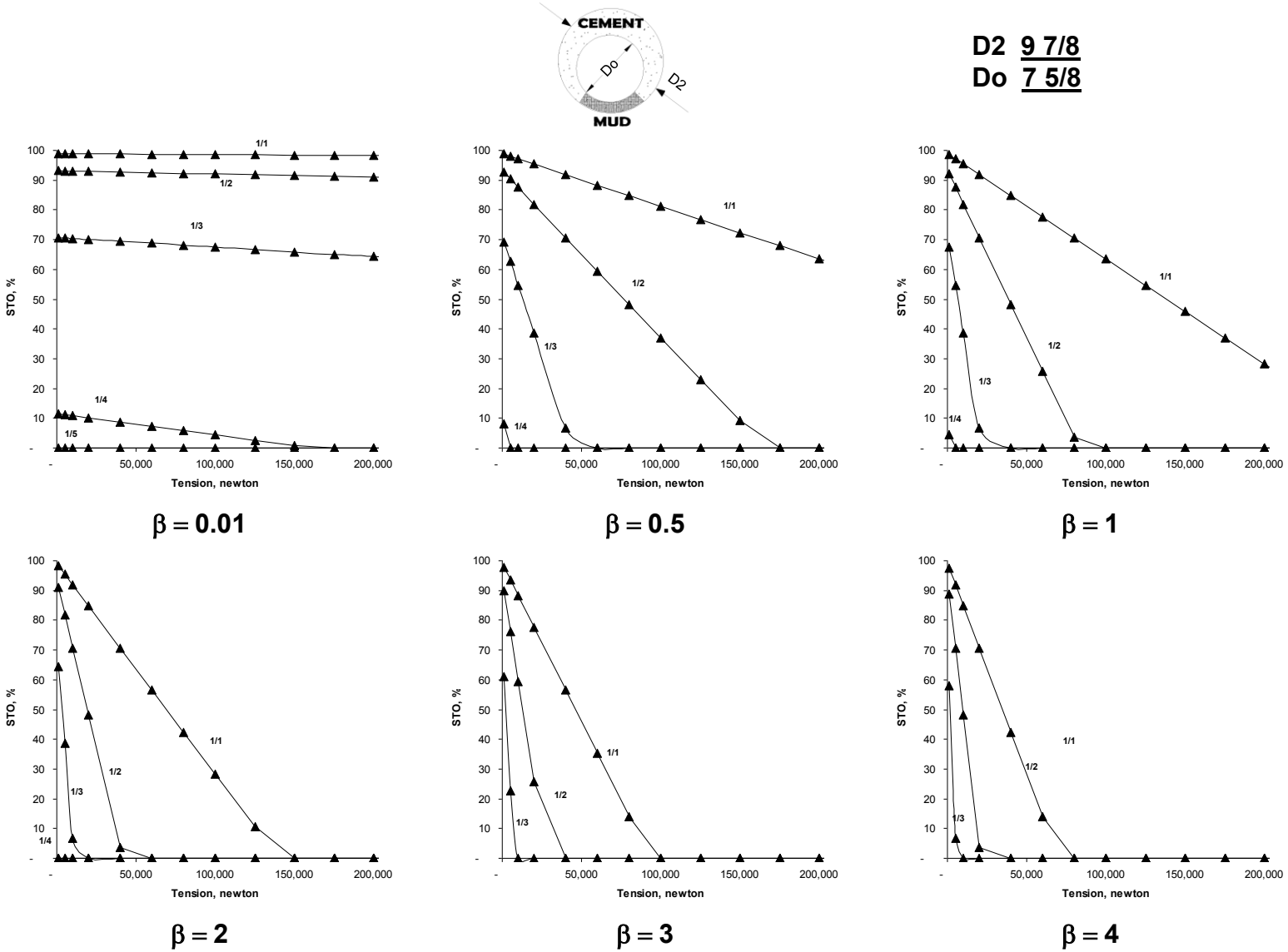

Figure 1g Casing standoff (STO) for straight, inclined wellbore with axial tension.

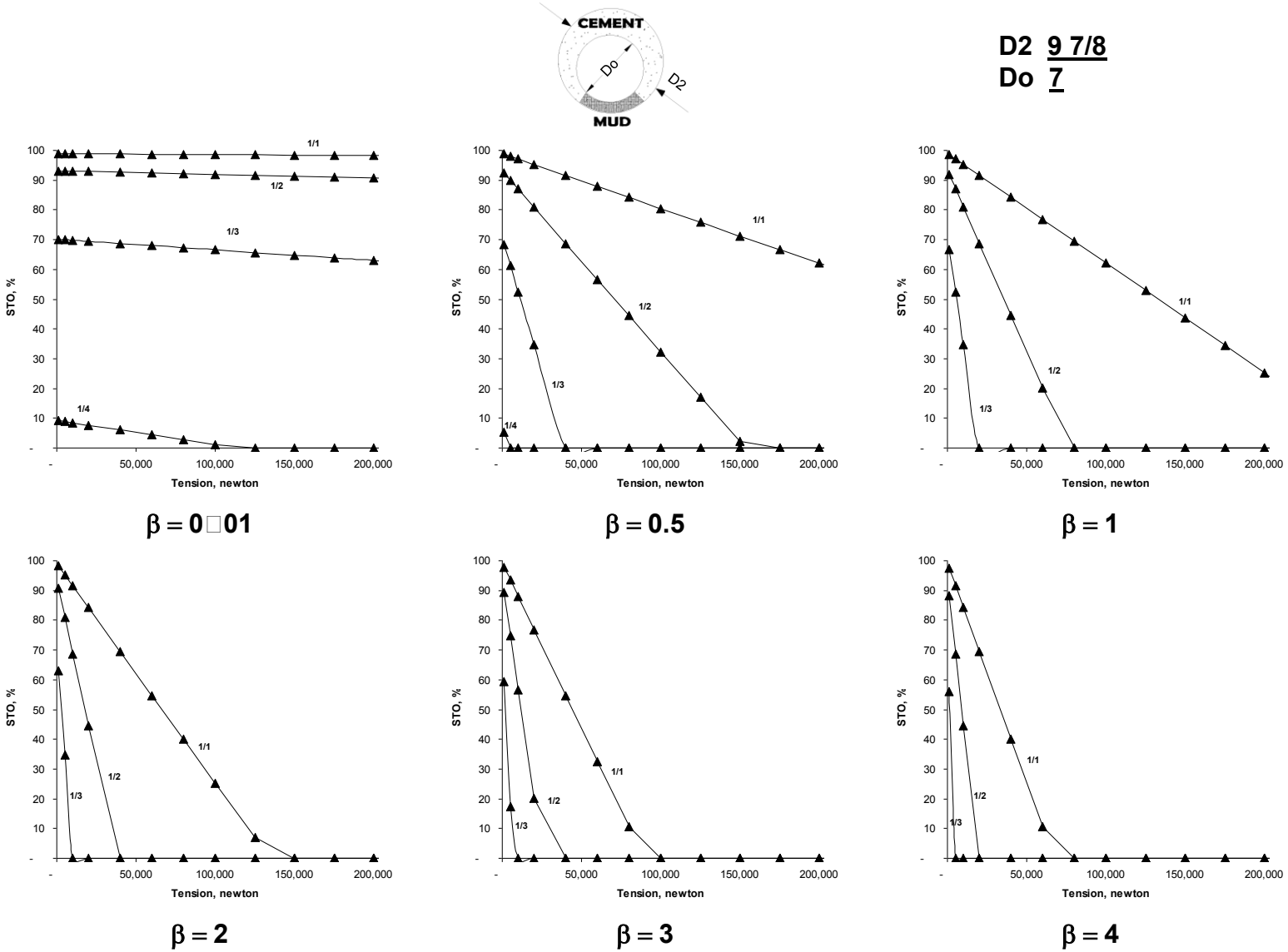

Figure 1h Casing standoff (STO) for straight, inclined wellbore with axial tension.

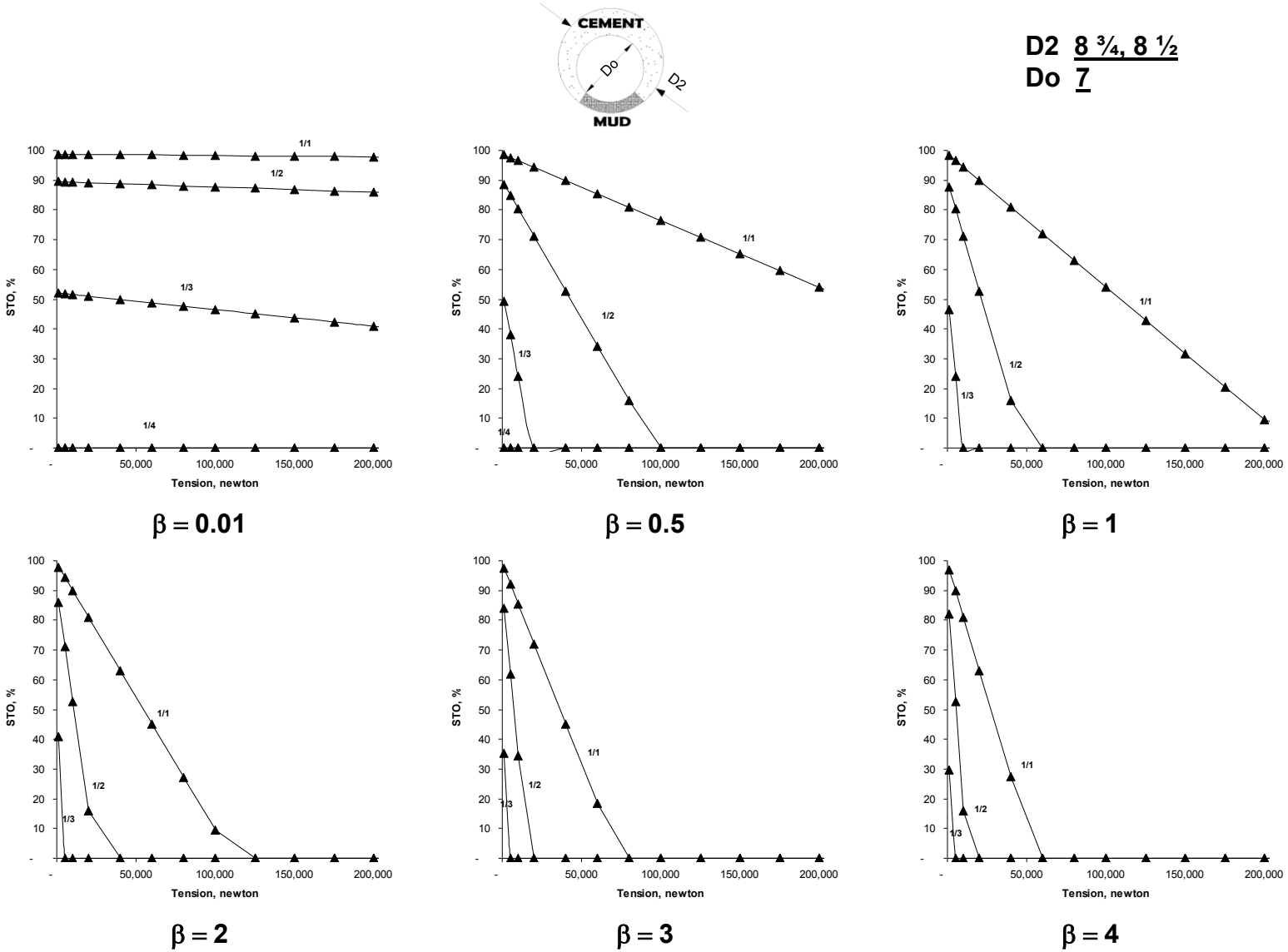

Figure 1i Casing standoff (STO) for straight, inclined wellbore with axial tension.

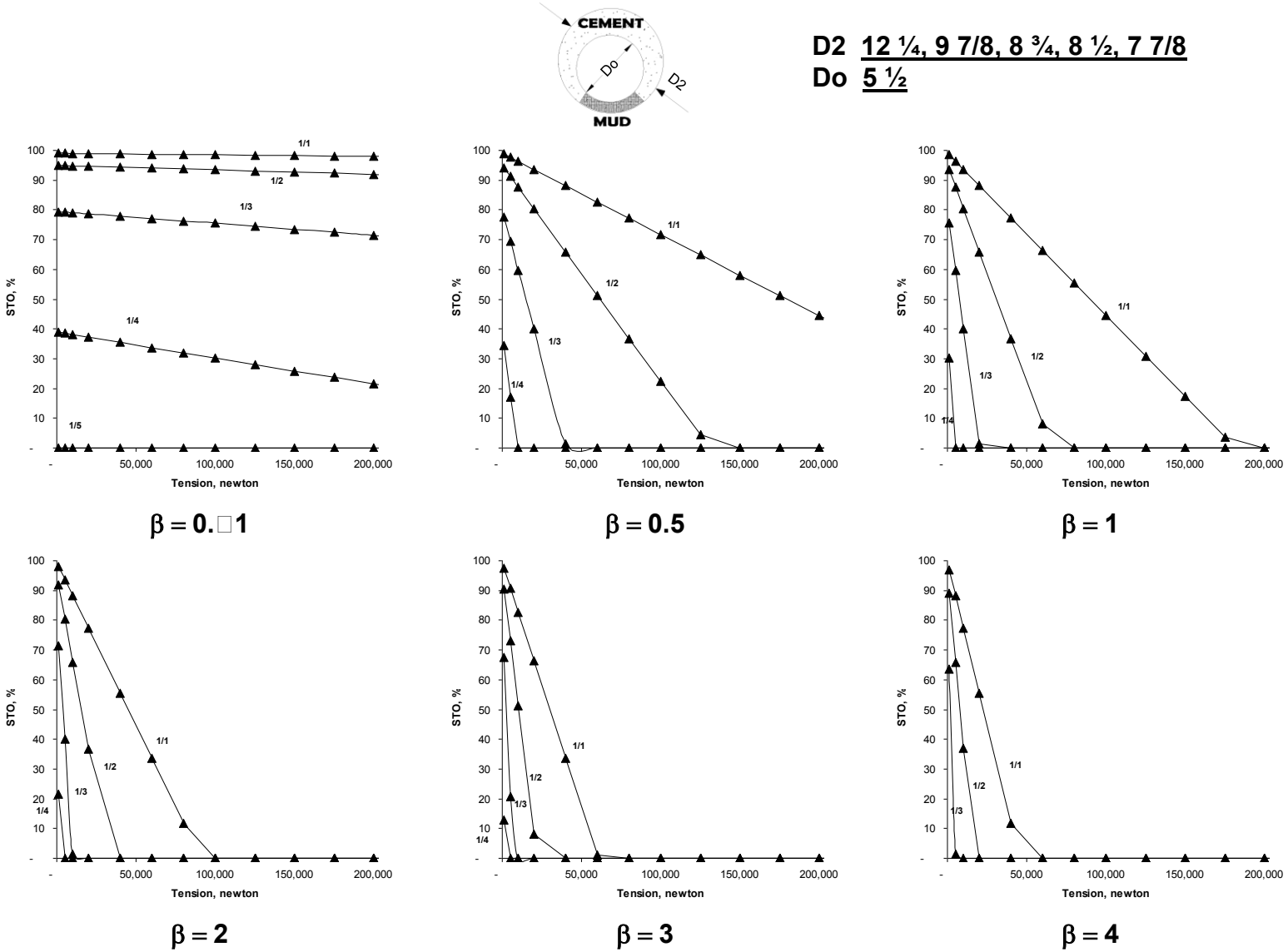

Figure 1j Casing standoff (STO) for straight, inclined wellbore with axial tension.

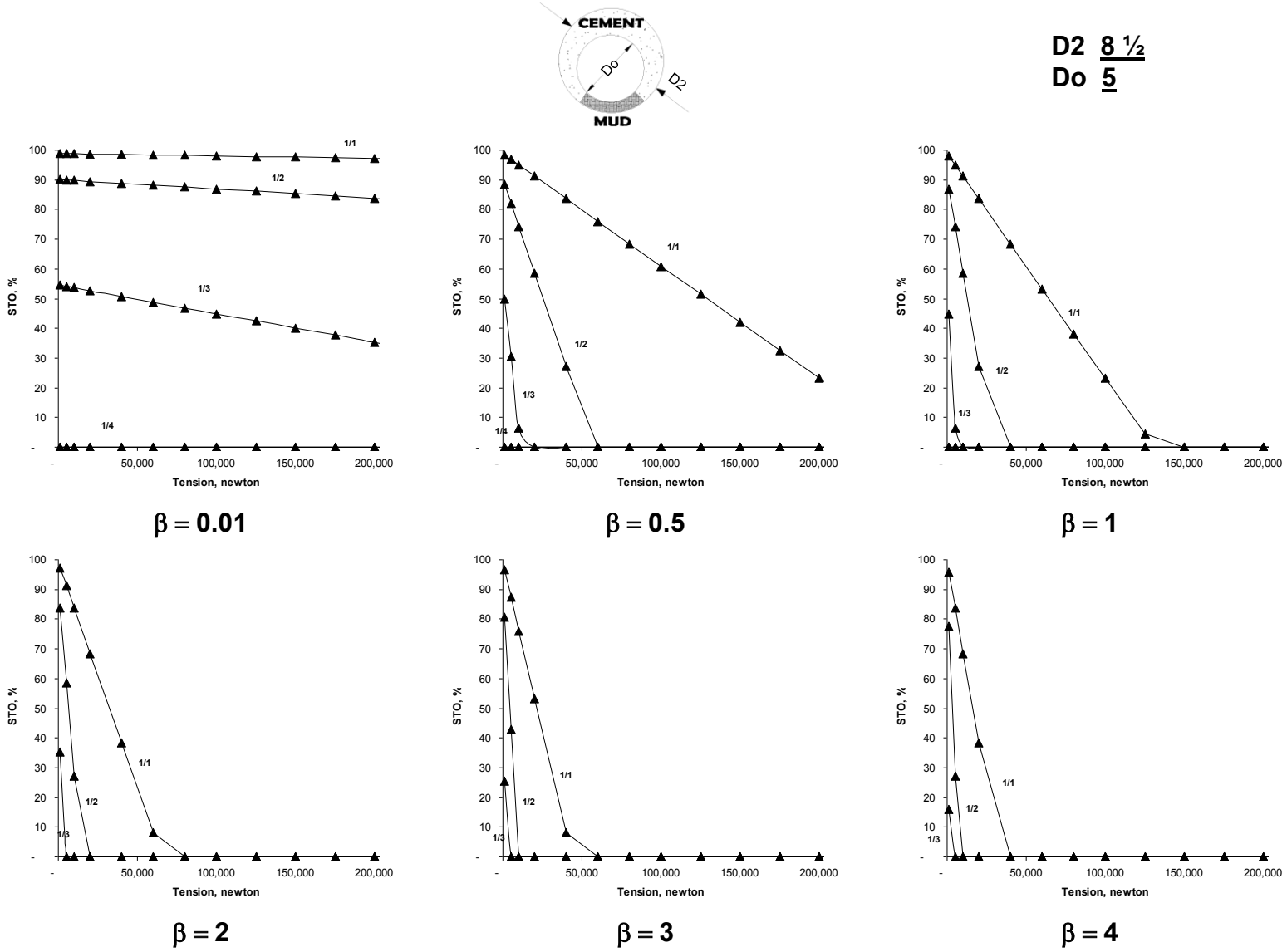

Figure 1k Casing standoff (STO) for straight, inclined wellbore with axial tension.

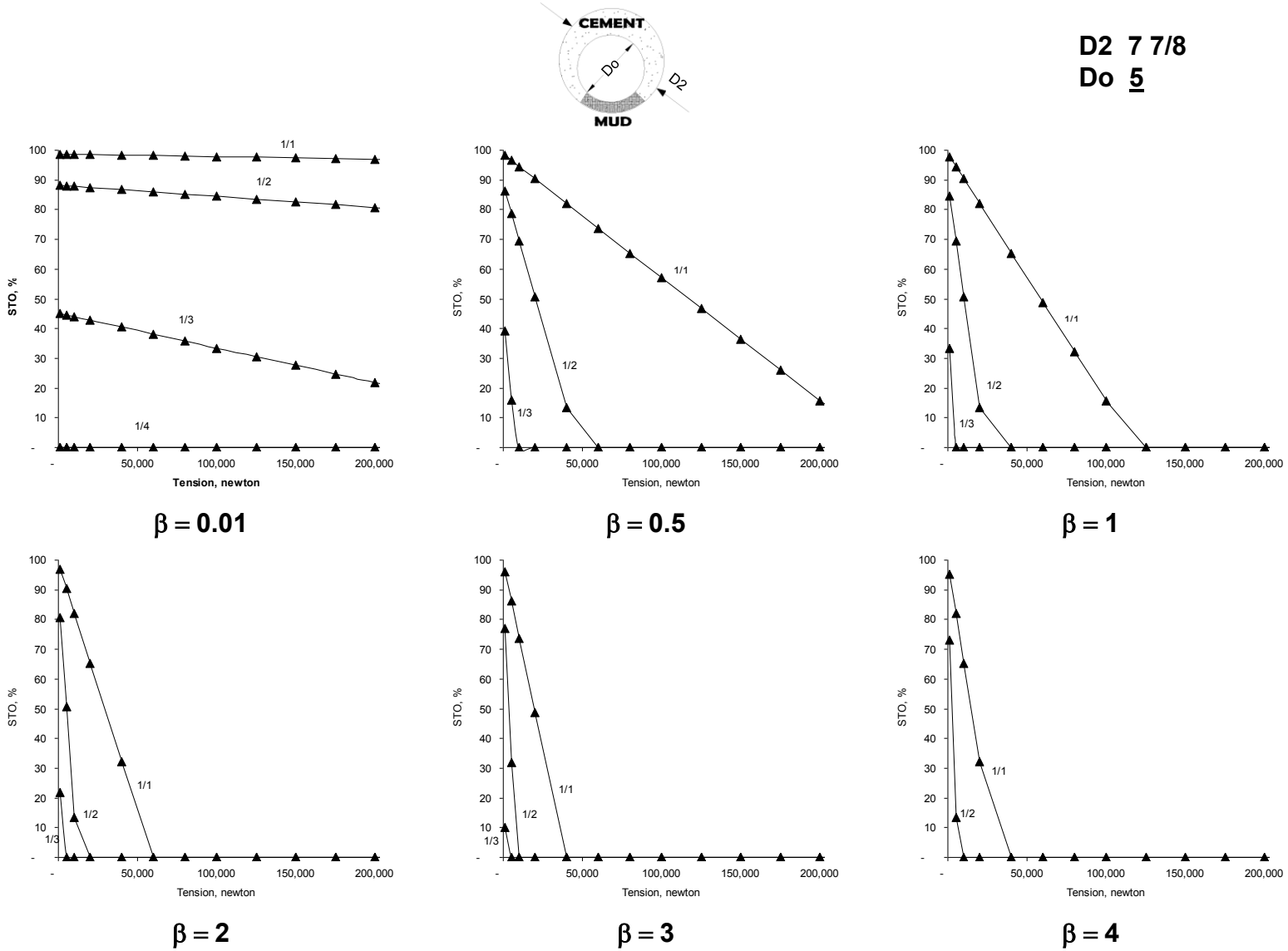

Figure 1l Casing standoff (STO) for straight, inclined wellbore with axial tension.

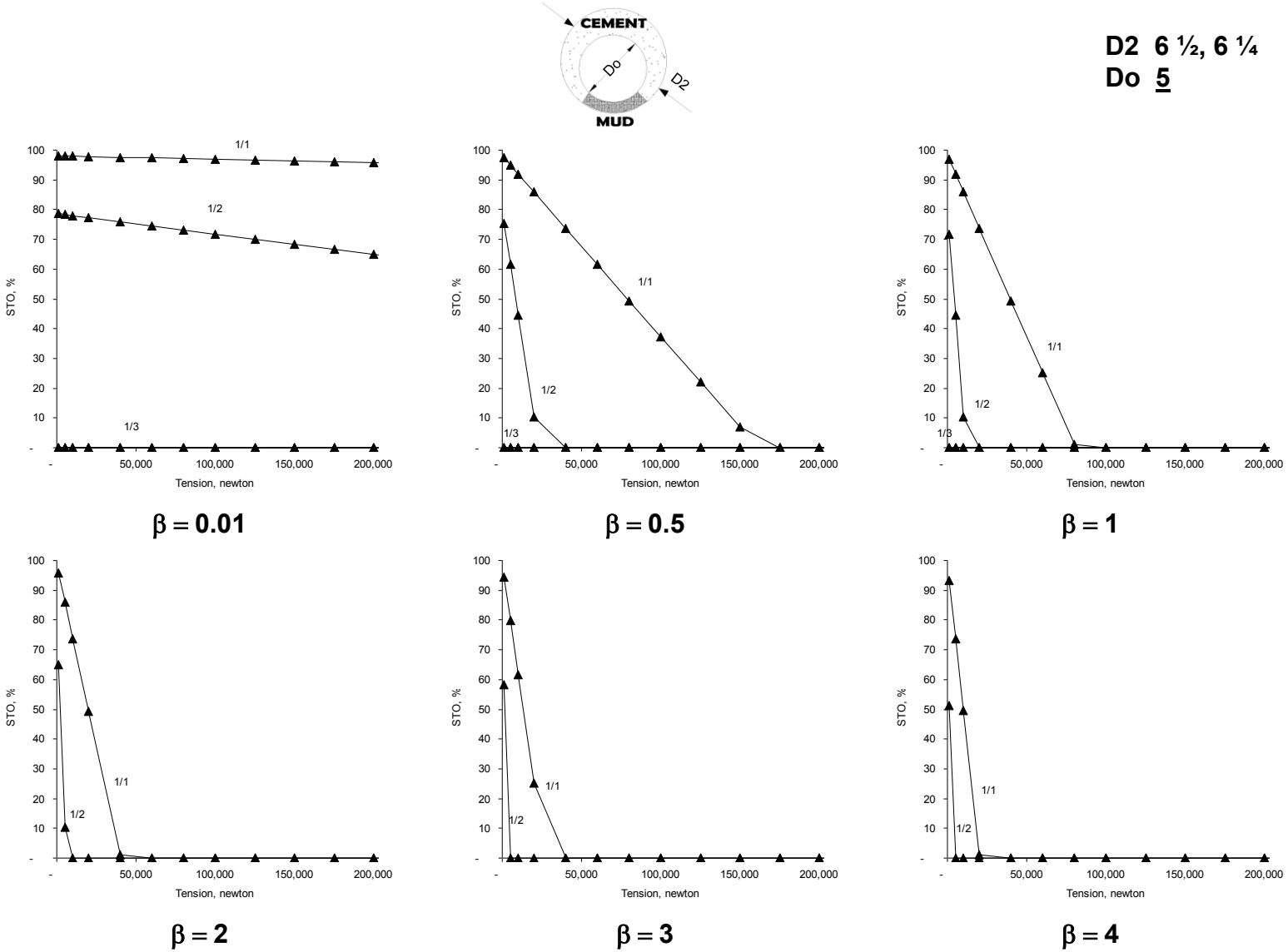

Figure 1m Casing standoff (STO) for straight, inclined wellbore with axial tension.